Mechanistic Insight into Human *ether-a-go-go*-related Gene (hERG) K^+ Channel Activation and Deactivation gating

by

Samrat Thouta

M.Sc., University of Leicester, 2009

B.Tech, Jawaharlal Nehru Technological University, 2008

Thesis Submitted in Partial Fulfillment of the
Requirements for the Degree of
Doctor of Philosophy

in the
Department of Biomedical Physiology and Kinesiology
Faculty of Science

SIMON FRASER UNIVERSITY
Summer 2017

Approval

Name: **Samrat Thouta**

Degree: **Doctor of Philosophy**

Title: **Mechanistic Insight into Human *ether-a-go-go*-related Gene (hERG) K^+ Channel Activation and Deactivation gating**

Examining Committee:

Chair: William Cupples
Professor

Dr. Thomas Claydon
Senior Supervisor
Associate Professor

Dr. Glen Tibbits
Supervisor
Professor

Dr. Peter Ruben
Supervisor
Professor

Dr. Nancy Forde
Internal Examiner
Associate Professor

Dr. Rikard Blunck
External Examiner
Associate Professor

Date Defended/Approved: June 15th, 2017

Abstract

hERG encodes the pore-forming α-subunit of the voltage-gated potassium channel that underlies the rapid delayed rectifier current, I_{Kr}, in the heart, which is essential for normal cardiac electrical activity and rhythm. Inherited mutations in, or pharmacological blockade of, hERG channels deplete the cardiac repolarization reserve, increasing the risk of life-threatening arrhythmias. The molecular bases of hERG gating events and drug binding are poorly understood. hERG channels display unique gating characteristics critical for their physiological function. They activate and deactivate slowly, yet inactivate and recover from inactivation rapidly. In addition, the promiscuous nature of drug interactions with hERG channels presents a therapeutic challenge for drug design and development. My thesis provides novel mechanistic and structural characterization of the unusual activation and deactivation gating processes of hERG. In my first study, I used a proline scan approach to define the activation gate region in hERG channels. Proximal substitutions (I655P-Q664P) impeded gate closure, trapping channels in the open state, while distal substitutions (R665P-Y667P) preserved normal gating, suggesting that Q664 marks the position of the activation gate in hERG. This is more than one helical turn lower than in related channels, which may allow for drug docking. Using two different approaches to measure voltage sensor gating in trapped open channels, I then demonstrated that slow activation is an intrinsic property of the voltage-sensing unit of hERG. In my second study, I showed that voltage-sensor stabilization slows hERG channel deactivation gating. I characterized the temporal sequence of events leading to voltage-sensor stabilization upon membrane depolarization. I showed that this occurs via two separable mechanisms, one derived from pore-gate-opening and the other from the voltage-sensing unit itself. In addition, I show that voltage sensor return in hERG channels is less energetically favourable than pore closure during repolarization and thus is what limits deactivation. Finally, I characterize the use of voltage clamp fluorimetry as a technique to track conformational rearrangements of the hERG voltage sensor associated with gating. These findings provide novel and in depth understanding regarding how hERG channels function and foundational knowledge relevant to finding targets for the treatment and management of cardiac arrhythmias.

Keywords: hERG; activation gate; proline scan; voltage-sensor stabilization; slow deactivation; voltage clamp fluorimetry.

Dedication

To my parents and my wife

Acknowledgements

Undertaking this PhD has been a truly life-changing experience for me and it would not have been possible to do without the support and guidance that I received from many people.

Firstly, it is a great pleasure to express my sincere thanks and deep gratitude to my supervisor Dr. Tom Claydon for his supervision, scrupulous guidance, scholarly encouragement and all the helpful suggestions through all various stages of my PhD. I am indeed highly privileged to have the opportunity of being his student. Without his support and constant feedback this PhD would not have been achievable.

Besides my supervisor, I would like to thank my committee members Dr. Glen Tibbits and Dr. Peter Ruben for their insightful comments, support and encouragement.

I would like to say a heartfelt thanks to Dr. May Cheng for teaching me electrophysiological techniques among other things. I am grateful to her, for her enthusiastic and illustrious guidance. My special thanks to Ji Qi for all her hard work in generating hERG constructs.

A big thank you to my lab mates Patrick Yu Shi, Christina Hull and Danielle Jeong for the stimulating discussions, for helping me in numerous ways during various stages of my PhD and for all the fun we had in the last six years. And of course, I would like to thank all the members of Molecular Cardiac Physiology Group. I have had a great time in the lab and it is because mostly due to you lot.

And finally, to my wife, Shalini, who has been by my side throughout this PhD, living every single minute of it, and without whom, I would not have had the courage to embark on this journey in the first place. Lastly this acknowledgment would be incomplete without expressing my indebtedness to my parents Srinivas and Rekha who have been a constant source of inspiration and support during my doctoral studies.

Table of Contents

List of Tables

List of Figures

Abbreviations and Acronyms

Amino Acid	3 letter code	1 letter code
Alanine	Ala	A
Arginine	Arg	R
Asparagine	Asn	N
Aspartate	Asp	D
Cysteine	Cys	C
Glutamate	Glu	E
Glutamine	Gln	Q
Glycine	Gly	G
Histidine	His	H
Isoleucine	Ile	I
Leucine	Leu	L
Lysine	Lys	K
Methionine	Met	M
Phenylalanine	Phe	F

Proline	Pro	P
Serine	Ser	S
Threonine	Thr	T
Tryptophan	Trp	W
Tyrosine	Tyr	Y
Valine	Val	V

A	Amplitude of fit
AP	Action potential
Å	Angstrom
Cav	Voltage-gated calcium channel
COVG	Cut-open vaseline gap
CNBHD	Cyclic nucleotide binding homology domain
C-terminus	Carboxy-terminus
Δt	Pulse/step durations
eag	*Ether-a-go-go-gene*
elk	*Ether-a-go-go-like* potassium channel
ECG	Electrocardiogram

e_o	Gating charge
FV	Fluorescence voltage relationship
GV	Conductance voltage relationship
GIRK	G-protein activated inward rectifier potassium channel
hERG	Human-*ether-a-go-go*
HCN	Hyperpolarization-activation cyclic nucleotide gated channel
I_{Kr}	Rapidly delayed rectifier potassium current
I_{Ks}	Slow delayed rectifier potassium current
IUPHAR	International Union of Pharmacology
k	Slope factor
K_{Ca}	Calcium-activated potassium channel
Kv	Voltage-gated potassium channel
K_{ir}	Inward rectifying potassium channel
LQTS	Long QT syndrome
$MgOR_2$	Ca^{2+} free oocyte ringer solution
MTSR	Methanethiosulphonate-rhodamdamine
mink	Minimal potassium channel subunit
MiRP1	Mink related peptide 1
Nav	Voltage-gated sodium channel

ND96	Extracellular recording solution
N-terminus	Amino-terminus
NMR	Nuclear magnetic resonance
PD	Pore domain
PMT	Photomultiplier tube
PAS	Per-Arnt-Sim domain
PVP	Proline-valine-proline
PCR	Polymerase chain reaction
QV	Gating charge voltage relationship
SEM	Standard error of the mean
τ	Time constant
Tdp	Torsade de pointes
TEVC	Two-electrode voltage clamp
TMRM	Tetramethylrhodamine-5-maleimide
TEA	Tetraethylammonium
VSD	Voltage sensing domain
$V_{1/2}$	Voltage at half maximal activation
VCF	Voltage clamp fluorimetry
WT	Wild type

Chapter 1. Introduction

1.1 Overview

Cardiac arrest is an electrical disturbance in the heart resulting in the abrupt loss of heart function. The electrophysiological behaviour of the heart is determined by ion channels. They establish and maintain the cardiac rate and rhythm. Dysfunction of ion channels can lead to life-threatening cardiac arrhythmias and sudden death (Roden et al. 2002). In the heart, the voltage-gated potassium channel Kv11.1 or human *ether-a-go-go-related gene* (hERG) is essential for regulating repolarization of the cardiac action potential (AP). Unlike other voltage-gated potassium (Kv) channels, hERG channels exhibit unusual gating properties that are crucial for their physiological function. Their unusual gating kinetics are important for timing the onset of repolarizing current during the AP. That being said, the molecular basis of the hERG channel's unusual gating kinetics is poorly understood. Investigating the structural determinants and gating mechanisms in hERG channels will improve our understanding of how these channels work and the processes underlying hERG function in health and disease. The outcome of these studies will be useful in laying the foundation for treatment and the prevention of cardiac disease and the development of safer drugs.

In this introduction, I will provide a general overview of potassium ion (K^+) channels with particular focus on the structural and functional aspects of Kv channels, followed by an in-depth review of the structural and molecular basis of hERG channel gating and drug binding. This introduction will set the stage for the focus of this thesis, which investigates the mechanistic basis of hERG gating function.

1.2 Potassium channel families

K^+ channels are the largest and most diverse group of ion channels, responsible for regulating the electrical activity of cell membranes (Gutman et al. 2005). These channels are integral membrane proteins, which contain a pore domain through which potassium ions diffuse. The first K^+ channel gene to be cloned was *Shaker*, a Kv channel from *Drosophila melanogaster.* A mutation in this gene produced a shaking phenotype in the fruit flies (Papazian et al. 1987). Since then, many other voltage and ligand-gated K^+

channel genes in flies, mammals and other organisms were identified (Jan & Jan 1997). Based on the phenotypic diversity, K^+ channels are broadly classified into four major types; six transmembrane (TM) Kv channels, Ca^{2+} dependent (K_{Ca}) channels, two TM inward rectifier (K_{ir}) channels and tandem pore domain (K_{2P}) or leak channels (Papazian et al. 1987; Miller et al. 2000; Hille 2001; Korn & Trapani 2005). A K^+ channel, regardless of which class it belongs to, is divided into two main parts: the pore domain (which facilitates the flow of K^+ ions) and a regulatory domain that senses various stimuli such as voltage or ligands. All of these channels exhibit pore-lining P-loops with an amino acid sequence - Thr/Ser-X-Gly-Tyr/Phe-Gly (Hille 2001) between the two most carboxy-terminal transmembrane spanning helices that form the K^+ selective pore (Choe 2002; Miller et al. 2000; Doyle et al. 1998). Among all types of K^+ channels, Kv channels constitute the largest family with some 40 genes (Gutman et al. 2005).

1.3 **Voltage-gated K^+ channels**

Kv channels are the transmembrane proteins that regulate the flow of K^+ out of the cell down their electrochemical gradient in response to a change in transmembrane potential. In response to the transmembrane potential change, Kv channels are either present in open, closed, or inactivated (non-conducting) states. The transition between these states is known as gating. Kv channels play a crucial role in regulating the electrical activity and functioning of excitable cells, including setting up the resting membrane potential, and modulating the duration and firing frequency of the action potential (Korn & Trapani 2005).

Kv channels are broadly classified into 12 subfamilies (see Table 1.1) Kv1.x to Kv12.x (Gutman et al. 2005). According to International Union of Pharmacology (IUPHAR), *Shaker* channels are referred to as Kv1.1, where 'K' stands for potassium channel, 'v' for voltage-gated, and '1' is the *Shaker* subfamily. Similarly, other drosophila genes are referred as *Shab* (Kv2.x), *Shaw* (Kv3.x) and *Shal* (Kv4.x). Kv5, 6, 8 and 9 assemble with other K^+ subunits to form functional channels. Kv7 channels also referred to as *KCNQ*, form heteromers with other subunits or interactions with accessory subunits. The *KCNH* subfamily genes encode Kv10.x (*eag*), Kv11.x (*erg*) and Kv12.x *(elk*) channels. hERG channels are also referred to as Kv11.1 or *KCNH2* (the gene product) and these are the subject of study in this thesis.

Table 1.1 Kv channels classification

Family	α - Subunit	Gene name	Category
Kv1 (*Shaker)*	Kv1.1	*KCNA1*	Delayed rectifiers
	Kv1.2	*KCNA2*	
	Kv1.3	*KCNA3*	
	Kv1.4	*KCNA4*	A-type transient current
	Kv1.5	*KCNA5*	Delayed rectifiers
	Kv1.6	*KCNA6*	
	Kv1.7	*KCNA7*	
	Kv1.8	*KCNA10*	
Kv2 (*Shab*)	Kv2.1	*KCNB1*	Delayed rectifiers
	Kv2.2	*KCNB2*	
Kv3 (*Shab*)	Kv3.1	*KCNC1*	A-type transient current
	Kv3.2	*KCNC2*	
	Kv3.3	*KCNC3*	
	Kv3.4	*KCNC4*	
Kv4 (*Shal*)	Kv4.1	*KCND1*	
	Kv4.2	*KCND2*	
	Kv4.3	*KCND3*	
KCNQ	Kv7.1	*KCNQ1*	Delayed rectifiers
	Kv7.2	*KCNQ2*	
	Kv7.3	*KCNQ3*	
	Kv7.4	*KCNQ4*	
	Kv7.5	*KCNQ4*	
KCNH	Kv10.1	*KCNH1/eag1*	
	Kv10.2	*KCNH5/eag2*	
	Kv11.1	*KCNH2/hERG*	
	Kv11.2	*KCNH6/erg2*	
	KV11.3	*KCNH7/erg3*	Delayed rectifiers
	Kv12.1	*KCNH8/elk1*	
	Kv12.2	*KCNH3/elk2*	
	Kv12.3	*KCNH4/elk4*	
Other Kv and electrically silent	Kv5.1	*KCNF1*	Modifier/silencer
	Kv6.1	*KCNG1*	
	Kv6.2	*KCNG2*	
	Kv6.3	*KCNG3*	
	Kv6.4	*KCNG4*	
	Kv8.1	*KCNV1*	
	Kv8.2	*KCNV2*	
	Kv9.1	*KCNS1*	
	Kv9.2	*KCNS2*	
	Kv9.3	*KCNS3*	

Functionally, Kv channels are grouped into two categories:

Delayed rectifiers - channels which show slow or no inactivation (Hille 2001). In the heart, delayed rectifiers play a crucial role in repolarization and termination of the action potential. In neurons, they control the action potential firing frequency, thus regulating excitability.

A-type transient current - channels which show fast inactivation (Hille 2001). In the heart, these channels rapidly repolarize the action potential thereby influencing the plateau potential and calcium entry.

1.3.1 **Kv channel structure**

In general, Kv channels share a common basic structure (Yellen 2002). In their simplest form, they exist as homotetramers, composed of four identical α subunits arranged around a central conducting pore (Fig.1.1B). Each α subunit contains six α-helical transmembrane helices (S1-S6), connected by five linker regions with both amino (N) and carboxy (C) terminal domains on the intracellular side of the membrane (Fig. 1.1A). Within the six transmembrane segments, the first four transmembrane segments (S1-S4) form the voltage-sensing domain (VSD). The VSD contains positively charged residues (Arginine or Lysine) spaced apart by hydrophobic residues in S4 and negatively charged residues in S1-S3 that confer sensitivity to changes in the membrane voltage (Papazian et al. 1987). The last two transmembrane segments (S5-S6) form the functional conducting pore domain (PD) connected with an intervening P-loop and selectivity filter, which confers a preference for the flow of potassium over other ions (Doyle et al. 1998). Membrane depolarization drives outward movement of the voltage sensor (S4) within the bilayer leading to the opening of the pore via the S4-S5 linker - which serves as a mechanical lever (Long et al. 2005b). In the following sections, I will outline key evidence provided by X-ray crystal structures of bacterial potassium channels (KcsA, MthK; (Doyle et al. 1998; Jiang et al. 2002a)) and the eukaryotic Kv channel (Kv1.2, Kv2.1/Kv1.2 paddle chimera; (Long et al. 2005a; Long et al. 2007)) and more recently cryo-EM structures of Kv10.1, Kv11.1 and $K_{Ca}1.1$ channels (Whicher & MacKinnon 2016; Wang & MacKinnon 2017; Tao et al. 2016) as well as functional probing of channel domains that have provided further insights into understanding of the structure-functional relationship of the voltage sensing and pore domain of Kv channels.

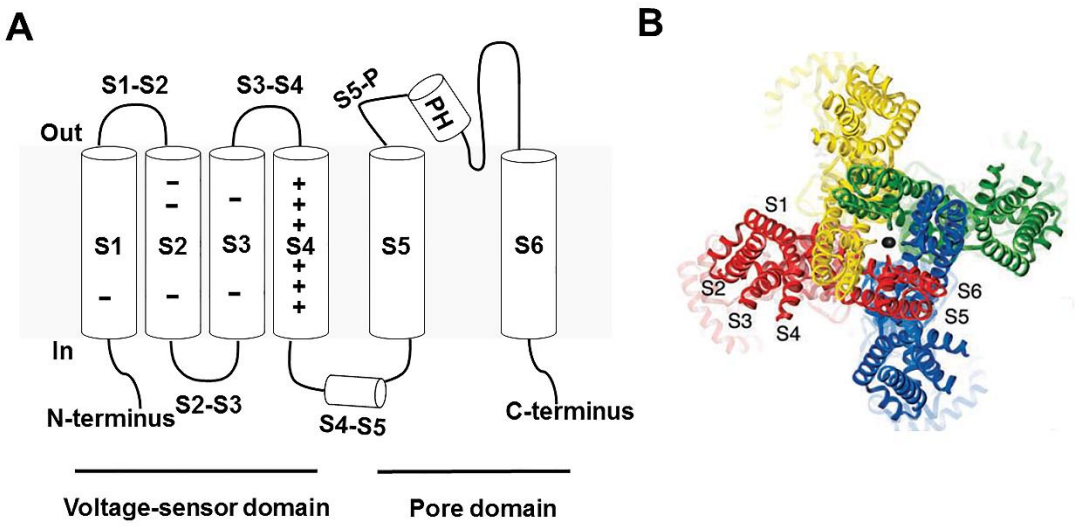

Figure 1.1 Structural features of Kv channels.
A, Schematic of a single α-subunit of a Kv channel comprises six α helical transmembrane segments (S1-S6). S1-S4 form a voltage sensor domain and S5-S6 the pore domain. ***B,*** Ribbon representation of the Kv1.2 crystal structure presented as a tetrameric assembly (Long et al. 2005a). Each subunit has been shown in a different colour. The model shows a view from the top view, extracellular side. Fig.1.1B is from Long et al., 2005a reprinted with permission from AAAS.

1.3.1.1. The pore region in K^+ channels

Pore gate

Early pharmacological studies on Kv channels showed that there is a gate region at the intracellular side of the pore. This gate regulates ion conduction across the pore by opening and closing. The first evidence came from a series of experiments by Dr Clay Armstrong that showed the application of tetraethylammonium (TEA) and its derivatives block the Kv channel of the squid axon when applied to the intracellular side. Apparently, TEA blocked the K^+ current only when the gate was opened (open channel blocker) by membrane depolarization (Armstrong 1966; Armstrong 1971; Armstrong & Hille 1972). In addition, upon membrane repolarization the gate closed rapidly, thereby trapping the TEA inside the pore suggesting that gate was located on the intracellular side of the membrane and there must be a vestibular cavity on the extracellular side of the gate in which TEA could reside (Armstrong 1974). The evidence for drug trapping mechanism of activation gate was best described in a mutant *Shaker* K^+ channel (I470C). In the presence of an intracellular blocker, decyltriethylammonium (C_{10}), membrane depolarization opened the channels rapidly and then relaxed to a new state where ~80%

of the channels were blocked. Upon membrane repolarization, unblocked channels closed to the normal resting state and blocked channels to a closed-blocked state, containing a trapped drug. Even after an extensive washout of the blocker, a positive voltage step opened only 20% of the channels rapidly, while the remaining 80% of the closed-blocked channels appeared to open slowly only after the release of the blocker (Holmgren et al. 1997). In *Shaker* channels, the location of the gate was identified by examining the state-dependent accessibility of engineered cysteines introduced in S6 region to methanethiosulphonate (MTS) reagents and Cd^{2+} (Liu et al. 1997; del Camino et al. 2000). These results showed that mutagenesis of the S6 region (T469-Y485) to small (alanine), bulky (tryptophan) and charged (aspartate) side chains either trapped the channel in the open state or prevented the channel from opening, and helped to confirm V478 and/or F481 as candidates for the *Shaker* gate (Hackos et al. 2002). Taken together, these data were consistent with the location of the gate at the intracellular side of the ion conduction pore in Kv channels.

In the year 1998, groundbreaking work from Roderick Mackinnon's group led to the determination of the first X-ray crystal structure of the K^+ channel, KcsA (Doyle et al. 1998). KcsA is a simple prokaryotic K^+ channel from bacteria *Streptomyces lividans* composed of four identical subunits arranged around a central conducting pore. Each subunit has two transmembrane α helices M1 and M2, which are analogous to S5 and S6 in *Shaker* channels. M1 is the outer helix and M2 is the inner helix that lines the inner cavity of the channel (Fig. 1.2A). The structure showed that the inner helix adopted an inverted teepee or cone-like structure at the intracellular end of the ion pore, which leaves a large aqueous pore cavity that could hold pore blockers like quaternary ammonium (QA) compounds just above an "activation gate", which controls the flow of ions between the pore and the cytoplasm. The activation gate was formed at the bundle crossing by the convergence of the inner helices (Fig. 1.2A), suggesting that the channel was crystallised in the closed state. At the outer end of the pore between the two transmembrane segments, there is a re-entrant P-loop, which contains the K^+ channel 'signature sequence' TVGYG (Fig. 1.2C).

This signature sequence combined from all the four subunits forms the selectivity filter. It is the selectivity filter, which confers a preference for the flow of K^+ ions over other ions. The amino acid residues of each subunit of the selectivity filter are lined by a backbone of carbonyl oxygen atoms that face towards the central axis of the pore. This

arrangement of oxygen atoms forms octahedral binding sites that mimic the hydration shell of K^+ ion in solution, and coordinate the dehydrated K^+ ions in a single file, separated by a single water molecule. A water-filled cavity lies between the selectivity filter and the activation gate.

In addition to KcsA, crystal structures of a prokaryotic calcium-gated K^+ channel, MthK, from the archeon *Methanobacterium thermoautotrophicum*, redefined the picture of the gate because the channel was crystallized in the open conformation (Jiang et al., 2002a). The MthK channel functions as a tetramer, in which the inner helices are bent ~30° and splayed outward at a conserved glycine residue which functions as a "gating hinge" (Jiang et al. 2002b). This gating hinge is observed in other K^+ channel crystal structures, such as KvAP, a Kv channel from *Aeropyrum pernix* (Jiang et al. 2003). The glycine hinges (Fig. 1.2A and B, red highlight) (Gly99 in KcsA, Gly83 in MthK and Gly220 in KvAP) are located in a similar position in these channels, suggesting a similar mechanism for the opening of the activation gate. Furthermore, this glycine hinge is not only restricted to K^+ channels, as bacterial voltage-gated Na^+ channels such as NaChBac from *Bacillus halodurans*, also have a conserved glycine (G219) residue located in the S6 helix, which serves as a gating hinge that is responsible for the bending of the inner helices to open the activation gate (Zhao, Yarov-Yarovoy, et al. 2004).

Similar to Mthk and KvAP, a eukaryotic Kv channel Kv1.2 (Fig. 1.2B), a homologue of *Shaker*, was also crystallised in the open confirmation (Long et al. 2005a). In this channel, the activation gate is formed at the bundle crossing by a conserved Proline-Valine-Proline (PVP) motif (Fig. 1.2B, yellow highlight), located in the lower region of the S6 helix. The PVP motif introduced a kink in S6 that allowed the helices to splay outward away from the central axis of the pore to create a large central cavity allowing electromechanical coupling with voltage sensor movements via the S4-S5 linker. (Long et al. 2005b). This PVP motif is highly conserved in Kv1-4 channels (Fig. 1.2C). In *Shaker* channels, mutating this motif led to a loss of channel function and/or alteration in channel gating (Labro et al. 2003). For example mutation of P475 in the PVP motif to Asp, trapped the channel in the open state producing constitutively active channels, suggesting that alterations to this motif could result in disruption of the structure of the S6 gate and thereby channel gating (Hackos et al. 2002).

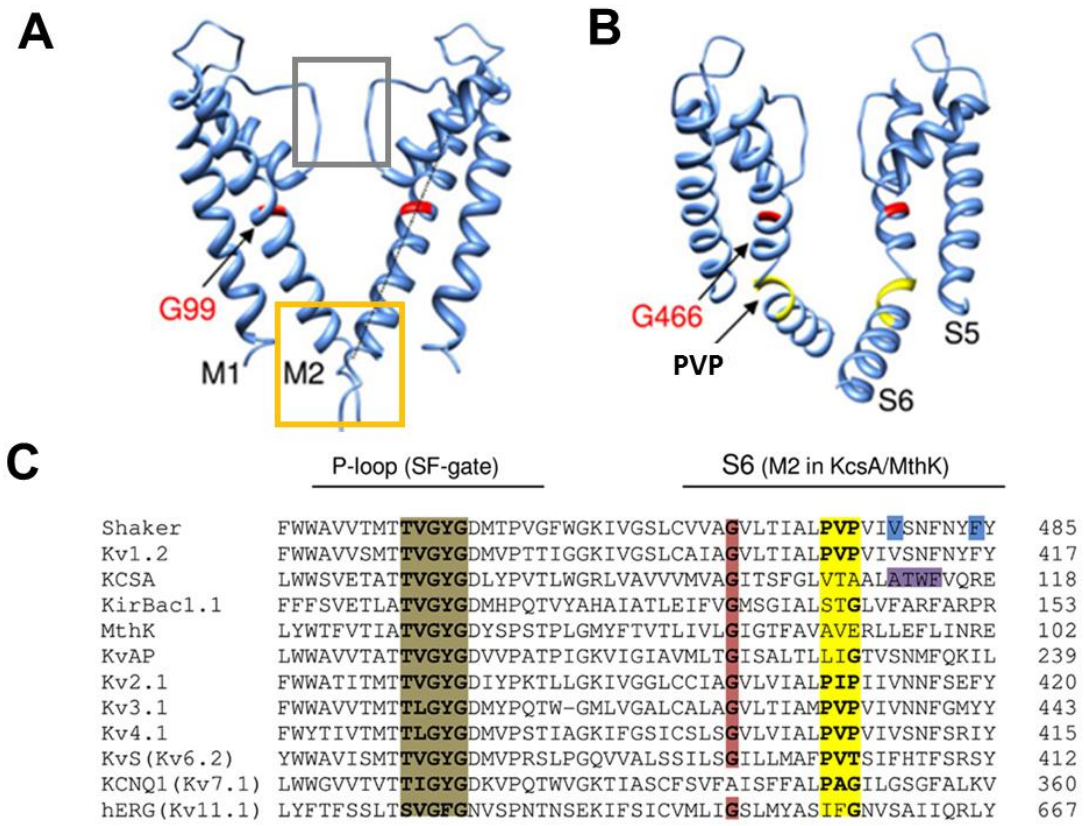

Figure 1.2 Structural features of the pore region in K^+ channels.
A and ***B***, side-view of the pore forming domain of the bacterial K^+ channel, KcsA, crystallized in the closed state (*A*) and the eukaryotic K^+ channel Kv1.2 crystallized in the open state (*B*). For clarity purpose, only two of the four subunits are shown in each case. Gray and orange boxes in *A* highlight the selectivity filter and activation gate, respectively. The conserved glycine hinge is highlighted in red (*A* and *B*) and the PVP motif is highlighted in yellow (*B*). ***C***, sequence alignment of the pore region in K^+ channels highlighting the selectivity filter, which contains the signature sequence - TVGYG (highlighted in brown). Highlighted in red and yellow are the highly conserved glycine residue and the PXP motif respectively. The gate regions in *Shaker* and KcsA channels is highlighted in blue (V478 and F484) and purple, respectively. Fig. *A-C* are reprinted and adapted with the permission of Creative Commons Attribution License (Labro & Snyders 2012)**.**

1.3.1.2 Voltage sensing in K^+ channels

Voltage sensor movement precedes channel opening

In the previous section, I discussed activation gating in the context of how the pore opens and closes. It is also equally important to understand how this opening and closing of the pore is coupled to the membrane voltage in Kv channels. What specific feature of the channel makes the opening and closing of the activation gate voltage sensitive? In real time, a voltage sensor detects the transmembrane voltage which

controls the activation gate opening and closing. In 1952, Hodgkin and Huxley (Hodgkin & Huxley 1952) proposed the idea of a voltage sensor that contains charged particles that are located in the membrane electrical field, which change their position in response to changes in the voltage. Many years later, we now know of these charged particles as gating charges. The S4 helix of each voltage sensing domain contains 4-8 positively charged residues (Arginine or Lysine) spaced at every third position (Liman & Hess 1991; Aggarwal & MacKinnon 1996; Yellen 1998; Bezanilla 2000). Movement of these gating charges across the electric field, as a result of a change in membrane voltage, induces pore opening, and may even be measured if ionic currents are eliminated by the application of pore blockers or by mutagenesis (Bezanilla 2000) as they generate transient current called a “gating current”.

Membrane depolarization evokes an ‘On’ gating current that corresponds to the movement of the voltage sensor charges from resting to activated states. Membrane repolarization elicits an ‘Off’ gating current that corresponds to the movement of voltage sensor charges returning to resting states. The time-integrals of both On and Off gating currents give charge movement and the voltage-dependence of gating charge transfer (QV) can be plotted. Plotting QV and pore conductance against voltage (GV) relationships on the same axis, it is apparent that the QV relation is noticeably left-shifted compared to the GV relation, suggesting that S4 movement precedes channel opening, i.e. it is energetically more favourable. This is consistent with the reports of Hodgkin-Huxley who showed that the voltage-sensors from four subunits moved independently prior to the channel opening (Hodgkin & Huxley 1952). It has also been shown that S4 traverses multiple closed states prior to the activated state (Perozo et al. 1994; Zagotta, Hoshi, Dittman, et al. 1994). In *Shaker* channels, gating current measurements suggested that channel opening occurs in one final cooperative step after all the VSDs of 4 subunits are activated (Zagotta, Hoshi & Aldrich 1994). Gating current recordings from *Shaker* channels suggested that the activation pathway involves two main steps: (1) early-closed state transitions, and (2) more major conformational changes of S4 (Perozo et al. 1994). Mutations in the *Shaker* S4 (S369I, I372L and S376T) - ‘ILT mutation’ - resulted in separation of the major component of charge movement (the QV is shifted to more negative voltages) from the final cooperative step and pore opening (the GV is shifted to more positive voltages) (Ledwell & Aldrich 1999). These data suggest that the ILT mutation separated the independent movements of S4

from the final cooperative step and pore opening, and showed that a fraction of voltage-dependence of gating charge is associated with pore opening (Smith-Maxwell et al., 1998a; Ledwell and Aldrich, 1999; Pathank et al., 2005).

Voltage sensor relaxation

In addition to resting and activated states, recent studies in *Shaker*, Kv1.2, Kv3.1 and Ci-VSP have shown that prolonged depolarization triggers the voltage sensor to engage in additional interactions that stabilize it in an alternate activated state termed the "relaxed state" (Villalba-Galea et al. 2008; Lacroix et al. 2011; Labro et al. 2012; Labro et al. 2015). This voltage sensor relaxation imparts a mode-shift behaviour (hysteresis), where the voltage-dependence of S4 return and subsequent pore closure occurs at more hyperpolarized potentials compared to that of S4 activation and pore opening. This observation illustrated that the voltage dependence of Kv channels is likely dynamic. The so-called mode-shift behaviour was first observed in Na^+ channels of the squid giant axon (Bezanilla 1982) and subsequently in *Shaker* (Lacroix et al. 2011; Labro et al. 2012), Kv1.2 (Labro et al. 2012), Kv3.1 (Labro et al. 2015), Kv7.2/Kv7.3 (Corbin-Leftwich et al. 2016), hERG (Piper et al. 2003; Tan et al. 2012; Hull et al. 2014; Goodchild et al. 2015), HCN (Bruening-Wright & Larsson 2007) and L-type voltage-gated calcium channels (Shirokov et al. 1992). The molecular mechanisms underlying voltage sensor relaxation are unknown. Initially, the time course of development of the mode-shift was correlated to C-type inactivation, suggesting that C-type inactivation is required for mode-shift to occur (Olcese et al. 1997). Other studies showed that mutations in the S4-S5 linker and S6, which uncouple the voltage sensor from the pore gate, abolish the mode-shift. This suggested that mode-shift originated from the mechanical load placed on the voltage sensor domain by the pore (Batulan et al. 2010; Haddad & Blunck 2011). However, voltage sensor relaxation was also reported in Ci-VSP, a voltage-sensitive phosphatase that comprises a voltage sensor domain, but no pore domain or C-type inactivation process. This demonstrated that relaxation may be an intrinsic property of the voltage sensor and not associated with inactivation (Villalba-Galea et al. 2008). Consistent with this, gating current recordings (Piper et al. 2003) and voltage clamp fluorimetry (VCF) measurements (Tan et al. 2012) in hERG channels showed that alterations of inactivation gating do not abolish relaxation. More recently, deletion of the pore domain in *Shaker* channels failed to prevent voltage sensor relaxation (Zhao & Blunck 2016). All of these observations indicated that the relaxation process emerged

from intrinsic behaviour of the voltage-sensing domain. Importantly, new evidence emerged in the literature indicating that voltage sensor relaxation may partially account for changes in the deactivation kinetics. In *Shaker* and Kv1.2 channels, applying depolarizing steps of increasing duration progressively slowed kinetics of charge return or pore gate closure during subsequent repolarization. The slowing of charge return or pore closure displayed a biphasic nature when plotted against increasing duration of the depolarizing pre-pulse. (Lacroix et al. 2011; Labro et al. 2012). Based upon kinetic association, the authors proposed that the faster component of slowing was associated with pore opening and is caused by stabilization of the activated voltage sensor by the open pore. The second, slower, stabilization of charge return was attributed to reconfiguration of the voltage sensor into the relaxed state. These studies showed that transition of the voltage sensor in *Shaker* and Kv1.2 channels to the relaxed state was slow, occurring over 2-4 s. More recently, Labro et al (2015) observed a very rapid component of charge return in Kv3.1 channels, which kinetically preceded pore gate opening, and was attributed to an ultra-fast relaxation mechanism. Furthermore, previous studies have shown that in *Shaker* channels, voltage sensor relaxation is critically dependent upon the length of the S3-S4 linker and to some extent to its amino acid composition. Gating current records from *Shaker* showed that shortening the length of the S3-S4 linker (31 amino acids) increased the extent of voltage sensor relaxation, whereas lengthening the linker had little effect (Priest et al., 2013).

The time-course of mode-shift due to voltage sensor relaxation varied from minutes in Na^+ channels (Bezanilla 1982) to seconds in *Shaker* and Kv1.2 channels (Labro et al. 2012; Lacroix et al. 2011), to several hundred milliseconds in hERG (Piper et al. 2003; Goodchild et al. 2015). The molecular mechanisms underlying voltage sensor relaxation and its divergent time courses in different channels remain unclear. In particular, the unusually rapid voltage sensor relaxation observed in hERG channels that appeared to occur on the timescale of a cardiac action potential has yet to be fully characterised. In Chapter 4, I show the systemic characterization of the time and voltage-dependence of voltage sensor relaxation in hERG channels.

Role of charged residues in gating

It has been widely acknowledged that the S4 region plays a crucial role in the functioning of Kv channels. As mentioned previously, the S4 region contains positively charged

residues, that are highly conserved in voltage-gated Na^+, K^+ and Ca^{2+} channels, that were proposed to move in response to changes in the membrane voltage (Sigworth et al. 1994). In particular, each S4 helix contains 4-8 positively charged residues (arginines or lysines) spaced apart by hydrophobic residues (Papazian et al. 1987). Gating current measurements from *Shaker* channels showed that upon membrane depolarization ~12 to 14 e_0 (gating charges) move across the membrane electric field, i.e. 3 to 4 e_0 per subunit (Aggarwal & MacKinnon 1996; Schoppa et al. 1992; Seoh et al. 1996). A recent study in *Shaker* revealed the manner in which these charges are translocated across the membrane electric field during voltage sensing (Tao et al. 2010). The outermost four arginines (R1-R4) lay along an aqueous cleft that projects into the phospholipid membrane and is accessible to the extracellular environment. The fifth positive charge is a lysine (K5) and is isolated from the aqueous cleft by a phenylalanine in S2 (F290) that forms a hydrophobic plug. F290, along with E293 and D316, acts a gating charge transfer centre, which catalyses the movement of S4 positive charges through the membrane. Interaction of the S4 lysine K5 with F290 stabilizes the activated state of voltage sensor, whereas interaction of the outer S4 arginine R1 with F290 stabilizes the resting state (Tao et al. 2010). Mutagenesis (Aggarwal & MacKinnon 1996; Seoh et al. 1996) and accessibility (Larsson et al. 1996) studies have shown that the outermost arginine residues (R1-R4) are exposed to the extracellular environment and carry most of the gating charges whereas the most intracellular lysine (K5) residue does not traverse the electric field. Neutralisation of the outer four charged residues altered the voltage-dependence of activation and reduced the size of the gating charges displaced, indicating that these charge residues are critical in dictating voltage sensitivity in these channels (Liman & Hess 1991; Logothetis et al. 1992; Lopez et al. 1991). This idea is further supported by the observation that a histidine scan of S4 showed that certain sites (R2H-R4H) in *Shaker* enabled proton transport across the membrane in the presence of pH gradient as the histidine shuttles across the membrane electric field in response to membrane depolarization (Starace et al. 1997; Starace & Bezanilla 2004). Furthermore, mutation of the first S4 arginine (R1) to smaller amino acids allowed permeability to metal ions, not through the pore but within the VSD (omega current) (Tombola et al. 2005). These studies show that the S4 region plays a crucial role in functioning of Kv channels.

In addition to the evidence described above, different fluorescence spectroscopic techniques have been used to understand how S4 moves. These include VCF, which allows visualisation of the conformational changes of S4 associated with channel gating, by site-specific attachment of a fluorophore to a cysteine residue (Mannuzzu et al. 1996; Cha & Bezanilla 1997), and fluorescence resonance energy transfer (FRET) and lanthanide-based resonance energy transfer (LRET), which can measure relative distance changes (Isacoff et al. 1999; Posson & Selvin 2008). Site-specific fluorescent labelling of S4 residues in *Shaker* showed changes in the fluorescence signal that complemented the movement of the S4 region as measured by gating currents (Labro et al. 2012). To date, numerous studies reported fluorescence measurements of voltage sensor movement using VCF in a variety of channels including *Shaker* (Mannuzzu et al. 1996; Cha & Bezanilla 1997), Kv1.2 (Horne et al. 2010; Claydon & Fedida 2007), Kv1.4 (Claydon & Fedida 2007), Kv1.5 (Claydon & Fedida 2007; Vaid et al. 2008), Kv7.1 (Osteen et al. 2012), Kv11.1 (Smith & Yellen 2002; Van Slyke et al. 2010; Es-Salah-Lamoureux et al. 2010; Tan et al. 2012; Thouta et al. 2014; Hull et al. 2014), hSkM1 Na^+ (Cha et al. 1999), BK_{Ca} K^+ (Savalli et al. 2006), HCN (Bruening-Wright & Larsson 2007), Nav1.5 (Varga et al. 2015) and Cav1.2 (Pantazis et al. 2014). These data used alone or in concert with gating current measurements, provide insight into the dynamics of voltage sensor movement during channel activation and deactivation.

Models of voltage sensor movement

Based upon the structural and biophysical insight outlined above, three basic conceptual models (Fig. 1.3) of the dynamics of gating movement of the voltage sensor have been proposed. (1) The helical screw or sliding helix model describes that upon membrane depolarization the S4 rotates along its axis, and at the same time, is translated across the membrane, thus moving the gating charges across the electric field. As a result, exposure of the S4 charges changes from the intracellular to the extracellular solution. Based on this model S4 would rotate 60° and move 4.5-5 Å outward, during activation. Later studies showed a 180° rotation and 13 Å change of distance (Keynes & Elinder 1999; Gandhi & Isacoff 2002; Ahern & Horn 2004). (2) The transporter or twist and tilt model describes S4 charges being located in a water crevice in contact with the intracellular solution at rest. During activation, the charges move into another water crevice that is in contact with the extracellular solution. This transit of S4 charges from one side of the membrane to the other by a tilt and rotation could be achieved a very

small movement, 2-3 Å, of S4 (Starace & Bezanilla 2004; Chanda et al. 2005). (3) The paddle model, derived from the crystal structure of the bacterial Kv channel KvAP (Jiang et al. 2003), describes S4 and the C-terminal of the S3 (S3b) as forming a paddle that moves through the membrane as a unit. At rest, S4 is located in the membrane, not far from the intracellular solution, and S3 is located on top of S4. During activation, S4 and S3 move to the outer side of the membrane with a displacement of 15-20 Å (Jiang et al. 2003; Ruta et al. 2005).

Current understanding of the gating movement of the voltage sensor converges more and more towards a single consensus model, where the positive charges of S4 are stabilized by pairwise interactions with negatively charged residues in S1-S3 aligned along the interface of S4 (Papazian et al. 1995). Upon channel activation, the S4 basic residues jump from one acidic residue to another leading to a conformational change of the voltage sensor. This movement of S4 has been projected to involve a combination of a tilt in the membrane, a rotation around the axis and small vertical and radial translations. This movement of S4 is transduced to the pore gate via S4-S5 linker (see below). In addition, it has been suggested that S4 adopts a 3_{10} helical conformation between resting and activated states and that sustained depolarization stabilizes the S4 in the relaxed state by transforming it from a 3_{10} to an α-helix (Villalba-Galea et al. 2008).

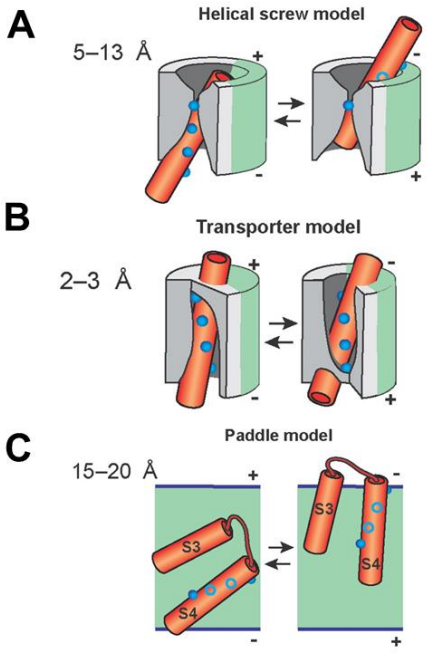

Figure 1.3 Models of voltage sensing.
Three structural models have been proposed to understand voltage-dependent S4 (red cylinders) movement. ***A***. Helical Screw model, ***B***. Transporter model and ***C***. Paddle model. The extent of S4 movement is reported on the side of each model. Fig. 1.3 is reprinted and adapted with the permission of Creative Commons Attribution (Tombola et al. 2006).

Electromechanical coupling

Available structural information along with biophysical data suggests that the voltage sensing domains are semi-independent functional units (Alabi et al. 2007; Long et al. 2005a; Long et al. 2007). However, significant progress has been made in understanding how the movement of voltage sensors is translated to the opening or closure of the pore gate. Combining the structures of Kv1.2 and Kv1.2/2.1 paddle chimera (Long et al. 2005a; Long et al. 2007) with a combination of electrophysiological and fluorescence spectroscopy has provided insight into the mechanism of what has been termed electromechanical coupling, the process of transferring energy from VSD to the PD, eliciting mechanical opening of the pore. The VSD is connected to the PD by a short amphipathic α-helical linker, the S4-S5 linker, which runs parallel to the intracellular side of the lipid bilayer with its hydrophobic side exposed to the lipid membrane while the hydrophilic side exposed to the cytoplasm (Long et al. 2005a). The S4-S5 linker lies in close position to the S6 helix of the adjacent subunit, near to the gate region, and provides a mechanism of electromechanical coupling between voltage sensing and pore regions.

The role of the S4-S5 linker in electromechanical coupling was first demonstrated in *Shaker* channels by Schoppa and Sigworth in 1998. Later in 2002, Lu et al showed that the S4-S5 linker interacts with the distal S6 to promote pore opening. They constructed a chimeric channel of *Shaker* and KcsA, by replacing the *Shaker* S4-S5 linker, along with the C-terminal S6 portion with the corresponding sequence of KcsA channel. This chimera abolished the voltage-dependent gating demonstrating that both the S4-S5 linker and distal S6 should be preserved in *Shaker* to maintain voltage control over channel gating (Lu et al. 2002). A similar chimeric approach between Kv1.5 and Kv1.2 showed that voltage-dependent gating requires specific interactions between the S4-S5 linker and the distal S6, which allow translation of voltage sensor movements to the pore (Labro et al. 2008). Recently, gating currents and VCF measurements from *Shaker*

channels showed that coupling between the S4-S5 linker and distal S6 stabilises the open state of the channel (Batulan et al. 2010). For example, mutations in the S4-S5 linker (I384N) and S6 (F584G) resulted in weak coupling or completely uncoupled voltage sensor movements from pore opening (Haddad & Blunck 2011). The importance of the S4-S5 linker in transducing voltage sensor motions to the pore gate in hERG channels has been extensively studied (Sanguinetti & Xu 1999; Ferrer et al. 2006; Tristani-Firouzi et al. 2002; Van Slyke et al. 2010; Hull et al. 2014) and will be discussed in detail in a later section. Interestingly, recent structural and functional studies in Kv10.1 (Whicher & MacKinnon 2016; Lörinczi et al. 2015; Tomczak et al. 2017), Kv11.1 (Wang & MacKinnon 2017; Lörinczi et al. 2015) and $K_{Ca}1.1$ channel (Tao et al. 2016) revealed that the coupling between voltage sensors and the pore in these channels may be different from the canonical model of Kv channels.

1.4 **Background of hERG channel**

In 1969, a novel genetic variant was discovered in the *Drosophila melanogaster* fruit fly, which caused rapid leg shaking when anesthetized with ether that resembled go-go dancers. The gene was named *ether-a-go-go* (*eag*) (Kaplan & Trout 1969), and was subsequently shown to code for a Kv channel (Warmke et al., 1991). Later, Warmke and Ganetzky cloned the human homolog of *eag* - the "human *eag*-related gene (hERG)" - by screening a human hippocampal cDNA library with a mouse homologue of the *eag* K^+ channel gene (Warmke & Ganetzky 1994). The hERG gene is now known as *KCNH2*, according to IUPHAR consensus nomenclature (Gutman et al. 2005), and the gene product is referred as Kv11.1 (or more often, hERG).

The hERG or *KCNH2* gene (located on chromosome 7 of region q36.1) shares 49% sequence homology with *eag* and *elk* (ether-a-go-go-like) genes (Warmke & Ganetzky 1994). hERG (Kv11.1) channels are expressed in several tissues and cell types, including neurons, smooth muscle and tumour cells (where the hERG channels influence cell proliferation, invasion and regulation of apoptosis). Two other genes hERG2 (Kv11.2) and hERG3 (Kv11.3) were found to be expressed in rat and human nervous systems, contributing to the neuronal excitability (Shi et al. 1997). However, hERG is highly expressed in cardiac cells, and this is where its function and dysfunction is best understood (Sanguinetti & Tristani-Firouzi 2006). An early study showed that there were two components of the outward delayed rectifier K^+ current (I_K) in ventricular

myocytes: a slow activating delayed rectifier K^+ current (I_{Ks}) and a rapid delayed rectifier K^+ current (I_{Kr}) (Noble & Tsien 1969).

In 1990, Sanguinetti and Jurkiewicz showed that these two components could be distinguished pharmacologically, due to varying sensitivities to class III antiarrhythmic drug, E-4031. E-4031 blocked the I_{Kr} current, but not the I_{Ks} (Sanguinetti & Jurkiewicz 1990). Subsequently, in 1995 two research groups (Trudeau et al. 1995; Sanguinetti et al. 1995) showed that heterologous expression of hERG channels in *Xenopus laevis* oocytes displayed a similar biophysical and pharmacological profile to that of native cardiac I_{Kr}. Later, in 1997 Wang et al. provided the first full quantitative characterization of hERG gating (Wang et al. 1997).

Our current understanding of the role of I_{Kr} in ventricular myocytes is derived primarily from studies of heterologous expression of the originally identified hERG1 isoform (Sanguinetti et al. 1995; Wang et al. 1997). However, several studies have suggested that native I_{Kr} is produced by heteromeric channels arising from the co-assembly of two different hERG gene products, hERG1a and hERG1b (Jones et al. 2004; Robertson et al. 2005; Jones et al. 2014). These two gene products are identical except for alternate 5' exons, which encode N-terminal domains of different sizes (Robertson et al. 2005). hERG 1b has a shorter N-terminus compared to hERG 1a. In heterologous expression systems, these two subunits form heteromeric channels and exhibit biophysical properties distinct from those of homomeric hERG 1a channels. There is also some evidence that hERG channels co-assemble with auxiliary β-subunits encoded by *KCNE* genes such as *KCNE1* (*min*K) and *KCNE2* (*MiRP1*). *KCNE1* has been suggested to be involved in upregulation of hERG current by increasing surface expression of channels without altering gating properties (McDonald et al. 1997). In contrast, co-assembly of *KCNE2* and hERG displayed fast deactivation kinetics and decreased trafficking to the cell surface (Abbott et al. 1999; Jentsch et al. 2000). However, other studies have questioned the physiological role of these auxiliary subunits. In 2004, Weerapura et al compared the biophysical and pharmacological properties of hERG with and without *KCNE2* coexpression. The data showed that coexpression with *KCNE2* did not modulate the pharmacological responses of hERG to I_{Kr} - blocking drugs. In addition, coexpression of *KCNE2* did not show any effect on hERG gating kinetics (Weerapura, Nattel, et al. 2002). Due to such discrepancy, the role of *KCNE2* in regulating hERG function is still a topic of debate.

1.5 **Physiological role of hERG channels**

As mentioned above, hERG channels are expresed in wide range of tissues, however their physiological function is best characterized in the heart (Sanguinetti & Tristani-Firouzi 2006). The cardiac action potential (AP) is divided into five distinct phases (phases 0 to 4, Fig.1.4B). Following the rapid depolarizing upstroke of the cardiac AP (phase 0) driven by the inward Na^+ current (I_{Na}), an initial early repolarization (phase 1) is predominantly carried by activation of the transient outward K^+ currents (I_{to}). This is followed by a much slower rate of repolarization (phase 2) known as the plateau phase. The prolonged plateau results from the balance between slowly activating inward Ca^{2+} currents mediated mostly by L-type Ca^{2+} channels ($I_{Ca,L}$) specifically Cav1.2 channel, which is highly expressed in ventricles and several delayed rectifier K^+ currents (I_K). $I_{Ca,L}$ inactivation and repolarizing delayed rectifier K^+ (I_{Kr} and I_{Ks}) and inwardly rectifying K^+ (K_{ir}) currents terminate the AP (phase 3). I_{Kr} conducted by hERG channels provides a critical resurgent repolarizing current, essential for repolarization (phase 3). This role of hERG channels is a result of unique gating properties (Fig. 1.4A). hERG channels activate (open) and deactivate (close) slowly, but inactivate (non-conducting state) and recover from inactivation rapidly. (See section 1.7 for detail description of hERG channel gating).

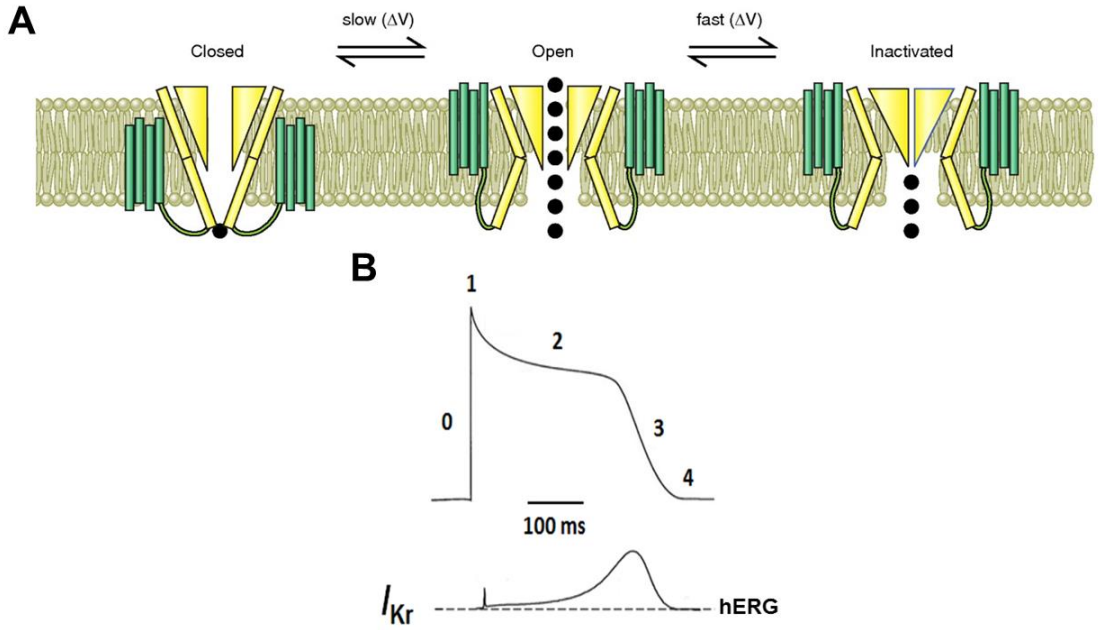

Figure 1.4 Unusual gating of hERG channels.
***A*,** Schematic of the hERG channel gating scheme representing the state transitions between the closed and open states being slower than transitions between open and inactivated states. ***B*,** Cardiac ventricular action potential waveform (*Top*) representing the five phases and schematic of rapid delayed-rectifier current, I_{Kr}, conducted by hERG channels (*Bottom*). Fig. 1.4A is reprinted and adapted with the permission of Creative Commons Attribution (Vandenberg et al. 2012).

The importance of these unique gating properties is underscored by the involvement of the hERG gene product in chromosome 7 with long QT syndrome (LQTS) (Curran et al. 1995; Kuchel et al. 2004) and blockade of the hERG channel by a diverse group of drugs causing LQTS (drug-induced LQT), a common cause of cardiac arrhythmia (J. S. Mitcheson et al. 2000; Vandenberg et al. 2001).

LQTS is a potentially lethal cardiac repolarization disorder associated with an increased risk of ventricular arrhythmias and sudden death (Sanguinetti & Tristani-Firouzi 2006). LQTS manifests as a prolongation of the QT interval observed in the electrocardiogram (ECG), which results from delayed ventricular repolarization leading to increased cardiac AP duration. The QT interval is defined as the time required for the repolarization of the ventricles during a single cardiac cycle. The symptoms of LQTS are frequently due to *torsade de points* (TdP), a unique arrhythmia that causes syncope (loss of consciousness) and can degenerate to the more lethal ventricular fibrillation and sudden cardiac death (Curran et al. 1995; Sanguinetti et al. 1996). In general, LQTS is classified into two major types; congenital (inherited) and acquired (drug-induced) LQTS. A total of 15 gene loci have been distinguished which are responsible for congenital LQTS of which three encode ion channels; *KCNQ1*, *hERG*, *SCN5A* and constitute the vast majority of cases (Nakano & Shimizu 2016). More than 500 LQTS associated mutations have been recognised in the hERG channel alone, which results in the variant long QT syndrome type 2 (LQTS2) (Perry et al. 2016). In general, LQTS2 is caused by inherited mutations in the hERG channel gene that result in the disruption of hERG channel function or dominant-negative suppression of I_{Kr} (Sanguinetti et al. 1996). Loss of function mutations arise from defective trafficking or defective gating of the hERG channel. The former is the most prevalent with missense mutations leading to mis-folding of channel subunit and degradation by the ubiquitin-protease enzyme pathway. In addition to inherited mutations, LQTS2 is also caused by blockade of hERG channels by a wide variety of drugs, which results in K^+ conduction block (J. S. Mitcheson et al. 2000; Tristani-Firouzi et al. 2001; Sanchez-Chapula et al. 2002). The structural basis of this

side effect of hERG channel block by diverse drugs (J. S. Mitcheson et al. 2000) is discussed in detail in section 1.8. Drug interactions with hERG are so prolific and the effects so potentially life-threatening, that testing compounds for hERG channel block is now mandated by the FDA for new drug approval (Sanguinetti & Tristani-Firouzi 2006; Mitcheson 2008). These observations highlight the importance of hERG channels in the maintenance of normal cardiac rhythm and their crucial role in health and disease.

1.6 **Structure of the hERG channel**

The first atomic structure of a K^+channel, KcsA, (Doyle et al. 1998) and the subsequent Kv channel structures, Kv1.2 (Long et al. 2005a; Long et al. 2005b) and the Kv1.2/Kv2.1 chimera, (Long et al. 2007) have revolutionized our understanding of ion conduction and voltage sensing in K^+ channels. These crystal structures have served as templates for homology models of hERG channels. To date, a combination of electrophysiological, spectroscopic and molecular dynamic simulations have provided the most significant insights into the structure-function relationships of hERG channels. However, very recently Mackinnon's group determined the structure of the *eag1* channel bound to the inhibitor calmodulin at 3.78 Å resolution (Whicher & MacKinnon 2016) and the hERG channel in a depolarized conformation at 3.8 Å resolution (Wang & MacKinnon 2017). These structures provide a template to better understand the gating properties of hERG channels and its role in the heart and drug discovery.

The hERG protein comprises 1159 amino acids and when fully glycosylated has a molecular weight of 155 kDa. Similar to other Kv channels, the hERG channel is tetrameric (homotetramer, Fig. 1.5A), each subunit has six α-helical transmembrane domains (S1-S6) (Swartz 2004; Cheng & Claydon 2012). Within the six transmembrane segments, the first four transmembrane segments (S1-S4) form the voltage-sensing domain; with S4, containing charged amino acids forming the main "voltage sensor". The last two transmembrane segments (S5-S6) form the functional conducting pore connected with an intervening P-loop. Membrane depolarization drives outward movement of the S4 within the bilayer leading to an opening of the pore via the S4-S5 linker which serves as a mechanical lever (Long et al. 2005a). In addition, the channel consists of a long intracellular cytoplasmic N- and C-terminal region. The N-terminal region contains an *eag* domain, which comprises a cap region and a Per-Arnt-Sim (PAS) domain, and a long linker region between the PAS and the S1 segment (Fig. 1.5A)

(Morais Cabral et al. 1998; Ng et al. 2011; Adaixo et al. 2013). The *eag* domain is highly conserved in *ether-a-go-go* subfamily channels. The C-terminus contains a C-linker region and a cyclic-nucleotide-binding homology domain (CNBHD) (Brelidze et al. 2012; Brelidze et al. 2013), which shares a structural similarity to the cyclic nucleotide-binding domains (CNBDs) of cyclic nucleotide-gated (CNG) and hyperpolarization-activated cyclic nucleotide-modulated (HCN) channels. Unlike HCN channels, hERG channels do not bind cAMP, because their nucleotide binding pocket is occupied by an intrinsic ligand - a short β-strand, which may modulate function (Brelidze et al. 2012; Brelidze et al. 2013; Haitin et al. 2013; Li, Ng, et al. 2014; Zhao et al. 2017). To date, NMR solution structures are available for the S4-S5 linker (Ng et al. 2012), PAS domain (Morais Cabral et al. 1998; F. W. Muskett et al. 2011; Ng et al. 2011; Adaixo et al. 2013) CNBHD (Li et al. 2016) and the membrane spanning regions such as S3 and S4 segments, S5P linker and pore helix (Pages et al. 2009; Torres et al. 2003; Li, Wong, et al. 2014). Accumulated studies have shown that domain-domain interactions play a crucial role in regulating hERG channel gating that is important for its physiological function (Morais-Cabral & Robertson 2015). Electrophysiological and biochemical studies showed that *eag* domain interacts with CNBHD and S4-S5 linker. Deletions of, or mutations within, the *eag* domain, CNBHD and S4-S5 linker have shown to alter hERG channel gating. In section 1.7.2 I have described in detail the interaction between these regions that are suggested to play an important role in regulating the slow deactivation process.

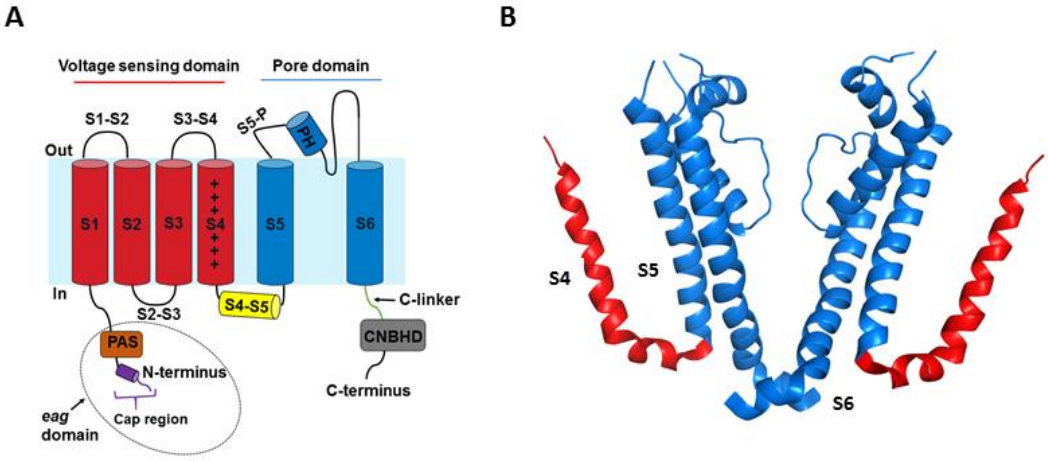

Figure 1.5 Structural features of hERG channels
***A*,** single α-subunit of a hERG channel comprises six α-helical transmembrane domains (S1-S6). The voltage sensor domain (S1-S4), S4-S5 linker and pore domain (S5-S6) are highlighted in red,

yellow and blue, respectively. hERG channels; comprise an intracellular N-terminus containing a PAS domain (amino acids 26-135) shown in brown and a Cap region (amino acids 1-25) shown in purple. Together these comprise the *eag* domain (amino acids 1-135). The C-terminus contains a C-linker (amino acids 666-748) shown in green and a CNBHD domain (amino acids 749-872) shown in gray. ***B***, side-view of the cryo-EM structure of the hERG channel in the activated state. For clarity, only two of the four subunits are shown. S4 highlighted in red and S5-S6 in blue.

1.7 **hERG channel gating**

Like other Kv channels, hERG channels undergo transitions between distinct closed, open and inactivated states. Unlike *Shaker*, hERG channels exhibit unusual gating properties. hERG channels activate and deactivate slowly, but inactivate and recover from inactivation rapidly and with a strong dependence on voltage (Sanguinetti et al. 1995; Trudeau et al. 1995) (Fig.1.4A). The result is that upon membrane depolarization, only a small outward current is generated, because the transition from closed to open states is slow (hERG activates in ~60 ms at +60 mV, whereas *Shaker* activates in <2 ms) (Hoshi & Ta 1994; Wang et al. 1997) and channels rapidly inactivate (Rasmusson et al. 1998). Although hERG inactivation is analogous to C-type inactivation in *Shaker*, it also has features that are unique. The rates of both hERG inactivation and recovery from inactivation are fast and voltage dependent (Schonherr & Heinemann 1996; Smith et al. 1996; P S Spector et al. 1996). Because inactivation is faster than channel activation, hERG currents are relatively small during depolarization. As a result, reduced hERG currents are observed at voltages typical of the plateau phase of cardiac AP (Schonherr & Heinemann 1996; Smith et al. 1996; P S Spector et al. 1996). Upon membrane repolarization, channels rapidly recover from inactivation into the open state giving rise to a large bolus of current before slow channel closure. This provides a significant contribution to the cardiac repolarization associated with the termination of the AP. The large current upon repolarization is manifested in electrophysiological experiments as a characteristic “hook” in the tail currents (Sanguinetti et al. 1995). The peak amplitude of tail currents reflects the proportion of channels activated during the preceding depolarization pulse, thus can be used to define the voltage-dependence of activation. Despite their critical role in determining cardiac excitability, the molecular bases of these unusual gating properties is poorly understood. Following is a description of what we currently understand about the structural and molecular basis of hERG activation, deactivation and inactivation.

1.7.1 **Structural and molecular basis of hERG activation gating**

Activation describes the process of transition from closed states to the open state. As mentioned above, changes in the membrane voltage result in the outward displacement of the voltage sensor, and this movement is coupled to the opening of the activation gate. This general principle is also attributed to hERG channels with regards to the role of VSD (Subbiah et al. 2004; Subbiah et al. 2005; Zhang et al. 2004); S4-S5 linker (Tristani-Firouzi et al. 2002; Van Slyke et al. 2010; Hull et al. 2014); and activation gate (Hardman et al. 2007; Wynia-Smith et al. 2008; Thouta et al. 2014). The discussion below is focused on what distinguishes hERG activation gating from other Kv channels, in particular, *Shaker* channels.

hERG activation gate

In hERG channels, experiments investigating drug block have been highly informative in providing evidence for the existence of an activation gate. Methanesulfonanilides such as MK-499 and dofetilide can access the intracellular cavity only when the channel is open (Peter S. Spector et al. 1996; J S Mitcheson et al. 2000). In the hERG S6 helix, two putative glycine hinge points have been identified. One is a highly conserved glycine residue (G648) (analogous to the G99 in KcsA and G466 in *Shaker*, (Fig. 1.2C). The other (G657) is located in a position corresponding to the second proline residue in the Pro-X-Pro motif in Kv channels (Fig. 1.2C). An alanine scan of these two glycine residues showed little effect on the voltage-dependence or kinetics of activation gating. Conversely, substitution of these glycine residues with proline or larger hydrophobic residues destabilised the closed state (Hardman et al. 2007). The authors proposed that, unlike other Kv channels, the hERG pore is more stable in the open state than the closed state and that the substitution at G648 or G657 further shifts the equilibrium towards the open state of the channel. Based on these observations, it was suggested that glycine residues at 648 and 657 were required for the tight packing of the S6 helices, but did not act as a hinge *per se* (Hardman et al. 2007).

The X-ray crystal structure of the Kv1.2 channel (Long et al. 2005a) showed a bending at the Pro-Val-Pro (PVP) motif, which was facilitated by the glycine hinge point (Fig. 1.2B). Extensive studies in *Shaker* suggest that the PVP motif is important in channel gating (Hackos et al. 2002) and that it forms the activation gate at the bundle crossing of

the S6 helix. The PVP motif introduces a kink in the S6 helix that allows the S6 helices to splay outward away from the central axis of the pore to create a large central cavity (del Camino et al. 2000; Del Camino & Yellen 2001; Hackos et al. 2002) allowing electromechanical coupling with voltage sensor movements via the S4-S5 linker (Long et al. 2005a; Long et al. 2005b). hERG channels lack the PVP motif leaving questions as to the location of the intracellular gate. A cysteine scan of the S6 helix attempted to define the hERG activation gate (Wynia-Smith et al. 2008). These authors proposed that the most important residues were grouped into two S6 microdomains. Substitution of the innermost residues, Q664, Y667 and S668 induced slow deactivation and constitutive opening at negative voltages. Mapping these residues onto energy-minimized models of the crystal structures of rKv1.2 (open state), MlotiK1, and KcsA (closed state) suggested they form a ringed domain, occluding the permeation pathway in the closed state. Interestingly, this occlusion site is approximately two helical turns below the location of the activation gate (V478) in *Shaker* channels. The second microdomain contained the valine residue V659, which was sensitive to various substitutions. Overall, these data suggest that the hERG activation gate and its coupling to the voltage sensing domain is different from that in other Kv channels such as *Shaker*.

The identification of the activation gate, its role in hERG channel gating, and how it is different from *Shaker* channels is the subject of Chapter 3 of this thesis.

hERG voltage sensing unit

As mentioned above, compared to many other Kv channels, hERG activation is slow. Previous studies suggested that activation of hERG channels is unusually slow as a result of rate limiting voltage sensor movement (Smith & Yellen 2002; Piper et al. 2003; Piper et al. 2005; Van Slyke et al. 2010). This is in contrast to *Shaker* channels, where voltage sensor activation is rapid and the opening of the activation gate is the rate limiting step (Cha & Bezanilla 1997; Smith-maxwell et al. 1998) The reason for slow and rate limiting voltage sensor movement in hERG channels is unclear.

It has been widely shown that in Kv channels, the S4 contains a high concentration of basic residues, and these are responsible for sensing voltages changes across the membrane. Similarly, the hERG S4 is comprised of seven basic residues; five arginines (R528, R531, R534, R537 and R541) and two lysines (K525 and K538). Mutagenesis

studies revealed critical roles of these basic residues in the S4. The first characterization of the hERG S4 region involved neutralisation of the charged residues.

A thermodynamic analysis of the shift in the voltage-dependence of activation showed that two mutants in particular caused the largest perturbation of activation. Compared to WT, R531Q caused a depolarizing shift in the GV (i.e. shifted the equilibrium towards the closed state), while K525Q caused a hyperpolarizing shift in the GV (i.e. shifted the equilibrium towards the open state). These data suggested that K525 and R531 contribute to the stabilization of WT channels in the closed and open state, respectively (Subbiah et al. 2004). Mutation of R531 also revealed some important differences with the activation gating in *Shaker* channels. In *Shaker* channels, the equivalent mutation (R371Q) caused a hyperpolarizing shift, an opposite effect to R531Q in hERG (Aggarwal & MacKinnon 1996; Seoh et al. 1996). It is also important to note that, in most Kv channels, the outermost S4 charge is arginine, but in hERG, it is lysine (K525). Charge reversal of K525 (K525R) did not restore WT like phenotype, suggesting that the specific lysine side chain at this position is more important than charge alone (Subbiah et al. 2004).

Followed by this initial characterization, cysteine (Zhang et al. 2004) and alanine (Piper et al. 2005) scans of hERG S4 revealed that outermost three charged residues (K525, R528 and R531) contributed to gating charges associated with channel activation. This was supported by the state dependent accessibility of these three residues to a membrane-impermeable thiol-modifying reagent (MTSET) during activation (Zhang et al. 2004). Using a smaller reagent (para-chloromercurybenzene sulfonate, pCMBS) with arguably better resolution of accessibility, another study showed that a stretch of S4 residues (L523 to L529), including the first two charged residues (K525 and R528), became externally accessible during depolarization (Elliott et al. 2009). In *Shaker* channels, S4 accessibility to MTSET and pCMBS reagents demonstrated translocation of four outermost arginine residues (R1-R4), consistent with the movement of ~12-14 e_0 gating charges across the electric field (Aggarwal & MacKinnon 1996; Seoh et al. 1996). The more limited movement of charge in hERG channels is consistent with measurement of a smaller number of gating charges, ~8 e_0, observed in hERG channels (Zhang et al. 2004). These functional measurements are further supported by the recent hERG channel structure with the voltage sensors in an activated conformation (Wang & MacKinnon 2017).

Similar to *Shaker*, hERG channels have three conserved negative counter charges in the voltage sensing unit (D456, D466 in S2 and D501 in S3), as well as three additional negative charges (D411 in S1, D460 in S2 and D509 in S3) that are only conserved in the *eag* family of Kv channels. Cysteine substitutions of these negative charges revealed their role in activation gating. Mutation of both D460 and D509 to cysteine produced a depolarizing shift in the GV as well as slowed activation kinetics compared to WT channels. In contrast, cysteine mutation of D411 produced a hyperpolarizing shift in the GV as well as accelerated activation kinetics. These data suggested that D460/D509 and D411 contribute to the stabilization of WT channels in the open and closed state, respectively (Liu et al. 2003). Taken together, interactions between K525-D411 and R531-D460/D509 have been proposed, suggesting a salt bridge pairing in the closed and open state, respectively (Zhang et al. 2005; Piper et al. 2008). In a recent study, Tao et al (2010) showed that in the *Shaker* channel, a highly conserved S2 Phe residue, F290 (F463 in hERG) along with two negative charges (E293 and D316), act as a gating charge transfer centre, which catalyses the movement of S4 charges across the electric field. Similar to *Shaker* channels, F463 in hERG, along with D466 (E293 in *Shaker*) suggested a similar charge transfer centre exists in hERG channels and interacts with K525 and K538 S4 residues (Cheng et al. 2013) consistent with the voltage sensor conformation in the hERG structure (Wang & MacKinnon 2017).

Overall, there appear to be some differences in the amount of charge moved across the membrane and the coupling between charged residues within the VSD in hERG channels compared with *Shaker*. However, what remains unclear is what makes hERG activation slow. It is reasonable to speculate that movement of the voltage sensor is slow, or perhaps opening of the activation gate is limiting, or alternatively there is less efficient electromechanical coupling between the VSD and PD via S4-S5 linker. To try to address this, it was important to examine the rate at which S4 traverses the electric field in response to a change in the membrane voltage. Voltage clamp fluorometry (VCF) measurements showed that a fluorophore (e.g. TMRM) attached to the S3-S4 linker by thiol reaction with a substituted cysteine residue at E518C, E519C (Smith & Yellen 2002), or L520C (Smith & Yellen 2002; Van Slyke et al. 2010; Es-Salah-Lamoureux et al. 2010) produced fluorescence changes that were well correlated with the time and voltage-dependence of channel activation. Some sites presented an additional fast phase of fluorescence change that might reflect inactivation, although manipulations that

altered inactivation (treatment with TEA or the G628C:S631C mutation) had no effect on the fast fluorescence component. These fluorescence data were further supported with the first gating current recordings from hERG channels, which displayed pronounced fast and slow components that differed ~100-fold in their kinetics (Piper et al. 2003). The authors showed that most of the charge movement (>95%) associated with hERG voltage sensor movement was slow (~50 ms); which is ~100 fold slower than *Shaker* gating currents, as shown by the fluorescence data. In addition, the fast gating current component did also not correlate with inactivation gating. Instead, the authors proposed that it likely represents transitions between closed states early in the activation pathway (Piper et al. 2003), although its mechanism is still unclear. Overall, the combination of early VCF and gating current measurements suggested that slow activation of hERG is due to slow movement of the voltage sensor, which is likely the rate-limiting step in the activation process. In Chapter 5, I present systemic characterization of the fluorescence tracking of hERG activation gating and discuss this in the light of recent data that challenges this initial concept.

In addition to gating current and VCF measurements of voltage sensor activation, envelope of tail experiments (used to measure the time course of activation in hERG channels, see section 2.4.3) revealed significant insight into the hERG channel activation pathway. These experiments showed that hERG activation is sigmoidal, which demonstrates the presence of multiple closed states that channels must transition through prior to opening (Wang et al. 1997). Analysis of activation kinetics suggested that the activation time course reaches saturation at depolarized voltages, which represents the presence of a voltage-independent step, which is a rate-limiting step at higher depolarized voltages (Wang et al. 1997; Piper et al. 2003; Subbiah et al. 2004). Because of the strong voltage-dependence of the deactivation rate, i.e. from the final closed to open state, the final transition must be voltage-dependent, requiring the voltage-independent step to happen before the final transition (Wang et al. 1997). In summary, a simple linear Markov model suggests that hERG gating involves transitions between three closed states (C1-C2-C3) preceding a final opening step (C3-O), with a voltage-independent step between C2 and C3 states. Subsequently, to describe the complex nature of hERG gating currents, Piper et al. (2003) proposed an updated Markov model by integrating previous *Shaker* models (Zagotta Hoshi Aldrich [ZHA] and Schoppa and Sigworth [S-S]) and the hERG model (Wang et al., 1997). In the Piper

model, each subunit independently traverses through two sequential, voltage-dependent steps, followed by concerted transitions to two sequential closed states and then to the final open state. This model was able to describe the salient features of both ionic and gating currents of hERG channels.

Coupling of VSD to PD in hERG channels

As in *Shaker* and other Kv channels, a large body of evidence suggests that the hERG S4-S5 linker is involved in transducing voltage sensor motions to the pore gate (Sanguinetti & Xu 1999; Tristani-Firouzi et al. 2002; Ferrer et al. 2006; Van Slyke et al. 2010; Hull et al. 2014). Charge reversal of D540 (D540K; in the hERG S4-S5 linker) caused re-opening of channels at hyperpolarized voltages, thus destabilizing the closed state (Sanguinetti & Xu 1999; J S Mitcheson et al. 2000). Subsequently, alanine substitution at R665 (in the distal S6) prevented re-opening in D540K channels, suggesting that D540 interacts with R665 to stabilize the closed state of the channel (Tristani-Firouzi et al. 2002). This idea was further supported by observations that cysteine residues at these two sites could be chemically cross-linked (Ferrer et al. 2006). Interestingly, this interaction also immobilised a portion of gating charge, confirming that the physical coupling restricted movement of the voltage sensor movement. Furthermore, several point mutations in the S4-S5 linker dramatically affected the voltage dependence or kinetics of the open-closed equilibrium in hERG channels (Alonso-Ron et al. 2008). In addition, mutation of the S4-S5 linker glycine residue (G546) to any other residue that reduced the α-helical propensity destabilized the closed state of the channel, suggesting that flexibility of the linker is important in regulating channel gating (Van Slyke et al. 2010). Overall, these data suggest that the S4-S5 linker connects voltage sensor motions with the pore gate and is involved in the coupling of charge movement with pore opening. Interestingly, recent structural evidence from closely related *eag* channels suggested that coupling in this sub-family of channels may differ from that in *Shaker*-like channels. The cryo-EM structure of the *eag1* channel is not domain-swapped and showed that the S4-S5 linker is a short loop, leading the authors to suggest that it does not function as a mechanical lever that influences the pore gate (Whicher & MacKinnon 2016). This idea is supported by the observation that voltage-dependent gating was not strongly influenced in hERG channels in which the physical continuity between the voltage-sensing and the pore domain was disrupted by expressing the two domains separately (Lörinczi et al. 2015). In this alternate model of

coupling, S4 in its down or resting state directly interacts with the C-linker region, which induces a bend in S6 to close the pore. During outward movement of S4 upon depolarization, the C-linker undergoes a rotation such that it loosens the bend in the S6 to open the pore (Whicher & MacKinnon 2016). This mechanism would allow the intracellular domains (PAS and CNBHD) of *eag* family members to interact with the voltage-dependent gating machinery. Interestingly, the recent cryo-EM structure of the hERG channel did not provide any structural evidence regarding the mechanism of voltage sensor coupling to the pore gate. However, the authors suggested that voltage sensor movement is transmitted to the pore gate through the S5-S6 interface (Wang & MacKinnon 2017). Therefore, the exact mechanism of coupling voltage sensor movement to pore gating in the *eag* family of channels and how it compares to *Shaker*-like channels is unclear. Furthermore, these recent studies are not readily reconciled with previous evidence demonstrating a strong influence of the S4-S5 linker on coupling. In Chapter 4, I discuss data showing that the linker appears to play a key role in coupling the pore to the voltage sensor during deactivation gating. Further studies are clearly needed to better define the bi-directional coupling between the voltage sensor and pore, and the role of other elements, such as the S4-S5 linker and the C-linker.

1.7.2 **Structural and molecular basis of hERG deactivation gating**

hERG channel deactivation is unusually slow and important for producing a resurgent current during repolarization of the cardiac AP. This is made evident by the observation that several LQT2 causing mutations reduce I_{Kr} current by accelerating hERG channel deactivation (Chen et al. 1999). Compared to other Kv channels, hERG channels have unique cytoplasmic regions (N-terminus, C-terminus and S4-S5 linker, see Fig 1.5B), and interactions between these regions are suggested to play an important role in regulating the slow deactivation process (Gustina & Trudeau 2011; de la Pena et al. 2011; Gianulis et al. 2013). However, the molecular determinants of slow deactivation remain elusive.

Numerous studies detail a critical role for the hERG N-terminus in regulating deactivation kinetics. hERG channels possess a long intracellular N-terminus (~390 amino acids), consisting of 1-135 amino acids referred to as the *eag* domain - a highly conserved region in the *eag* channel family (Fig. 1.5B) (Warmke & Ganetzky 1994; Morais Cabral et al. 1998). Deletion of the entire N-terminus (Δ2-354 or Δ2-373) dramatically accelerated

hERG deactivation gating (Schönherr & Heinemann 1996; Wang et al. 1998). A subsequent study showed that even the deletion of the first 25 residues (referred to as N-Cap domain) resulted in a similar phenotype to the deletion of entire N-terminus (Wang et al. 1998). Consistent with this, application of a peptide corresponding to the first 1-16 residues restored the slow deactivation phenotype in ∆2-373 channels (Wang et al. 2000). Recent NMR structures of residues 2-135 revealed that N-Cap domain encompasses a flexible tail (1-12 residues) followed by an amphipathic α-helix (13-23 residues) (Li et al. 2010; F. W. Muskett et al. 2011; Ng et al. 2011). Mutations in the tail region or amphipathic α-helix resulted in a significant acceleration of the rate of the channel closure (F. W. Muskett et al. 2011; Ng et al. 2011; Adaixo et al. 2013). X-ray crystal structures of the *eag* domain (Morais Cabral et al. 1998), showed that, unlike the PAS domain (residues 26-135), the N-Cap domain did not form a stable structure. This supports a dynamic role for the N-Cap domain and an important role in trafficking of hERG channels to the membrane. Overall, there is compelling data to suggest that the N-terminus, comprising the PAS domain and the flexible tail, is critically important in stabilizing the channel in the open state.

In addition to the well-described role of the N-terminus in modifying hERG deactivation kinetics, two recent studies suggested a role for the N-terminus in generating mode-shift behaviour (Goodchild et al. 2015; Tan et al. 2012). Mode-shift in hERG channels has been used to describe the observation that the voltage-dependence of channel deactivation is shifted by ~-30 mV relative to that of activation. Using VCF to track voltage sensor rearrangements, Tan et al (2012) showed that deletion of the distal N-terminus (∆2-25) or distal point mutations (R4A, R5A and G6A) reduced mode-shift of the pore without altering mode-shift of the voltage sensor. The authors proposed that perturbation of the N-terminus caused pore closure ahead of voltage sensor return leading them to suggest that voltage sensor return is rate limiting for pore gate closure during deactivation in WT channels and that the N-terminus is an adapter required for coupling the pore to the voltage sensor during deactivation gating (Tan et al. 2012). However, another study examining hERG voltage sensor gating currents showed that deletion of the N-terminus (∆2-135), accelerates charge return and that closure of the pore gate is the limiting step for voltage sensor return. In this study, mode-shift of both pore gate and voltage sensor return were reduced by deletion of N-terminus, leading the authors to propose that mode-shift behaviour is associated with open-pore stabilization

induced by N-terminus with rest of the channel such as C-terminus (Goodchild et al. 2015). This controversy and the paucity of data describing the mechanistic role of N-terminus, and other regions such as S4-S5 linker and voltage sensor, in determining mode-shift drove the systematic characterization of mode-shift behaviour and its coupling to deactivation gating in hERG channels is described in Chapter 4 of this thesis.

Deletions in the C-terminus, in particular in the CNBHD, dramatically accelerate hERG channel deactivation kinetics, similar to deletions in the N-terminus (Gustina & Trudeau 2011). Indeed, application of a recombinant *eag* domain could not restore slow deactivation in both *eag* domain and CNBHD deleted channels. This suggests that interaction between N-and C-termini of hERG channels is critical in regulating deactivation gating. Spectroscopic experiments using FRET provide further evidence of a direct interaction between the PAS and CNBHD (Gianulis et al. 2013), and are consistent with structural evidence, which shows that isolated PAS and CNBHD domains from the closely related *eag* family (mouse *eag*1) form multiple interactions (Haitin et al. 2013).

In addition to the C-terminus, it has been proposed that the N-terminus also interacts with the S4-S5 linker to regulate deactivation gating. Notably, modification of a cysteine introduced at G546 in the S4-S5 linker with N-ethylmaleimide (NEM) accelerated deactivation in a manner similar to N-terminal deletion as if the bulky adjunct group impeded the action of the N-terminus (Wang et al. 1998). Consistent with a role for the S4-S5 linker, a VCF study showed that alterations in the S4-S5 linker, modified pore closure by altering S4 return (Van Slyke et al. 2010). Furthermore, the proximity of the N-terminus and S4-S5 linker was demonstrated by reversible cross-linking of a cysteine introduced at V3 in the N-terminus and Y542 in the S4-S5 linker (de la Pena et al. 2011). In an alternative approach, titration of a protein fragment corresponding to residues 1-135 in the presence of an S4-S5 linker peptide that included nine residues (R541-V549), showed chemical shifts of several residues within the N-terminal region, indicative of specific interactions between the N-terminus and S4-S5 linker peptide (Li et al., 2010). Taken together, these data suggest a direct functional interaction between the S4-S5 linker and N-terminus.

In addition to the role of the S4-S5 linker in modifying deactivation kinetics, a recent VCF study showed that the S4-S5 linker modulates mode-shift behaviour in hERG channels.

Mutations in the S4-S5 linker largely reduced the mode-shift of ionic current without altering mode-shift of voltage sensor movement (Hull et al. 2014), suggesting that S4-S5 linker is critical for coupling pore gate and voltage sensor during deactivation. The role of the S4-S5 linker in deactivation gating is discussed in detail in Chapter 4 of this thesis.

1.7.3 **Structural and molecular basis of hERG inactivation gating**

Following activation, maintained depolarization induces most Kv channels to enter into a non-conducting, or inactivated state, through a process known as inactivation. This non-conducting state is quite distinct from the deactivated state of the channel. Inactivation gating in Kv channels, such as *Shaker*, have been well described and shown to be of two distinct types, referred to as N-and C-type inactivation (Rasmusson et al. 1998). N-type inactivation occurs in the order of milliseconds, and involves block of the conduction pathway by an N-terminus tethered particle that binds at the intracellular mouth of the pore via a ball and chain mechanism (Hoshi et al. 1990; Zagotta et al. 1990). Initial characterization experiments involving deletion of the N-terminus abolished N-type inactivation and revealed a slower inactivation process, referred to as C-type inactivation (Hoshi et al. 1991). C-type inactivation involves conformational rearrangements of the outer mouth of the pore (Hoshi & Armstrong 2013). Mutations in this region (e.g. T449 in *Shaker* channels) altered C-type inactivation (López-Barneo et al. 1993) and external TEA slowed C-type inactivation (MacKinnon & Yellen 1990; Choi et al. 1991) leading to the suggestion that the process involves a collapse of the outer pore.

Unlike *Shaker* channels, hERG channels lack an N-type inactivation process. Instead inactivation in hERG channels is analogous to the C-type inactivation observed in *Shaker*. Upon membrane depolarization, hERG channels exhibited strong inward rectification which was associated with rapid C-type inactivation kinetics (Smith et al. 1996; P S Spector et al. 1996) instead block of the outward currents by Mg^{2+} or polyamines - the mechanism that was shown to be responsible for the rectification of inward rectifier K^+ channels, K_{ir} (Ficker et al. 1994). In addition, application of external TEA slowed the inactivation in hERG channels and mutations at position S631 (at the outer mouth of the pore) analogous to T449 in *Shaker* altered inactivation (Schönherr & Heinemann 1996). Indeed, several mutations in the outer pore region either reduced inactivation (S631A, N588K, N588E) or completely abolished inactivation (S620T, G628C+S631C) (Herzberg et al. 1998; Ficker et al. 1998; Yang et al. 2004). In addition,

mutations in the turret region dramatically affected inactivation gating (Jiang et al. 1999; Liu et al. 2002). Furthermore, the closely related *eag* channel, which does not inactivate, exhibited rapid inactivation upon transfer of the pore helix and selectivity filter from hERG channels (Herzberg et al. 1998).

However, C-type inactivation in hERG exhibits some unique features from that of *Shaker* channels. In hERG, inactivation was shown to be intrinsically voltage-dependent, i.e. not coupled to the voltage-dependence of activation (Perry et al. 2013) and both the onset and recovery from inactivation occurs much faster than in *Shaker* channels (Sanguinetti et al. 1995; Schonherr & Heinemann 1996; Smith et al. 1996; Wang et al. 1997). The voltage of half-maximal ($V_{1/2}$) inactivation is ~-90 mV compared with a $V_{1/2}$ of activation of -20 mV (Schönherr & Heinemann 1996). Zhang et al. (2004) examined the contribution of voltage sensor charges to the voltage-dependence of hERG inactivation. Their mutagenesis study showed that the apparent gating charge during inactivation was not altered upon neutralization of the positively charged S4 residues (Zhang et al. 2004). In addition, an alanine scan of S4 identified mutations that have profound effects on activation but minimal effect on inactivation and *vice versa*. These data defined two distinct regions on the S4 that contribute differentially to hERG activation and inactivation (Piper et al. 2005). In the absence of a strong link between S4 movement and voltage-dependence of inactivation, some evidence suggested that the S5-P turret region may impart the dependence on membrane potential (Clarke et al. 2006; Torres et al. 2003; Liu et al. 2002). hERG channels comprise a long S5-P linker, known as the turret region that is ~40 amino acids compared with ~12-15 amino acids in other Kv channels. Jiang et al. (1999) first suggested that the S5-P linker is involved in inactivation gating when mutations of H578 and H687 disrupted inactivation gating (Jiang et al. 1999). Subsequently, a cysteine scan of the entire S5-P linker region also revealed sites that abolished inactivation when mutated (Liu et al. 2002). In addition, the recent hERG cryo-EM structure demonstrated that some subtle rearrangements of the selectivity filter might correlate with the rapid hERG inactivation gating. In particular, residue F627 in the selectivity filter is uniquely positioned and suggested to play a key role in regulating hERG inactivation gating (Wang & MacKinnon 2017). However, further investigation is required to substantiate this suggestion.

Recently, a more global model that involves complex rearrangements throughout the channel that are initiated by K^+ efflux from the pore has been proposed to underlie

inactivation in hERG channels. The widespread rearrangements of the channel during inactivation is analogous to the sequential motions that are required to open and close a Japanese puzzle box (Ng et al. 2011; M. D. Perry et al. 2013; Matthew D. Perry et al. 2013; Perry et al. 2015). Despite intense study, the molecular mechanism underlying inactivation in hERG channels and the basis of its unusual kinetics and voltage-dependence remains unresolved.

1.8 Determinants of high-affinity drug binding in hERG channels.

Compared to other Kv channels, hERG channels are highly sensitive to block by a very wide range of drug compounds. This predisposes drug-induced, or acquired, LQTS2, which is more common than the inherited form. Various studies have shown that hERG channels are blocked by a wide variety of structurally and functionally diverse drugs such as antiarrhythmics, antihistamines, antipsychotics, gastrointestinal motility agents and antibiotics with high affinity (Sanguinetti et al. 1995; Roden et al. 2002). Drug blockade of hERG channels reduces the K^+ conductance resulting in decreased cardiac current (I_{Kr}), prolongation of the cardiac AP leading to LQTS2. Individuals with LQTS2 are prone to increased risk of *torsade de pointes* (TdP), a ventricular arrhythmia that can degenerate to ventricular fibrillation and sudden death. Indeed, the development of new and safe medications requires routine hERG screening and it has been estimated that ~60% of new molecules developed for potential therapeutic use block hERG channels, halting their further development (Raschi et al. 2008). Therefore, advances in understanding of the structural and molecular basis of the high sensitivity of hERG channels to a wide group of drugs is essential and helps in the explanation of the pharmacological promiscuity of this channel.

The high sensitivity of hERG channels towards a diverse range of compounds suggests that it has an unusual drug-binding site compared to other Kv channels (Mitcheson 2008). It is well established that that majority of drugs bind in the central cavity of the hERG pore region and that channel opening is required in order to bind (Mitcheson & Perry 2003; Kamiya et al. 2006). Structural modelling of the hERG pore region based on the closed- state KcsA crystal structure revealed two major differences between hERG and other Kv channels that may explain high drug affinity in hERG channels (J. S. Mitcheson et al. 2000). Firstly, as mentioned before, hERG channels lack a PVP motif in

S6 (Fig 1.2C). This motif introduces a kink in the S6 helices and limits the size of the inner cavity (del Camino et al. 2000). The absence of the kink in the S6 helices is thought to create a larger inner cavity such that drugs can be better accommodated in the inner cavity of hERG than in other Kv channels. Secondly, hERG possess two aromatic residues (Y652 and F656) in S6 that have been shown to be crucial for high-affinity drug block (J. S. Mitcheson et al. 2000). These residues are unique to hERG and are Ile and Val (non-aromatic residues) in other Kv channels. The interaction of drugs with Y652 and F656 aromatic residues seems to involve hydrophobic and electrostatic interactions suggesting that these residues interact with drugs through cation-π interactions or π-stacking interactions. There is also evidence that upon pore opening the aromatic residues Y652 and F656 rotate to face towards the large central cavity of the channel (Chen et al. 2002; Fernandez et al. 2004; Mitcheson 2008). In addition to the mutagenesis and modelling studies, the cryo-EM structure of hERG channels revealed unusual features of the inner cavity that provided significant insight into why hERG is so susceptible to a wide group of drugs. The structure showed that the central cavity is small and surrounded by four hydrophobic pockets, i.e. one for each subunit, that connects the pore cavity just below the selectivity filter. A narrow constriction in the pore cavity that exhibited a negative electrostatic potential, compared to other K^+ channel cavities, could explain why many drugs block hERG (Wang & MacKinnon 2017). Compounds that are common culprits for causing acquired LQT syndrome contain positive charges or have a positive electrostatic potential.

Inactivation may also play a role in high drug binding affinity in hERG channels (Ficker et al. 1998; Herzberg et al. 1998; Weerapura, Hébert, et al. 2002; Ficker et al. 2001; Perrin et al. 2008a). The closely related *eag* channel, which does not inactivate, shows 100-fold less sensitivity to the hERG blocker dofetilide, yet upon introduction of inactivation by mutagenesis, the *eag* channels showed high sensitivity to dofetilide (Ficker et al. 1998; Ficker et al. 2001). In the same study, the authors showed that a mutation, S620T, that abolishes hERG inactivation also showed reduced affinity to drug block.

As part of the routine screening of pharmacological compounds under development for their ability to block hERG channels, several hERG channel activator small molecules have been identified. These include RPR260243 (Kang et al. 2005), NS1643 (Casis et al. 2005), PD118057 (Xu et al., 2008), A935142 (Su et al. 2009), ICA-105574 (Gerlach et al. 2010) and Ginsenoside Rg3 (Choi et al. 2011). These activators share an ability to

increase repolarizing current and shorten cardiac AP duration and thus may have possible significant therapeutic potential when treating individuals suffering from LQTS. Based on current understanding, these hERG channel activators are grouped into Type1 or Type 2, depending on their mechanism of action. Type 1 activators, such as RPR260243 and Ginsenoside Rg3, primarily target deactivation, severely slowing its kinetics leading to increased hERG current. Type 2 activators, such as NS1643 and ICA-105574, primarily target inactivation and induce a positive shift in the voltage-dependence of C-type inactivation (Sanguinetti 2014). This categorization is inherently limited, since for example, a secondary effect of RPR260243 is to increase hERG current by attenuating C-type inactivation (Kang et al. 2005; Perry et al. 2007), and a secondary effect of NS1643 is to shift the voltage dependence of activation to hyperpolarized voltages. However, the discovery of hERG channel activator compounds is of considerable interest and better understanding of their mechanism of action will lead to novel therapeutic opportunities. Indeed, in recent years, additional hERG activators have been identified and their mechanism of action been described (for reviews, see Perry et al. 2010; Zhou et al. 2011).

1.9 **Objectives**

The overall objective of this thesis was to understand the structural determinants and molecular basis of the unusual gating properties in hERG cardiac potassium channels. I used a combination of mutational analysis, two-electrode voltage clamp (TEVC), voltage-clamp fluorimetry (VCF) and cut open vaseline gap (COVG) electrophysiology techniques to study wild-type (WT) and mutant hERG channels expressed in *Xenopus* oocytes to:

(1) define the location of the intracellular pore gate in hERG channels (Chapter 3).

(2) provide the first comprehensive characterization of mode-shift behaviour and the slowing of hERG channel deactivation as a result of voltage sensor relaxation (Chapter 4).

(3) characterize fluorescence reports of voltage sensor movement in hERG channels to understand the mechanism underlying slow activation gating in hERG channels (Chapter 5).

Chapter 2. Materials and Methods

2.1 Molecular biology - Generation of hERG channel mutants

hERG channel constructs were incorporated into the expression vector pBluescript SKII and expressed in *Xenopus laevis* oocytes. Mutagenesis of amino acids was achieved using conventional overlap extension polymerase chain reaction (PCR) (Ho et al. 1989) with primers synthesised by Sigma Genosys (Oakville, ON) and the high-fidelity DNA polymerase enzyme, Pf*u*Turbo. Constructs were transformed into DH5α competent cells and a Qiagen miniprep kit was used to extract the plasmid DNA. Mutant constructs were sequenced using Eurofins MWG Operon (Huntsville, AL) to ensure no off-target errors were integrated during PCR cycling, although errors are rare when using P*fu*Turbo polymerase. Once the desired mutation was achieved, constructs were linearized using *XbaI* restriction endonuclease thus creating a template for *in vitro* transcription. cRNA was transcribed from linear cDNA using the mMessagemMachine T7 Ultra cRNA transcription kit (Ambion, Austin, TX), which integrates polyadenylation of the 3′-tail and an anti-reverse cap analog (ARCA) to increase translation and to stabilize target RNA within the cell. These features significantly improve membrane surface expression, which is particularly important for studying hERG channels. To prevent cRNA degradation, the cRNA was precipitated using 50 µl of $LiCl_2$ at -20 °C for 2 h and stored at -80 °C. For my projects, the Claydon lab technician, Ji Qi, made all of the constructs to be tested.

2.2 Expression system

Throughout this study, I focused on understanding how hERG ion channels function at the molecular level. In particular, I investigated the molecular determinants that underlie hERG channel gating. To answer these questions, I used a suitable expression system that has low endogenous ion channel expression and into which the channel under investigation can be exogenously expressed through the *Xenopus laevis* oocyte expression system. Although there were other common expression systems, such as Chinese Hamster Ovary (CHO) or Human Embryonic Kidney (HEK) mammalian cell

lines, there are advantages of the *Xenopus* oocyte system: (1) the large size (up to 1.3 mm in diameter) which facilitates easy manipulation and allows penetration with two recording electrodes to perform TEVC recordings; (2) oocytes faithfully express foreign RNA that has been injected into them facilitating electrophysiological measurements and any associated biochemical procedures; (3) the oocytes can be readily harvested in large numbers; (4) the cells are hardy, require simple culture conditions and survive *in vitro* for up to several weeks; (5) the expression level can be easily controlled by the amount of RNA injected; (6) having relatively few endogenous channels (expressed at very low levels) oocytes permit the study of the channel of interest in virtual isolation (Goldin 1991); (7) for VCF studies, oocytes facilitate high expression level of channels, the animal pole of the oocyte being black in color reduces the background fluorescence. Fluorophores are impermeable to the oocyte membrane and (8) in addition, co-expression of channel subunits at once is easily possible in oocytes rather than mammalian cells (Papke & Smith-Maxwell 2009) although this is not the focus of my studies. Despite these advantages, there are some caveats for oocyte recordings.

Limitations: Although endogenous currents are small, sometimes they can contaminate the electrophysiological recordings if, for example, the channels in question produce only small currents (for example mutants with low expression). Another limitation is the occurrence of large capacitance upon membrane potential clamp resulting from the large size of the cell. The time constant of charging the membrane is large, because of the high surface area, which translates to a large membrane capacitance. For instance, in recording from channels that activate rapidly, important kinetics can be lost during the settling time of the clamp. To reduce this effect, I used an amplifier that can clamp the membrane within ~1 ms which means that fast kinetics are not generally lost. Moreover, in gating currents, cut open vaseline gap (COVG) only clamps a small portion of the membrane and allows compensation for the capacitance quite well.

2.2.1 **Oocyte preparation and injection**

In accordance with the Simon Fraser University Animal Care Committee, and Canadian Council on Animal Care protocols and procedures, female *Xenopus laevis* frogs were terminally anaesthetized by placing them in 2g/L tricane (ethyl-3-aminobenzoate methanesulphonate) solution (Sigma-Aldrich) for 10-15 min. Both the leg and tail were pinched to ensure lack of a reflex response. Following a small abdominal incision, the

ovarian lobes were then removed and partial digestion of follicular layers was achieved by treatment with 1mg/ml collagenase type 1A in a calcium-free solution (MgOR2) (in mM: 96 NaCl, 2 KCl, 20 $MgCl_2$, 5 HEPES, titrated to pH 7.4 with NaOH) for ~1 h. Collagenased oocytes were washed several times with MgOR2 solution and healthy stage V or VI oocytes (presence of a light colored vegetal pole and dark animal pole, separated by a clear band) were sorted and placed in SOS+ medium (in mM: 96 NaCl, 2 KCl, 1.8 $CaCl_2$, 1 $MgCl_2$, 5 HEPES, 2.5 sodium pyruvate, 100 mg/L gentamycin sulphate and 5% horse serum, titrated to pH 7.4 with NaOH) for ~ 15 to 20 min to further loosen up the follicular layer (determined by a cap formation) before manual removal of the remaining follicular layer with fine-tip forceps. It was important to remove the follicular layer completely for two reasons (1) the follicular layer can be a barrier to the injection pipette that can potentially result in cell damage during cRNA injections; (2) the follicular layer contains endogenous channels and transporters that can result in contamination of electrophysiological recordings (Goldin 1991; Bossi et al. 2007). Isolated oocytes were incubated in SOS+ solution before injection. Injection glass pipettes were made using a P-87 Flaming/Brown Micropipette puller (Sutter Instrument Co.) and tips were manually broken with forceps to get a beveled shape. Injection glass pipettes were then filled with mineral oil and mounted on to a Drummond digital micro-dispenser. The mineral oil was dispensed onto a piece of parafilm and RNA was then pipetted onto the mineral oil and sucked up into the injecting pipette. Generally, ~20 oocytes were then injected with 50 nl (5-15 ng) of cRNA each. Once the injection was completed, the oocytes were incubated in SOS+ solution at 19 °C for 24-72 h prior to the electrophysiological recordings. For gating currents and VCF recordings, oocytes were incubated for 3-4 days to achieve high expression. In general, oocytes were cultured in SOS+ solution, which was replaced every day. For control experiments, uninjected oocytes were used. Since defolliculated oocytes contain few endogenous channels, ionic currents recorded from these cells are negligible in comparison with cRNA-injected oocytes, but they serve as useful controls for measuring background current and fluorescence levels and resting membrane health. All chemicals were purchased from Sigma-Aldrich (Mississauga, Canada).

2.3 **Electrophysiology**

2.3.1 **Two-electrode voltage clamp (TEVC)**

Wild-type (WT) and mutant hERG channel ionic currents were recorded using the TEVC technique. In brief, TEVC includes two intracellular microelectrodes, a voltage electrode that measures the membrane voltage relative to bath ground, and the other, a current electrode that injects the current proportional to the difference between the command and measured membrane voltage. This current represents the flow of ions through ion channels that are expressed in the membrane. When a command voltage is set, a pre-amplifier detects the membrane voltage and sends the output to a feedback amplifier, in this case an OC-725C amplifier (Warner instruments, Haden, CT). This amplifier serves as a negative feedback system; it subtracts the membrane voltage from the command voltage and sends an output to the current electrode. Thus, it produces a current equal and opposite to the ionic current. A silver chloride (AgCl) electrode placed in the bath chamber serves as a reference electrode. All signals were digitized using a digidata 1440 A/D convertor and computer-driven protocols were performed using pClamp 10.2 software (Axon Instruments, Foster City, CA). The recording electrodes were made from thin-walled borosilicate glass with a resistance of 0.2 -2.0 MΩ when filled with 3 M KCl, which ensures high conductivity between the AgCl electrode and the recording solution. Since the concentration of KCl within the borosilicate glass recording electrodes is high compared to the recording solution, a liquid junctional potential was created and this was electrically corrected before impaling the electrodes into the oocyte.

In this thesis, the majority of recordings were performed at room temperature (20-22 °C) while oocytes were bathed in an external ND96 solution (in mM: 96 NaCl, 3 KCl, 0.5 $CaCl_2$, 1 $MgCl_2$ and 5 HEPES, titrated to pH 7.4 with NaOH) and perfused at a flow rate of 1 ml/min. In the case of proline mutant channels (see Chapter 3), recordings were performed while the oocytes were bathed in an external ND96 solution containing 30 mM K^+ rather than 3 mM K^+ to highlight the inward current observed with hyperpolarization. In addition, 0.5 mM $CdCl_2$ (see Chapter 3) was added to the ND96 solution in some experiments to modify gating. All current signals were acquired at a sampling rate of 10 kHz with a 4 kHz low-pass Bessel filter.

2.3.2 **Voltage-clamp fluorimetry (VCF)**

Advances in fluorescence spectroscopy techniques, such as VCF, allow direct observation of protein structural dynamics in real time. The fluorescence measurements allow visualization of the conformational changes associated with the channel gating. This fluorescence technique has proven to be a powerful tool in investigating the relationship between ion channel dynamic structure and its function (Bezanilla et al., 1999; Cha & Bezanilla, 1997; Claydon et al., 2006; Mannuzzu et al., 1996).

VCF involves site-specific attachment of a fluorophore, often tetramethylrhodamine-5-maleimide (TMRM; Invitrogen), to a cysteine amino acid residue engineered at a specific position of interest within the channel. When the channel undergoes state transitions during gating, the fluorophore gets exposed to a different cellular environment causing a change in the fluorescence signal that reflects the conformational changes occurring in the protein at or near the fluorophore (Mannuzzu et al. 1996). VCF allows simultaneous measurement of the fluorescence emission changes associated with channel rearrangements along with ionic current measurements using TEVC. This therefore provides an encompassing and unparalleled report of channel behavior.

The membrane impermeant thiol-reactive fluorescent probe, TMRM was used for fluorescent labelling in most of the VCF experiments in this thesis. TMRM covalently binds to cysteine residues substituted at S3-S4 linker sites (G516 to L520C; see Chapter 3 and 5) and has a maximum light absorption at 542 nm and a maximum emission at 567 nm. In the present study, two native extracellular cysteines in the S1-S2 linker (C445 and C449) were replaced with valines (referred to as C-less in this study), to prevent non-targeted labelling. On the day of the experiment, oocytes were incubated in a depolarizing solution (in mM: 99 KCl, 1 $MgCl_2$, 5 HEPES, 2 $CaCl_2$, titrated to pH 7.4 with NaOH) containing 5 µM TMRM for 30 min at 10°C in the dark. Oocytes were then washed with an ND96 solution and maintained in the dark until recordings. Two-electrode voltage clamp fluorometry experiments were performed with a Nikon TE2000S inverted microscope with an epifluorescence attachment and a Hamamatsu photomultiplier tube (PMT) detection module (Carin Research, Kent, UK). For fluorescence recordings, a 100 W mercury arc lamp was used to excite TMRM with light that passes through a 525 nm band-pass (45 nm) excitation filter (Omega Optical, Brattleboro, VT) via a dichroic mirror (560 nm long pass) and 20x objective lens to the oocyte in the recording bath chamber. Fluorescence emission was collected via the

same 20x objective lens and filtered through a 565 nm long pass emission filter before being collected by the PMT module (Fig. 2.1). During VCF experiments, ionic currents and voltage signals were measured simultaneously along with fluorescence signals. The signal-to-noise ratio of fluorescence recordings was improved by recording the average of a number of sweeps. To account for photobleaching, the fluorescence recorded during voltages at which there was no channel opening was subtracted. All fluorescence signals were acquired at a sampling rate of 10 kHz with a 4 kHz low-pass Bessel filter.

In some experiments, I used a different fluorophore methanethiosulphonate-rhodamine (MTSR; Toronto Research Chemicals) (see Chapter 4). MTSR has similar spectroscopic profiles to TMRM. However, on an experimental day, oocytes were labelled with 5 µM MTSR in the depolarizing solution for 1 min on ice in the dark.

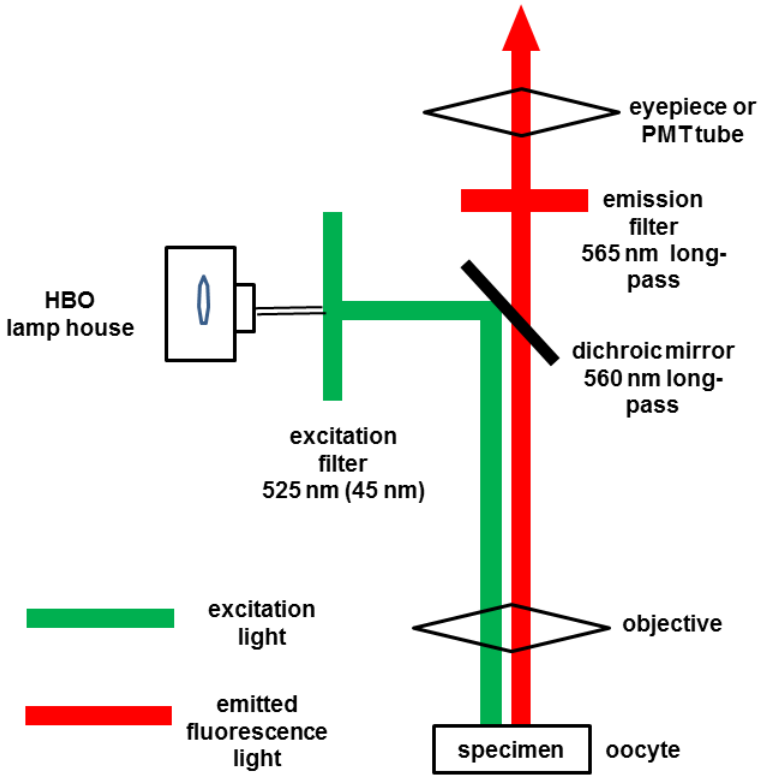

Figure 2.1 Schematic of VCF set up.
***A*,** Fluorescence emission from fluorophores attached to a specific channel site is recorded from individual oocytes using a Nikon TE2000S inverted microscope with an Epi-fluorescence attachment and photomultiplier tube (PMT) detection module. Fluorophore molecules are excited by light provided from a 100W mercury lamp (HBO lamp) and passed through a 525 nm bandpass excitation filter. The light is then reflected by a long pass dichroic mirror through a 0.75 NA 20x objective lens to the oocyte. Resulting fluorescence emission is collected via the same 20x objective and dichroic mirror before being filtered by a 565 nm long pass emission filter. The filtered emissions are then passed to a Cairn PMT module.

2.3.3 **Cut-open Vaseline-gap (COVG)**

Gating current (intra-membrane charge movement) recordings from oocytes expressing WT and mutant hERG constructs were collected using the COVG voltage clamp technique using a CA-1B amplifier (Dagan, Minneapolis, MN). COVG is suitable to achieve low-noise recordings with fast clamp speed and provides the ability to modulate the intracellular and extracellular environment of the cell. In COVG, a part of the oocyte membrane is isolated by a vaseline-gap and cytoplasmic fluid is exchanged by permeabilizing the remaining membrane (Taglialatela et al. 1992). Briefly, COVG involves mounting the oocyte into the middle of three chambers that were electrically independent and separated by vaseline gaps (Fig. 2.2A and B). The voltage clamp circuit was then assembled around the oocyte by six agar bridges and one intracellular electrode (Fig. 2.2B). The three chambers, from top to bottom, are referred to as the top/recording chamber (contains the oocyte membrane under voltage clamp and from which membrane currents are recorded), the guard chamber (acts as an electric guard shield) and the bottom chamber (provides access to the inside of the cell). The recording and guard chamber contain holes (~0.6 mm) to accommodate the oocyte. These holes were lined with vaseline so that the three chambers were electrically isolated, thus forming a vaseline-gap. Connections between the chambers and the electrical circuits were made via agar bridges and AgCl electrodes filled with 1 M NaCl. Typically, agar bridges were made of glass capillary tubes, and were bent on both the ends and had an internal platinum wire (to increase the capability of passing high-frequency currents). The lower part of the oocyte was exposed to the bottom chamber and was permeabilized with 0.1 % saponin, so that the cytosolic fluid is electrically continuous with the internal solution in the lower chamber. In contrast, recording and guard chambers contained external solution. Two separate voltage clamps were used to clamp the recording and guard chamber solutions to the inverse of the command voltage, each requiring two agar bridges. The third voltage clamp injects the current intracellularly through the bottom chamber, to maintain the oocyte interior at ground as measured by the tip of the electrode impaling the oocyte in the top chamber. Thus, the membrane was effectively clamped to the command voltage.

In the present study, all COVG signals were digitized at 50 kHz, low-pass filtered at 10 kHz (using an ITC-16 interface, HEKA electronics) and recorded using Patchmaster software (HEKA electronics). Extracellular solution in the top and guard chamber

contained (in mM 120 tetraethyl ammonium hydroxide (TEA-OH), 120 2-(N-Morpholino) ethane sulfonic acid (MES), 10 HEPES and 0.5 $Ca(OH)_2$, titrated to pH 7.4 with MES and was supplemented with the hERG blocker terfenadine (20 µM) to inhibit ionic current. Internal solution contained (in mM): 120 TEA-OH, 120 MES, 10 HEPES, 2 EGTA, titrated to pH 7.4 using MES. To achieve the cut-open configuration, 0.1% saponin was added to the bottom chamber for 30-60 s to permeabilize the oocyte membrane. Upon electrical access, saponin was replaced with internal solution. Prior to gating current recordings, the membrane was held at -10 mV for ~30 min to ensure depletion of endogenous K^+ ions from the cytosol of the oocyte. Microelectrodes were pulled from borosilicate glass and had a resistance of 250-500 kΩ when filled with 3 M CsCl. Capacitive currents were partially compensated using the amplifier's analogue circuitry. Unless otherwise stated, linear leak subtraction was performed online with a P/-8 protocol.

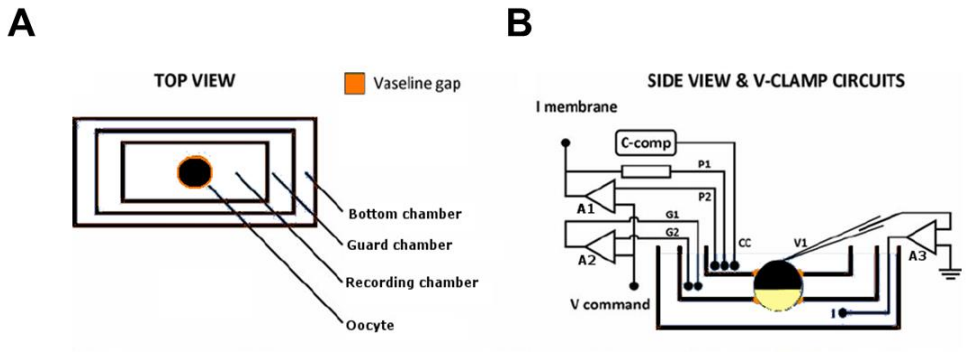

Figure 2.2 Schematic of COVG set up
A, Top-view of the three COVG chambers, from top to bottom, referred to as the recording, guard and bottom chambers. The oocyte is positioned surrounded by a vaseline rim highlighted in orange. ***B,*** Side-view of the setup showing the chambers and electronics. The oocyte is mounted into the middle of the chambers, highlighting the vaseline gaps in orange and a schematic representation of the voltage clamp circuitry (A1, A2 and A3) assembled around the oocyte showing V1 as intracellular electrode and P1, P2, G1, G2, CC and I as agar bridges. The dashed line represents the membrane of the oocyte placed in the bottom chamber and permeabilized with 0.1% saponin.

2.4 **Voltage protocols**

Due to the unusual kinetics of hERG gating, measurement of these gating characteristics is not straightforward. However, there are now well-established standard protocols that are routinely used. This section outlines these standard protocols used to record ionic currents; they are also represented as a schematic in Fig. 2.2. It is important to note that, depending on the biophysical properties of the mutants or experimental

conditions (gating currents or VCF measurements), the individual parameters such as the voltages and pulse durations were modified. Thus, any modifications to these voltage protocols are annotated as an *inset* in the relevant figure, or described in the figure legend.

2.4.1 **Activation**

To determine the voltage-dependence of activation, as shown in Fig. 2.2A, oocytes were held at -80 mV and subjected to 2 s depolarizing steps to +50 mV in 10 mV increments (P1) to activate and inactivate channels followed by a 2 s hyperpolarizing step to -110 mV (P2) to recover channels from inactivation and allow for deactivation. Peak tail currents during P2 pulse following recovery from inactivation were plotted against voltage and fitted with a Boltzmann function (see section 2.5.1). In Chapter 4, I explored the correlation between the slow activation of hERG and the position of the voltage-dependence of activation relationship.

2.4.2 **Deactivation**

To determine the voltage-dependence of deactivation, as shown in Fig. 2.2B, oocytes were held at -80 mV and subjected to a 500 ms depolarizing step to +60 mV (P1) to activate and inactivate channels, followed by 8 s steps (P2) from –110 mV to +40 mV in 10 mV increments to recover channels from inactivation and allow for deactivation followed by a repolarizing step to -110 mV (P3) for 100 ms. Peak tail currents after recover from inactivation during P3 pulse were plotted against voltage and fitted with a Boltzmann function (see section 2.5.1). As I explored in Chapter 4, because hERG channels deactivate slowly, 8 s or greater duration P2 pulses were required to measure the steady-state voltage dependence of deactivation.

2.4.3 **Activation Kinetics**

To determine the time course of activation, an envelope of the tails protocol was used (Wang et al., 1997). In brief, as shown in Fig. 2.2C, oocytes were held at -80 mV and then depolarized to +60 mV (or to a different test pulse depending on the voltage of interest) for successive increasing durations from 10 to 500 ms (in 10 ms increments) to activate and inactivate channels. At the end of each test pulse, the membrane was

hyperpolarized to -110 mV to recover channels from inactivation followed by deactivation. Peak tail current during the -110 mV pulse was plotted against the preceding test pulse duration. Data points during the late phase of activation were fitted with a single exponential function as described in section 2.5.2.

2.4.4 **Deactivation Kinetics**

To determine deactivation kinetics, as shown in Fig. 2.2D, oocytes were held at -80 mV and subjected to a 500 ms depolarizing P1 step +60 mV to activate and inactivate channels, followed by 4 s P2 steps from -110 mV to -40 mV in 10 mV increments to recover channels from inactivation followed by deactivation. The current decay during P2 was fitted with a double exponential function as described in section 2.5.3.

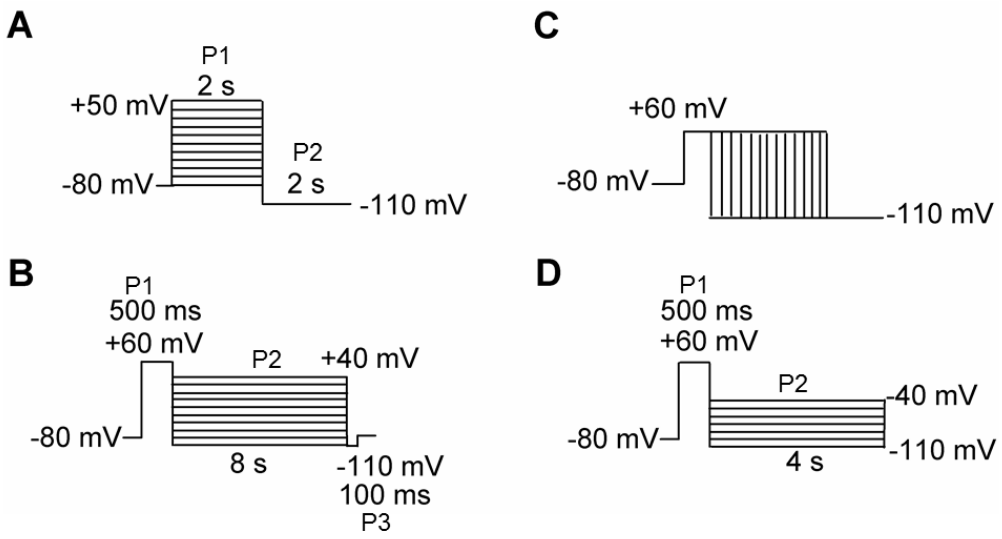

Figure 2.3 Standard voltage protocols used to characterize hERG gating properties.

A, voltage protocol used to measure the voltage-dependence of activation. ***B*****,** voltage protocol used to measure the voltage-dependence of deactivation. ***C*****,** voltage protocol used to measure activation kinetics, ***D*****,** voltage protocol used to measure deactivation kinetics.

2.5 **Data Analysis**

Data throughout this study were analysed using Clampfit 10.3 (Axon Instruments), SigmaPlot11 (Systat Software, San Jose, CA), or IGOR Pro (Wavemetrics, Lake Oswego, OR) software. Unless otherwise noted, data were presented as mean ± SEM. n represents the total number of cells recorded. Statistical analysis was performed using a

Student's *t*-test or one-way analysis of variance (ANOVA) where appropriate. A p-value of < 0.05 is taken as a statistically significant difference. In figures, arrows indicate the zero current level and dotted lines are to guide the eye.

2.5.1 **Voltage-dependence relationships**

Conductance-voltage (GV) relationships describing the voltage-dependence of activation and deactivation were obtained from ionic current traces as described above. In all cases, peak tail current amplitudes were normalized to the maximum tail current amplitude. Fluorescence-voltage (FV) relationships were obtained from the fluorescence signal amplitude at the end of the test pulse. Charge versus voltage (QV) relationships were obtained by integrating off gating currents at -100 mV (for activation), or on gating currents at 0 mV (for deactivation). Calculated integrals were normalized to total charge moved and were plotted as a function of the preceding test pulse voltage. GV, FV and QV curves were fitted with the Boltzmann equation:

$$y = 1/ (1+\exp (V_{1/2} - V)/k)$$

where y is the relative conductance, fluorescence or charge movement, normalized to the maximum conductance (G/G_{max}), fluorescence (F/F_{max}) or charge movement (Q/Q_{max}), $V_{1/2}$is the half-activation or deactivation, V is the test voltage and *k* is the slope factor.

2.5.2 **Time course of activation**

The time course of activation was derived from single exponential fits of data plotting the peak tail current against depolarization duration. The tau was derived from:

$$f(t) = A^{*} \exp (t/\tau) + C,$$

where A is the amplitude of the fit, t is time, τ is the time constant of activation and C is the residual current. The time course of fluorescence change upon depolarization was derived from single exponential fits using the same equation.

2.5.3 **Time course of deactivation**

To determine the time course of ionic current deactivation and off-gating current kinetics, the decay phase of deactivating tail currents or off gating currents were fitted with a double exponential fit:

$$f(t) = A_{slow}\exp(-t/\tau_{slow}) + A_{fast}\exp(-t/\tau_{fast}) + C,$$

where A is the amplitude of the fit, t is time, τ is the time constant of deactivation, and C is the residual current function.

Chapter 3. Proline scan of the hERG channel S6 helix reveals the location of the intracellular pore gate.

This chapter describes the work published in the article listed below with some formatting changes to suit the thesis style and an additional brief overview paragraph. I contributed to the most of the work presented in this chapter. I performed all of the ionic current and VCF experiments and Dr. Stan Sokolov performed all of the gating current experiments. I analyzed the majority of the data, and made the majority of the figures and wrote the first draft of the manuscript. I also presented this work in poster format at the Biophysical Society - 2013, Philadelphia, USA.

Thouta, S., S. Sokolov, Y. Abe, S.J. Clark, Y.M. Cheng, T.W. Claydon. 2014**.** Proline scan of the hERG channel S6 helix reveals the location of the intracellular pore gate. *Biophys.J*. 106:1057-1069.

3.1 **Overview**

Comparison of X-ray crystal structures of K^+ channels in closed (Fig. 1.2A) and open states (Fig. 1.2B) and extensive studies on *Shaker* (Liu et al. 1997; Hackos et al. 2002), suggested that the activation gate regulates ion conduction through the pore by opening and closing. Data suggest that the activation gate is formed at the bundle crossing by a conserved proline-valine-proline (PVP) motif located on the lower region of S6 helix. The PVP motif introduces a kink in the S6 helix that allows for electromechanical coupling with voltage sensor motions via the S4-S5 linker. hERG channels lack the PVP motif and therefore the location of the activation gate and how it is coupled with S4 movement is less clear. This raises questions about the origins of the unusually slow activation kinetics of hERG channels, as well as their ability to accommodate a wide array of bulky pharmacological compounds. Here, we define the location of the gate by introducing a proline kink at different positions along the length of inner S6 helix, from I655 to Y667. This is a useful approach, because introduced proline residues disrupt α-helices below their point of introduction. By monitoring the perturbation of the gate as we introduced a proline residue down the length of the S6 helix, we could effectively map where the proline introduction stopped perturbing gate function, and thus locate the functional gate region. We found that proline substitution at proximal positions trapped the activation gate open, leading to constitutive channel current. In contrast, substitutions below Q664 preserved channel gating. This suggests that the position of the intracellular activation gate is formed at Q664 and the data provided the first detailed map of the position of the gate in hERG channels. These data suggest that the activation gate is one helical turn lower in S6 helix in hERG than in *Shaker*-like channels. This finding is consistent with a previous homology model-based prediction (Wynia-Smith et al. 2008) and a more recent structural description of the hERG (Wang & MacKinnon 2017) and *eag* channel (Whicher & MacKinnon 2016). The lower gate position would likely increase the size of the pore cavity allowing greater drug access. Using voltage clamp fluorimetry and gating current analysis we also characterized voltage sensor movement in a trapped-open channel to understand what underlies the unusually slow activation of hERG channels. We report what we interpreted as intrinsic hERG voltage sensor movements, and demonstrated that these are uncharacteristically slow. We proposed that this underlies slow activation of hERG channels.

3.2 **Introduction**

The human *KCNH2* gene encodes the pore forming α-subunit of the cardiac voltage-gated K^+ (Kv) channel Kv11.1 or human-*ether-a-go-go-related* gene (hERG). hERG channels underlie the rapid delayed rectifier current, I_{Kr}, in the heart that is essential for repolarization of the cardiac action potential and consequently normal cardiac electrical activity and rhythm (Sanguinetti et al. 1995; Trudeau et al. 1995). In contrast to other Kv channels, hERG channels display unusual gating characteristics, which include slow activation and rapid voltage-dependent inactivation that restrict repolarizing current upon initial membrane depolarization, and slow deactivation and rapid recovery from inactivation that allow channels to revisit and dwell in the open state upon repolarization, thus producing a resurgent repolarizing current that aids terminal repolarization of the action potential. Despite orchestrating such a unique role for hERG channels in cardiac physiology, the mechanisms underlying the unusual gating behaviors in hERG channels are not well understood. In particular, neither the location of the intracellular pore gate, nor the manner in which it is coupled to the voltage-sensing unit of the channel, are well defined. This is of principal interest, because hERG channels are targeted by many pharmaceutical agents, the majority of which block by entering the pore via the intracellular activation gate and are limited by the unusually slow opening of the pore gate. Drug binding that reduces hERG channel function, as with congenital mutations, has been shown to prolong the duration of the action potential and lead to long QT syndrome, a potentially life-threatening ventricular repolarization disorder that is associated with increased vulnerability to arrhythmia, ventricular fibrillation and sudden cardiac death (Curran et al. 1995; Sanguinetti et al. 1996). Moreover, recent advances in the discovery of hERG channel openers as therapeutics have identified sites of action that involve direct interactions with the voltage sensing unit that may modify activation/deactivation gating (Durdagi et al. 2012). These observations underscore the need to understand the structural determinants of the hERG channel pore gate and the mechanistic basis of electromechanical coupling in these channels.

Evidence for gated access to the K^+ channel pore comes from reports of state-dependent blockade by intracellular quaternary ammonium derivatives, which blocked the open channel pore and could even be trapped by closure of the activation gate (Armstrong 1966; Armstrong 1971; Armstrong & Hille 1972; Holmgren et al. 1997). In

Shaker channels, the location of the activation gate was defined by examining state-dependent accessibility of engineered cysteines within S6 to methanethiosulfonate reagents and Cd^{2+} (Liu et al. 1997; Del Camino & Yellen 2001). These results showed that modification of Val^{478} occurred in both closed and open states, but that access was limited to the open state for sites deeper within the pore. Mutagenesis of S6 residues to small, bulky, or charged side chains helped to confirm Val^{478} and/or Phe^{481} as candidates for the *Shaker* gate (Hackos et al. 2002). These data were corroborated by evidence that the gate could be trapped in the closed conformation by introducing tryptophan at Val^{478}, which suggested that Val^{478} forms a hydrophobic seal at the lower limit of the pore gate that acts as a steric barrier for K^+ permeation (Kitaguchi et al. 2004). Such functional evidence for the location of the gate is consistent with evidence from structures crystallized in open and closed states (Doyle et al. 1998; Jiang et al. 2002b; Long et al. 2005b), which suggest that ion conduction is gated by the opening of an intracellular pore gate created as the lower S6 helices swing away from the midline of the pore (Jiang et al. 2002b). In Kv channels, a conserved Pro-Val-Pro (PVP) motif introduces a kink in the S6 helices that brings them into contact with the S4-S5 linker to provide electromechanical coupling between voltage sensor movements and the S6 pore gate (Long et al. 2005a; Long et al. 2005b). Disruption of the highly conserved PVP motif dramatically alters gating, suggesting that it contributes to the structural form of the intracellular gate (Hackos et al. 2002), one helical turn above the Val^{478}steric barrier.

hERG channels lack the S6 PVP motif raising questions as to the location of the gate and how it is coupled to voltage sensor movement. One study using a cysteine scan approach showed that inner hERG S6 helix mutations could alter gate function, primarily by disrupting the energetics of channel closing, resulting in a standing conductance at negative voltages (Wynia-Smith et al. 2008). Interestingly, mutation of Ser^{660} (which corresponds to *Shaker* Val^{478}) did not alter hERG gating suggesting that the location of the activation gate may be different in hERG channels. This is consistent with a brief report that introduction of PVP into hERG channels prevented channel closure (Fernandez et al. 2004). Here, we define the location of the hERG activation gate by introducing a proline-induced kink at positions along the length of the inner S6 helix from, Ile^{655} to Tyr^{667}. Examining the pattern of gate perturbation by the engineered proline enabled us to define the boundary of the activation gate as Gln^{664}, more than one full helical turn below the gate position in *Shaker*-like Kv channels. Voltage-clamp

fluorimetry (VCF) and gating current data show that proline introduction disrupts coupling of voltage sensor movement with the pore gate, isolating the gate and trapping it in the open state. We characterize these reports of voltage sensor movement and charge transfer in a trapped-open channel, and show that a component of voltage sensor movement appears to be intrinsically slow in hERG channels expressed in *Xenopus* oocytes.

3.3 Materials and Methods

3.3.1 Molecular biology

hERG channel constructs were incorporated into the pBluescript SKII vector and expressed in *Xenopus laevis* oocytes. Mutations were engineered using conventional overlap extension PCR with primers synthesized by Sigma Genosys (Oakville, Ontario). All mutant constructs were sequenced using Eurofins MWG Operon (Huntsville, AL) to ensure no errors were integrated during PCR cycles. Wild-type (WT) and mutant constructs were linearized using *XbaI* restriction endonuclease and cRNA was transcribed *in vitro* using the mMessage mMachine T7 Ultra cRNA transcription kit (Ambion, Austin, TX).

3.3.2 Oocyte preparation and injection

In accordance with Simon Fraser University Animal Care Committee and Canadian Council on Animal Care protocols and procedures, oocytes were isolated from female *Xenopus laevis* frogs that were terminally anesthetised by immersion in 2g/L tricaine solution (Sigma Aldrich) for 10-15 min. Selection and injection of oocytes was performed as described previously (Van Slyke et al. 2010).

3.3.3 Data acquisition

Current and voltage signals were collected using conventional two-electrode voltage clamp with an OC-725C amplifier (Warner Instruments, Handen, CT). Signals were digitized and acquired using a digidata 1440 A/D convertor and pClamp 10.2 software (Axon Instruments, Foster City, CA). In proline mutant channels, recordings were made with cells exposed to a modified ND96 solution that contained 30 mM [K^+] (in mM: 69

NaCl, 30 KCl, 5 HEPES, 0.5 $CaCl_2$, 1 $MgCl_2$, titrated to pH 7.4) so as to increase the driving force for ion flow. In all other cases, unless otherwise stated, standard ND96 (i.e., with 96 mM NaCl, 3 mM KCl) solutions were used. Where applicable, 0.5 mM $CdCl_2$ was added to the ND96 solution and perfused at a flow rate of 1ml/min. Recording microelectrodes were made from borosilicate glass with a resistance of 0.2-2.0 MΩ when filled with 3 M KCl. Current signals were acquired at a sampling rate of 10 kHz and with a 4 kHz low-pass Bessel filter. Recordings were performed at 20-22 °C.

3.3.4 **Voltage protocols and data analysis**

Data were analyzed using Clampfit 10.3 (Axon Instruments), SigmaPlot11 (Systat Software, San Jose, CA) or IGOR Pro (Wavemetrics Inc, Lake Oswego, OR) software. Steady-state conductance-voltage (GV) relationships were determined from peak tail currents recorded during a voltage step to -110 mV applied following 2 s depolarizing pulses (holding potential, -80 mV). Many proline mutant channels passed inward current at -80 mV. In these cases, a holding potential of -30 mV was used, since this correlated reasonably well with the reversal potential in the modified, 30 mM external [K^+], ND96 solution. In all cases, peak tail current amplitudes were normalized to the maximum tail current amplitude. The relationship between the steady-state current activation, fluorescence changes or charge movement, and membrane voltage were fitted (where possible) with a Boltzmann function: $y=1/(1+\exp(V_{1/2} - V)/k)$, where y is the relative conductance, fluorescence or Q_{off} normalized with respect to maximal conductance, fluorescence or Q_{off}, $V_{1/2}$ is the voltage of half-activation, V is the test voltage and *k* is the slope factor. Rectification factor was calculated as previously described (Sanguinetti et al. 1995) using: $R=I/Gn(V-E_{rev})$, where R is the rectification factor, I is the membrane current, G is the slope conductance calculated from the fully activated current-voltage relationship, n is the activation variable (which was set at 1.0 because data were collected from fully activated channels, i.e. following a voltage step to +60 mV), V is the test voltage and E_{rev} is the measured reversal potential. To determine the rate of channel activation, an envelope of tails activation protocol was used. Peak tail currents at -110 mV were measured following step to +60 mV of varying duration (10-500 ms). The holding potential was -80 mV. Activation time course was derived from single exponential fits of data plotting the peak tail current against depolarizing pulse duration: tau was derived from $f(t)=A*\exp(t/\tau)+C$, where A is the amplitude of the fit, t is time, τ is

the time constant of activation, and C is the residual current. The time course of fluorescence change upon depolarization was derived from single exponential fits using the same equation. All data are expressed as mean ± SEM. In the figures, arrows indicate the zero current level and dotted lines are to guide the eye. Voltage protocols are depicted in figures and described in details in figure legends.

3.3.5 **Voltage clamp fluorimetry (VCF)**

The G516C mutation in the S3-S4 linker was introduced as a site for fluorophore labeling with the impermeant thiol-reactive fluorescent probe, tetramethylrhodamine-5-maleimide (TMRM; Invitrogen). To prevent possible modification of the fluorescence emission from G516C, two native extracellular cysteines in the S1-S2 linker (C445 and C449) were replaced with valine (Es-Salah-Lamoureux et al. 2010). Oocytes were labeled with 5 µM TMRM in a depolarizing solution (in mM: 99 KCl, 1 $MgCl_2$, 5 HEPES, and 2 $CaCl_2$, titrated to pH 7.4) for 30 min at 10°C in the dark. Two-electrode voltage-clamp fluorimetry experiments were performed as described previously (Van Slyke et al. 2010). Fluorescence-voltage (FV) relationships were determined from fluorescence signal amplitude at the end of the test pulse.

3.3.6 **Gating current measurement using cut-open oocyte voltage clamp**

Cut-open voltage-clamp experiments were performed using a CA-1B amplifier (Dagan, Minneapolis, MN) with the vaseline gap technique (Stefani & Bezanilla 1998). Data were digitized at 50 kHz, low-pass-filtered at 10 kHz (using an ITC-16 interface, HEKA Elektronics), and recorded using Patchmaster software (HEKA Elektronics). Gating current recordings were performed 4-6 days after oocyte RNA injection. Microelectrodes pulled from borosilicate glass had resistances of 250-500 k when filled with 3 M KCl. Extracellular solution in the top and guard chambers contained (in mM): 120 TEA-MES, 10 HEPES, 2 Ca-MES (titrated to pH 7.4). The hERG blocker terfenadine (100 µM) was added to the external solution to inhibit ionic current. Internal solution contained (in mM): 120 TEA-MES, 10 HEPES, 2 EGTA (titrated to pH 7.4). Recording bath temperature was maintained at 21 °C with a Peltier device run by a TC-10 temperature controller (Dagan, Minneapolis, MN). To achieve the cut-open configuration, 0.1% saponin was added to the bottom bath for 30-60 s to permeabilize the oocyte membrane. Upon electrical

access, saponin was washed out and replaced with intracellular solution. Oocytes expressing WT or G516C hERG were held at a holding potential of 100 mV. Oocytes expressing I663P/G516C were held at 0 mV, since gating charge movement was apparent in the negative voltage range. Capacitative transients were partially compensated with the amplifier's analog circuitry. Linear leak subtraction was performed online by using a P/-8 protocol. Typical non-leak-subtracted WT hERG gating current records are shown in Fig. S1 in the supporting material (see section 3.7), along with examples of recordings from uninjected oocytes. On-gating currents ($I_{g,on}$) were evoked by 100 ms steps from the holding potential to test potentials from -90 to +50 mV for WT and G516C channels, or from -10 to -160 mV for I663P/G516C. Off-gating ($I_{g,off}$) currents were recorded for 100 ms upon return to the holding potential. Charge-voltage (Q_{off}/V) relationships were determined by integrating $I_{g,off}$ and plotting the off-gating charge (Q_{off}) against test potential.

3.4 **Results**

3.4.1 **Introduction of the PVP motif into hERG traps the channel in the open state**

Fig. 3.1 characterizes the effects of introducing the PVP motif into the S6 helix of hERG channels, by the triple mutation I655P/F656V/G657P, on activation, deactivation and inactivation gating properties. Fig. 3.1,A-C, compare the relative open probability of WT and PVP mutant channels over a range of voltages. Typical WT currents recorded in response to depolarizing voltage steps from a holding potential of -80 mV are shown in Fig. 3.1A. Normalized peak tail current amplitudes in response to repolarization to -110 mV were used to plot the voltage-dependence of channel activation (Fig. 3.1C). These WT data show that the relative open probability is low at -80 mV (relative P_o (-80 mV) = 0.02 ± 0.01) and maximal at +40 mV, and that the relationship between voltag e and open probability is well described by a Boltzmann function ($V_{1/2}$ = -27.4 ± 1.4 mV; k = 8.7 ± 0.1 mV; n = 6). Fig. 3.1B shows typical hERG PVP currents recorded in response to voltage steps from -140 to +40 mV followed by repolarization to -110 mV (holding potential, -30 mV, see Materials and Methods). In contrast to WT channels, the normalized peak tail current amplitudes from hERG PVP channels (Fig. 3.1C) show that the mutant channels are trapped in the open state over a wide range of voltages,

passing inward current at hyperpolarized potentials (relative P_o (-110 mV) = 0.91 ± 0.02, n = 4) that did not appear to deactivate.

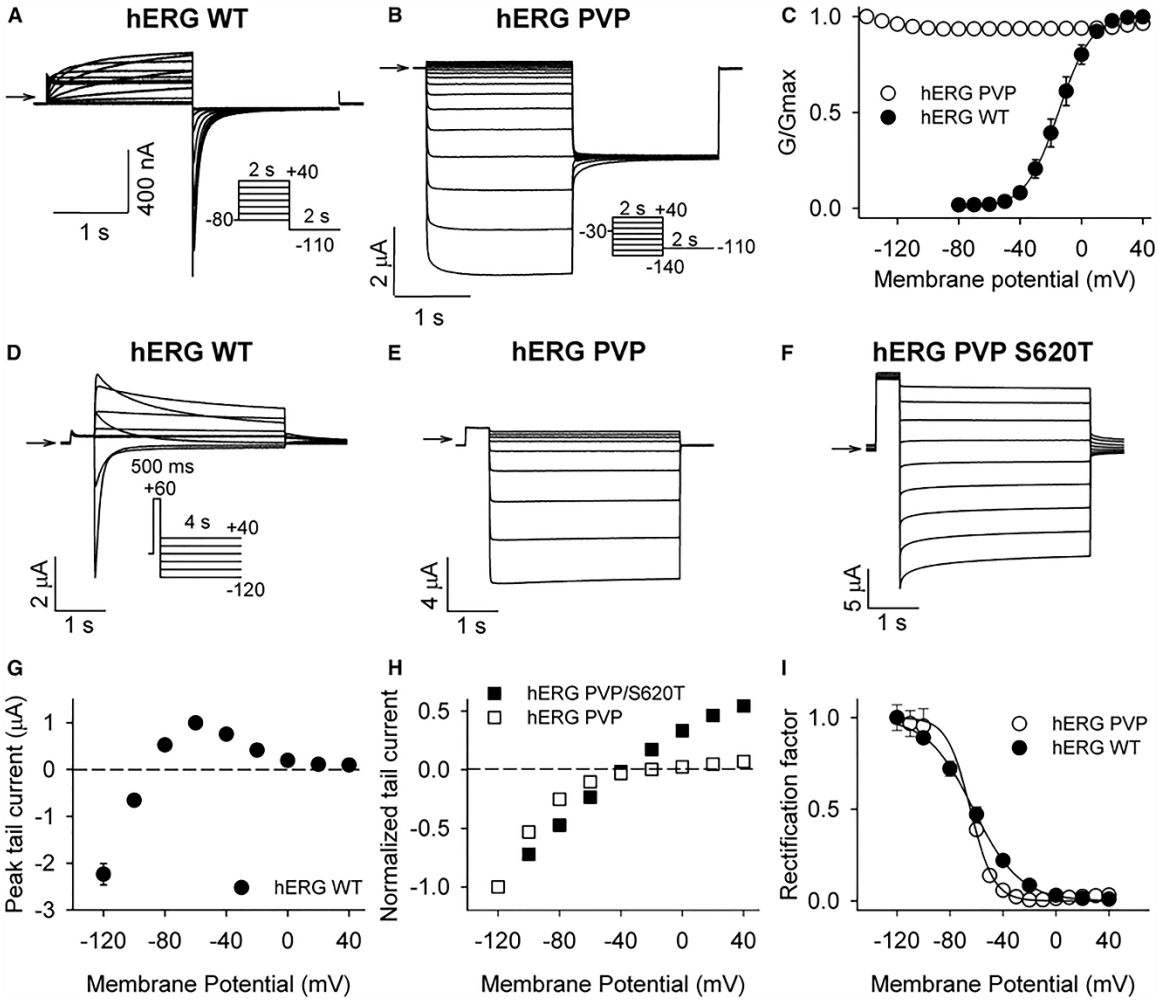

Figure 3.1 Introduction of the PVP motif perturbs the activation gate, but not inactivation.

A* and *B*,** Typical current traces from WT (*A*) and PVP mutant (*B*) channels evoked during 2 s depolarizing voltage steps from -80 mV (or from -140 mV in the case of PVP) to +40 mV (in 10 mV increments) followed by a 2 s hyperpolarizing step to -110 mV. Because PVP channels were trapped open, a holding potential of -30 mV was used as this approximated the reversal potential. WT currents were recorded in ND96 solution and from a holding potential of -80 mV. ***C, Mean WT (n = 6) and PVP mutant (n = 4) conductance-voltage (GV) relations constructed from peak tail current amplitudes. G/G_{max} reflects the relative conductance at each voltage normalized to that +40 mV. WT, but not PVP mutant, data could be fitted with a Boltzmann function, which yielded values of -27.4 ±1.4 and 8.7 ± 0.1 mV for $V_{1/2}$ and *k,* respectively. ***D-F,*** Typical current traces from WT, PVP and PVP/S620T channels evoked during 4 s repolarizing voltage steps from +40 to -120 mV applied following a 500 ms step to +60 mV to activate channels (holding potential was -80 mV for WT and -30 mV for PVP and PVP/S620T). ***G* and *H***, Fully activated WT (*G*), PVP (*H*) and PVP/S620T (*H*) instantaneous tail current voltage relations. Current amplitudes were normalized in (*H*) to compare rectification in the two constructs. (*I*) Rectification factor for WT and

PVP channels calculated from the data in *G* and *H* (see Materials and Methods) as a measure of the voltage-dependence of inactivation in each channel. Data were fitted with a Boltzmann function. $V_{1/2}$ and *k* values were -61.7 ± 2.9 and 16.4 ± 0.3 mV for WT (n = 8), and -64.6 ± 1.0 and 8.8 ± 0.9 mV for PVP (n = 3), respectively.

Fig. 3.1, D-I, suggest that the effects of the PVP substitution are limited to the open-closed equilibrium, since hERG PVP channels display strong inward rectification that is abolished by the S620T pore mutation, which inhibits inactivation. Fig. 3.1D and E show WT and PVP mutant channel tail currents in response to steps to a range of potentials following a 500 ms pulse to +60 mV to maximally activate the channels. In Fig. 3.1G and H, the peak tail current amplitude is plotted as a function of test voltage. Strong rectification was observed in both WT and PVP mutant channels. To quantify and compare rectification in the two channel types, we calculated the rectification factor (Fig. 3.1I; see Materials and Methods) from the fully activated tail current data in Fig. 3.1D and E. The data were fitted with a Boltzmann function, which described similar voltage dependencies of rectification in the two channels: the $V_{1/2}$ of WT rectification was -61.7 ± 2.9 mV compared with -64.6 ± 1.0 mV in PVP channels (although the slope factor, *k*, was altered: *k* was 16.4 ± 0.3 and 8.8 ± 0.9 mV, respectively). In WT hERG channels, rectification can be abolished by the outer pore S620T mutation, which inhibits inactivation (Ficker et al. 2001). Fig. 3.1F and H demonstrate that the S620T mutation also largely abolished rectification in hERG PVP channels. Taken together, the data shown in Fig. 3.1 indicate that inactivation is preserved in hERG PVP channels and that the predominant effect of the substitution is on the activation gate, biasing the open-closed equilibrium in favor of the open state.

3.4.2 Proline scan of S6 reveals location of the activation gate in hERG channels

We exploited the trapped-open phenotype observed following the PVP substitution within S6 to investigate the location of the pore gate. Our rationale was that the PVP mutation prevented the intracellular pore gate from closing by introducing a kink in the lower portion of S6 that reoriented the helices such that tight steric closure of the gate was prevented. Alternatively, the mutation could have disrupted the mechanical coupling of the gate with the voltage sensor, rendering it non-responsive to changes of transmembrane potential. We hypothesized that by scanning down the S6 helix with single proline mutations a point would be reached at which proline introductions would

no longer trap channels open, because the substituted site occupied a position below the gate. A similar approach was used previously to define the location of the gate in Kir3.4 inward rectifier channels, which also lack the PVP motif (Jin et al. 2002). Fig. 3.2 shows the results of the individual proline scan of S6 on hERG channel gating. Fig. 3.2A and B illustrates typical currents recorded from substitutions that trapped the hERG channel gate open (I663P) or did not markedly affect gating (L666P). It is clear that I663P channels conduct robust currents during hyperpolarization as if the pore activation gate was trapped-open and that the tail currents report maximal channel opening at all test potentials from -140 mV to +40 mV. In contrast, L666P channels were closed at -80 mV and only activated upon depolarization. As in WT channels, repolarization of L666P channels to -110 mV produced large transient tail currents indicative of channel closing during deactivation. Fig. 3.2C demonstrates mean I663P and L666P GV relations. The results from each site studied in the proline scan are summarized in Fig. 3.2D. Here, the relative open probability is plotted for WT, the PVP mutant, and each individual proline substitution, from I655P to Y667P. We found a clear pattern to the effects of proline introductions within S6, with proximal substitutions (Q664P and above) trapping channels open, as in the PVP mutant, and distal substitutions (R665P and below) preserving WT-like activation gate function (see Table S1; section 3.7). Fig. 3.2E shows a homology model of the hERG channel pore with the region scanned by proline substitutions highlighted. That proline residues at and below Arg^{665} did not alter closing, while all residues above disrupted normal gate function, strongly suggests that the position of the intracellular gate lies at Gln^{664}.

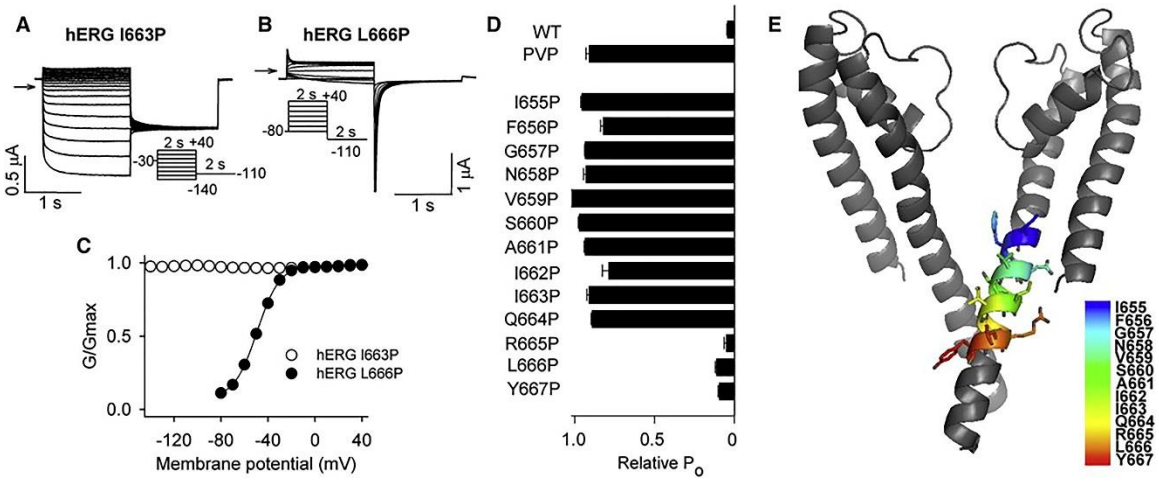

Figure 3.2 Mapping the location of the hERG channel pore gate using a proline scan.

A and ***B***, Typical hERG I663P (*A*) and L666P (*B*) current traces evoked by 2 s voltage steps from –140 mV (or from -80 mV in the case of L666P) to +40 mV followed by a 2 s repolarizing step to -110 mV. ***C,*** Mean L666P (n = 6) and I663P mutant (n=4) GV relations constructed from peak tail current amplitudes. G/G_{max} reflects the relative conductance at each voltage normalized to that +40 mV. L666P, but not I663P mutant, data could be fitted with a Boltzmann function, which yielded values of -51.2 ± 0.5 and 11.2 ± 0.3 mV for $V_{1/2}$ and *k*, respectively. ***D***, Plot of the relative open probability (P_o) for WT, the PVP mutant and each of the individual proline substitutions from I655P to Y667P (n = 5). P_o values were calculated from GV curves constructed as in Fig. 3.1C and 3.2C. For WT and WT-like gating mutants, the P_o at -80mV was used and for trapped-open mutants, the relative conductance at -110 mV was used. ***E***, Homology model of the hERG pore region (based on the MlotiK1 structure; co-ordinates from (Wynia-Smith et al. 2008) with inner S6 residues I^{655} to Y^{667} highlighted.

3.4.3 Proline substitutions in the inner S6 helix affect deactivation gating.

Fig. 3.3 presents more detailed information of the gating behavior observed in each of the proline mutant channels. In Fig. 3.3A typical traces recorded in response to a range of potentials following depolarization to +60 mV are shown. It is clear that R665P, L666P and Y667P showed WT-like deactivation properties (see also Table S1, section 3.7), whereas proline substitutions at Gln^{664} and above exhibited very little closing even with a 4 s voltage step to -110 mV. Interestingly, the extent of closing in these cases was variable. For example, deactivation was negligible in G657P, S660P and I663P channels, but more pronounced in I662P (although significant inward current remained after 4 s). In Fig. 3.3B, the percentage deactivation observed at the end of 4 s repolarizing pulses to different potentials is plotted for each mutant. Although this isochronal measurement may not reflect steady-state conditions in all mutants, these data nevertheless provide for meaningful comparison of the extent of deactivation across channels. Fig. 3.3B illustrates that R665P, L666P and Y667P channels, like WT, deactivate in a voltage-dependent fashion and that at potentials negative to -80 mV deactivation is essentially complete after 4 s. In contrast, deactivation was negligible at all test potentials in G657P, S660P and I663P channels, and the remaining mutant channels (with the exception of V659P; see below) showed some deactivation at strongly hyperpolarized potentials as if the dependence on voltage were shifted to a more hyperpolarized range. These data suggest that G657P, S660P and I663P mutations trap the hERG channel gate open, whilst I655P, F656P, N658P, A661P, I662P and Q664P strongly bias the open-closed equilibrium towards the open state. Fig. 3.3C shows the position of the S6 helix residues tested in a helical wheel representation.

Interestingly, G657, S660 and I663 lie along the same face of the S6 helix as the pore-lining Phe^{656}, and are within two turns of one another, suggesting that a proline-induced kink in this defined locale induces the most severe disruption of gate closure.

3.4.4 **Hyperpolarization activates V659P channels**

Data for deactivation of V659P channels are not represented in Fig. 3.3B, because this mutant displayed an unusual, and interesting, phenotype. These channels appeared trapped-open (Fig. 3.2D), but upon strong hyperpolarization (≤ -90 mV) we observed a slow increase in inward current as if channels were slowly activating at these voltages. Such behavior is reminiscent of the well-studied hyperpolarization-induced activation of hERG D540K channels (Ferrer et al. 2006; Tristani-Firouzi et al. 2002; Sanguinetti & Xu 1999; J S Mitcheson et al. 2000) and this prompted us to further characterize the putative slow activation observed in V659P channels. Fig. 3.4A shows typical currents recorded from hERG V659P channels in response to a protocol designed to measure the voltage dependence of the slowly activating current. In this protocol, voltage steps were applied from -140 mV to +40 mV and were followed by a step to -130 mV that allowed recovery from inactivation and quantification of the fraction of activated channels in the preceding pulse. Analysis of the current traces revealed that V659P, like other trapped-open proline mutant channels, pass inward non-deactivating current upon hyperpolarization between the holding potential (-30 mV) and -80 mV. However, unlike in any other proline mutant tested, further stronger hyperpolarization, i.e. -90 mV and more negative, induced a secondary slowly activating component of current in V659P channels that increased in amplitude with hyperpolarization such that it accounted for ~60 % of the inward current at -140 mV. To quantify this, we plotted the peak tail current amplitude recorded at -130 mV in Fig. 3.4B (*tail currents are shown on an expanded timescale in the inset to* Fig. 3.4A). The slowly activating hyperpolarization-induced increase in V659P channel conductance was well described by a Boltzmann function with values for $V_{1/2}$ and k of -99.7 ± 0.7 and 8.9 ± 0.2 mV, respectively. Fig. 3.4C shows that the hyperpolarization-activated conductance does not reflect altered recovery from inactivation, since the phenotype was preserved in hERG V659P/S620T channels in which inactivation is removed. These data suggest that the V659P mutation introduces a hyperpolarization-induced slow activation of channels, with a voltage dependence that is

similar to that created by the hERG S4-S5 linker mutation, D540K (-117 mV (Sanguinetti & Xu 1999; Tristani-Firouzi et al. 2002; Ferrer et al. 2006)).

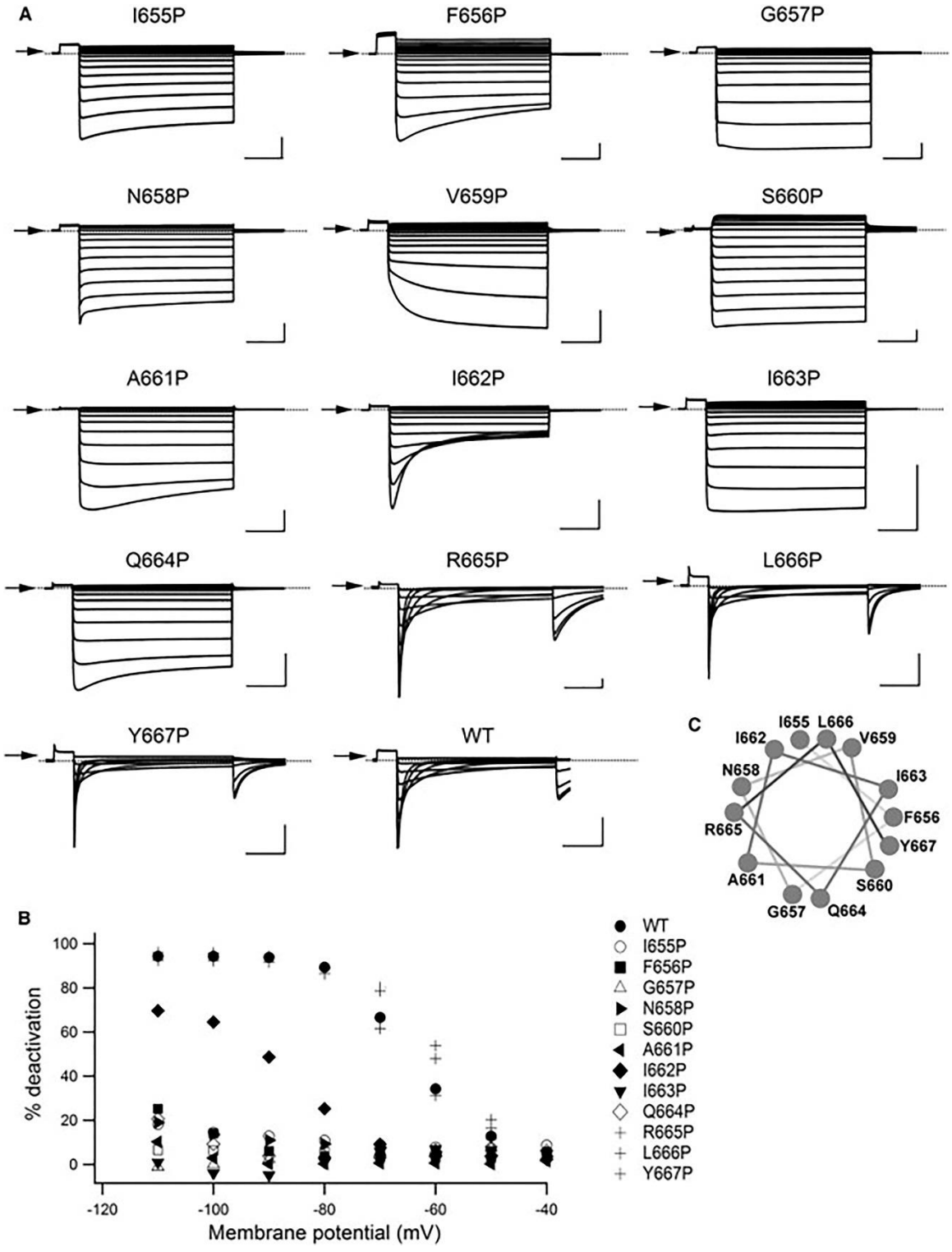
A
I655P
F656P
G657P
N658P
V659P
S660P
A661P
I662P
I663P
Q664P
R665P
L666P
Y667P
WT
C
I655
L666
I662
V659
N658
I663
F656
R665
Y667
A661
S660
G657
Q664
B
% deactivation
100
80
60
40
20
0
-120
-100
-80
-60
-40
Membrane potential (mV)
WT
I655P
F656P
G657P
N658P
S660P
A661P
I662P
I663P
Q664P
R665P
L666P
Y667P

Figure 3.3 Proline substitutions in the inner S6 helix affect deactivation gating.
A*,** Typical current traces evoked from proline substitutions within the hERG S6 (I^{655} to Y^{667}) in response to 4 s voltage steps from -110 mV to +40 mV (or from -110 to -40 mV in the case of WT, R665P, L666P, Y667P) following a 500 ms depolarization to +60 mV. In each panel, scale bars represent 2 µA of current and 1 s time. ***B*,** Plot of the percentage deactivation observed at the end of the 4 s repolarization for each mutant (n = 5-6). ***C, Helical wheel representation showing the relative position of the inner S6 helix residues tested.

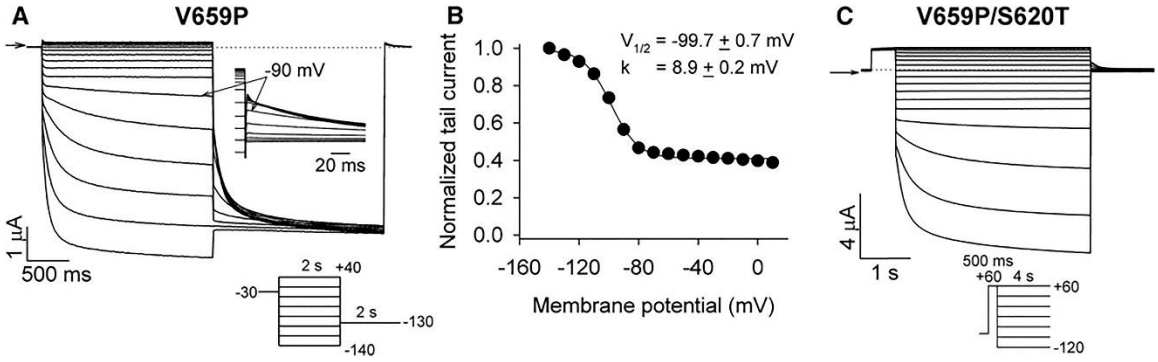

Figure 3.4 The V659P mutant is activated by hyperpolarization.
A*,** Typical hERG V569P current traces evoked from a holding potential of -30 mV in response to voltage steps applied from -140 mV to +40 mV, followed by a test pulse to -130 mV. The inset shows an expanded view of the tail currents recorded at -130 mV. ***B*,** Plot of the dependence of the instantaneous tail current amplitude (recorded at -130 mV) on the preceding voltage step. Mean peak tail current amplitudes were normalized to the peak tail current recorded following a step to -140 mV (n = 5). Data were fitted with a Boltzmann function, which yielded values for $V_{1/2}$ and *k* of -99.7 ± 0.7 and 8.9 ± 0.2 mV, respectively. ***C, Typical hERG V659P/S620T current traces evoked in response to 4 s hyperpolarizing steps from -120 to +60 mV following a 500 ms depolarization to +60 mV.

3.4.5 Proline substitutions in hERG S6 trap the activation gate open by disrupting coupling between the voltage sensor and pore

The mechanism by which voltage sensor coupling occurs with pore domains that lack the PVP motif is incompletely understood. We therefore investigated whether proline substitutions that trap open the activation gate (e.g. I663P) do so by altering the coupling between voltage sensor and pore. To assess this, we used two approaches to report on voltage sensor movement: voltage clamp fluorimetry (VCF) to provide a report on physical movements and gating current recordings using cut-open oocyte voltage clamp to provide a report on intra-membrane charge movement (Fig. 3.5). Fig. 3.5A shows typical fluorescence responses to changes in membrane voltage reported by TMRM attached at G516C in the S3-S4 linker (see Materials and Methods). This site was chosen as a site for TMRM-labelling, since it produced the most robust voltage-

dependent fluorescence response of all cysteine introductions tested in this region (G516C-L520C; data not shown). The fluorescence change upon depolarization and repolarization is slow and is consistent with previous fluorescence reports from hERG L520C (Smith & Yellen 2002; Es-Salah-Lamoureux et al. 2010; Tan et al. 2012). Fig. 3.5B compares the FV relationship constructed from peak fluorescence measurements from G516C channels with the GV relationship constructed from ionic tail current measurements. The FV and GV relationships had $V_{1/2}$ values of -27.0 ± 3.3 and -31.6 ± 1.9 mV, respectively, and *k* values of 15.8 ± 0.7 and 12.6 ± 0.7 mV. To correlate the fluorescence reports from G516C with the movement of gating charge, we recorded gating currents in both WT hERG and the G516C construct (Fig. 3.5C). Both channels displayed qualitatively similar gating current profiles that are very similar to previously reported records from WT hERG expressed in *Xenopus* oocytes (Piper et al. 2003; Piper et al. 2005; Goodchild & Fedida 2014; Abbruzzese et al. 2010). We observed pronounced fast and slow on-gating current ($I_{g,on}$) components, the latter of which contributes most significantly to total charge movement (Piper et al. 2003; Piper et al. 2005; Abbruzzese et al. 2010; Goodchild & Fedida 2014), although, like others, we could not resolve the very fast component of charge movement reported from hERG channels expressed in human embryonic kidney cells (Wang et al. 2013). Integration of off-gating charge (Q_{off}) during a 100 ms repolarization step to -100 mV allowed comparison of the voltage-dependence of gating charge displacement with that of the fluorescence report from G516C channels (Fig. 3.5D). In these experiments, the TMRM fluorophore attached at G516C in the S3-S4 linker of hERG reports reconfigurations occurring with a voltage-dependence that closely matches that of the bulk of gating charge movement, which approximates that of the GV relationship. Recently, the slow movement of the bulk of gating charge was shown to precede, in kinetic terms, opening of the pore gate (Goodchild & Fedida 2014). Therefore, as a further test of whether the fluorescence report from G516C reflects voltage sensor movement, we measured the kinetics of the fluorescence change upon depolarization and compared this with the kinetics of pore opening recorded from a standard envelope of tails experiments (see Materials and Methods). The TMRM fluorescence report from hERG G516C channels activated with a tau of 55.9 ± 3.3 ms at +60 mV (n = 5), while pore gate activation occurred with a tau of 98.6 ± 4.1 ms at +60 mV (n = 4). These data support the idea that the fluorescence report from G516C tracks the slowly moving bulk of voltage sensor gating charge.

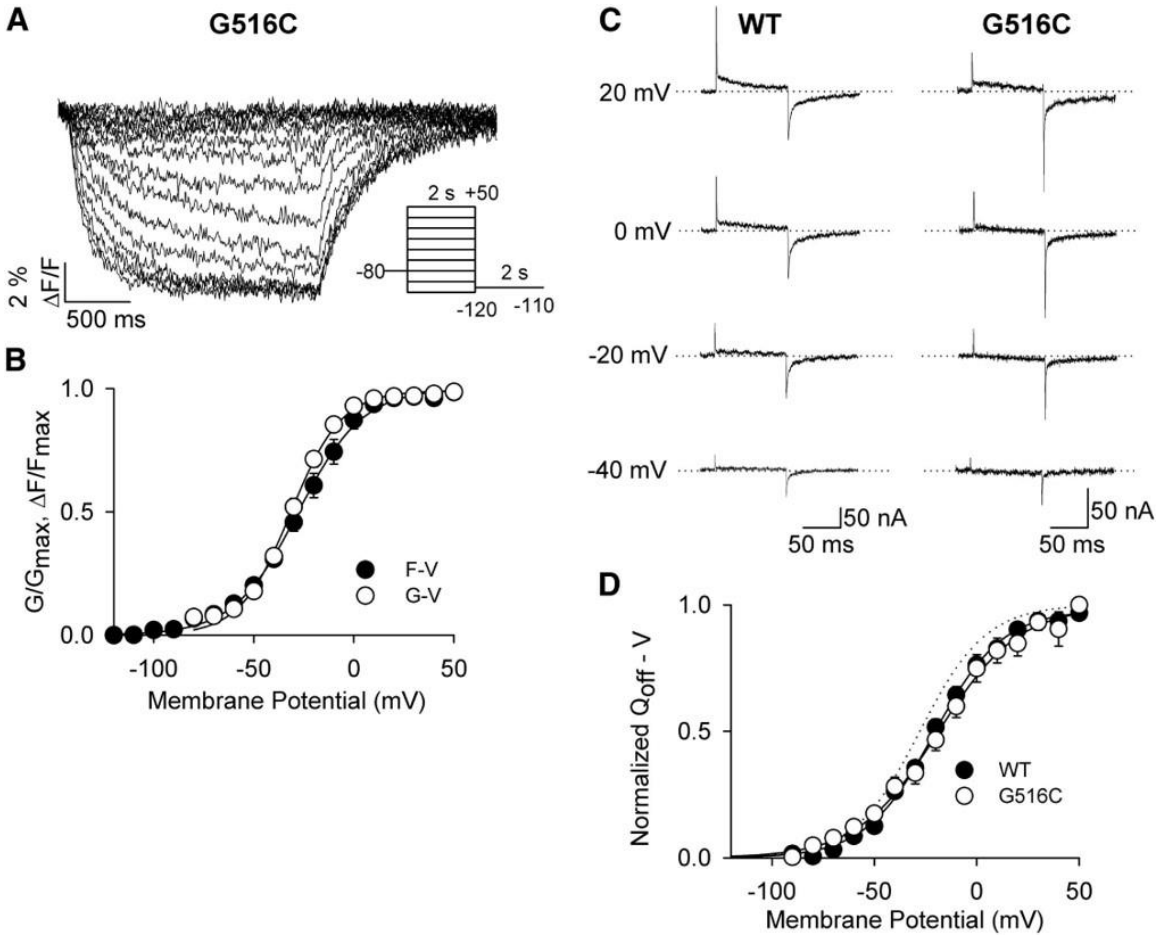

Figure 3.5 Reports of voltage sensor movement in hERG channels.
A, Typical fluorescence reports from TMRM-labeled hERG G516C channels evoked during 2 s voltage steps from -120 mV to +50 mV (holding potential -80 mV) followed by a 2 s repolarizing step to -110 mV. ***B***, Plot of mean GV and FV relations. GV data derived from peak tail current amplitudes were normalized to the peak tail current following a step to +50 mV. FV data derived from the fluorescence amplitude at the end of the 2 s depolarizing steps were normalized to the fluorescence amplitude at +50 mV. Data were fitted with a Boltzmann function. $V_{1/2}$ and *k* values were -31.6 ± 1.9 and 12.6 ± 0.7 mV for the G-V relation (n = 5), and -27.0 ± 3.3 and 15.8 ± 0.7 mV for the FV relation (n = 5), respectively. ***C***, Typical WT and G516C gating currents evoked by 100 ms pulses to the indicated test voltages from a holding potential of -100 mV. ***D***, Mean $Q_{off}V$ relationships for the two channels constructed from normalized $I_{g,off}$ records. Data were fitted with a Boltzmann function. $V_{1/2}$ and *k* values were -20.9 ± 2.4 and 17.9 ± 1.5mV for WT (n = 7), and -16.1 ± 4.4 and 21.7 ± 2.0 mV for G516C (n = 7), respectively. The dashed line represents the FV relation of hERG G516C shown in panel *B*.

We next examined voltage sensor movement in the I663P/G516C construct, which displays the trapped-open phenotype, to understand whether the introduction of a proline kink in S6 alters the conformational changes in S4 associated with channel gating. Fig. 3.6 shows fluorescence and gating current records from I663P/G516C

channels. Since gating charge movement was apparent in the negative voltage range, test pulses were applied from a holding potential of 0 mV. Consequently, for purposes of consistency, we also used a holding potential of 0 mV for the VCF experiments. Fig. 3.6A shows typical fluorescence reports from TMRM-labeled I663P/G516C channels in response to 2 s steps to voltages ranging from 0 mV to -180 mV (in -20 mV increments). The fluorescence changes from I663P/G516C channels are similar to those from G516C in that depolarization induces quenching of the fluorophore signal and hyperpolarization causes dequenching. The voltage-dependence of the fluorescence report upon hyperpolarization from 0 mV is shown in Fig. 3.6B. A Boltzmann fit yielded values of -111.0 ± 1.02 and 10.8 ± 0.3 mV for the $V_{1/2}$ and k, respectively. Gating current measurements during 100 ms hyperpolarizing steps from a holding potential of 0 mV (Fig. 3.6C) confirm that the voltage sensing domain in I663P/G516C channels is functional. $I_{g,on}$ and $I_{g,off}$ records were qualitatively similar to those of WT and G516C channels, but the voltage-dependence was shifted in the negative direction. The mean Q_{off} observed in seven oocytes is plotted against the hyperpolarizing step potential in Fig. 3.6D. We were unable to reach saturating potentials for gating charge movement in this construct due to instability of the oocyte membrane and the presence of endogenous chloride currents at potentials more negative than -160 mV and therefore the data could not be fitted with a Boltzmann function. Despite this, the observed voltage-dependence of gating charge appears to correlate reasonably well with the voltage-dependence of fluorescence changes (Fig. 3.6B).

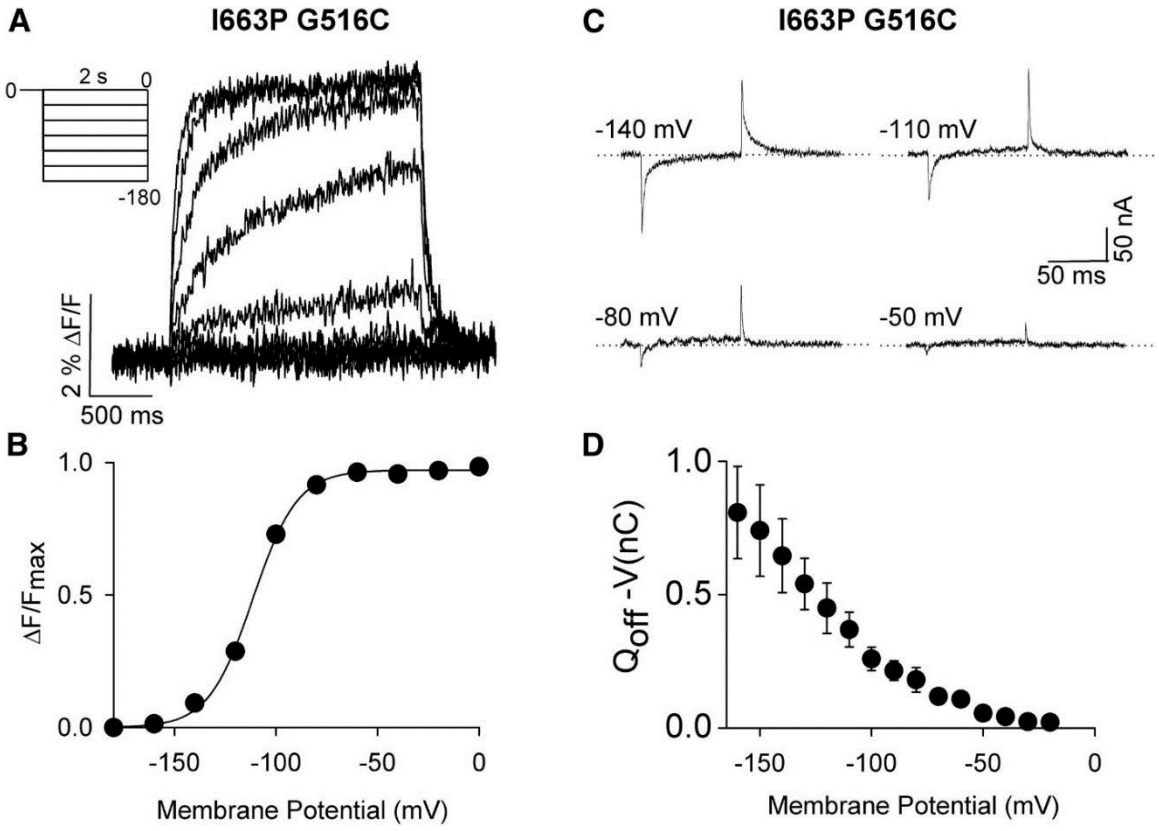

Figure 3.6 Detection of voltage sensor movement in trapped-open hERG channels.

A, Typical fluorescence reports from TMRM-labeled hERG I663P/G516C channels evoked during 2 s voltage steps from a holding potential of 0 mV to -180 mV in 20 mV increments. ***B***, Mean FV (n = 5) relation from I663P/G516C fluorescence. Data were fitted with a Boltzmann function, which yielded $V_{1/2}$ and *k* values of -111.0 ± 1.0 and 10.8 ± 0.3 mV, respectively. ***C***, Typical hERG I663P/G516C gating currents evoked by 100 ms pulses to the indicated test voltages from a holding potential of 0 mV. ***D***, Mean Q_{off}-V relationship (n = 7) constructed from integration of $I_{g,off}$ over time.

As further confirmation that the fluorescence report from I663P/G516C channels reflected conformational changes of the voltage sensor, we used Cd^{2+} as a tool, since it is known to shift the voltage-dependence of gating charge movement to more positive potentials, as well as to slow the development of on-gating charge and accelerate that of off-gating charge (Abbruzzese et al. 2010). Fig. 3.7A displays typical fluorescence reports from I663P/G516C channels in the absence and presence of 0.5 mM Cd^{2+} (close to the reported *IC50* (Abbruzzese et al. 2010)). In these experiments, a 2 s voltage step from the holding potential of -30 mV to -120 mV (P1) reported voltage sensor movement during deactivation, and this was followed by voltage steps from -180 to 0 mV (P2) to study the voltage-dependence of activation. It is clear that the fluorescence report upon hyperpolarization to -120 mV (P1) was accelerated in the presence of Cd^{2+}, consistent

with the acceleration of off-gating charge reported previously (Abbruzzese et al. 2010). Fig. 3.7B shows plots of FV relations measured from peak fluorescence amplitudes during P2, and GV relations measured with the protocol described in Fig. 3.2A, in the absence and presence of Cd^{2+}. Conductance-voltage relationships confirm that Cd^{2+} does not affect the trapped-open pore at any voltage in the range studied (-140 mV to +40 mV). Boltzmann fits of fluorescence data yielded $V_{1/2}$ and k values of -86.1 ± 2.6 and 14.4 ± 1.0 mV under control conditions and -53.7 ± 0.8 and 13.9 ± 0.8 mV with 0.5 mM Cd^{2+}. The ~30 mV right-shift of the fluorescence report in the presence of 0.5 mM Cd^{2+} is entirely consistent with the reported effects on the voltage-dependence of gating charge movement (Abbruzzese et al. 2010). Taken together, the data in Fig. 3.6 and 3.7 indicate that the fluorescence report from G516C tracks the voltage sensor movement in the trapped-open I663P channels. The data from both fluorescence and intra-membrane charge movement measurements suggest that introduction of a proline-induced kink in the S6 helix disrupts the electromechanical coupling of S4 with the pore gate such that the gate is effectively isolated and trapped in the open conformation.

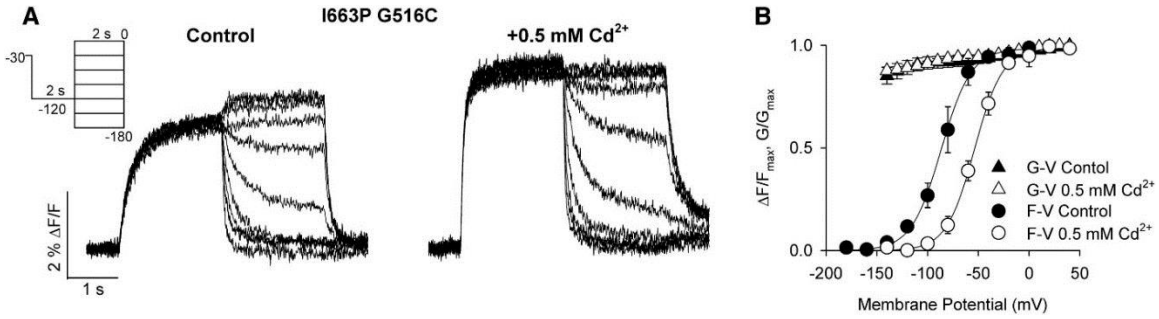

Figure 3.7 Effect of Cd^{2+} on the fluorescence report of voltage sensor movement.

A, Typical fluorescence reports from TMRM-labeled hERG I663P/G516C channels in the absence and presence of 0.5 mM Cd^{2+}. Fluorescence reports were evoked during 2 s steps to voltages from 0 to -180 mV in 20 mV increments, following a 2 s pre-pulse to -120 mV from a holding potential of -30 mV***. B,*** Comparison of mean GV and FV relations in the absence and presence of 0.5 mM Cd^{2+}. GV relations were constructed from peak tail current amplitudes as in Fig. 3.2*A* both in control (n = 4) and in the presence of 0.5 mM Cd^{2+} (n = 4), respectively. FV data were fitted with a Boltzmann function, which yielded $V_{1/2}$ and k values of -86.1 ± 2.6 and 14.4 ± 1.0 mV in control (n = 5), and -53.7 ± 0.8 and 13.9 ± 0.8 mV in the presence of 0.5 mM Cd^{2+} (n = 5), respectively.

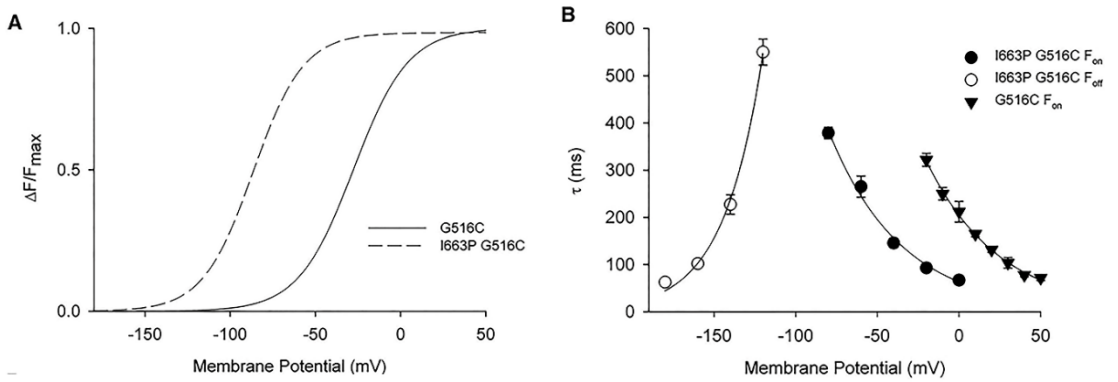

Figure 3.8 Characteristics of voltage sensor movement with disrupted coupling to the pore.

***A*,** Comparison of the voltage-dependence of the fluorescence report of voltage sensor movement in G516C channels with and without the I663P mutation, which disrupts the coupling of the voltage sensor with the pore gate. Data taken from Fig. 3.5*B* and 3.7*B* are compared on the same axes. ***B*,** Mean tau values from single exponential fits of fluorescence signals from G516C during depolarizing voltage steps in the absence and presence of the I663P mutation using: $f(t)=A*\exp(-t/\tau)+C$, where A is the amplitude of the fit, t is time, τ is the time constant of deactivation, and C is the residual current. Tau values from fits of fluorescence changes during deactivation in I663P/G516C channels are also shown.

Characterization of channels in which voltage sensor movement is uncoupled from pore opening, e.g. *Shaker* ILT, has proven valuable in understanding the mechanisms of voltage-dependency in ion channels (Smith-Maxwell et al. 1998; Smith-maxwell et al. 1998; Ledwell & Aldrich 1999; Pathak et al. 2004). Similar tools for dissociating gating steps in the activation pathway of hERG channels have, however, been less forthcoming. Fig. 3.8A plots the voltage-dependence of the fluorescence report of voltage sensor movement from G516C with and without the I663P mutation on the same axes (data from Fig. 3.5B and 3.7B).

The I663P mutation resulted in a left-shifted dependence of voltage sensor activation on membrane potential. Fig. 3.8B compares the time course of voltage sensor activation and deactivation as reported by fluorescence in I663P/G516C channels. Voltage-sensor activation tau values are also plotted for G516C channels for purposes of comparison. In both cases, voltage-sensor activation tau values report relatively slow activation. These data indicate that after accounting for the shift in the voltage-dependence, the rate of voltage sensor activation is similar in channels in which coupling with the pore is intact (G516C) or perturbed (I663P/G516C). This result suggests that the slow charge movement observed in hERG channels expressed in *Xenopus* oocytes (Fig. 3.5C and 3.6 C, see also (Piper et al. 2003; Piper et al. 2005; Abbruzzese et al. 2010; Goodchild &

Fedida 2014)) is an intrinsic property of the voltage sensing unit and does not appear to be imparted by its coupling to the pore.

3.5 Discussion

3.5.1 Location of the hERG activation gate

In this study, we have used a proline scan approach to define the location of the intracellular activation gate in hERG channels. Prolines substituted at or above Gln^{664} trapped channels in the open state, whilst substitutions below (at Arg^{665}, Leu^{666}, Tyr^{667}) showed WT-like activation and deactivation properties (Fig. 3.2 and 3.3, Table S1), suggesting that the gate is formed at Gln^{664}. A similar proline scan approach was previously used to identify the location of the intracellular activation gate in Kir3.4 inward rectifier channels (Jin et al. 2002), which, like hERG, lack the PVP motif. In Kir3.4 channels, introduction of proline residues on the outer face of S6 resulted in constitutively activated channels, whilst proline substitutions on the inner face trapped the pore closed (Jin et al. 2002). Molecular modeling suggests that introduction of proline creates a kink in the helix that may bend the lower portion away from the permeation pathway, trapping the activation gate in the open state (Jin et al. 2002). The structural consequences of proline residues within an *α*-helix are well described; avoidance of steric clashes with i - 4 (where the proline is at position i) and the loss of hydrogen bonds with i - 3 and i - 4 increase helix flexibility N-terminal to the proline favouring a kink of ~20º away from the helix axis (Barlow & Thornton 1988; von Heijne 1991; MacArthur & Thornton 1991; Cordes et al. 2002). Given this, it is reasonable to conclude that the proline substitutions in hERG (and Kir3.4) induce a kink that re-orients the S6 helix N-terminal to the introduced proline residue. Surprisingly, our results in hERG demonstrate that all proline substitutions from Ile^{655} to Gln^{664} disrupted pore gate closing suggesting that these sites lie above the steric constriction site of the gate. In contrast, our data indicate that Arg^{665}, Leu^{666} and Tyr^{667} are below the gate, because they do not impede gate closure.

In the majority of cases, a proline-induced helical kink occurs within i - 4 and i (Barlow & Thornton 1988; von Heijne 1991; MacArthur & Thornton 1991; Cordes et al. 2002). Our functional data suggest that a proline at Gln^{664} marks the boundary of gate disruption and we have interpreted this to imply that Gln^{664} forms the gate, just as the PVP-induced

kink in *Shaker*-like channels is often referred to as the activation gate. This would place the gate more than one helical turn below that described in Kir3.4 (Jin et al. 2002) and *Shaker* (Liu et al. 1997; Hackos et al. 2002) channels and is consistent with previous predictions of hERG activation gate architecture (Wynia-Smith et al. 2008). These predictions were made based on cysteine substitution data, which showed that cysteines at specific positions within S6 induced a standing conductance at hyperpolarized potentials, as if channel closure were impeded (Wynia-Smith et al. 2008). When the sites affected were mapped onto a structural model constructed using the MlotiK1 cyclic nucleotide gated channel, the data suggested that Gln^{664} may create the steric barrier that occludes ion flow. Our functional data using an alternative approach support and confirm that Gln^{664} likely forms the intracellular activation gate in hERG channels and that the gate position is lower in S6 than in other K^+ channels, such as *Shaker* and Kir3.4. Recently, a cryo-EM structure of the hERG channel was determined and showed that the activation gate is formed at Gln^{664} (Wang & MacKinnon 2017), thus supporting our functional evidence.

Proline substitutions within S6 that trapped the activation gate open did so with minimal effect on inactivation gating. However, we did observe a steeper voltage-dependence of inactivation in hERG PVP (and hERG I663P; data not shown) mutant channels compared to WT (Fig. 3.1I). These data suggest that the voltage sensitivity of inactivation may be enhanced in trapped-open channels. This requires further study, however, because inactivation in hERG channels is not strongly coupled to activation and the derivation of its unusual dependence upon voltage is unclear. For example, some evidence suggests that a micro domain of S4 imparts inactivation voltage-dependence (Piper et al. 2005), whereas other data suggest a role for the S5-P turret region (Liu et al. 2002; Torres et al. 2003; Clarke et al. 2006). More recently, more global complex rearrangements throughout the channel that are initiated by K^+ exit from the pore have been proposed to regulate inactivation in hERG channels (Wang et al. 2011). Although strong conclusions cannot be drawn from the data in this regard, they demonstrate that inactivation is conserved in the trapped-open channels.

3.5.2 **Disruption of coupling between the voltage sensor and the pore**

It is interesting to note that all proline substitutions above the gate trapped channels open, rather than producing an α-helical pattern where prolines on one face of the helix

stabilized the open gate and those on the opposite side stabilized the closed gate, as was observed in Kir3.4 (Jin et al. 2002). We interpret this to mean that any proline-induced perturbation of the S6 helix, no matter the orientation, disrupts gate closure. Although, the peculiar kinetics of mutants such as F656P, V659P and I662P suggests that individual positions of proline substitutions have specific effects on the ability of the modified pore gate to approach steric closure, i.e. a non-conducting conformation. One possibility is that proline mutant channels are trapped open because the mutations immobilize the voltage sensor in the activated 'up' configuration. In this case the voltage sensors would not respond to changes in membrane potential and channels would not close upon hyperpolarization. However, our fluorescence and gating current reports (Figs. 3.5-3.7) show intact voltage sensor movement in I663P trapped-open channels. The close correlation of our intra-membrane charge measurements and fluorescence signals in the same construct (Fig. 3.6 and 3.7) suggest that both approaches report upon voltage sensor movement. The demonstration that the fluorescence signals are also manipulated by Cd^{2+} (Fig. 3.7), well known to specifically co-ordinate with and modify voltage sensor behavior (Abbruzzese et al. 2010), provides further support for this conclusion. In addition, our fluorescence data from G516C show that the fluorescence report of voltage sensor movement occurs with a similar voltage-dependence to that of pore opening, but precedes, kinetically, opening of the pore gate. These data are consistent with a recent comparison of hERG gating currents recorded with cut-open voltage clamp (Goodchild & Fedida 2014) and whole cell patch clamp in mammalian cells (Wang et al. 2013), which showed that a prominent slow phase of voltage sensor movement carries the bulk of charge that moves ahead of, but with a voltage-dependence that is similar to that of channel opening. Finally, our data showing voltage-dependent fluorescence signals that correlate with gating currents in I663P channels, which do not show any signs of pore constriction at the activation gate strengthen the notion that fluorophore probes attached to S3-S4 linker residues report local rearrangements of the voltage sensor.

Taken together, we interpret our data to indicate that the S6 proline mutations disrupt the coupling of the voltage sensor movement to the intracellular pore activation gate. Such disruption may occur by structurally perturbing the interaction between the S4-S5 linker and lower S6 so that S4 motion is no longer electromechanically coupled to the pore, or by altering the structure of S6 so that S4-S5 linker work applied during repolarization is

not sufficient, or is not applied in the appropriate direction, to actuate closure of the permeation pathway gate.

3.5.3 Voltage sensor movement in the absence of normal coupling to the pore gate

We observed fluorescence changes and gating currents from I663P/G516C channels, in which the activation gate is trapped open, that were similar to those from G516C channels, in which normal gate function is preserved, although with altered voltage-dependence (Fig 3.8). This supports the previous suggestion (Tan et al. 2012) that fluorescence signals from the hERG S3-S4 linker report on voltage sensor conformational changes that are distinct from pore opening. Observation of the fluorescence signal characteristics in I663P channels allows scrutiny of voltage sensor movement in the absence of normal coupling to the pore. The data in Fig. 3.8B indicate that slow voltage sensor activation is an intrinsic property of the voltage-sensing unit of hERG.

3.5.4 Hyperpolarization-induced activation in V659P channels

The V659P mutant phenotype was of particular interest and warranted further investigation (Fig. 3.4). This mutant channel passed robust inward current at -80 mV, just as in other trapped open proline mutant channels; however, upon stronger hyperpolarizing steps of ≤ - 90 mV an additional slowly activating voltage-dependent conductance was evident. These data are strikingly similar to hyperpolarization-activated cyclic nucleotide gated (HCN) channel gating and are also reminiscent of the hERG D540K S4-S5 linker mutant phenotype, which re-opens into a hyperpolarized activated state (J S Mitcheson et al. 2000; Sanguinetti & Xu 1999; Tristani-Firouzi et al. 2002), as well as the hyperpolarization-activated conductance induced in NaChBac channels containing S6 proline substitutions (Zhao, Scheuer, et al. 2004). These data suggest that the substituted proline at V659 creates an additional open state that is accessed upon strong hyperpolarization ($V_{1/2}$ = -99.7 mV) and that is distinct from the open state occupied at potentials more positive than -80 mV. A similar two open-state model has been proposed for hERG D540K channels (Sanguinetti & Xu 1999).

3.6 **Conclusion**

From these studies, we conclude that the location of the intracellular gate in hERG channels is at Gln^{664}, at least one helical turn below that in *Shaker* channels. Proline introductions at or above this position disrupt the coupling of the pore gate from the voltage sensor movement, trapping channels in the open state. VCF and gating currents from these trapped-open channels suggest that voltage sensor movement is intrinsically slow in hERG channels.

3.7 **Supplementary Material**

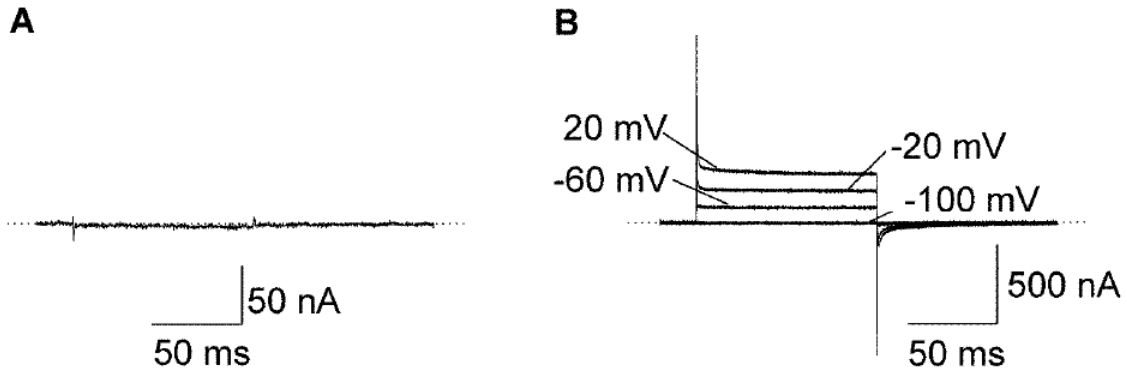

Figure S1 Non-leak subtracted gating current recordings from WT hERG channels and current recordings from un-injected oocytes.

A, Leak- and capacity-subtracted current in an un-injected oocyte in response to a +20 mV step from a holding potential of -100 mV. ***B***, Non-subtracted currents in an oocyte expressing WT hERG in response to depolarization to the indicated voltage from a holding potential of -100 mV.

Table S1: Activation and deactivation parameters of WT and gated S6 mutant hERG channels.

	Activation		Deactivation (at -110 mV)		
	$V_{1/2}$ (mV)	k (mV)	τ_{fast} (ms)	τ_{slow} (ms)	n
WT	-27.4 ± 1.4	8.7 ± 0.1	95 ± 9	650 ± 136	6
R665P	-47.1± 0.9	7.1 ± 0.4	104 ± 15	715 ± 183	5
L666P	-51.6 ± 0.5	11.2 ± 0.4	36 ± 2	306 ± 20	6
Y667P	-47.2 ± 1.7	10.9 ± 0.2	28 ± 2	222 ± 8	5

Activation parameters for WT and mutant channels were determined from Boltzmann fits to the voltage-dependence of peak tail current amplitudes. Deactivation time constants were measured from tail currents recorded in response to repolarizing voltages steps between -120 mV and +40 mV applied following a 500 mc pulse to +60 mV to fully activate channels. The decay phase of deactivating tail currents was fitted with a double exponential function: $f(t) = A_{slow} \cdot \exp(-t/\tau_{slow}) + A_{fast} \cdot \exp(-t/\tau_{fast}) + C$, where A is the amplitude of the fit, t is the time, τ is the time constant of deactivation, and C is the residual current.

Chapter 4. Stabilization of the activated hERG channel voltage sensor by depolarization involves the S4-S5 linker

This chapter describes the work published in the article listed below with some formatting changes to suit the thesis style and an additional brief overview paragraph. I contributed to most of the work presented in this chapter. I performed ionic (WT and ∆2-135 channels) and gating current (∆2-135 and G546L channels) experiments. Christina Hull and Patrick Shi performed some of the ionic current experiments in hERG mutant channels and Dr. May Cheng performed WT gating currents. I analyzed the majority of the data, and made the majority of the figures and wrote the first draft of the manuscript. I presented this work in poster format at the Biophysical Society - 2015, Baltimore, USA.

Thouta, S.*, Hull, C.M.*, Shi, Y.P., Sergeev, V., Young, J., Cheng, Y.M., T.W. Claydon 2017**.** Stabilization of the activated hERG channel voltage sensor by depolarization involves the S4-S5 linker *Biophys.J*. 112:300-312:

***These authors contributed equally to this work**

4.1 **Overview**

Having identified the position of the hERG channel gate and discovered that activation gating appeared to be dictated by intrinsically slow voltage sensor activation, I next studied the transitions of channels from the activated to the deactivated state in hERG channels. In particular, I focused on events that occur upon opening of the pore that seemed, from reported studies, to limit channel closure and might therefore be responsible for the characteristically slow deactivation gating in hERG channels. It is well described that membrane depolarization causes the voltage sensor (S4) of Kv channels to undergo conformational changes that lead to pore opening. However, recent studies in the archetypal *Drosophila* Kv channel, *Shaker*, have shown that sustained depolarization stabilizes the S4 voltage sensor in a relaxed state (Lacroix et al. 2011; Labro et al. 2012). Voltage sensor relaxation imparts mode-shift to the channel such that the voltage-dependence of activation and deactivation differ. Mode-shift due to voltage sensor relaxation was recently demonstrated in hERG channels, where relaxation of the S4 may be involved in slow deactivation and contribute to the repolarizing current during the cardiac action potential (Tan et al. 2012; Hull et al. 2014; Goodchild et al. 2015). Despite potentially orchestrating such a unique role for hERG channels, relaxation of the voltage sensor and its coupling to the pore in the control of deactivation was unclear and poorly characterized. In the present study, we have provided the first full characterization of voltage sensor relaxation in hERG channels and investigated the underlying molecular mechanisms. We revealed that prolonged depolarization of hERG channel activation resulted in a biphasic slowing of pore closure and gating charge return. These data suggested that the fast component of slowing of charge return with prolonged depolarization is associated with opening of the hERG pore gate, and a second slow component was consistent with the process of relaxation (Lacroix et al. 2011; Labro et al. 2012). We demonstrated that the slowing of charge return following depolarization is responsible for the apparent mode-shift reported in hERG channels, and, importantly, that the extent of mode-shift recorded depends on the duration of the recording protocols. By measuring activation and deactivation at steady state, we showed that the "true" mode shift of gating currents was ~40 mV, much greater than ionic currents (~15 mV). This suggested that voltage sensor return is less energetically favorable upon repolarization than pore gate closure. Lastly, experiments with an N-terminal deletion (Δ2-135) construct revealed that, whilst deletions of the N-terminus accelerated the

kinetics of gating charge return, they did not alter the stabilization of the activated voltage sensor imparted by the open-pore or the relaxation process. Instead, we showed that S4-S5 linker mutation, G546L, impeded the faster phase of voltage sensor stabilization without attenuating the slower phase, demonstrating a key role for the S4-S5 linker in communicating between the voltage sensor and the pore gate during deactivation.

4.2 **Introduction**

The human *ether-a-go-go* related gene (hERG) encodes the pore forming α-subunit of the cardiac rapid delayed rectifier potassium current, I_{Kr}. This current contributes to cardiac repolarization and consequently normal cardiac excitability and rhythm. Upon membrane depolarization, hERG channels activate slowly and inactivate rapidly, but upon repolarization, channels recover from inactivation into the open state. Slow deactivation of open channels produces a resurgent repolarizing current that aids termination of the cardiac action potential. Despite the critical role in determining cardiac excitability, the molecular basis of slow hERG channel deactivation is currently unclear.

Like other voltage-gated K^+ (Kv) channels, hERG channels are a tetrameric assembly of six α-helical transmembrane segments (S1-S6), with S1-S4 forming the voltage-sensing domain, which transitions between resting and activated states in response to membrane depolarization, and S5-S6 forming the conducting pore domain. Numerous studies support a role for the hERG S4-S5 linker in transducing voltage sensor motions to the pore gate (Ferrer et al. 2006; Hull et al. 2014; Van Slyke et al. 2010; Sanguinetti & Xu 1999; Tristani-Firouzi et al. 2002); however, recent structural (Whicher & MacKinnon 2016) and functional (Lörinczi et al. 2015) evidence suggests that voltage sensing may be coupled to the pore in hERG by an alternate mechanism that is divergent from *Shaker*-like Kv channels.

Activation and deactivation pathways in hERG, and other channels, are not symmetrical, but rather exhibit hysteresis, or mode-shift behavior, where the energy landscape during deactivation is different from that during activation. This results in a separation of the voltage dependencies of activation and deactivation such that more energy is required to return channels to the deactivated state than to activate them (Hull et al. 2014; Bezanilla 1982; Bruening-Wright & Larsson 2007; Goodchild et al. 2015; Piper et al. 2003;

Shirokov et al. 1992; Tan et al. 2012). Stabilization or immobilization of voltage sensor charges has been observed in a number of channels in response to depolarization and this can be mediated by factors outside of the voltage sensor, such as the N-type inactivation particle or other intracellular pore blockers that prevent closure of the pore gate (Bezanilla et al. 1991; Choi et al. 1993), the permeant ion species (Chen et al. 1997), or inactivation (Fedida et al. 1996; Olcese et al. 1997). Recent studies in *Shaker,* Kv1.2 and Kv3.1 channels, as well as the voltage-sensitive phosphatase, Ci-VSP, have suggested that sustained depolarization also induces an intrinsic reconfiguration of the voltage sensor into a "relaxed" state that stabilizes the activated state (Lacroix et al. 2011; Labro et al. 2012; Villalba-Galea et al. 2008). These studies propose that relaxation retards return of the voltage sensor during deactivation resulting in mode-shift behaviour. The mechanistic basis of relaxation is unclear, but its presence in WT Ci-VSP (which comprises a voltage sensor domain, but no pore domain or inactivation process, both with and without its phosphatase load) has been interpreted to indicate that relaxation is an intrinsic property of the voltage sensor (Villalba-Galea et al. 2008). In support of this idea, voltage sensor relaxation in *Shaker* is also sensitive to both the length and composition of the S3-S4 linker (Priest et al. 2013). Other studies have shown that mutations in the S4-S5 linker and S6 of *Shaker* channels, which uncouple the voltage sensor from the pore gate, also impede mode-shift behaviour, suggesting that mode-shift might originate from the mechanical load placed on the voltage sensor domain by the pore (Batulan et al. 2010; Haddad & Blunck 2011). Others have also suggested that voltage-independent gating steps might underlie mode-shift behaviour, rather than voltage sensor-mediated relaxation (Shirokov 2011). Importantly, a recent study (Labro et al. 2012) demonstrated in *Shaker* and Kv1.2 channels that stabilization of the activated voltage sensor due to pore opening can be kinetically separated from that due to relaxation of the voltage sensor. More recently, Labro et al. (Labro et al. 2015) observed a very rapid component of charge stabilization in Kv3.1 channels, which kinetically preceded pore gate opening, and was attributed by the authors to an 'ultra-fast' relaxation mechanism. These studies emphasize the presence of a stabilization of the activated voltage sensor being an intrinsic property of the voltage sensing unit, but the mechanistic basis underlying relaxation is currently illusive.

Despite the physiological importance of slow deactivation in hERG channels, relaxation of the voltage sensor and stabilization of the activated voltage sensor by the pore in the

control of deactivation has largely been overlooked in these channels. Two recent studies investigating the effects of the N-terminal domain on hERG mode-shift behaviour (Tan et al. 2012; Goodchild et al. 2015) reported differing effects leaving questions regarding the role of the N-terminus in stabilizing activated voltage sensor charges and the sequence of events that leads to retardation of deactivation and mode-shift behavior.

This study aims to better understand the control of hERG channel deactivation by characterizing hERG gating currents and ionic currents during prolonged voltage steps that allow for measurement of activation and deactivation and on- and off-gating charge under steady-state conditions. Using several mutations as tools, we define key steps in the deactivation pathway that limit voltage sensor return to produce the physiologically relevant resurgent hERG current in cardiomyocytes.

4.3 Materials and Methods

4.3.1 Molecular biology

Wild-type (WT) and mutant hERG channel constructs were prepared for expression in *Xenopus laevis* oocytes as previously described (Cheng et al. 2013).

4.3.2 Oocyte preparation and injection

Oocytes were isolated from female *Xenopus laevis* frogs and injected with WT or mutant hERG cRNA in accordance with the Simon Fraser University Animal Care Committee, and Canadian Council on Animal Care protocols and procedures and as described previously (Cheng et al. 2013).

4.3.3 Electrophysiology

Whole-cell membrane current recordings from oocytes expressing WT or mutant hERG constructs were collected using two-electrode voltage clamp with an OC-725C amplifier (Warner Instruments). Signals were digitized and acquired using a Digidata 1440 A/D convertor and pClamp 10.2 software (Axon Instruments, Foster City, CA). Recordings were performed at room temperature (20-22°C.) while oocytes were perfused with ND96 solution (in mM: 96 NaCl, 3 KCl, 0.5 $CaCl_2$, 1 $MgCl_2$ and 5 HEPES, titrated to pH 7.4

with NaOH) at 1 mL/min. Reagents were purchased from Sigma Aldrich. Recording microelectrodes were made from thin-walled borosilicate glass (World Precision Instruments) with a resistance of 0.2-2.0 MΩ when filled with 3 M KCl. Current signals were digitized at a 10 kHz sampling frequency and low pass filtered at 4 kHz (Bessel filter). Gating current recordings were collected using the vaseline gap cut-open voltage clamp technique with a CA-1B amplifier (Dagan, Minneapolis, MN) and recorded using Patchmaster software (HEKA electronics; ITC-16 interface) as previously described (Thouta et al. 2014). The hERG blocker terfenadine (20 μM) was added to both external and internal solutions to inhibit ionic current. Prior to gating current recordings, the membrane was held at -10 mV for ~30 min to aid K^+ depletion from the cytosol to reduce the driving force for residual ionic currents. Recording microelectrodes were made from thin-walled borosilicate glass with a resistance of 250-500 KΩ when filled with 3 M CsCl. Capacitative currents were compensated using the analog circuitry of the amplifier. Linear leak subtraction was performed online using a P/-8 protocol. Typical non-leak-subtracted WT hERG gating current records and examples of recordings from uninjected oocytes are shown in Fig. S2 in the supporting material (see section 4.6).

4.3.4 **Data analysis**

Data were analysed using Clampfit 10.3 (Axon Instruments), SigmaPlot11 (Systat Software, San Jose, CA), or IGOR Pro (WaveMetrics, Lake Oswego, OR) software. Steady-state conductance-voltage (GV) relationships were obtained from peak tail currents. Charge versus voltage (QV) relationships for activation and deactivation were obtained by integrating off-gating currents at -100 mV, or on-gating currents at 0 mV, respectively. Calculated integrals were normalized to the total charge moved and were plotted as a function of the preceding test pulse voltage. GV and QV curves were fitted with the Boltzmann equation: $y=1/(1+\exp(V_{1/2}-V)/k)$, where y is the relative conductance or charge movement, normalized to maximum conductance (G/G_{max}) or charge movement (Q/Q_{max}), $V_{1/2}$ is the voltage at which half maximal conductance was recorded or half of the total charge had moved, V is the test voltage and *k* is the slope factor. Ionic current deactivation and off-gating current kinetics were fitted with a double exponential function yielding fast and slow components. We report the fast time constant for ionic current deactivation since current decay at -110 mV was dominated (>85%) by the fast component, which did not change appreciably in any of our experiments. For off-gating

currents, we report the weighted tau, which expresses the fast and slow components of current decay weighted according the relative amplitude of each component, as a simplified best-approach for the quantification of the bi-exponential off-gating current (Fig. S3, see section 4.6). This approach was taken because the mechanistic basis for the two components is unclear, and because the relative amplitude of the two components changed with depolarizing step duration (Fig. S3). Unless otherwise noted, data are expressed as mean ± SEM. n represents the number of oocytes tested. In figures, arrows indicate the zero current level.

4.4 Results

4.4.1 Prolonged depolarization stabilizes the activated hERG voltage sensor

hERG channel deactivation kinetics are characteristically slow, but the mechanistic basis for this is unclear. Moreover, previous evidence suggests that hERG channels follow a different energetic pathway during deactivation from that during activation resulting in a mode-shift (Tan et al. 2012; Hull et al. 2014; Goodchild et al. 2015), but this pathway has not been characterized. We sought to better understand the deactivation pathway in hERG channels by exploring the transition of activated channels to deactivated states that results in mode-shift behaviour. Fig. 4.1 shows the effects of the duration of depolarization on the kinetics of hERG channel pore closure during deactivation. Depolarizing steps to different voltages and of variable duration were applied to activate channels followed by a test pulse to -110 mV to deactivate channels. Typical ionic current traces (Fig. 4.1A) recorded in response to this voltage protocol show that deactivation, which at -110 mV is dominated by a fast component, slowed as the duration of the depolarizing step was increased. This slowing is highlighted in Fig. 4.1B by the scaled deactivation traces recorded following 50, 500 and 15,000 ms depolarizing steps to +60 mV. Fig. 4.1C shows the time constant of channel deactivation plotted against the duration of the depolarizing pulse. These data, from experiments using three different depolarizing voltages, show that increasing the duration of the depolarization step slows hERG channel deactivation kinetics. In each case, the relationship could be fitted with a bi-exponential function with the two phases of slowing yielding τ-values of 93 ± 5 ms (relative amplitude 0.42 ± 0.03) and 4.3 ± 0.5 s (relative amplitude 0.58 ± 0.03) with a depolarization to +60 mV (n = 6).

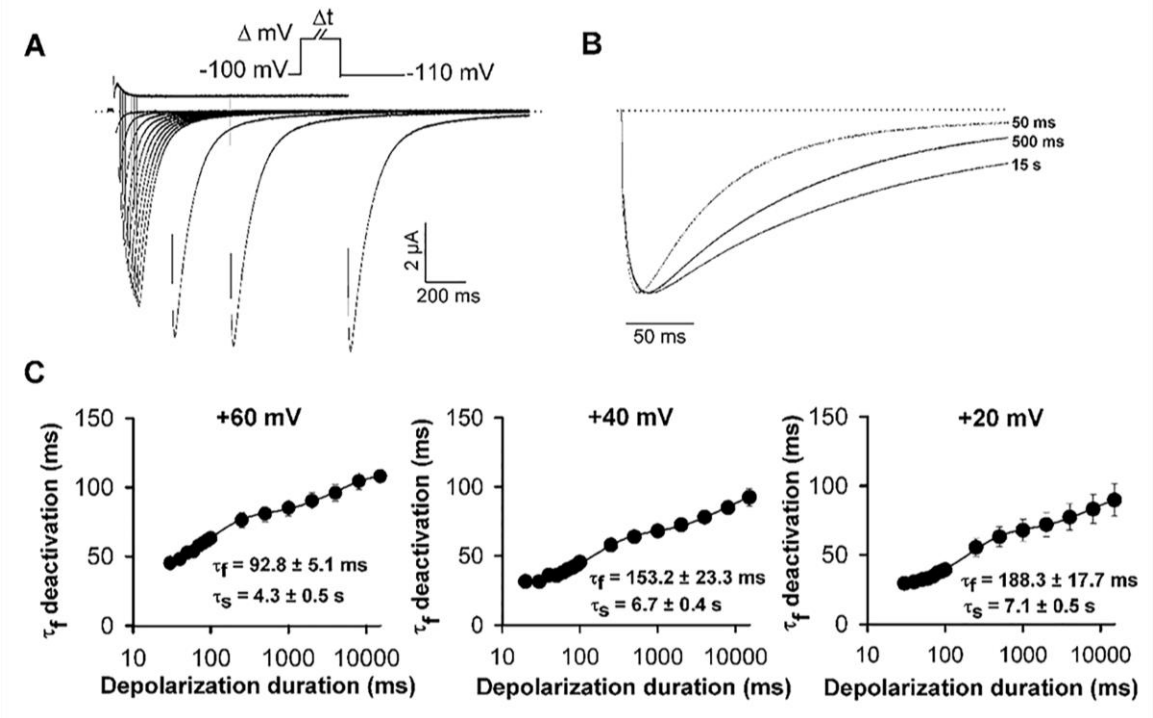

Figure 4.1 Pre-pulse dependent slowing of WT hERG channel deactivation.
A*,** Typical current traces from WT channels recorded in response to the protocol shown in which the depolarizing test pulse (+60 mV) duration (Δt, in ms) was varied. ***B*,** Superposition of normalized ionic deactivation tail current traces from *A*, recorded at -110 mV following 50, 500 and 15,000 ms steps to +60 mV to highlight the change in deactivation. ***C, Plot of mean tau fast component of deactivating current (τ_f deactivation) as a function of increasing depolarization duration at +60 mV, +40 mV, and +20 mV (n = 6, 5 and 4, respectively). Data were fitted to a double exponential function: τ_f deactivation (t) = A_{slow}*exp(-t/τ_s) + A_{fast}*exp(-t/τ_f) + C.

A similar biphasic slowing of deactivation has been observed in *Shaker* and Kv1.2 channels where the fast phase correlated with the kinetics of pore opening (Labro et al. 2012). Although the kinetics of the faster phase of hERG deactivation slowing shown in Fig. 4.1C are an order of magnitude slower than reported for *Shaker* and Kv1.2 (Labro et al. 2012), they approximated the time course of the relatively slow activation of hERG channels measured from envelope of tails experiments (Van Slyke et al. 2010). This correlation suggests that rearrangements of the hERG pore gate during activation retard pore closure. The more delayed component of deactivation slowing in Fig. 4.1C occurred in response to more prolonged depolarizations that exceeded the time course of pore opening. It is interesting that this slower deactivation delay in hERG channels occurred with kinetics that are similar to those reported in *Shaker* and Kv1.2 channels (Labro et al. 2012), despite the marked difference in the kinetic properties of both activation and inactivation in hERG channels.

To understand the mechanistic basis of slowed channel deactivation because of depolarization in hERG channels, on- and off-gating charge was measured from voltage sensor gating current recordings. Fig. 4.2A shows a typical WT hERG gating current record in response to a 250 ms step depolarization to +60 mV, which highlights the complex kinetics associated with charge transit across the membrane as has been reported previously in these channels (Piper et al. 2003; Piper et al. 2005; Thouta et al. 2014; Abbruzzese et al. 2010; Goodchild & Fedida 2014). Both on- and off-gating currents display pronounced fast and slow phases of decay. Fig. 4.2B shows on- and off-gating current recordings in response to a +60 mV depolarizing step of varying duration followed by a repolarizing step to -110 mV. Off-gating kinetics depended greatly on the duration of the depolarizing step. Fig. 4.2C shows a plot of the weighted τ of off-gating charge against depolarizing step duration, which revealed a bi-exponential relationship that could be described with tau values of 34 ± 5 ms (relative amplitude 0.54 ± 0.02) and 2.5 ± 0.4 s (relative amplitude 0.46 ± 0.02; n = 6). This dependence of the kinetics of voltage sensor return upon depolarization duration is qualitatively similar to the ionic current measurements of channel deactivation in Fig 4.1. Together, these data suggest that slowed deactivation gating in response to prolonged depolarization occurs because of stabilization of the voltage sensor in the activated configuration.

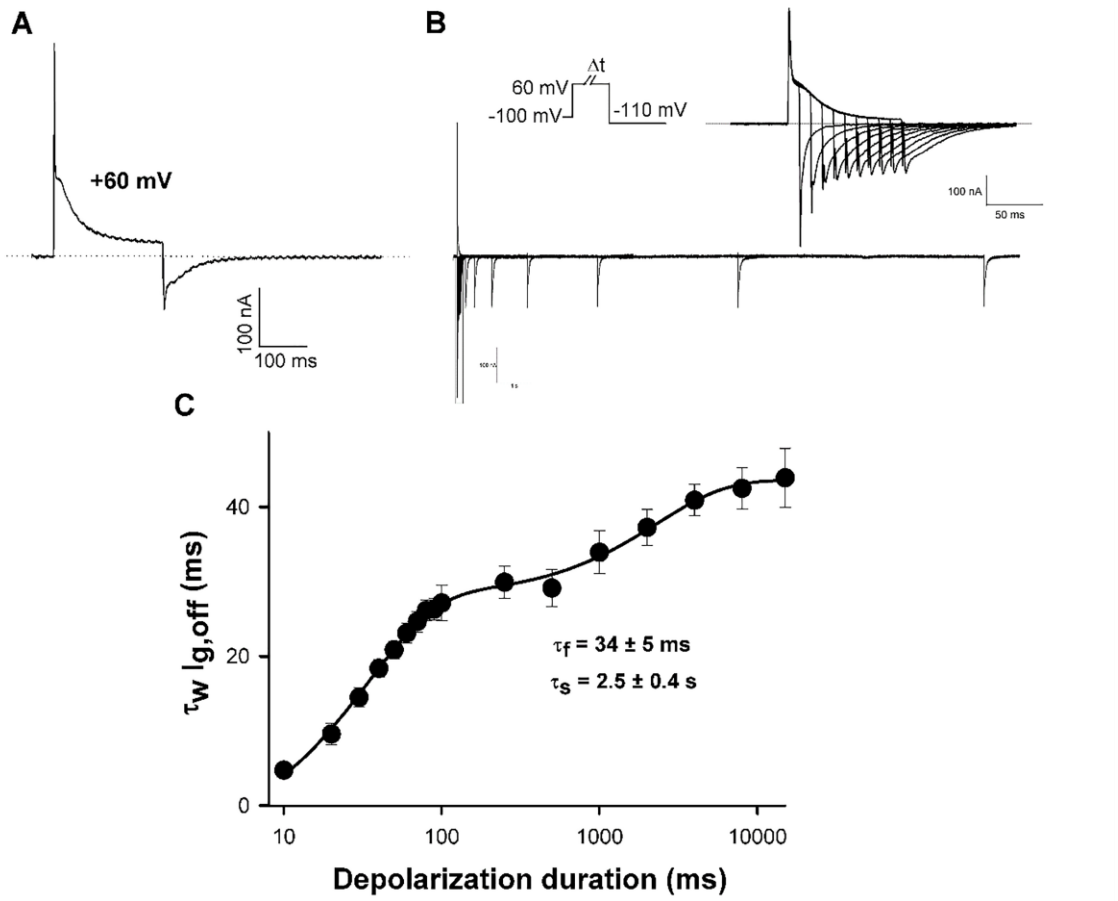

Figure 4.2 Stabilization of the hERG activated voltage sensor by prolonged depolarization.

A, Typical hERG WT gating current traces recorded in response to a 250 ms step depolarization to +60 mV from a holding potential of -100 mV. ***B*****,** Typical hERG gating current traces recorded in response to the protocol shown in which the depolarizing test pulse duration was varied. ***(Inset)****,* currents following shorter durations on an expanded time scale to highlight the off-gating current decays. ***C,*** Plot of the mean weighted tau of the off-gating current (τ_w $I_{g,off}$) as a function of increasing depolarization duration at +60 mV (n = 6). Data were fitted to a double exponential function: $\tau_w I_{g,off}(t) = A_{slow*}\exp(-t/\tau_s) + A_{fast*}\exp(-t/\tau_f) + C$.

4.4.2 Perturbation of the S4-S5 linker disturbs communication of the sate of the pore gate to the voltage sensor during deactivation

We have previously shown that sites within the S4-S5 linker profoundly influence the open-closed equilibria in hERG channels. Mutation of one site in particular, G546, left-shifts the voltage dependence of activation gating by ~50 mV, suggesting that flexibility of the connecting linker stabilizes closed channel states during activating voltage steps (Van Slyke et al. 2010). Interestingly, we found here that the G546L mutation impeded the influence of the pore on the stability of the activated hERG voltage sensor pore

during repolarization. Fig. 4.3 shows the dependence of ionic current deactivation and voltage sensor off-gating current upon the duration of the depolarizing step applied to G546L channels. The relationship between deactivation rate and depolarizing step duration was no longer biphasic in the mutant channels, but could be described by a single exponential (n = 6). This same effect was observed in measurements of the slowing of off-gating with increasing depolarizing step duration, which could also be fitted with a single exponential function (n = 5). The data show that the fast phase of slowing of pore closure and gating charge return, which in WT channels associated with channel opening, was no longer prominent in G546L channels. Significant slowing of channel deactivation in the mutant channels only occurred following durations much longer than the time course of channel opening (~43 ms (Van Slyke et al. 2010)). These data suggest that the depolarization-induced stabilization of the activated voltage sensor position by the open pore gate and voltage sensor relaxation are separable. The G546L mutation apparently impedes the faster phase of off-gating current slowing that is due to stabilization of the voltage sensor by the open pore gate while leaving the relaxation-induced stabilization of the activated voltage sensor and open pore intact.

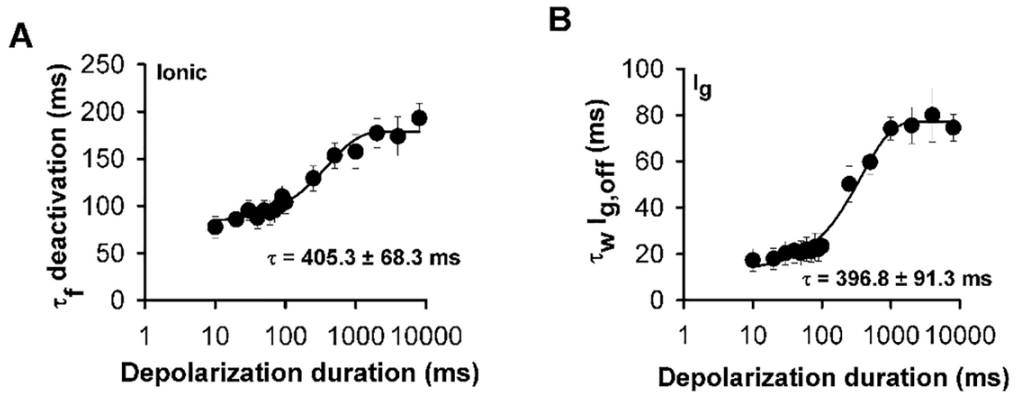

Figure 4.3 Perturbation of the S4-S5 linker impedes pore-induced stabilization of the activated voltage sensor.

A* and *B, Plot of mean tau fast component of deactivating current (τ_f deactivation) and the mean weighted tau of the off-gating current (τ_w $I_{g,off}$) as a function of increasing depolarization duration at +60 mV, respectively (*A*, n = 6; *B*, n = 5). Data were fitted to a single exponential function: τ_f deactivation (t) = $A_*\exp(-t/\tau)$ + C (*A*) and τ_w $I_{g,off}$ (t) = $A_*\exp(-t/\tau)$ + C (*B*).

4.4.3 **Characterization of mode-shift behaviour in hERG channels**

The above data suggest that opening of the hERG channel intracellular pore gate and a slower relaxation process stabilize the voltage sensor in its activated state. This process would be expected to alter the energetic landscape experienced by the voltage sensor during its return upon repolarization. Indeed, what has been called mode-shift behaviour of hERG channels has been documented in a number of studies (Piper et al. 2003; Tan et al. 2012; Hull et al. 2014; Goodchild et al. 2015). These studies present, however, differing reports of the extent of mode-shift and the effects of, for example, deletion of the N-terminus. To try to reconcile these observations, we sought to characterize and correlate mode-shift behaviour of the pore gate and the voltage sensing domain taking particular care in our attempts to make measurements as close to steady-state conditions as possible.

Mode-shift in hERG channels is prominently displayed when activation and deactivation steps of physiological duration are applied, such as in Fig. 4.4A. These data demonstrate a profound apparent mode-shift with the voltage-dependence of activation and deactivation separated by ~65 mV on the voltage axis. We sought to characterize the mode-shift behaviour of hERG channels and the effect of mutations to better understand how open channel transitions stabilize the activated voltage sensor. Understanding that the unusually slow activation and deactivation gating kinetics of hERG channels may influence the measurement of the mode-shift, we first set out to measure the “true” mode-shift from steady-state measurements, since this has not been done before. The data in Fig. 4.4B and C show that the large separation of activation and deactivation in Fig. 4.4A derives largely from the non-steady-state measurement of the intrinsically slow kinetics of these two processes and that measurement of steady-state activation and deactivation, and consequently “true” mode-shift, in hERG channels requires long step durations. Fig. 4.4B shows the dependence of the activation-voltage relationship on the duration of the depolarizing voltage step. Depolarizing steps of 8 s or more are required to measure steady-state voltage-dependence of activation (-32.8 ± 0.3 mV, n = 6), as has been described previously (Cheng et al. 2013; Viloria et al. 2000).

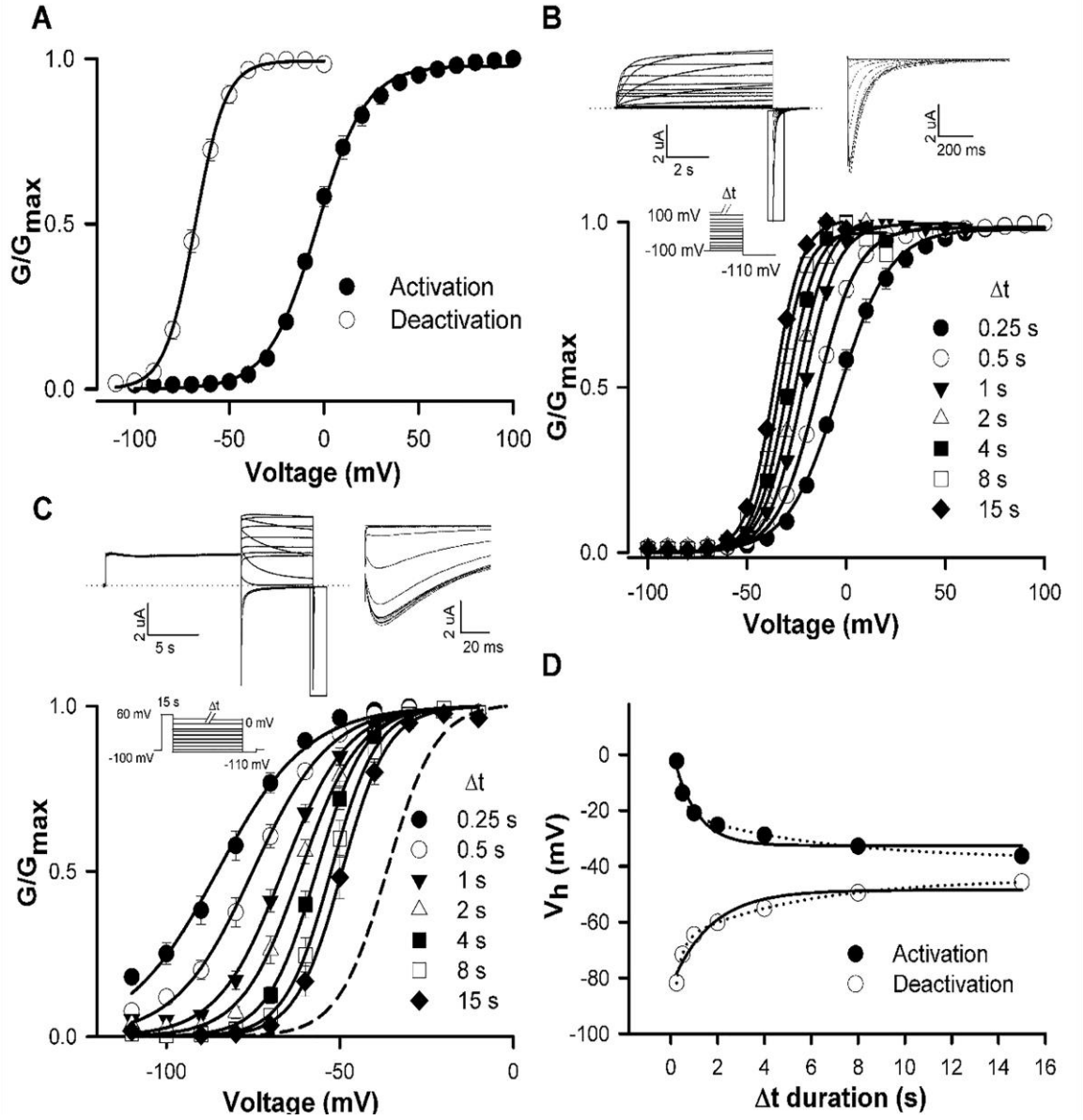

Figure 4.4 Measurement of "true" mode-shift in WT hERG channels.

A, Plot of mean WT hERG GV relationships for activation and deactivation measured with voltage steps of physiological duration. For activation, oocytes were held at -100 mV and subjected to 250 ms depolarizing steps to +100 mV in 10 mV increments followed by a repolarizing voltage step to -110 mV. For deactivation, oocytes were held at -100 mV and subjected to a 250 ms depolarizing step +60 mV and then to 750 ms voltage steps to -110 mV in 10 mV increments followed by a repolarizing voltage step to -110 mV. Data were fitted with a Boltzmann function. ***B* and *C***, *Top,* Typical WT ionic current traces recorded during protocols to measure activation (*B*) and deactivation (*C*) at steady-state. For activation, oocytes were held at -100 mV and subjected to 8 s voltage steps to +60 mV in 10 mV

increments, followed by a 3.5 s repolarizing step to -110 mV. For deactivation, oocytes were held at -100 mV and subjected to a 15 s depolarizing step +60 mV followed by 8 s repolarizing voltage steps from -110 mV to +40 mV in 10 mV increments and then a 100 ms repolarizing step to -110 mV. *Inset* shows currents on an expanded time scale to highlight the peak tail current. *Bottom,* Plot of WT hERG mean GV relationships for activation (*B*) and deactivation (*C*) constructed from normalized peak tail currents (n = 6) following the different pre-pulse durations. For both activation and deactivation, the protocols were repeated in the same cell with different Δt durations and the mean $V_{1/2}$ and *k* values were obtained by fitting each data set to a Boltzmann function (see Table 4.1). These data demonstrate the approach towards steady-state activation and deactivation GV relations with increasing Δt duration. The dashed line in *C* represents the steady-state activation GV relation of WT hERG shown in *B*. ***D***, Relationship between $V_{1/2}$ of activation and deactivation with the Δt duration, as determined from the data presented in *B* and *C*. Data are fitted with extrapolated single (solid line) or double (dotted line) exponential functions. Single exponential extrapolated steady-state values for activation and deactivation $V_{1/2}$ were -33 and -48 mV. The equivalent values for double exponential fits were -38 and -45 mV, respectively.

Fig. 4.4C shows that slow hERG channel deactivation also influences measurement of the $V_{1/2}$ of the voltage-dependence of deactivation. Using a 15 s depolarizing step to fully activate channels, repolarizing voltage steps to different voltages were applied for different durations. The data show that allowing slow deactivation to reach steady-state shifted the voltage-dependence of deactivation to more depolarized potentials (see Table 4.1 for Boltzmann fit parameters). Fig. 4.4D plots the dependence of the $V_{1/2}$ of the activation and deactivation voltage relationships on step duration. These data demonstrate that recording activation and deactivation at steady-state greatly alters the measured report of the mode-shift of the WT channel. Extrapolated single exponential fits of the data approximate that the “true” mode-shift in hERG channels is ~15 mV. Double exponential fits yielded a value of ~7 mV and the better fit suggests that although the single exponential provides a reasonable estimate, longer durations may be required to determine the exact value of the “true” mode-shift. This approximated mode-shift represents the separation of the voltage-dependencies of activation and deactivation that is not dependent upon the step duration. These data highlight the influence of voltage step duration on the reporting of the voltage-dependence of both activation and deactivation gating in hERG channels, and consequently, the extent of mode-shift.

Fig. 4.5 shows measurement of the “true” mode-shift of gating charge movement in hERG channels. Fig. 4.5A shows on-gating charge-voltage relationships constructed from recordings of the off-gating current during repolarization from depolarizing steps of different duration. The $V_{1/2}$ of steady-state on-gating charge movement was -42.9 ± 1.3 mV (n = 3). The dependence of the $V_{1/2}$ of the off-gating charge movement on step duration is shown in Fig. 4.5B and is summarized in Fig. 4.5C (see Table 4.2 for

Boltzmann fit parameters). Extrapolated single and double exponential fits of the dependence of the $V_{1/2}$ of on- and off-gating charge on step duration show that the approximated “true” voltage sensor mode-shift is ~40 mV. This is much greater than the ionic current mode-shift (~15 mV). Fig. 4.5D demonstrates this by directly comparing the steady-state voltage dependence of ionic current activation and deactivation on the same axis as the steady-state voltage-dependence of on- and off-gating charge movement. The plot shows that upon repolarization the hERG channel pore closes at voltages that do not return significant charge. For example, at -50 mV, the open probability of the pore is reduced by approximately 80% when only roughly 20% of charge returns. These data show that, upon repolarization, pore closing is more energetically favourable than the return of the gating charges.

4.4.4 The role of the N-terminus in stabilizing the activated voltage sensor and mode-shift

The N-terminus is well known to modify hERG deactivation gating by slowing pore closure; however, the underlying mechanism is unclear. Some insight came from two recent studies (Tan et al. 2012; Goodchild et al. 2015) which investigated the role of the N-terminus in mode-shift behaviour; however, the reported effect of N-terminal deletion on mode-shift differed. We reasoned that these findings might be reconciled based on our findings above that the apparent mode-shift is influenced by the recording step duration. To test this, we measured mode-shift behaviour in channels lacking the distal N-terminus (∆2-135) with step durations that were long enough to record activation and deactivation at steady-state. We also measured the effect of N-terminal deletion on stabilization of the activated voltage sensor.

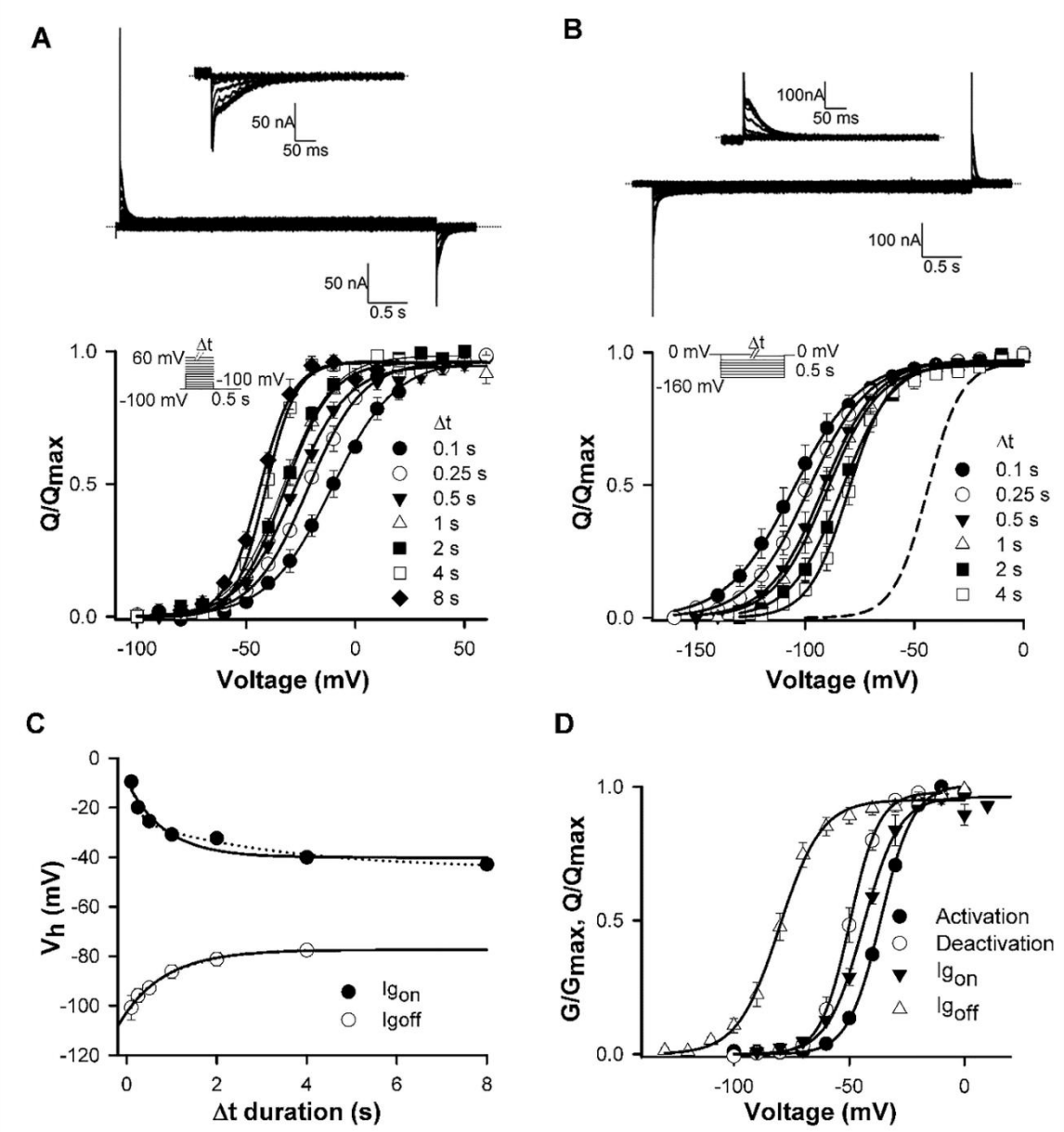

Figure 4.5 Uncoupling of the voltage sensor from the pore during deactivation. ***A*** **and** ***B*****,** ***Top****,* Typical WT on-gating (*A*) and off-gating (*B*) currents. For on-gating currents, oocytes were held at -100 mV and subjected to 4 s voltage steps to +60 mV in 10 mV increments. Gating charge moved was determined from the integral of the off-gating current measured during the 500 ms step back to -100 mV. ***A*****,** ***inset,*** Off-gating currents are enlarged for clarity. For off-gating currents, oocytes were held at 0 mV and subjected to 4 s repolarizing steps to -160 mV in 10 mV increments. Gating charge moved was determined from the integral of the on-gating currents measured during the 500 ms step back to 0 mV. ***B*****,** ***inset*****,** On-gating currents are enlarged for clarity. ***Bottom,*** Plots of mean WT hERG QV relationships for on-gating (*A*) and off-gating (*B*) measured with varying depolarizing or repolarizing pulse durations (Δt). For both on- and off-gating, mean $V_{1/2}$ and *k* values were obtained by fitting to a Boltzmann function (see Table 4.2). The dashed line in *B* represents the steady-state on-gating QV relation shown in *A*. ***C,*** Relationship between $V_{1/2}$ of on- and off-gating with Δt duration, as determined from *A* and *B*. Data are fitted with extrapolated single (solid line) or double (dotted line) exponential functions.

Single exponential extrapolated steady-state values for on- and off-gating $V_{1/2}$ were -40 and -77 mV. The equivalent values for double exponential fits were -45 and -77 mV, respectively. ***D*,** Summary of the steady-state GV and QV relations highlighting the uncoupling of voltage sensor return from pore closure.

Table 4.1 Activation and Deactivation GV Boltzmann fit parameters for WT hERG channels with different depolarizing step durations (Δt)

	Activation GV			Deactivation GV		
Δt (s)	$V_{1/2}$ (mV)	*k* (mV)	n	$V_{1/2}$ (mV)	*k* (mV)	n
0.1	-	-	-	-	-	-
0.25	-2.2 ± 1.6	13.5 ± 2.3	6	-81.8 ± 2.0	11.8 ± 0.4	6
0.5	-13.7 ± 0.8	10.1 ± 1.7	6	-71.6 ± 0.8	9.8 ± 0.6	6
1	-20.8 ± 0.2	8.8 ± 1.3	6	-64.6 ± 0.4	7.7 ± 0.5	6
2	-25.3 ± 0.5	8.1 ± 1.2	6	-60.1 ± 0.6	6.6 ± 0.4	6
4	-28.8 ± 0.8	7.7 ± 1.2	6	-55.0 ± 0.4	6.2 ± 0.4	6
8	-32.8 ± 0.3	7.1 ± 1.2	6	-49.5 ± 0.5	5.7 ± 0.4	6
15	-36.3 ± 0.4	6.8 ± 1.1	6	-45.7 ± 0.4	5.5 ± 0.4	6

Table 4.2 $I_{g,\,on}$ and $I_{g,\,off}$ QV Boltzmann fit parameters for WT hERG channels with different depolarizing step durations (Δt)

	Ig, on QV			Ig, off QV		
Δt (s)	$V_{1/2}$ (mV)	*k* (mV)	n	$V_{1/2}$ (mV)	*k* (mV)	n
0.1	-9.5 ± 2.3	15.5 ± 0.5	5	-100.8 ± 5.0	15.5 ± 0.7	6
0.25	-19.9 ± 1.3	14.1 ± 0.8	7	-95.9 ± 2.7	15.2 ± 0.5	6
0.5	-25.5 ± 1.4	14.7 ± 1.4	7	-92.8 ± 2.2	12.3 ± 0.7	7
1	-30.9 ± 1.4	11.8 ± 0.5	7	-86.2 ± 2.8	12.7 ± 1.0	7
2	-32.3 ± 1.4	12.0 ± 1.3	6	-81.2 ± 2.7	12.0 ± 1.4	4
4	-40.0 ± 1.6	7.6 ± 0.9	4	-77.5 ± 2.3	10.1 ± 1.2	7
8	-42.9 ± 1.4	8.4 ± 0.4	3	-	-	-
15	-	-	-	-	-	-

Fig. 4.6, A-C, demonstrates the measurement of "true" mode-shift in hERG Δ2-135 channels. These data show that, as in the case of the WT channel, the apparent mode-shift is highly dependent upon the voltage step durations used for recording both activation and deactivation (see Table S1 (section 4.6) for Boltzmann fit parameters,). The "true" mode-shift in hERG Δ2-135 channels is ~6 mV, which is similar to the approximated value in WT channels. These data suggest that the N-terminal domain does not play a significant role in mode-shift behaviour. Consistent with this, Fig. 4.6, D-G shows the effect of depolarizing step duration on ionic current deactivation and gating charge return in hERG Δ2-135 channels. The data show that both channel deactivation

and gating charge return were faster in hERG Δ2-135 channels compared with WT hERG channels. However, most interestingly, both measures were slowed by increased depolarization step durations in a biphasic manner. Channel deactivation was slowed with τ_{fast} and τ_{slow} values of 59.8 ± 4.5 ms (relative contribution 0.37 ± 0.02) and 2.6 ± 0.6 s (relative contribution 0.63 ± 0.02), respectively (n = 5). Gating charge return was slowed with tau fast and tau slow values of 12.7 ± 1.4 ms (relative contribution 0.26 ± 0.02) and 4.3 ± 1.5 s (relative contribution 0.73 ± 0.02), respectively (n = 12). These data demonstrate that, as in the case of WT channels, depolarization slowed voltage sensor return in a biphasic manner with a fast phase of slowing of both charge return and channel deactivation that occurred over a similar time-frame to channel opening (hERG Δ2-135 activation τ = 73 ± 7 ms at +60 mV, n = 6). These data show that while deletion of the N-terminus accelerates the kinetics of voltage sensor return, both open pore- and relaxation-induced stabilization of the voltage sensor are preserved in hERG channels lacking the N-terminus. These data show that voltage sensor stabilization in response to depolarization is preserved in hERG channels lacking the N-terminus.

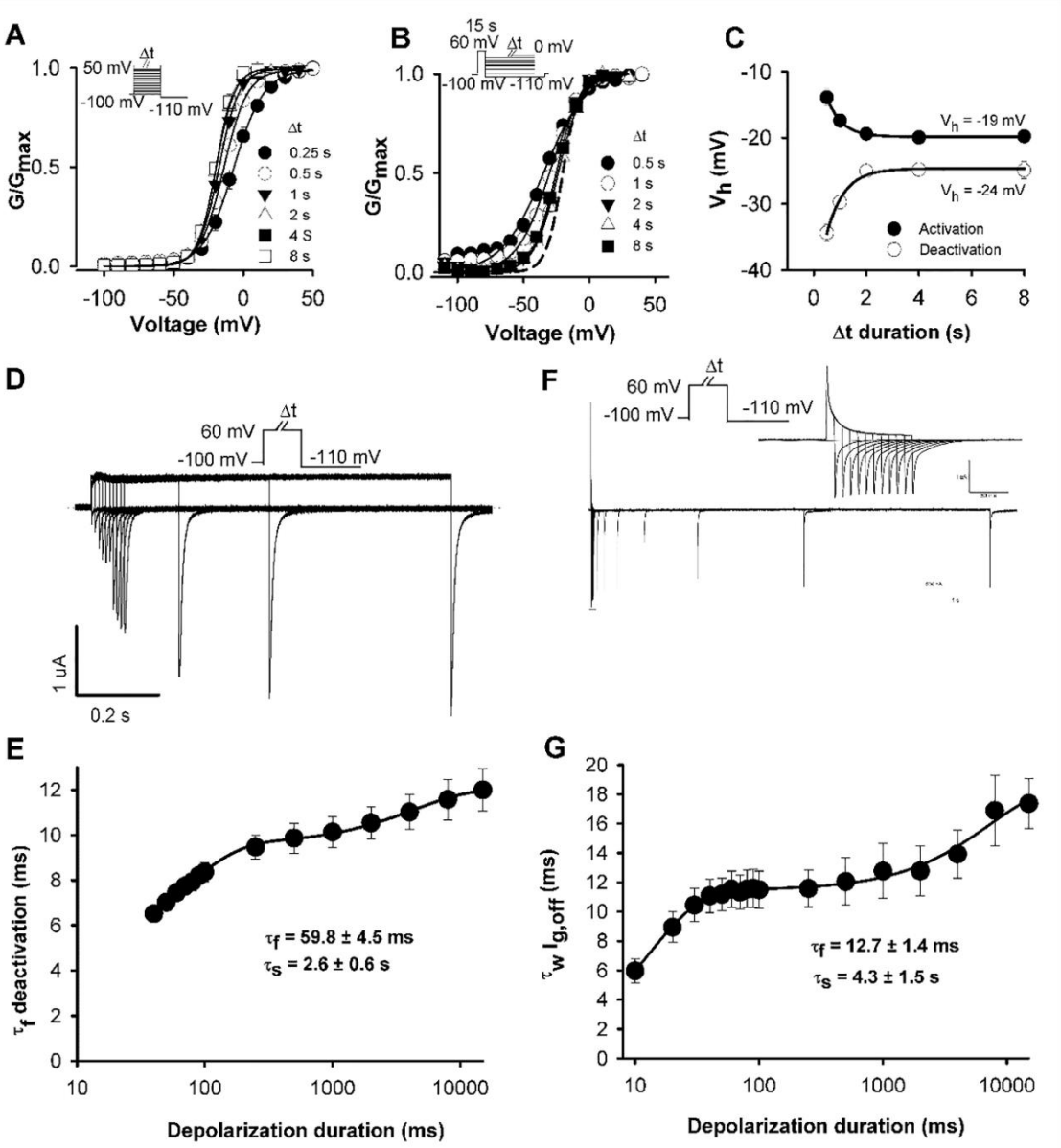

Figure 4.6 Effect of deltion of the distal N-terminus on voltage sensor stabilization.

A* and *B, Plot of mean hERG Δ2-135 GV relationships for activation (*A*) and deactivation *(B*) constructed from normalized peak tail currents with different prepulse durations (n = 5). Activation and deactivation were recorded in the same cells with different Δt durations and the mean $V_{1/2}$ and *k* values were obtained by fitting each data set to a Boltzmann function (see Table S2, section 4.6). These data demonstrate the approach towards steady-state activation and deactivation GV relations with increasing Δt duration. The dashed line in B represents the steady-state activation GV relation of hERG Δ2-135 in *A*. ***C,*** Relationship between $V_{1/2}$ of activation and deactivation with the Δt duration, as determined from the data in *A* and *B*. Data are fitted with an extrapolated exponential function. ***D* and *F*,** Typical ionic (*D*) and gating *(F*) current traces from hERG Δ2-135 channels recorded in response to the protocol shown in which the depolarizing test pulse duration was varied. Inset in *F* shows currents on an expanded time scale to highlight the off-gating current decay. ***E* and *G***, Plot of the mean tau fast component of deactivating ionic

current (τ_f deactivation) and the mean weighted tau of the off-gating current ($\tau_w I_{g,off}$) as a function of increasing depolarization duration at +60 mV, respectively. Data were fitted to a double exponential function: τ_f deactivation (t) = $A_{slow*}\exp(-t/\tau_s) + A_{fast*}\exp(-t/\tau_f) + C$ (*E*) and $\tau_w I_{g,off}$ (t) = $A_{slow*}\exp(-t/\tau_s) + A_{fast*}\exp(-t/\tau_f) + C$ (*G*).

4.4.5 Accelerated deactivation kinetics result in an apparent reduction in mode-shift

The data in Fig. 4.4 and 4.5 show that incomplete measurement of channel deactivation and gating charge return in WT hERG channels produces an apparent mode-shift behaviour that does not reflect “true” mode-shift behaviour. We reasoned that fast deactivation in channels lacking the N-terminus allows more complete measurement of deactivation and creates an apparent loss of mode-shift when compared with WT channels in which deactivation is slower and requires voltage steps of 8 s or more to reach steady-state (Fig. 4.4). Consistent with this, when standard voltage step durations were used, measurements of the voltage-dependence of activation and deactivation in WT channels resulted in an overestimation of the mode-shift (Table 4.3). In numerous mutant channels, fast deactivation gating meant that the voltage-dependence of deactivation was closer to steady-state and resulted in an apparent reduction in mode-shift behaviour. This was the case for mutations made at sites throughout the hERG channel, such as R4D and R5E in the N-terminus, D456A in S2, E480R in the S2-S3 linker, D509A in S3, R537K, R541G, Y542G and E544G in the S4-S5 linker. Table 4.3 shows that in each of these cases, the apparent reduction in mode-shift behaviour could be explained by accelerated kinetics of channel deactivation.

4.4.6 S3-S4 linker does not influence stabilization of activated hERG channel states

Our data in hERG channels are consistent with previous studies in other Kv channels in that they suggest that a slow voltage sensor stabilization or relaxation occurs due to prolonged depolarization. Previous studies suggest that this property is intrinsic to the voltage sensor and one study showed that the S3-S4 linker plays a role in stabilizing the activated configuration of the voltage sensor in response to prolonged depolarization in *Shaker* channels (Priest et al. 2013). This study predicted greater voltage sensor stabilization in channels with shorter S3-S4 linker lengths, although linker composition, such as the negative charge cluster, EEED, were also suggested to play a role. To investigate the role of the relatively short hERG S3-S4 linker and its composition in the

stabilization of the activated state, mode-shift was measured in WT hERG channels and compared with mutant channels in which the short, 9-residue, S3-S4 linker was replaced with the longer, 31-residue, linker from *Shaker* channels (hERG/Sh), or in which the 9 residues of the native hERG S3-S4 linker were replaced with glycine amino acids (hERG/9G; Fig. 4.7A). Fig. 4.7B shows mean activation and deactivation-voltage relationships for each of these constructs (see Table S3 for Boltzmann fit parameters). These experiments were designed with non-steady-state pulse durations so that a loss of mode-shift because of linker perturbation would be detectable compared to the mode-shift recorded in WT channels. The mean mode-shift that we recorded was –31.3 ± 2.0 mV (n = 5), –34.5 ± 1.2 mV (n = 5), and -28.8 ± 1.1 (n = 4) mV in WT, hERG/Sh and hERG/9G channels, respectively. Given this lack of effect of the S3-S4 linker, a putative role of the S1-S2 linker in mediating voltage sensor stabilization was also investigated. Truncation of the majority of the S1-S2 linker produced non-functional channels, but channels in which a negative charge cluster, ETEE, in the S1-S2 linker were neutralized to glutamine residues (Fig. 4.7C) were functional. The mean mode-shift in ETEE/QQQQ mutant hERG channels (Fig. 4.7D) was –24.5 ± 2.9 mV (n = 5), which was not significantly different from that in WT channels –24.1 ± 4.5 mV (n = 5). These data suggest that the extracellular S3-S4 linker does not play a role in stabilizing the activated hERG voltage sensor configuration as has been shown in other channel types, indicating that other regions within the hERG voltage sensing unit that are yet to be identified may contribute to the mode-shift phenomenon.

Table 4.3 Correlation of apparent mode-shift with deactivation kinetics

	Activation GV			Deactivation GV			Mode-shift		Deactivation $\tau - \tau_f$ (ms)	
	$V_{1/2}$ (mV)	k (mV)	n	$V_{1/2}$ (mV)	k (mV)	n	$V_{1/2}$ (mV)	n	-110 mV	n
WT	-22.8 ± 1.1	10.8 ± 0.7	9	-54.2 ± 1.6	7.8 ± 0.4	9	-31.4 ± 2.1	9	94.8 ± 9.3	8
R4D	-14.9 ± 1.0	9.2 ± 0.3	5	-22.8 ± 1.1	7.5 ± 0.8	5	-7.8 ± 1.6	5	27.5 ± 2.5	4
R5E	-17.6 ± 2.0	9.6 ± 0.3	5	-30.1 ± 1.4	7.8 ± 0.5	5	-12.5 ± 1.0	5	47.9 ± 5.7	4
D456A	-1.0 ± 1.2	7.5 ± 0.4	5	-7.0 ± 1.0	7.5 ± 0.6	5	-6.0 ± 0.9	5	35.8 ± 2.5	5
E480R	-2.8 ± 0.6	10.0 ± 0.2	5	-14.0 ± 1.7	8.4 ± 0.5	5	-11.8 ± 2.3	5	47.0 ± 3.5	5
D509A	14.3 ± 1.5	11.0 ± 0.2	4	8.3 ± 0.7	9.9 ± 0.7	4	-6.0 ± 1.4	4	22.0 ± 2.0	4
R537K	-8.6 ± 3.7	8.0 ± 0.3	6	-9.8 ± 3.7	8.3 ± 0.4	6	-1.2 ± 0.7	6	55.2 ± 2.3	5
R541G	-35.2 ± 1.5	13.2 ± 0.5	5	-41.7 ± 1.2	11.7 ± 0.4	5	-6.5 ± 0.6	5	42.8 ± 1.6	7
Y542G	-4.9 ± 2.1	14.8 ± 1.0	5	-14.9 ± 1.4	11.1 ± 0.7	5	-10.0 ± 1.6	5	12.9 ± 0.5	9
E544G	-22.4 ± 0.5	8.5 ± 0.1	7	-25.3 ± 0.8	7.5 ± 0.2	7	-2.9 ± 0.6	7	18.9 ± 0.6	5

Activation GV relations were collected from oocytes held at -80 mV and subjected to 2 s depolarizing steps to +50 mV in 10 mV increments followed by a 2 s step to -110 mV. Deactivation GV relations were collected from oocytes held at -80 mV and subjected to a 500 ms depolarizing step +60 mV followed by 8 s steps from –110 mV to +40 mV in 10 mV increments followed by a repolarizing step to -110 mV. Boltzmann fits were used to obtain the $V_{1/2}$ and k values. Deactivation tau was obtained by fitting the deactivation tail current decay with a double exponential function. Tau fast is reported, since current decay at -110 mV was dominated (>85%) by the fast component.

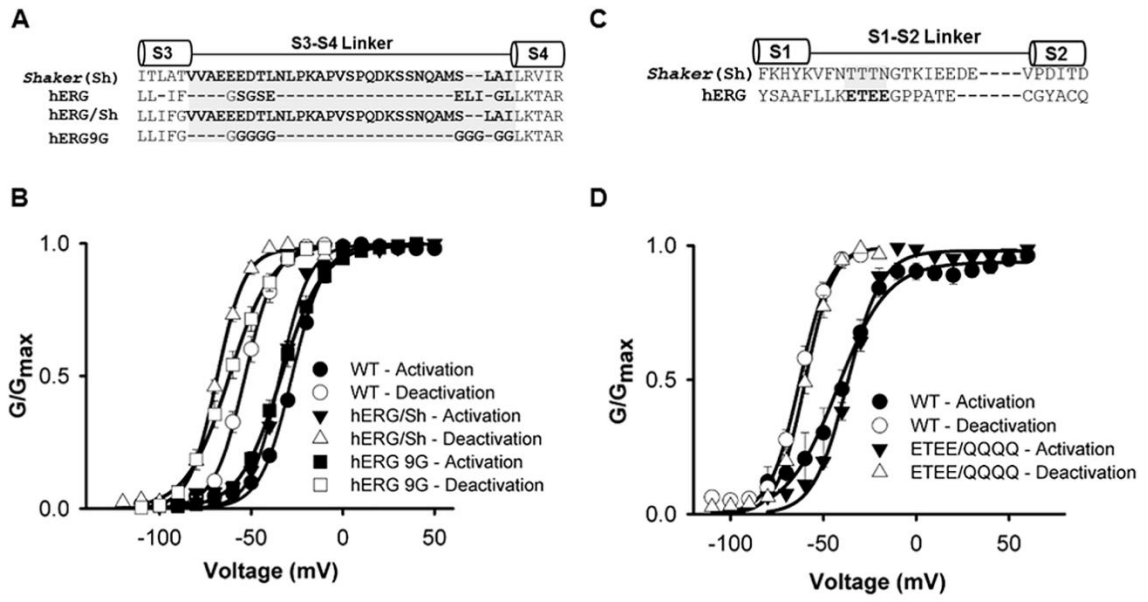

Figure 4.7 Mode-shift in hERG channels is not dependent upon S3-S4 or S1-S2 linker strutcture.

***A* and *C*,** Sequence alignment of the S3-S4 (*A*) and S1-S2 (*C*) linker in *Shaker* and hERG channels. ***B and D*,** Plots of mean GV relationships for hERG WT, hERG/Sh and hERG 9G (*B*) and hERG ETEE/QQQQ (*D*) activation and deactivation constructed from normalized peak tail currents. Mean $V_{1/2}$ and *k* values were obtained by fitting each data set to a Boltzmann function (see Table S3, section 4.6).

4.5 **Discussion**

This study provides, to our knowledge, novel insight into the link between activation and deactivation gating in hERG channels. The data show that the activated voltage sensor configuration is stabilized by depolarization via two separable mechanisms, one that derives from the open pore gate and another from within the voltage sensing unit itself. We have characterized the mode-shift behaviour that this produces by measuring activation and deactivation, as well as on- and off-gating currents, at steady-state and this shows that the pore gate in hERG channels can close while the voltage sensors remain in their activated position. Lastly, we demonstrate that coupling between the pore gate and voltage sensor during deactivation is impeded by perturbation of the S4-S5 linker, but remains intact in Δ2-135 channels.

4.5.1 **Pre-pulse dependent slowing of hERG deactivation**

Biphasic slowing of deactivation in response to increasing depolarizing step duration, such as that which we characterize in hERG channels in Fig. 4.1 and 4.2, has been observed in *Shaker* and Kv1.2 channels (Lacroix et al. 2012; Labro et al. 2012; Villalba-Galea et al. 2008). In these channels, the faster phase of deactivation slowing was kinetically associated with pore opening, which was interpreted by the authors to suggest that rearrangements of the pore gate during activation limit pore closure. The slower phase of deactivation slowing occurred with depolarization durations that exceeded the time course of channel activation. Both components of the slowing of channel deactivation correlated well with measurements of gating charge return leading the authors to conclude that the slowed deactivation emanated from events intrinsic to the voltage sensor that were influenced by the opening of the pore. Our data in hERG channels are consistent with this interpretation and suggest that both mechanisms are conserved features of gating in hERG channels. Firstly, the time course of channel opening and the faster component of deactivation slowing with increasing depolarization duration are reasonably well correlated despite the fact that activation of the pore gate in hERG channels is approximately 10-fold slower than in *Shaker* and Kv1.2 channels. This is consistent with a role for pore opening in the retardation of closing. Interestingly, the tau of the fast phase of slowing of gating charge return (34 ms) was faster than that of deactivation gating (93 ms) in hERG channels. This suggests that the faster slowing of charge return may occur in response to events earlier in the activation pathway (35-40% of channels are open after a 35 ms at +60 mV (Van Slyke et al. 2010)), while the faster slowing of pore closure during deactivation appears to occur in response to events later in the activation pathway when channels are fully activated.

It is interesting that the time course of the slower component of voltage sensor slowing was similar in hERG channels (~2.5 s) to that reported (~1.1 s) in *Shaker* and Kv1.2 channels (Labro et al. 2012) despite the fact that inactivation properties are quite distinct in the different channels. The delayed phase was attributed to a relaxation process whereby the voltage sensor assumes a more stable lower energy state in response to prolonged depolarization (Lacroix et al. 2011; Labro et al. 2012). Several lines of evidence suggest that relaxation is an intrinsic voltage sensor property that is distinct from inactivation mechanics. For example, relaxation is preserved in a voltage sensor protein that lacks a pore domain (Ci-VSP (Villalba-Galea et al. 2008)) and therefore the

effector of inactivation (Labro et al. 2012). However, others have suggested that delayed charge return may result from voltage-independent steps that are a prelude to, or associated with, the inactivation process (Shirokov 2011). The similar kinetics of the slow process despite stark differences in inactivation properties (*Shake*r and Kv1.2 inactivation occurs on the timescale of seconds and is voltage-independent, whereas hERG inactivation is strongly voltage-dependent and occurs with a tau of a few milliseconds at depolarized potentials) leads us to suggest that the relaxation process is unrelated to inactivation in hERG channels.

4.5.2 **S4-S5 linker coupling during deactivation**

Several studies have suggested that the S4-S5 linker that connects the voltage sensor domain with the pore domain is involved in the coupling of charge movement with pore gate opening (Ferrer et al. 2006; Hull et al. 2014; Sanguinetti & Xu 1999; Tristani-Firouzi et al. 2002; Van Slyke et al. 2010; Alonso-Ron et al. 2008). However, recent evidence suggests that the mechanism of coupling in hERG channels may be different from that in other *Shaker*-like Kv channels. The recent cryo-EM structure of the *eag* channel reveals that the S4-S5 linker in *eag*, and related channels such as hERG, may be too short to function as a mechanical lever that influences the pore gate (Whicher & MacKinnon 2016). This idea is supported by the observation that activation gating is not strongly influenced in channels in which the physical connection between the S4-S5 linker and the pore domain is disrupted (Lörinczi et al. 2015).

We have previously shown that mutation of G546, to any other residue that reduced α-helical propensity, shifted the voltage-dependence of activation ~50 mV to more hyperpolarized potentials (Van Slyke et al. 2010). This suggested to us that G546 is an important site that mediates the open-closed equilibria in hERG channels. Here, we have used mutation of G546 in the S4-S5 linker as a perturbation tool to investigate the role of the S4-S5 linker in deactivation gating. We were further driven to investigate the S4-S5 linker by the observation that disruption of the physical connection between the voltage sensor and pore domains, while not influencing activation greatly, impacted deactivation gating significantly (Lörinczi et al. 2015). Furthermore, evidence from *Shaker* channels suggests that the S4-S5 linker couples the pore and voltage sensor during deactivation based on the observation that specific interactions between residues in the S4-S5 linker and the pore control mode-shift behavior (Haddad & Blunck 2011).

Fig. 4.3 shows that the G546L mutation appeared to specifically impede the faster component of voltage sensor stabilization that is associated with opening reconfigurations of the pore gate without attenuating the slower relaxation phase, since there is no obvious phase of slowing of charge return and deactivation gating that occurs on the same time scale as pore opening. This suggests that S4-S5 linker perturbation interferes with pore-to-voltage sensor coupling during deactivation. An alternate possibility is that the fast phase of slowing is preserved in G546L channels, but that it occurs in response to much shorter duration pre-pulse steps than tested here. However, if this were the case, the proportion of this phase would be dramatically reduced compared with WT channels, and would still be temporally dissociated from activation of the pore gate of the channel. Thus, we interpret the data to indicate that the S4-S5 linker perturbation interferes with the influence of the pore gate on the stability of the voltage sensor and supports a role for the short helical connector in communicating reconfigurations of the open pore to the voltage sensor. It is also possible that reduced flexibility of the linker in the G546L mutant channel limits the configurations of the pore gate that are associated with increased stability of the activated voltage sensor, but our data cannot distinguish between these mechanisms. In either case, the data from the mutant channel suggest that in WT channels the pore drives one aspect of voltage sensor return, and a separable relaxation mechanism drives a slower stabilization of the activated voltage sensor. This latter mechanism appears therefore to originate from upstream of the S4-S5 linker, further supporting the conclusion that it originates from within the voltage sensor itself. Taken together, these data suggest that voltage sensor return and closing of hERG channels is dually regulated by the pore gate upon opening, and by intrinsic voltage sensor rearrangements. These processes are predicted to dictate slow deactivation in hERG channels enabling the provision of a resurgent cardiac repolarizing current. Interestingly, a recent study showed that the drug retigabine preferentially stabilized Kv7.2/Kv7.3 channels in the relaxed state (Corbin-Leftwich et al. 2016), suggesting that selective targeting of the relaxed state in these channels, or hERG channels for that matter, may offer therapeutic potential.

The influence of S4-S5 linker perturbation on communication between the pore and voltage sensor during deactivation described in this study is significant given the recent structural description of *eag* channels (Whicher & MacKinnon 2016). Based upon the short length of the S4-S5 linker, the authors interpreted these structures to demonstrate

that the mechanism of voltage-dependence in the *eag* family of channels (which includes hERG) may differ from the classical S4-S5 linker-mediated electromechanical coupling described in *Shaker*-like channels. An alternate mechanism involving integration of the PAS domain and CNBHD by calmodulin was proposed to gate the *eag* intracellular pore independent of voltage changes. Voltage sensor motions during activation were predicted to alter interactions of the S4-S5 linker with S6, which then positions S4 to interact with the C-linker region and open the pore. Our data are consistent with this model of voltage sensing. Firstly, Fig. 4.5 provides functional evidence supporting the structural observation that the pore gate can close with voltage sensors in the activated position. Secondly, Fig. 4.3 shows that the S4-S5 linker influences the communication of pore gate reconfigurations upon opening to the activated voltage sensor. This is consistent with the observed interaction between the S4-S5 linker and the lower portion of S6 when the voltage sensors are in the activated position in the *eag* structure (Whicher & MacKinnon 2016).

4.5.3 **Characterization of mode-shift behavior in hERG channels**

Stabilization of activated states during depolarization results in delayed charge return and channel deactivation, which has been described as mode-shift behaviour. Mode-shift has been reported in hERG channels (Piper et al. 2003; Tan et al. 2012; Hull et al. 2014; Goodchild et al. 2015), but is dependent on recording conditions. This makes comparison of the effects of mutations challenging. In Fig. 4.4 and 4.5, we characterized the mode-shift of ionic current and of charge movement in hERG channels by measuring steady-state activation and deactivation, and on- and off-gating current respectively. These data show that the “true” mode-shift of the pore gate is ~15 mV while that of the voltage sensor is ~40 mV. From these data, we draw two conclusions. Firstly, the reporting of mode-shift is highly dependent upon the kinetics of activation and deactivation and the step durations used to record on-gating/activation and off-gating/deactivation. We observed an apparent loss of mode-shift in many mutant channels (Table 4.3) that could be accounted for by faster deactivation kinetics than observed in WT channels. Secondly, mode-shift of the voltage sensor is significantly greater than that of the pore gate. This observation demonstrates that voltage sensor return is less energetically favourable than pore closure upon repolarization and demonstrates the important role for voltage sensor relaxation in stabilizing the hERG

activated voltage sensor and limiting its return. This finding is consistent with a previous observation of the dissociation between voltage sensor return and pore closure caused by a pharmacological activator compound (Abbruzzese et al. 2010). Furthermore, our data also provide supporting functional evidence for the recent cryo-EM structural prediction of the related *eag* channel, which captures the channel in a state in which the pore gate is closed, but the voltage sensor is in the activated configuration (Whicher & MacKinnon 2016). We may also interpret the data in Fig. 5.5D to demonstrate that not all charges must return upon repolarization for the pore gate of hERG channels to close. hERG channel gating schemes include independent voltage sensor transitions (Piper et al. 2003), which supports the idea that the pore may close is response to return of only a portion of gating charge. Indeed, a role for individual voltage sensor subunits within the channel tetramer has been documented (Gagnon & Bezanilla 2009).

4.5.4 **The role of the N-terminus in coupling during mode-shift**

Deletion of the N-terminus of hERG channels accelerates deactivation kinetics suggesting that the cytoplasmic domain stabilizes the open state of the pore gate (Morais Cabral et al. 1998; F.W. Muskett et al. 2011; Ng et al. 2011; Wang et al. 1998; Tan et al. 2012; Goodchild et al. 2015). The desire to understand this fundamental mechanism is underscored by the observation that inherited mutations, such as R56Q in the N-terminus, accelerate deactivation and predispose Long QT syndrome and sudden cardiac death (Chen et al. 1999). Two studies recently reported the effects of deletion of the N-terminus on mode-shift behaviour in an attempt to address this question, but the reported effects differed (Tan et al. 2012; Goodchild et al. 2015). Here, using steady-state measurements of activation and deactivation, we demonstrate that mode-shift of the pore gate in Δ2-135 hERG channels is similar to that in WT channels. Moreover, coupling between the pore gate and voltage sensor appears intact, since voltage sensor return was slowed by channel opening in a similar biphasic manner to that observed in WT channels. These data suggest that the N-terminus does not abolish the stabilizing influence of the pore on the voltage sensor. It is interesting, however, that the fast phase of slowing of gating charge return and pore gate closure were accelerated in Δ2-135 channels compared with WT channels ($P<0.05$). This implies that perturbation of the N-terminus accelerates the kinetics of open pore stabilization of the activated voltage sensor. A possible interpretation of this finding is that deactivation in WT channels is

limited by transitions occurring as the pore opens that stabilize the open pore and the activated voltage sensor. Truncation of the N-terminus apparently accelerates these transitions and this could underlie the faster deactivation kinetics in Δ2-135 channels. Further studies are required to clarify this influence of the N-terminus on the stability of the activated voltage sensor.

4.6 **Supplementary Material**

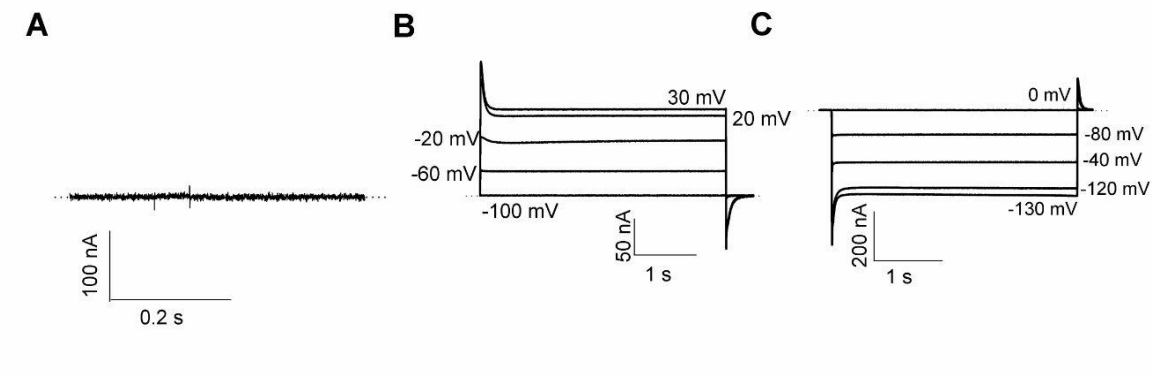

Figure S2 Gating current recordings from WT channels and un-injected oocyytes.
A, Representative leak and capacity subtracted currents recorded from un-injected oocyte in response to a -100 mV step from a holding potential of 0 mV. ***B and C***, Non-leak subtracted WT hERG currents recorded in response to depolarization (*B*) and repolarization (*C*) to the indicated voltages from a holding potential of -100 mV and 0 mV respectively.

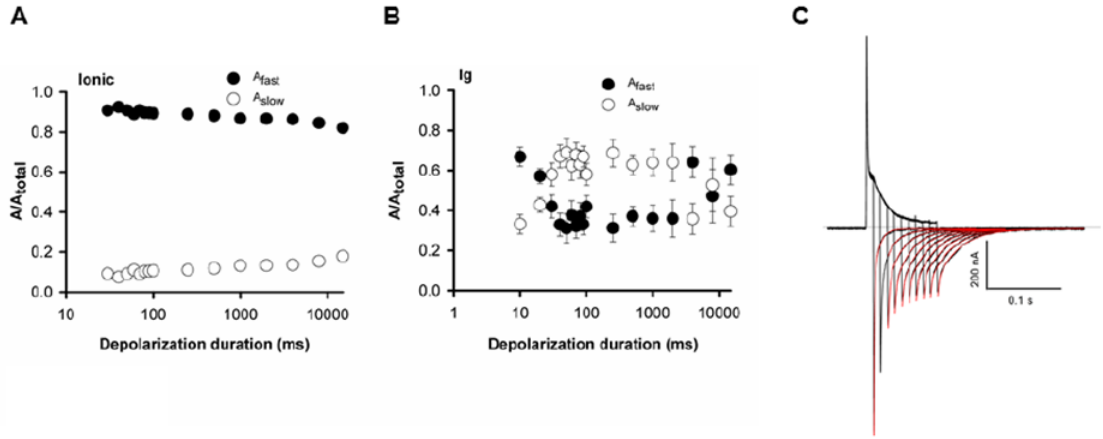

Figure S3 Dependence of relative amplitudes of the fast and slow phases of current decay on pre-pulse duration.
A and B, Plot of mean relative amplitudes of the phases of deactivating (*A*) and off-gating current decay (*B*) measured at -110 mV against depolarizing step duration. (*C*) Representative hERG WT gating current traces as in Fig. 4.2B inset showing double-exponential fits (red lines) of off-gating current decays.

Table S2: Activation and deactivation GV Boltzmann fir parameters for hERG Δ2-135 channels with different depolarizing step durations (Δt)

	Activation GV			Deactivation GV		
Δt (s)	$V_{1/2}$ (mV)	k (mV)	n	$V_{1/2}$ (mV)	k (mV)	n
0.25	-6.7 ± 2.1	10.6 ± 0.6	5	-	-	-
0.5	-13.8 ± 1.3	8.4 ± 0.4	5	-34.3 ± 1.2	16.2 ± 1.5	5
1	-17.3 ± 0.6	7.2 ± 0.3	5	-29.7 ± 1.0	12.7 ± 0.5	5
2	-19.4 ± 0.4	6.6 ± 0.4	5	-24.7 ± 0.9	9.1 ± 0.8	5
4	-19.9 ± 0.5	6.5 ± 0.4	5	-23.2 ± 0.5	9.4 ± 0.9	5
8	-19.7 ± 0.8	6.4 ± 0.5	5	-24.9 ± 1.3	9.4 ± 0.5	5

Table S3: Activation and deactivation GV Boltzmann fit parameters for hERG S3-S4 and S1-S2 linker mutant channels

	Activation GV			Deactivation GV			Mode-shift	
	$V_{1/2}$ (mV)	k (mV)	n	$V_{1/2}$(mV)	k (mV)	n	$V_{1/2}$ (mV)	n
WT hERG	-21.5 ± 0.5	7.9 ± 0.1	5	-52.8 ± 1.7	8.1 ± 0.3	5	-31.3 ± 2.0	5
hERG/Sh	-34.1 ± 0.7	8.0 ± 0.2	5	-68.1 ± 1.0	7.8 ± 0.3	5	-34.5 ± 1.2	5
hERG 9G	-33.3 ± 2.2	11.2 ± 0.3	4	-62.0 ± 2.8	11.2 ± 0.4	4	-28.8 ± 1.1	4
ETEE/QQQQ	-35.8 ± 2.6	8.9 ± 0.9	5	-59.3 ± 4.0	7.3 ± 0.9	5	-24.5 ± 2.9	5

To compare the effect of mutations on the extent of mode-shift, activation and deactivation were measured using non-steady-state durations. Activation GV relations were collected from oocytes held at -80 mV and subjected to 2 s depolarizing steps to +50 mV in 10 mV increments followed by a 2 s step to -110 mV. Deactivation GV relations were collected from oocytes held at -80 mV and subjected to a 500 ms depolarizing step +60 mV followed by 8 s steps from –110 mV to +40 mV in 10 mV increments followed by a repolarizing step to -110 mV. Boltzmann fits were used to obtain the $V_{1/2}$ and k values.

Chapter 5. Fluorescence tracking of hERG activation gating

This chapter describes unpublished work. I contributed to the most of the work presented in this chapter. I designed and performed all of the experiments, analyzed the majority of the data, and made the majority of the figures.

5.1 Introduction

Voltage-gated potassium (Kv) channels activate and deactivate when the membrane is depolarized and repolarized, respectively. Kv channels derive their electrical sensitivity from positively charged residues in the voltage sensor (S4). The S4 charges sense changes in the membrane potential, which initiates a conformational change that is coupled to the opening or closing of the ion-conducting pore. The dynamics of the voltage sensor in the archetypal *Shaker* Kv channel have been assessed by measuring gating currents using cut-open vaseline gap (COVG) (Bezanilla 2000), S4 state-dependent accessibility experiments (Larsson et al. 1996), and voltage-clamp fluorimetry (VCF), a technique that has been employed to directly observe protein structural dynamics in real time (Mannuzzu et al. 1996). VCF has proven to be a powerful technique in understanding the fundamental aspects of channel gating, because it provides insight that is not obtained with other techniques. For example, while studies using X-ray crystallography or cryo-EM have provided great insight into the structure of ion channels, these structures provide snapshots in time of the channel under investigation. COVG, on the other hand reveals detailed and quantitative description of intramembrane charge movement, but does not provide information regarding the dynamic conformational changes of the channel during transitions between different states. VCF provides insight here by enabling the simultaneous measurement of fluorescence emission changes associated with channel rearrangements along with ionic current measurements. In addition, VCF also enables visualization of conformational changes of the channel associated with electrically silent transitions, such as inactivation or drug bound states (Claydon et al. 2007). Thus, VCF can provide an encompassing and unparalled view of the relationship between channel function and its dynamic structure.

Previous studies have shown that fluorescence emission reports from fluorophores such as tetramethylrhodamine-5-maleimide (TMRM) covalently attached to a cysteine amino acid introduced in the S3-S4 linker provide a reliable measure of the time- and voltage-dependence of S4 movement during channel gating. In *Shaker*, Kv1.2, Kv1.4, Kv1.5 and Kv7.1 channels, fluorophores attached at this position reveal S4 movement as a rapid change in fluorescence emission that correlates well with the displacement of the charge, measured by gating currents (Mannuzzu et al. 1996; Cha & Bezanilla 1997; Vaid et al. 2008; Horne et al. 2010; Osteen et al. 2010). In addition to Kv channels, VCF measurements from Nav and Cav channels have revealed mechanisms of gating which could not have been learned from static structural studies. For example, VCF protocols have been established for Na^+ channels to probe the interaction between the voltage sensors of the different domains and fast inactivation (Cha et al. 1999). Recently, fluorescence reports from Cav1.2 channels have revealed that each voltage sensor of the different domains exhibits a distinct time-and voltage-dependence of activation kinetics (Pantazis et al. 2014). These data demonstrated the utility of VCF to study conformational rearrangements in different ion channel families.

The unusual gating characteristics in hERG Kv channels provide an attractive target for study using VCF. hERG activates and deactivates slowly, yet inactivates and recovers from inactivation rapidly. These unusual gating properties afford hERG channels a critical role in the repolarization of the cardiac action potential and termination of excitability (Sanguinetti & Tristani-Firouzi 2006), but are not well understood. Throughout my studies, I have used VCF to study gating in hERG channels, usually combining the approach with other measures for validation. For example, I have studied the molecular basis of activation and deactivation gating in Chapters 3 and 4, and have used a combined approach of ionic current, gating current and VCF measurements to gain mechanistic insight. Such measurements have precedent in the literature. Charge movement in hERG channels has been measured previously by measuring gating currents (Piper et al. 2003; Piper et al. 2005; Wang et al. 2013; Goodchild & Fedida 2014; Goodchild et al. 2015; Thouta et al. 2014), and voltage sensor dynamics has been reported using VCF (Smith & Yellen 2002; Es-Salah-Lamoureux et al. 2010; Van Slyke et al. 2010; Tan et al. 2012; Hull et al. 2014; Thouta et al. 2014; Guo et al. 2015). However, a recent study suggested differing reports of voltage sensor movement from these two different approaches (Goodchild et al. 2015). This has raised the question as

to whether fluorescence measurements from the outer section of S4 of hERG channels provide a faithful report of S4 movement. In this Chapter, I aim to determine the ability of VCF to track voltage sensor movement and therefore the validity of the technique to inform on hERG S4 gating. I have provided the most comprehensive yet characterization of the fluorescence reports from numerous sites within the hERG channel voltage sensor from two different fluorophores. I have quantified the kinetics and voltage-dependence of the fluorescence report of S4 movement in hERG channels and highlighted the importance of the holding potential to ensure that a complete fluorescence profile is measured. These findings demonstrated that VCF does appear to report on S4 movement, which precedes opening of the pore gate both kinetically and energetically. The data are consistent with gating current records of intra-membrane charge movement and demonstrate that fluorescence changes from an S4-mounted fluorophore provide a faithful recapitulation of the dynamics of voltage sensor movement in hERG channels.

5.2 Materials and Methods

5.2.1 Molecular biology

hERG channel constructs were subcloned into the expression vector pBluescript SKII and expressed in *Xenopus* oocytes. All mutant constructs were generated using conventional overlap extension PCR as described previously (see Section 2.1).

5.2.2 Oocyte preparation and injection

Xenopus laevis frogs were terminally anaesthetized by placing them in 2g/2L tricane solution (Sigma Aldrich) for 10-15 min. Stage V and VI oocytes were isolated and injected as described previously (see Section 2.2.1).

5.3 Data acquisition

Wild-type (WT) and mutant hERG channel ionic currents were studied using two-electrode voltage clamp with an OC-725C amplifier (Warner Instruments). All signals were digitized using a 1440 A/D convertor and pClamp 10.2 software (Axon Instruments). All recordings were performed while oocytes were bathed in an external ND96 (96 mM NaCl, 3 mM KCl, 5 mM HEPES, 0.5 mM $CaCl_2$, 1 mM $MgCl_2$, titrated to

pH 7.4 with NaOH) solution. Microelectrodes made from borosilicate glass had a resistance of 0.2-2.0 MΩ when filled with 3 M KCl. Current signals were acquired at a sampling rate of 10 kHz with a 4 kHz low-pass filter. Recordings were performed at 20-22°C.

5.3.1 **Voltage clamp fluorimetry (VCF)**

Five adjacent residues in the S3-S4 linker region, G516C-L520C, were individually introduced as a site for fluorophore labelling with either tetramethylrhodamine-5-maleimide (TMRM, Invitrogen) or methanethiosulfonate-rhodamine (MTSR; Toronto Research Chemicals) fluorophore. Both TMRM and MTSR are membrane impermeant thiol-reactive fluorescent probes. TMRM has a maleimide-linker, which covalently binds to the engineered cysteine residues. MTSR has a methanethiosulphonate (MTS) group as the sulfhydryl regent that binds with cysteine residues. In comparison to other dyes, rhodamines are widely used as external labels in VCF for a number of reasons: (1) these dyes have a large Stokes Shift. TMRM has a maximum light absorption at 542 nm and a maximum emission at 567 nm and MTSR has a maximum light absorption at 565 nm and a maximum emission at 586 nm. This means that they can be excited with a standard mercury or metal halide lamp and the emission spectra can easily be collected with a long pass filter without significant contamination of excitation light; (2) TMRM and MTSR have high molar extinction coefficients (e.g. TMRM has an extinction coefficient near 110 000 $M^{-1}cm^{-1}$), which means rhodamines are efficient absorbers; (3) rhodamines have high fluorescence quantum yield, resulting in high fluorescence intensities; and (4) rhodamines have high photo-stability, meaning that they can undergo multiple excitations before being destroyed in their excited state, i.e. photo bleaching.

Two native cysteines in the S1-S2 linker (C445 and C449) were removed and replaced with valine residues to prevent off-target labelling within the channel. Throughout this Chapter, these background mutations are not mentioned, e.g. the construct C445V:C449V:G516C is referred to as G516C. For TMRM experiments, oocytes were incubated in a depolarizing solution (in mM: 99 KCl, 1 $MgCl_2$, 5 HEPES, 2 $CaCl_2$, titrated to pH 7.4 with NaOH) labelled with 5 μM TMRM for 30 min at 10°C in the dark. For MTSR experiments, oocytes were incubated in depolarizing solution labelled with 5 μM for 1 min on ice in the dark. Two-electrode VCF experiments were performed as described previously (see Section 2.32). To account for the majority of fluorophore

bleaching during excitation, the fluorescence signal recorded at potentials at which there was no channel opening was subtracted from the test signal.

5.3.2 **Data analysis**

Data throughout this study was analyzed using Clampfit10.3 and SigmaPlot11 software. Conductance-voltage (GV) relationships were derived from normalized peak tail current amplitudes. Fluorescence-voltage (FV) relationships were derived from the fluorescence signal amplitude at the end of the test pulse. To improve the signal-to-noise ratio of fluorescence recordings, all the fluorescence reports were collected from the average of a number of sweeps. GV and FV curves were fitted with the Boltzmann equation: $y = 1/(1+ \exp(V_{1/2} - V)/k)$, where y is the relative conductance or fluorescence normalized to the maximum conductance (G/G_{max}) or fluorescence (F/F_{max}), $V_{1/2}$ is the half-activation voltage, V is the test voltage and *k* is the slope factor. To determine the rate of channel activation, an envelope of tails protocol was used (see Fig. 2.2C). Peak tail currents at -110 mV were measured following the step to +60 mV of varying duration (10–500 ms). The holding potential was -80 mV. Activation time course was derived from single exponential fits of data plotting the peak tail current against depolarizing pulse duration: tau was derived from $f(t)=A*\exp(t/\tau) + C$, where A is the amplitude of the fit, t is time, τ is the time constant of activation, and C is the residual current. The time course of fluorescence change upon depolarization was derived from single exponential fits using the same equation. All data are expressed as mean ± SEM (n = number of oocytes). In figures, arrows indicate the zero-current level and dotted lines are to guide the eye. Voltage protocols are either depicted in figures or described in detail in the figure legends.

5.4 **Results**

To get an overall picture of the conformational rearrangements of the voltage sensor associated with slow activation of hERG channels, I performed a systematic fluorescence scan of the S3-S4 linker region (from residue G516C to L520C) with two different fluorescent probes (TMRM and MTSR), and analyzed the relationship between the fluorescence changes and ionic currents from three TMRM-labeled cysteine-substituted residues (G516C, E519C and L520C). These cysteine-substituted sites are

located in the S3-S4 linker and outer end of S4 (Fig. 5.1A and B). To prevent possible modification of the fluorescence emission from fluorophores labelling native cysteine residues, two endogenous cysteines in the S1-S2 linker (residues C445 and C449), were replaced with valine (Fig. 5.1A and B). For comparison, the sequence alignment of the S3-S4 linker in *Shaker* and hERG channels is shown in Fig. 5.1C. The underlined residues in *Shaker* have been shown to provide a reliable report of the S4 movement using VCF (Mannuzzu et al. 1996). In *Shaker*, changes in the fluorescence signal occurred with similar voltage-dependence as the gating charge movement.

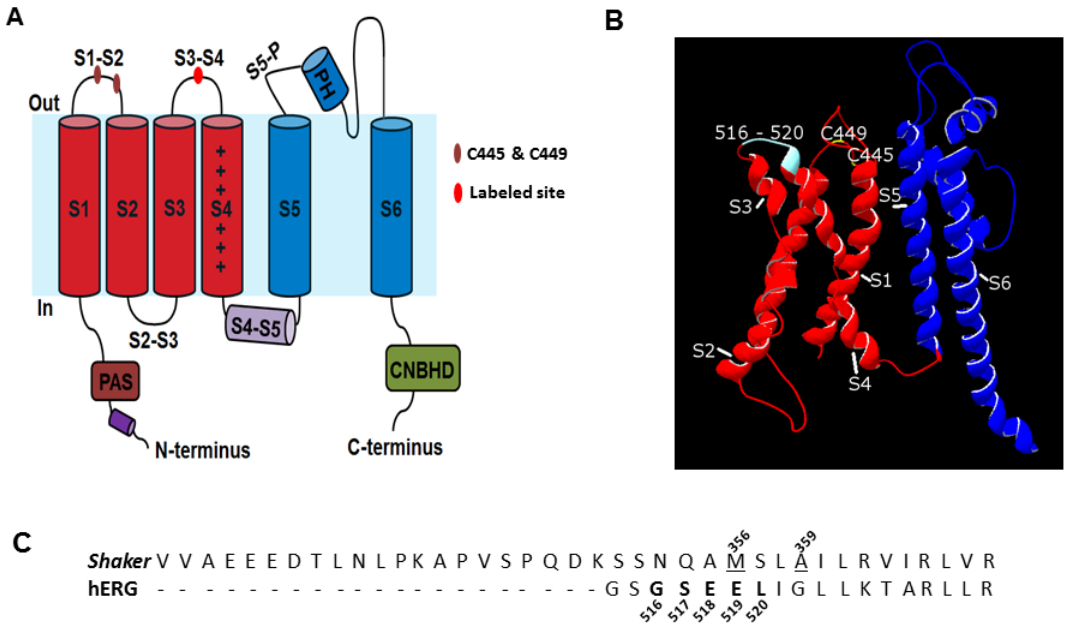

Figure 5.1 Structure of the hERG channel and location of cysteine substitutions.

A, Cartoon transmembrane topology of a hERG channel α-subunit showing relative positions of the two native cysteines, C445 and C449, in the S1-S2 linker (brown circles), and the engineered cysteine mutants within the S3-S4 linker (red circle) used to covalently bind the fluorescent dye. ***B,*** Homology model of the hERG voltage sensing domain (S1-S4, red) and pore domain (S1-S6, blue) generated based on the cryo-EM structure of the Kv10.1 *(eag*1) channel (Whicher & MacKinnon 2016). The voltage-sensing domain is in an open conformation highlighting the location of the introduced cysteines in the S3-S4 linker (residues G516 to L520, cyan) and two native cysteines in S1-S2 linker (residues C445 and C449, yellow). ***C***, Sequence alignment of the S3-S4 linker in *Shaker* and hERG channels. The residues shown in bold in the hERG sequence were individually mutated to cysteine and labeled with fluorescent dyes in the present study. The underlined residues in *Shaker* have been shown to provide a reliable report of voltage sensor movement using VCF (Mannuzzu et al. 1996).

5.4.1 **Effects of cysteine mutants on the voltage-dependence of hERG activation**

Before performing VCF experiments, it was important to characterize the influence of the cysteine substitutions on hERG channel gating. Gating behaviour observed in each of the TMRM-labeled cysteine mutants (G516C, E519C and L520C) is shown in Fig. 5.2. Fig. 5.2, A-C compares the relative open probability of the G516C, E519C and L520C with WT channels over a range of voltages. GV relations were fitted with a Boltzmann function which yielded $V_{1/2}$ and k values of -25.6 ± 0.6 and 8.8 ± 0.5 mV for WT (n = 6), -31.6 ± 1.8 and 12.6 ± 0.7 mV for G516C (n = 5), -20.7 ± 1.5 and 14.5 ± 0.4 mV for E519C (n = 7), and -25.4± 1.2 and 14.8 ± 0.8 mV for L520C (n = 4). The voltage-dependence of activation in all three mutants following modification with TMRM was not significantly different from WT hERG activation gating properties (P>0.05, ANOVA) (Fig. 5.2). These data suggested that cysteine substitutions in the S3-S4 linker have minor, if any effect on the hERG channel activation gating process that I intend to report upon.

5.4.2 **Fluorescence scanning of the hERG S3-S4 linker region**

For an improved understanding of the fluorescence tracking of channel rearrangements, I labeled residues G516C to L520C with two different fluorophores, TMRM and MTSR (Fig. 5.3). Both TMRM and MTSR are derived from rhodamine labels, with a net charge of 0 at physiological pH. Typical fluorescence signals from TMRM (Fig. 5.3A) and MTSR (Fig. 5.3B) labelled oocytes expressing the identified mutant were recorded in response to a single voltage step from -80 mV to +60 mV and then returning to -110 mV. Measurements using either TMRM or MTSR at most sites tested yielded similar fluorescence signals, where the fluorescence changed with a single component: a marked quenching of fluorescence upon depolarization. However, measurements using TMRM and MTSR at S517C and E519C, on the other hand, showed very different fluorescence signals. While the fluorescence changes of TMRM-S517C and MTSR-E519C showed a single component, the fluorescence signal from MTSR-S517C and TMRM-E519C showed two distinct components. The two components have very different time courses and the fluorescence change in each component occurred in opposing directions. For example, upon membrane depolarization, the fluorescence signal from E519C-TMRM revealed an initial rapid decrease followed by a slow increase. Upon repolarization, the fluorescence rapidly decreased and then slowly increased. In

addition, while the fluorescence signal for S517C-MTSR showed fast and slow components similar to E519C-TMRM, the fluorescence changes occurred in the opposite direction. Interestingly, E518C labeled with both TMRM and MTSR showed a biphasic fluorescence change upon repolarization. There was a small rapid downward deflection with TMRM and a rapid upward deflection with MTSR that preceded the bulk of the de-quenching during repolarization.

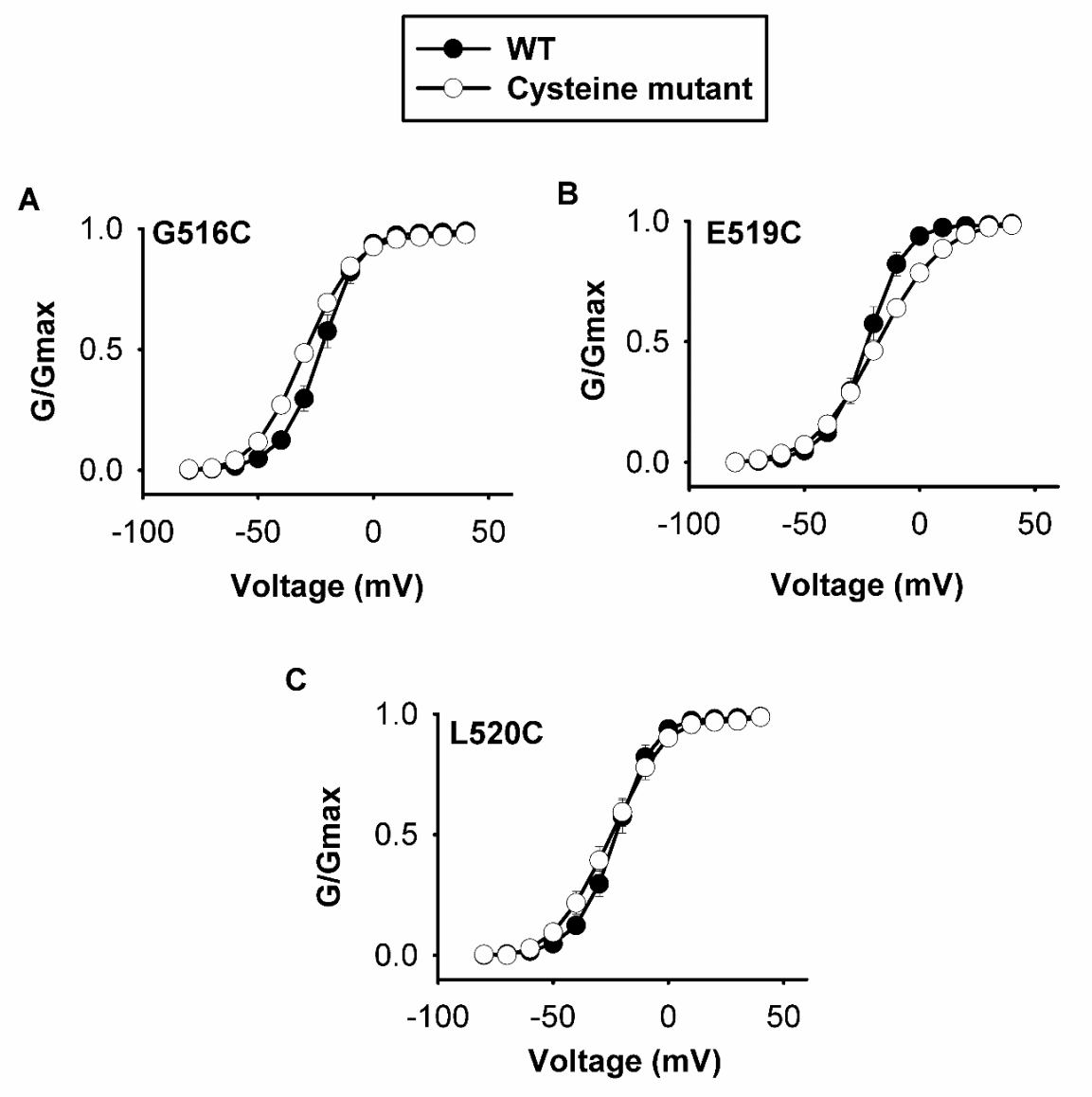

Figure 5.2 Activation gating of TMRM-labeled G516C, E519C and L520C channels.

A-C, Plot of mean WT and cysteine mutant GV relations for activation gating, constructed from peak tail current amplitudes. Data were fitted with a Boltzmann function. $V_{1/2}$ and *k* values were -25.6 ± 0.6 and 8.8 ± 0.5 mV for WT (n = 6), -31.6 ± 1.8 and 12.6 ± 0.7 mV for G516C (n=5), -20.7 ± 1.5 and 14.5 ± 0.4 mV for E519C (n = 7), and -25.4± 1.2 and 14.8 ± 0.8 mV for L520C (n=4). The data suggested that all the three cysteine mutants activate with a similar voltage-dependence to that in WT channels.

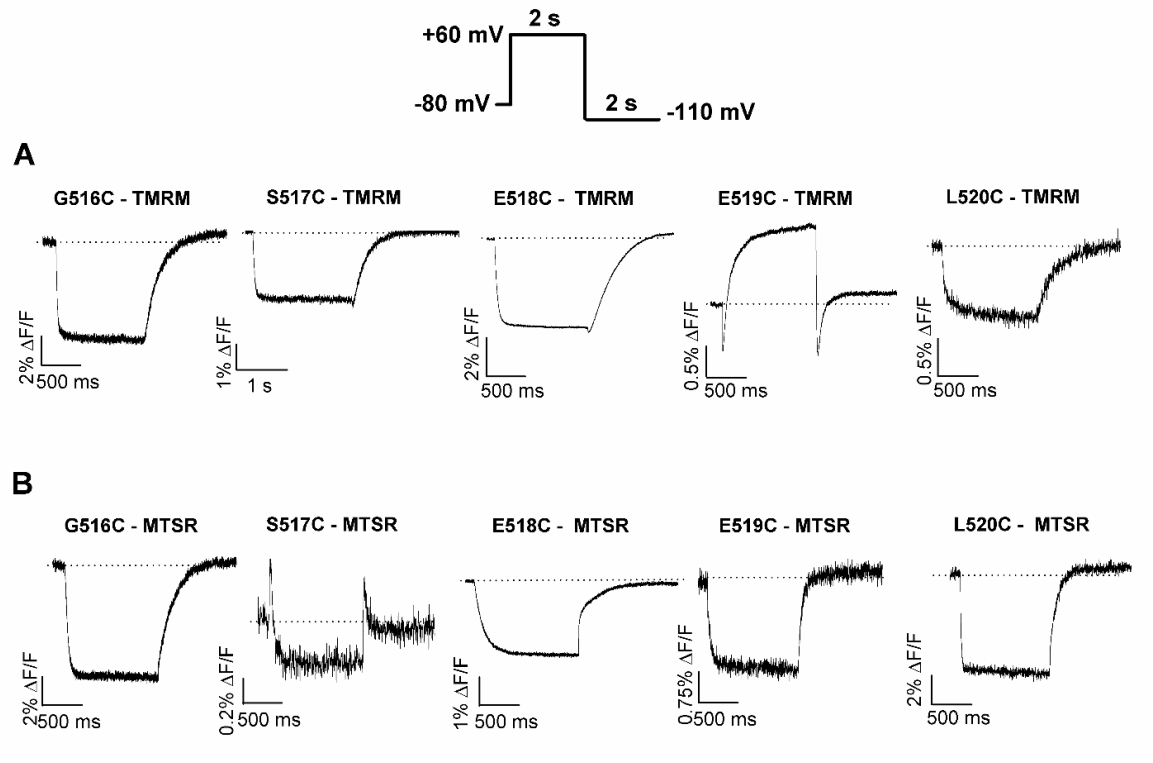

Figure 5.3 Fluorescence reports from TMRM and MTSR attached at positions in the S3-S4 linker region.

A* and *B, Representative TMRM (*A*) and MTSR (*B*) labeled hERG fluorescence signals recorded in response to a single voltage step protocol (centre).

5.4.3 Relationship between fluorescence signals and ionic conductance

A few previous studies from laboratories other than our own have reported VCF measurements of hERG gating (Smith & Yellen 2002; Es-Salah-Lamoureux et al. 2010; Tan et al. 2012) to probe the connection between S4 movement and pore opening. However, these studies showed differing reports, leaving questions regarding the fluorescence measurements in hERG channels. The first VCF study on hERG channels acquired fluorescence signals from TMRM attached in the S3-S4 linker (E518C, E519C

and L520C) each of which reported slow and fast fluorescence emissions that were not correlated well with the expected gating charge movement. The slow fluorescence from L520C showed a voltage-dependence (FV) that overlaid GV relationship of activation, while fast fluorescence from E518C and E519C did not correlate with activation and instead was associated with inactivation gating. These data suggested that in hERG channel voltage sensor movement is slow like pore opening and closing (Smith & Yellen 2002). Soon after the first VCF study, hERG gating currents recorded in oocytes showed that the kinetics of the charge movement were remarkably slow, and the QV relation was noticeably left-shifted compared to GV relation, suggesting that S4 movement precedes channel opening (Piper et al. 2003). This was in contrast to the previous VCF data, which showed a strong overlap of the FV and GV relation (Smith & Yellen 2002). Furthermore, a recent report of VCF has questioned findings of the previous VCF data, and instead associated slow fluorescence with opening and closing of the pore (Es-Salah-Lamoureux et al. 2010). Due to such discrepancies between the VCF and gating current measurements, further investigation is required to test the validity of the fluorescence report in hERG channels and understand the underlying mechanism of the slow hERG activation gating.

To address this, I characterized the voltage-dependence of the fluorescence report of S4 movement to compare with ionic currents during activation gating. Typical fluorescence traces from TMRM-labeled hERG G516C (Fig. 5.4A), E519C (Fig. 5.4C) and L520C (Fig. 5.4E) channels are shown in Fig. 5.4 (left). Fluorescence reports were recorded during 2 s depolarizing steps from varying voltages in 10 mV increments, followed by a 2 s repolarizing step to -110 mV. The holding potential was -80 mV. FV and GV relations for G516C (Fig. 5.4B), E519C (Fig. 5.4D) and L520C (Fig. 5.4F) channels were compared in Fig. 5.4 (right).

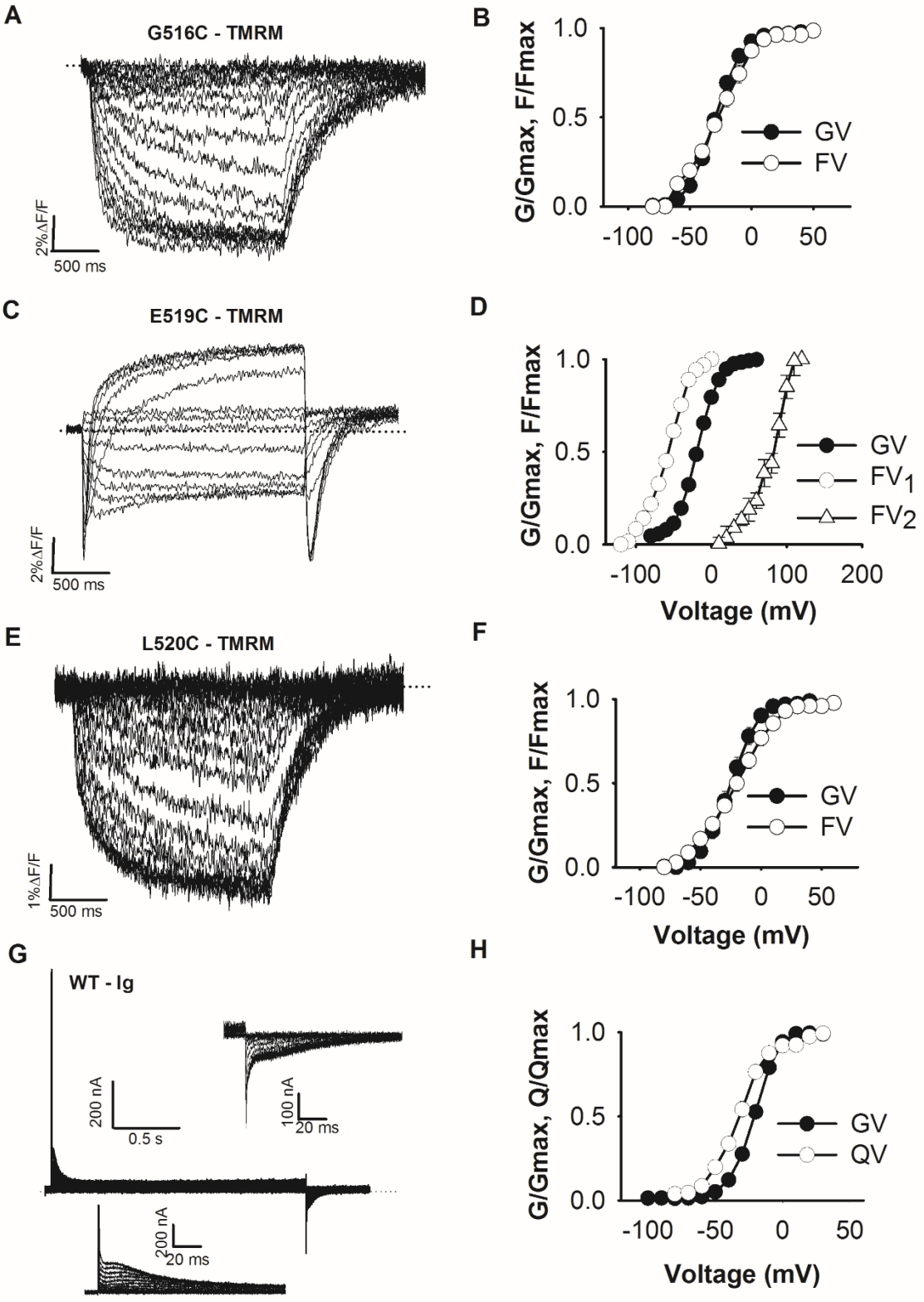
A
G516C - TMRM
2%ΔF/F
500 ms
B
G/Gmax, F/Fmax
1.0
0.5
0.0
-100 -50 0 50
GV
FV
C
E519C - TMRM
2%ΔF/F
500 ms
D
G/Gmax, F/Fmax
1.0
0.5
0.0
-100 0 100 200
Voltage (mV)
GV
FV1
FV2
E
L520C - TMRM
1%ΔF/F
500 ms
F
G/Gmax, F/Fmax
1.0
0.5
0.0
-100 -50 0 50
Voltage (mV)
GV
FV
G
WT - Ig
200 nA
0.5 s
100 nA
20 ms
200 nA
20 ms
H
G/Gmax, Q/Qmax
1.0
0.5
0.0
-100 -50 0 50
Voltage (mV)
GV
QV

Figure 5.4 Relationship between the fluorescence report of voltage sensor movement and ionic current activation.

Left, Typical fluorescence reports from TMRM-labeled hERG G516C (*A*), E519C *(C*) and L520C (*E*) channels evoked during 2 s depolarizing voltage steps in 10 mV increments (holding potential -80 mV), followed by a 2 s repolarizing step to -110 mV. ***Right,*** Comparison of mean GV and FV relations for each mutation. GV data derived from peak tail current amplitudes were normalized to the peak of tail current following a step to +50 mV. FV data derived from the peak fluorescence and were normalized to the maximum fluorescence amplitude. Boltzmann fits of the data gave $V_{1/2}$ and *k* values for GV and FV relations of -31.6 ± 1.8 and 12.6 ± 0.7 mV (GV), and -27.1 ± 3.3 and 15.8 ± 0.7 mV (FV), respectively, for G516C (*B*, n = 5); -20.7 ± 1.5 and 14.4 ± 0.4 mV (GV), and -50.6 ± 3.1 and 16.1 ± 0.8 mV (FV1),and +80.1 ± 4.7 and 16.2 ± 7.1 mV (FV2) respectively, for E519C (*D,* n = 5); and -25.0 ± 0.5 and 11.0 ± 0.4 mV (GV), and -22.4 ± 1.2 and 17.0 ± 1.0mV (FV), respectively, for L520C (*F,* n = 4). ***G***, Typical WT gating currents evoked by 2 s voltage steps in 10 mV increments from a holding potential of -100 mV. *Insets* show on- and off- gating currents on an expanded time scale to highlight the gating current decays. ***H***, Plot of mean hERG WT QV and GV relations. The QV relation was constructed from normalized Ig_{off} records. A Boltzmann fit of the data gave $V_{1/2}$ and *k* values of −22.8 ± 0.2 and 8.2 ± 1.3 mV (GV), and −32.3 ± 1.4 and 12.0 ± 1.3 mV (QV) for WT (n = 6).

The single component fluorescence change observed with TMRM-attached at G516C or L520C presented a voltage-dependence that is similar to that of ionic current activation. The FV and GV relations had $V_{1/2}$ and *k* values of -31.6 ± 1.8 and 12.6 ± 0.7 mV (GV), and -27.1 ± 3.3 and 15.8 ± 0.7 mV (FV), for G516C (n = 5); -25.0 ± 0.5 and 11.0 ± 0.4 mV (GV), and -22.4 ± 1.2 and 17.0 ± 1.0mV (FV), for L520C (n = 5). On the other hand, the more complex fluorescence signal from E519C channels reported events occurring with different voltage-dependencies. The rapid initial fluorescence quenching reported by E519C channels upon depolarization had a voltage-dependence that saturated near 0 mV with an FV1 that was hyperpolarized from the GV relation: FV1, $V_{1/2}$ = -50.6 ± 3.1 mV and GV, $V_{1/2}$ = -20.7 ± 1.5 mV. The second, slower component of fluorescence saturated near +100 mV and had a voltage-dependence, FV2, which was right-shifted compared to GV relation: FV2, $V_{1/2}$ = +80.1 ± 4.7 mV). To correlate the fluorescence reports with the movement of gating charge, I also recorded gating currents from WT hERG channels. Typical WT gating current traces recorded in response to 2 s depolarizing steps from varying voltages in 10 mV increments, followed by a 2 s repolarizing step to -100 mV are shown in Fig. 5.4G. Similar to previous studies, I observed fast and slow gating current components, the latter of which carries the bulk of charge movement (Piper et al. 2003; Piper et al. 2005; Goodchild & Fedida 2014; Thouta et al. 2014; Goodchild et al. 2015; Thouta et al. 2017). In these experiments, where I have taken care to match depolarization duration, it is evident that the QV relationship lies to the left of the GV relationship indicating a lower energetic barrier to charge movement than pore opening, indicative of charge movement preceding pore opening. The fast fluorescence

component from TMRM-E519C (FV1) appeared to recapitulate this left-shifted position relative to the GV relation; however, the more simple fluorescence signals from G516C and L520C at the top of S4 appeared to overlay the GV relationship, questioning whether the signal tracks charge movement, or an event that is coupled with the voltage-dependence of pore gate opening.

5.4.4 The fluorescence report from TMRM attached at L520C depends upon the holding potential

To explore this further, and to address the unexpected observation that the fluorescence signal from the top of S4 at some, but not all, positions appeared to follow the voltage-dependence of pore opening rather the charge movement, I examined the effect of the holding potential on the fluorescence reports. I reasoned that a holding potential of -80 mV may not be hyperpolarized enough to return the voltage sensor to its fully rested state, and therefore that the fluorophore report might be underestimated. To test this, I recorded the fluorescence report from TMRM attached at L520C during depolarizing voltage steps from a holding potential of -80 mV or following a 2 s pre-pulse to -120 mV. I found that oocytes did not tolerate long periods of holding the membrane at -120 mV and opted instead to hold at -80 mV and apply a 2 s pre-pulse to -120 mV immediately preceding depolarizing test voltage steps. Fig. 5.5A and C show typical fluorescence traces recorded with the two different holding potentials and mean FV and GV relationships measured at 2 s are shown in Fig. 5.5B and D. The fluorescence traces showed a robust fluorescence de-quenching initiated by the pre-pulse to -120 mV. This strongly suggests that the fluorescence report of voltage sensor movement from TMRM at L520C is not fully at baseline at a holding potential of -80 mV. Because of this, the FV relation recorded from a holding potential of -80 mV missed some of the fluorescence report and differed significantly from the FV recorded with a pre-pulse to -120 mV. The $V_{1/2}$ of the FV was -48.9 ± 0.9 mV from a holding potential of -120 mV (n = 4) compared with -25.0 ± 0.5 mV from a holding potential of -80 mV (n = 4). In contrast, the holding potential had no effect on the GV relationship (Fig. 5.5E). The outcome is that the FV was ~-30 mV left-shifted from the GV relationship when all of the fluorescence change is captured by holding at -120 mV. This was consistent with the relative position of the QV relationship and is indicative of a lower energetic barrier to voltage sensor movement than pore opening upon depolarization (Fig. 4.4H). These data demonstrated that the

fluorescence report from TMRM attached at L520C provides a representation of voltage sensor movement that is consistent with measures of charge movement.

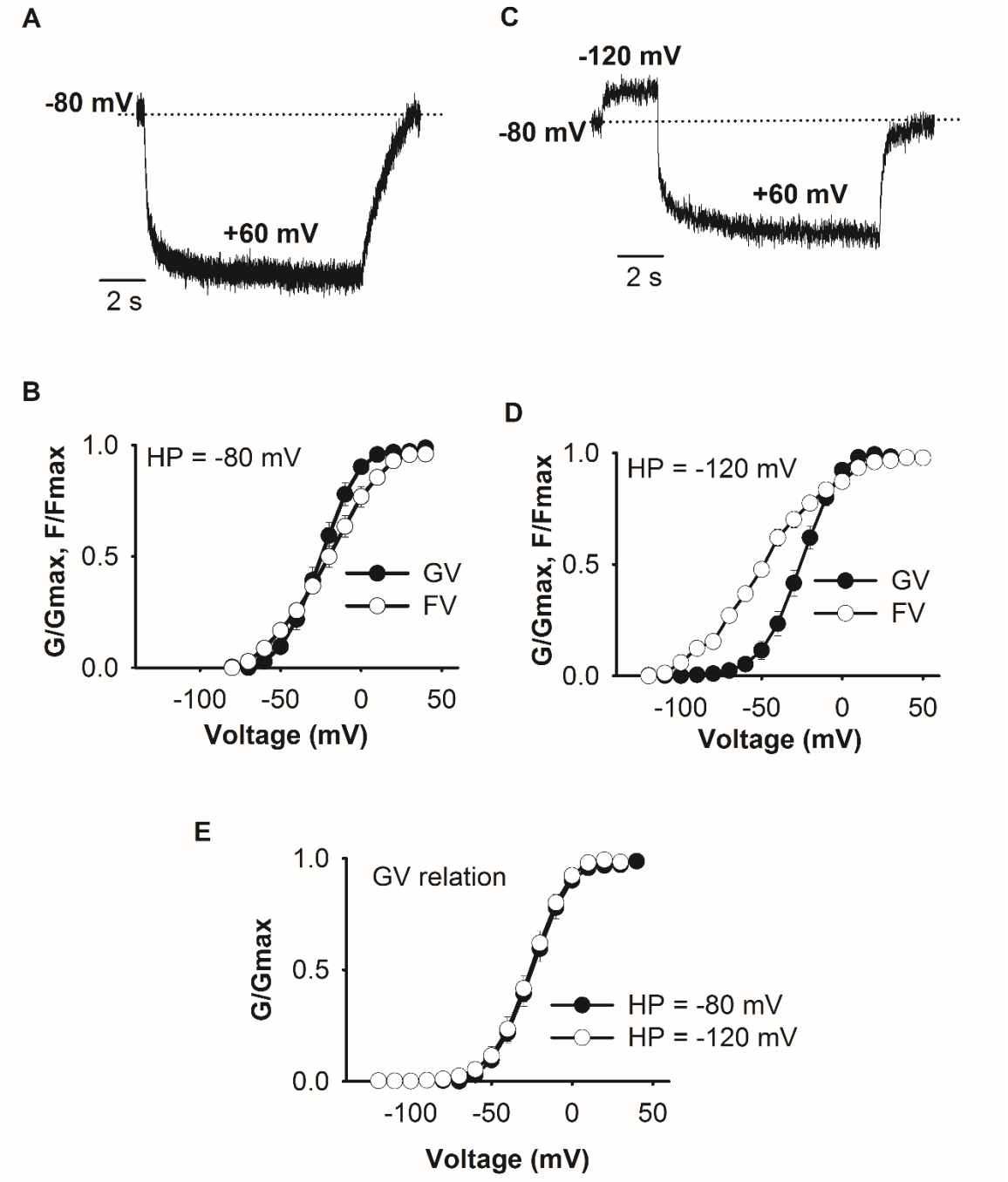

Figure 5.5 Detection of S4 movement from TMRM-attched L520C channels at voltages negative to channel activation.

A and ***C,*** Typical fluorescence reports from TMRM-labeled L520C channels evoked during a voltage pulse to +60 mV from a holding potential (HP) of -80 mV (*A*) or after a prepulse to -120 mV (*C*) ***B*** and ***D,*** comparison of mean GV an FV relationships for each condition. Boltzmann fits

of the data gave $V_{1/2}$ and k values for GV and FV relationships of -25.0 ± 0.5 and 11.0 ± 0.4 mV (GV) and -22.4 ± 1.2 and 17.0 ± 1.0 mV (FV) for HP = -80 mV (n = 4); and -25.8 ± 0.3 and 11.5 ± 0.8 mV (GV) and -48.9± 0.9 mV and 20.2 ± 0.8 (FV) for HP = -120 mV (n = 4). ***E***, Plot of the GV relations obtained from the two different holding potentials on the same axes (data from *B* and *D*) highlighting that the GV relationship is not effected by the holding potential.

5.4.5 The fluorescence report of voltage sensor movement kinetically precedes that of pore opening

In other Kv channels, such as *Shaker*, voltage sensor activation kinetically precedes pore opening, as evidenced by gating current measurements and VCF fluorescence reports (Bezanilla 2000; Mannuzzu et al. 1996; Cha & Bezanilla 1997). I aimed to test if the fluorescence report from sites in the outer S4 that report upon voltage sensor movement, report earlier or faster movement than that of pore opening and the resulting flow of ionic current in hERG channels. To investigate this, I measured the kinetics of the fluorescence change upon depolarization from a number of sites and compared this with the kinetics of pore opening measured under the same conditions. The kinetics of fluorescence quenching upon depolarization (red) and channel activation (black) from TMRM attached at G516C (A), E519C (C) and L520C (E) are shown in Fig. 5.6. The time course of opening of the pore during activation at +60 mV was measured using an envelope of tails voltage protocol in which peak tail current amplitude was assessed following depolarizing pulses (+60 mV) of increasing duration. Experiments were performed in TMRM-labeled oocytes. The time course of the fluorescence report of voltage sensor activation was measured by fitting the fluorescence signal at +60 mV to a single exponential function. The TMRM fluorescence report from hERG G516C, E519C and L520C channels activated at +60 mV with tau values of 33.5 ± 1.3 ms (n = 5), 67.1 ± 1.9 ms (n = 5) and 59.3 ± 3.0 ms (n = 5), respectively. In each case, this was faster than the time course of opening of the pore gate. Pore gate activation from the same constructs at +60 mV occurred with tau values of 98.5 ± 4.1 ms (n=4), 108.1 ± 5.3 ms (n = 4) and 78.1 ± 2.2 ms (n = 4), for hERG G516C, E519C and L520C, respectively. These data further support the conclusion that fluorescence reports from G516C (B), E519C (D) and L520C (F) track voltage sensor movement.

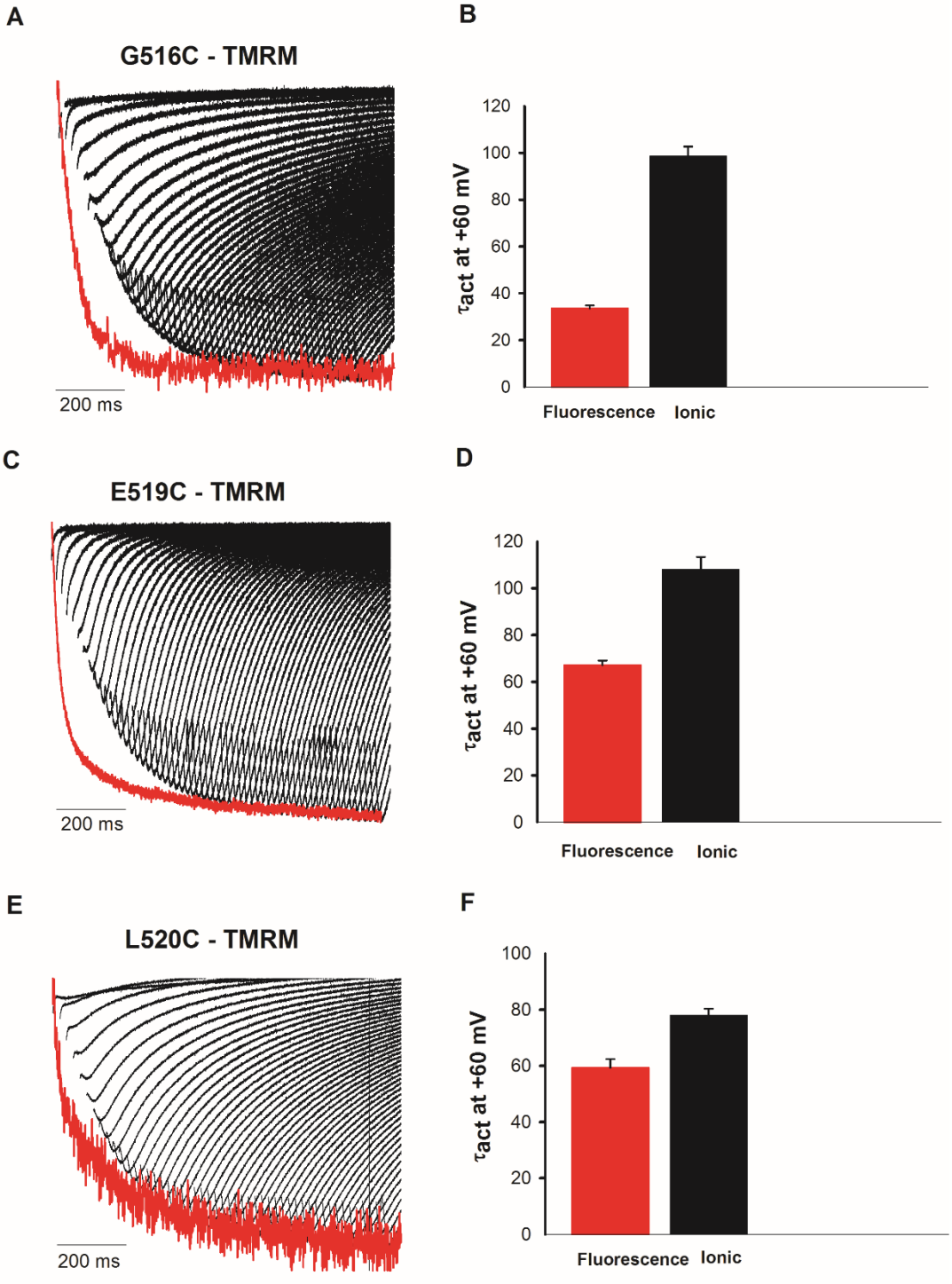
A
G516C - TMRM
200 ms
B
τact at +60 mV
120
100
80
60
40
20
0
Fluorescence
Ionic
C
E519C - TMRM
200 ms
D
τact at +60 mV
120
100
80
60
40
20
0
Fluorescence
Ionic
E
L520C - TMRM
200 ms
F
τact at +60 mV
100
80
60
40
20
0
Fluorescence
Ionic

Figure 5.6 Fluorescence report of voltage sensor movement kinetically precedes pore gate opening in hERG channels.

Left, Typical ionic current (black) and fluorescence (red) traces from TMRM-labeled hERG G516C (*A*), E519C (*C*) and L520C (*E*) channels. Ionic currents were recorded during an envelope of tails protocol (see section 2.4.3) to measure the time course of activation of ionic current at +60 mV. The fluorescence signal was recorded during a depolarization to +60 mV. ***Right,*** Comparison of the time course of activation of ionic current and fluorescence of each construct. The black bars represent the activation tau obtained from exponential fits to the peak tails (black traces in *left*) and the red bar represents the exponential fit of the fluorescence change upon depolarization to +60 mV for 2 s (red trace in *left*). These data show that the fluorescence report of voltage sensor movement is faster than ionic current activation, suggesting that the voltage sensor moves ahead of pore gate opening.

Fig. 5.7 shows example fluorescence traces recorded from *Shaker* A359C (A) and hERG L520C (B), to compare the relative kinetics of voltage sensor movement. Fluorescence emission from *Shaker* channels is monophasic, with a quenching upon depolarization to +60 mV that occurs with a time course ~10 times faster than that observed in hERG channels. This finding suggests that voltage sensor movement in hERG is slow, and likely limits activation. This is consistent with the observation that gating current measurements recorded in oocytes show a prominent slow phase of charge movement (Piper et al. 2003; Piper et al. 2005; Goodchild & Fedida 2014; Thouta et al. 2014; Goodchild et al. 2015; Thouta et al. 2017).

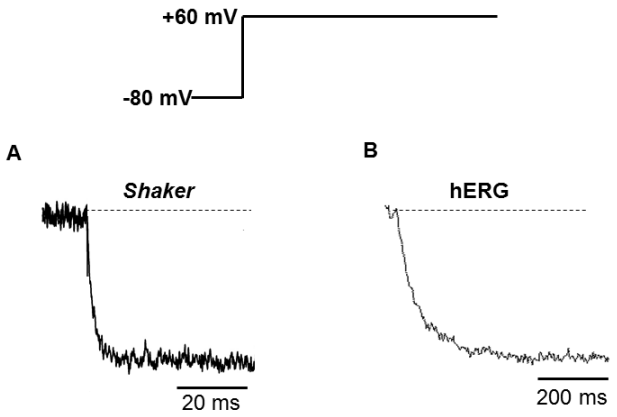

Figure 5.7 Comparison of voltage sensor movement in *Shaker* and hERG channels.

A and ***B,*** example fluorescence traces from TMRM-labeled *Shaker* A359C (*A*) and hERG L520C (*B*). Fluorescence signals were recorded in response to a depolarizing step from -80 mV to +60 mV. Data show that the fluorescence report of voltage sensor movement in *Shaker* channels is faster than hERG channels, indicating that movement of the voltage sensor appears to be slow in hERG channels and this might contribute to slow hERG channel activation.

5.5 Discussion

In this study, I have performed a detailed VCF study in hERG channels to investigate the ability of fluorophores attached to the outer voltage sensor to provide a faithful report of voltage sensor movements during activation gating. To do this, I compared the time course and voltage-dependence of fluorescence and ionic currents using equivalent protocols. My key findings are: (1) I observed qualitatively similar profiles of fluorescence change reporting voltage sensor movement from different sites on the outer voltage sensor, with a couple of exceptions; (2) I found that the fluorescence report of voltage sensor movement kinetically precedes channel opening; (3) I showed that fluorescence changes from TMRM-labeled L520C produce an FV relationship that is left-shifted from that of the GV when all fluorescence changes were captured. Taken together, these data suggested that fluorophores labelling sites at the top of the voltage sensor provide reliable reports of the voltage-dependence and kinetics of voltage sensor movement in hERG channels.

5.5.1 Previous VCF measurements in hERG channels and the ability of fluorophores to track voltage sensor movement

A few previous studies from laboratories other than our own have reported VCF measurements of hERG gating (Smith & Yellen 2002; Es-Salah-Lamoureux et al. 2010; Tan et al. 2012) to probe the connection between S4 movement and pore opening. Initial VCF reported fluorescence signals from three adjacent sites located in the S3-S4 linker region, but did not remove the native cysteines in the S1-S2 linker (Smith & Yellen 2002). The authors showed that the fluorescence signal from TMRM at each site (E518C, E519C, or L520C) contained a slow component, but that the report from E518C and E519C also showed a fast component of fluorescence change. The authors showed that the fast component presented similar kinetics and voltage-dependence to the rapid C-type inactivation process in hERG channels. However, alterations in the inactivation process made by pore mutations, or by TEA application, did not alter the fast fluorescence component, leading the authors to suggest that the fast report may reflect voltage sensor transitions associated with inactivation, rather than inactivation itself, or an electrochromic effect of the fluorophore. However, neither conclusion is particularly satisfying, since it has been shown that inactivation does not derive its voltage dependence from S4 (Zhang et al. 2004), and an electrochromic effect would be

expected to be very much more rapid than the observed changes. Smith and Yellen (2002) described the time course and voltage-dependence of the slow component of fluorescence from TMRM-L520C as closely matching the kinetics and voltage-dependence of activation (GV). This led the authors to suggest that voltage sensor movement limits opening of the pore in hERG channels. In agreement with this finding more recent fluorescence reports from E518C labelled with MTSR showed a slow fluorescence emission that displayed a time-and voltage-dependence that is in close association with channel activation (Tan et al., 2012). Taken together, these data suggested that the slow changes in the fluorescence reflect conformational changes of S4 that underlie the unusual slow activation in hERG channels and have led to the conclusion that slow voltage sensor movement, rather than pore opening, is rate-limiting for activation in hERG channels. Such a conclusion was consistent with previous Markov modeling schemes (Wang et al. 1997), which identified a rate-limiting step early in the activation pathway that preceded pore opening. This scheme is, however, in contrast to the fluorescence reports from *Shaker* (Mannuzzu et al. 1996; Cha & Bezanilla 1997) channels, where fluorescence reports from analogous positions (A359C in *Shaker*) were rapid and the voltage-dependence of fluorescence (FV) reported was left-shifted by ~20 mV relative to the GV relationship, indicative of S4 movement that precedes channel opening. Another group revisited this idea and performed VCF in hERG channels showing that the two native cysteines in the hERG S1-S2 linker, C445 and C449, modified the fluorescence signals reported by the S4-labeled positions (Es-Salah-Lamoureux et al. 2010). These authors showed that removing these native cysteines enabled a cleaner measure of fluorescence signals from fluorophore linked sites. In particular, substitution of native cysteines with valine modified the overall fluorescence emission from the TMRM labeled hERG E519C in the S3-S4 linker. As in the previous work (Smith & Yellen 2002), fluorescence signals from TMRM-labeled E519C upon membrane depolarization showed two kinetic components. Unlike Smith and Yellen, these authors attributed the fast component of fluorescence change to rapid S4 movement and the slow component to events associated with pore gate opening (Es-Salah-Lamoureux et al. 2010). These authors showed that the voltage-dependence of the fast component was best described by a double Boltzmann function with one majority component that was left-shifted to the GV relation, and comparable with the gating charge QV relationship described in WT hERG channels (Piper et al., 2003, 2005). This led the authors to suggest that S4 movement in hERG channels precedes

pore gate opening, and is not rate-limiting in the activation pathway (Goodchild & Fedida 2014, Wang et al., 2013; Goodchild et al., 2015). The authors showed that the second component of the fast fluorescence of TMRM-E519C showed an FV relation that was right-shifted from the GV and attempted to correlate this with the fast component of on-gating charge (Q_{on}), described in previous studies (Piper et al., 2003). Interestingly, this component of fluorescence was not present in S620T:E519C, inactivation-removed, channels. However, in the gating current measurements, the fast Q_{on} was still present in the inactivation-removed mutant, leaving the underlying basis for the second component of fast fluorescence from E519C channels elusive. These different studies thus arrive at different conclusions as to what the fast and slow fluorescence components recorded from the hERG voltage sensor reflect, and this has led to differing interpretations about whether the voltage sensor or the pore limits slow activation in hERG channels. Using a systematic scan of voltage sensor sites and two different fluorophores, my data were able to reconcile some of these previous findings.

5.5.2 TMRM and MTSR labelling in the S3-S4 linker induces fluorescence changes with both fast and slow components

To my knowledge, I have performed the most comprehensive examination of fluorescence reports from the hERG voltage sensor to date. For most sites, labelling with either TMRM or MTSR yielded similar fluorescence profiles: a single component of fluorescence change. However, MTSR at S517C and TMRM at E519C reported fluorescence changes with both fast and slow components. Interestingly, TMRM at S517C and MTSR at E519C reported only a single fluorescence component (Fig. 5.3).

To examine the correlation between the voltage-dependence of the fluorescence signals and ionic currents, I measured isochronal FV and GV protocols. Fig. 5.4 shows that the fluorescence signal from G516C and L520C reported an FV relationship that overlaid the GV relationship. In contrast, the initial rapid quenching from TMRM-E519C upon depolarization has two components, with one component (FV_1) hyperpolarized compared to GV. Another component, FV_2, showed a voltage-dependence that had a more depolarized voltage-dependence than the GV. These observations were consistent with previous findings of Es-Salah-Lamoureaux et al. 2010. Interestingly, recent gating current recordings from hERG WT expressed in mammalian cells reported two distinct charge systems with an extremely rapid gating charge component (Q1) that carries less

charge (~30 %) and a slow charge component (Q2) that carries the bulk of the charge (~70%) (Wang et al. 2013). Interestingly, the voltage-dependence of the rapid quenching of the TMRM-E519C (FV1) closely correlated with the voltage-dependence of the Q1 component which had a $V_{1/2}$ of -55 mV (Wang et al. 2013). Thus, the fast component of fluorescence in E519C may reflect early voltage sensor transitions associated with the activation pathway, and is consistent with the FV1 relation being more negative compared to that of GV relationship.

This fast fluorescence component was only observed from TMRM-E519C and MTSR-S517C, and was not observed from the second fluorophore at the same site. The differences in these signals may be due to the differences in the linker size (maleimide vs MTS), such that the orientation of the fluorophore's transition dipole could be different with the different fluorophores thereby causing a change in the fluorescence quenching. Alternatively, the distance between the quencher and the fluorophore could be different and responsible for the difference in the fluorescence signals. It is also apparent that the change in the fluorescence is not only dependent on the site of the labelling, but also the surrounding protein residues, which can interact with and quench the fluorophore. Further investigation is required to better understand the differences between the TMRM and MTSR fluorescence signals at S517C and E519C positions.

5.5.3 Slow fluorescence changes from TMRM-L520C channels report on voltage sensor movement

What then is the relationship between the slow fluorescence change reported from the majority of sites and voltage sensor and pore gating? Voltage-sensor movements in Kv channels show a separation of gating charge movement and pore opening during voltage-dependent gating (Bezanilla 2000). For example, simultaneous ionic and fluorescence recordings show that the TMRM fluorophore in *Shaker* reports a monophasic fluorescence change upon depolarization that occurs with a time-course and voltage-dependence that precede pore opening (Mannuzzu et al. 1996; Cha & Bezanilla 1997). However, the monophasic fluorescence changes from TMRM-G516C and L520C showed no separation between the FV and GV relationships (Fig. 5.4B and F). This raises the question as to whether the fluorescence signal from these sites reports on S4 movement or other conformational changes occurring in or near the pore that are associated with pore activation. To address this, I investigated whether, in

TMRM-L520C, the measurement of the fluorescence signal might be systematically underestimated. I reasoned that movements at negative potentials that would contribute to the FV relation might be missed by holding at -80 mV. My data showed a robust fluorescence de-quenching when the membrane potential was hyperpolarized from -80 to -120 mV and that the FV relationship was shifted to more negative potentials when holding at -120 mV. The shift of the FV relation was pronounced, shifting by ~-30 mV. Furthermore, the FV relation recorded from holding potential of -120 mV showed a hyperpolarized shift in compared to GV (Fig. 5.5D) that was comparable with the separation between the QV and GV relationship in hERG channels (Fig. 5.4H). These findings indicated that previous measurements of fluorescence from this site underestimated the signal because the voltage sensor did not fully returned to its resting state at -80 mV. My data show that the slow fluorescence from the TMRM-L520C channels tracks the voltage-dependence of voltage sensor movements rather than pore opening. In addition, this FV relationship of TMRM-L520C channels from a holding potential of -120 mV closely resembled the voltage-dependence of the slow gating component (Q2) that carries the bulk of the gating charge as described in the cut-open oocyte (Piper et al. 2003; Goodchild & Fedida 2014) and patch clamp in mammalian cells (Wang et al. 2013). In my experiments, comparisons between GV, FV and QV were made by using protocols with same depolarizing pulse duration (2 s), since I have shown in Chapter 4 that the GV of activation and QV of on-gating shifts left if the step duration is prolonged, which would lead to a separation between GV and QV. The data presented here show that fluorescence reports of TMRM-L520C channels track the voltage-dependence of S4 movement. Further study is required to measure fluorescence reports from other remaining sites, such as G516C, S517C, and E518C to determine the effect of holding potential on the fluorescence report from these sites.

5.5.4 Slow voltage sensor movement underlies the slow hERG activation

Recent gating current records from hERG channels expressed in oocytes (Piper et al. 2003; Goodchild & Fedida 2014; Goodchild et al. 2015) or mammalian cells (Wang et al. 2013) showed that the prominent slow phase of voltage sensor movement carries the bulk of gating charge that moves faster than pore opening. Therefore, to further test whether the slow fluorescence report from hERG channels might reflect voltage sensor movement, rather than pore opening, I measured the kinetics of the slow fluorescence

change upon depolarization and compared this with the kinetics of pore opening recorded from a standard envelope of tails protocols. The data showed that the time course of the fluorescence change from TMRM in G516C, E519C and L520C channels is faster than ionic current activation (Fig. 5.6). This finding is consistent with the slow fluorescence report from these sites reporting on an event that is associated with voltage sensor movement, rather than pore opening. In comparison to the fluorescence report of voltage sensor movement in *Shaker* channels, the reports from hERG channels are slow (Fig. 5.7), consistent with the slow movement of the bulk of charge observed in gating current measurements (Piper et al. 2003; Wang et al. 2013; Goodchild & Fedida 2014; Thouta et al. 2014; Goodchild et al. 2015).

5.5.5 Synopsis of hERG gating currents and fluorescence measurements

The initial gating current recordings of hERG channels expressed in oocytes revealed fast and slow gating charge components that differed ~100-fold in their kinetics and exhibited different QV relationships; the slow being left-shifted from the GV and the fast being ~50 mV right-shifted from the GV (Piper et al. 2003). The authors indicated that the slow component carries the bulk of the gating charge and was implicated as the reason for slow activation of hERG. Subsequent gating current recordings from hERG channels expressed in mammalian cells and with a faster clamp speed showed fast (Q1) and slow (Q2) gating charge systems that were both much faster than channel opening and exhibited similar QV relationships that are hyperpolarized relative to the GV relationship. The authors suggested that S4 movements are not rate-limiting in hERG slow gating, implying that downstream events may have more effect on the delay of pore opening (Wang et al. 2013). To address the differences between the gating currents recorded in different expression systems, a recent study directly compared gating currents recorded from COVG in oocytes and whole cell patch clamp in mammalian cells (Goodchild & Fedida 2014). The study reported a prominent slow phase of voltage sensor movement that carries the majority of charge that can be resolved in COVG of oocytes, but not in mammalian cells. These data suggested that the slow component of gating charge is more easily resolved in oocytes, perhaps because the slow IgON was too small to clearly resolve in mammalian cell recordings and that mammalian cells could not tolerate the long duration depolarizing steps required to resolve the slower movement of charge. This slowly moving bulk of voltage sensor charge preceded, both

kinetically and energetically, pore gate opening. These data provide some clarity as to the fluorescence reports from different sites in the S3-S4 linker. Sites that produce fluorescence reports that kinetically precede pore gate opening and with a voltage-dependence that is left-shifted to GV relation are consistent with measurements of the movement of the bulk of the gating charge. The data presented in Fig 5.6 show that the slow fluorescence report from G516C, E519C and L520C tracks voltage sensor movement that precede pore opening. Taken together with the data showing that the FV relation of L520C is left-shifted from the GV relationship (Fig 5.5D), these data support the idea that the slow fluorescence report from L520C is consistent with the kinetics and voltage-dependence of movement of the bulk of the gating charge in hERG channels. Interestingly, the voltage-dependent components of the fast fluorescence change reported from E519C correlated with the voltage-dependence and kinetics of the fast gating charge component (Q1) described in the hERG gating currents recorded from mammalian cells. This fast charge component has been suggested to reflect early voltage sensor transitions between the closed states of the channel. Overall, these data support the idea that slow S3-S4 linker fluorophore reports track slow voltage sensor motions that carry the bulk of gating charge.

Chapter 6. General Discussion and Future Direction

The work presented in this thesis has been an investigation into the molecular mechanisms of hERG potassium channel activation and deactivation gating. The main questions raised involve the determination of the structural basis of the activation gate, the mechanism underlying the slow activation gating of hERG, and the key steps involved in the hERG deactivation pathway. The aim of this final chapter is to discuss the context of the findings reported in this thesis in the broader scope of ion channel biology, and to discuss some future directions of hERG research.

6.1 hERG Activation

6.1.1 Nature of the hERG activation gate

The majority of drugs that block hERG do so by entering the pore via the intracellular activation gate. Numerous studies have identified key residues within the intracellular pore required for high-affinity block of hERG channels, such as Y652 and F656 in the S6 helix, as well as T623, S624 and V625 in the pore helix (Mitcheson et al. 2000). Despite this structural information, there remains significant interest in understanding the structural elements of the hERG activation gate and how it contributes to high-affinity drug binding since the unusually slow opening of the gate limits the accessibility of drugs to their binding site.

The activation gate in the majority of Kv channels is formed at the bundle crossing by the convergence of the inner S6 helices near a conserved proline-valine-proline (PVP) motif, which introduces a kink in the helices that allows for electromechanical coupling with voltage sensor motions (Jiang et al. 2002b). I described in section 1.7.1 that hERG channels lack the PVP motif and the location of the gate and how it is coupled to voltage sensor movement was poorly understood. This is particularly important because slow activation of hERG channels is fundamental to the critical role these channels play in the heart and also regulates drug blocker access. Despite this, the mechanism underlying slow activation in hERG channels is unclear. In Chapter 3, I initially investigated the functional impact of introducing the PVP motif into hERG channels. In contrast to WT channels, introduction of the PVP motif trapped the hERG channels in the open state

producing constitutively active hERG channels that passed inward current at hyperpolarized voltages that did not appear to deactivate (Fig. 3.1). Based on these initial results, I introduced single proline residues at different positions along the length of the inner S6 helix, from I655 to Y667, to determine whether each proline mutant gated as WT or PVP-phenotype (Fig. 3.2). A similar approach was previously used to define the location of the pore gate in Kir3.4 G protein-sensitive inwardly rectifying potassium (GIRK) channels, which also lack the PVP motif. In Kir3.4 channels, the introduction of a proline at S176 (equivalent to M651 in hERG) resulted in constitutively active channels. A proline scan of the lower portion of the helices revealed an α-helical periodic pattern of gate perturbation, whereby prolines introduced on the same face of a helix to S176 stabilized the open state of the gate, while those on the opposite face stabilized the closed state (Jin et al. 2002). The periodicity of open gate stabilization stopped one helical turn above the narrowest part of the intracellular pore that is formed by F187. Using a similar approach, proline scan of the hERG inner S6 helix, from I655 to Y667 revealed that gate perturbation occurred with proximal substitutions (I655 to Q664), as in the PVP mutant, and distal (R665 to Y667) substitutions preserved WT like gating, strongly suggesting that the position of the intracellular activation gate in hERG channels is formed at Q664 (Fig. 3.2D). These data suggest that the activation gate in hERG channels is one full helical turn below the location of the gate (V478) in *Shaker* channels. Thus, using a very different approach, these data support the Wynia Smith et al. work, where they showed cysteine substitution at Q664, Y667 and S668 produced constitutive active channels, and when mapped onto a homology models these sites formed a gating ring, with the ion conduction barrier at Q664 (Wynia Smith et al. 2008). Subsequent to publication of my study showing the location of the gate (Chapter 3), a cryo-EM structural prediction of *eag* (Whicher & MacKinnon 2016) and hERG channels (Wang & MacKinnon 2017) has been published. These structures demonstrate the lack of a PVP motif and show the position of the gate (Q476 in *eag* and Q664 in hERG) being below the position occupied by the gate in *Shake*r, consistent with my functional experimental findings. This lower gate position likely increases the size of the hERG channel pore cavity allowing greater drug access. In contrast, the hERG cryo-EM structure showed that the pore cavity is small exhibiting a highly electronegative potential with extended pockets. However, the authors did not provide any quantitative analysis to confirm that the pore cavity is small. I assume that the presence of extended hydrophobic pockets and narrow constriction in the pore cavity appear to suggest that the hERG channels

comprises a small volume of pore cavity. Therefore, more data is required to understand the precise mechanism of drug binding. Thus, in addition to unique pore-lining aromatic residues, hERG presents pore geometry that is conducive to drug binding. These features appear to underlie the unique involvement of hERG channels in the generation of acquired LQTS.

6.1.2 **Voltage sensor movements in a trapped-open hERG channel**

With the aim of understanding whether the hERG trapped open channel phenotype was the result of altered electromechanical coupling or altered voltage sensor movement, I measured fluorescence reports and gating currents from I663P trapped-open channels (Fig. 3.6). It was possible that proline substitutions in the S6 had broken the coupling between voltage sensor movement and the pore gate, thereby isolating the gate and trapping it in the open state. Alternatively, the proline substitutions may have allosterically altered the coupling of S6 with the S4-S5 linker such that they effectively immobilized the voltage sensor. Both fluorescence and gating currents revealed that voltage sensor movement in I663P trapped-open channels was intact and exhibited similar conformational changes to channels in which normal gate function was preserved. These data suggested that I663P channels trap the activation gate open as a result of uncoupling of the voltage sensor from the pore (Fig. 3.6). Typically, such uncoupling would be expected to result in a separation of the QV (or FV) and GV relationships. However, we do not see this phenomenon in I663P channels as the pore is open independent of voltage. It is possible that the pore gates between two open states in response to voltage sensor movements. However, I cannot discern between this possibility and an uncoupling of the voltage sensor from the pore from my data in chapter 3. This could be further investigated, for example, by tracking movements of the inner pore gate using fluorescent unnatural amino acids (fUAAs) during voltage sensor gating.

I realized that such uncoupling of the pore (via I663P) allowed scrutiny of voltage sensor movement in isolation from constraints induced by the pore. In a comparison of the fluorescence report of voltage sensor movement in G516C channels with and without the I663P mutation, my data showed that a component of voltage sensor movement appears to be intrinsically slow. I interpreted this to indicate that this likely underlies slow activation gating in hERG channels (Fig. 3.8). This conclusion is consistent with gating

currents measured from hERG WT channels. Charge movement in hERG channels is complex, presenting two distinct components that differed in kinetics and voltage-dependence. Measurements of gating currents using cut-open oocyte showed an initial rapid component with a time course of ~ 0.5 ms followed by a slow decaying component carries the bulk of the gating charge, which displayed a voltage-dependence (QV) that is hyperpolarized to the GV relationship and is ~100-fold slower than the fast component (Piper et al. 2003; Piper et al. 2005; Goodchild & Fedida 2014; Thouta et al. 2014; Goodchild et al. 2015). Furthermore, the first gating current measurements of hERG WT expressed in mammalian cells revealed two gating charge systems (Q1 and Q2) with similar voltage-dependencies and different kinetics. The Q1 charge system was extremely rapid and caries less charge (30%). It is followed by a large slow component (Q2) that carries the bulk of the charge (70%) (Wang et al. 2013). However, in each report of gating currents recorded from hERG channels, a prominent slow component is evident, which carries the majority of charge. My findings are also consistent with Markov kinetic schemes, which require a rate-limiting step between closed states early in the activation pathway to effectively model hERG activation gating characteristics (Wang et al. 1997). These findings suggest that a slow component of charge movement associated with the voltage sensor limits the activation gating of hERG channels.

6.1.3 Trapped-open hERG channel provide a potential model to study drug binding in hERG channels

The trapped open hERG channel phenotype (e.g. I663P) offers a unique opportunity to study the mechanism of drug binding in hERG channels. There is considerable debate regarding the role of inactivation in determining the high-affinity binding of drugs in hERG channels. Inactivation in hERG channels has a characteristic and unusual voltage-dependence that may contribute to high-affinity drug binding. Consistent with this, *eag* channels which are closely related to hERG channels do not inactivate and are less sensitive to drug block. When mutations that introduce inactivation are engineered into *eag*, the channel becomes sensitive to drug binding (Ficker et al. 2001). Other studies have also shown reduced drug sensitivity in hERG mutant channels that either reduce inactivation (S631A, N588K, N588E) or completely abolish inactivation (S620T, G628C+S631C) (Ficker et al. 1998; M. J. Perrin et al. 2008). However, mutations that enhance inactivation, such as G648A, F627Y and S641A, showed reduced affinity for drug block by the anti-arrhythmic drug MK-499 (J. S. Mitcheson et al. 2000). In addition,

different mutations that either accelerated or abolished inactivation showed no change in the IC50 for cocaine block (Guo et al. 2006). Furthermore, using hERG concatemers a recent study showed that S620T and S631A mutations reduced drug sensitivity by a mechanism that is independent of their effects on inactivation gating (Wu et al. 2015). These studies suggest uncertainty as to the role of inactivation in determining high affinity drug binding in hERG channels.

A reason for such conflict might be due to difficulties in measuring the effects of inactivation, since its kinetics are rapid, and drugs must wait for slow opening of the activation gate to bind. This makes it difficult to assess the state-dependence of drug binding. The studies described above took an approach to manipulate inactivation by introducing mutations in the pore region and from the effect on binding affinity, inferred the importance of inactivation gating in drug binding. However, pore mutations may alter drug binding independent of their effect on gating, for example by allosterically modifying the pore structure, or by altering channel selectivity.

My trapped-open I663P hERG construct provides a novel experimental paradigm to study the role of inactivation in drug binding. Because hERG I663P channels are trapped in the open state over a wide range of voltages (Fig. 3.2), and inactivation is slightly altered by the mutation, it is possible to evaluate the role of inactivation in determining the high drug binding affinity of hERG channels. I have preliminary data which compared the extent of block by cisapride, terfenadine and dofetilide at voltages where inactivation is maximum (e.g. +40 mV) with voltages where inactivation is minimal (e.g. -120 mV) in trapped-open I663P channels. These preliminary data showed that the extent of block by all three drugs does not correlate with the voltage-dependence of inactivation and did not show a strong dependence of binding upon voltage. Once extended, these experiments will provide better insight into the molecular mechanisms underlying the unusually high-affinity drug binding in hERG channels.

6.1.4 **The V659P mutation is activated by hyperpolarization**

Interestingly, V659P mutant channels revealed an unusual phenotype in which the channels appeared trapped open but passed an additional slowly activating and voltage-dependent inward current upon strong hyperpolarization (Fig. 3.4A). This phenotype is reminiscent of the well-studied hyperpolarization-induced activation of hERG D540K and

HCN channels (Sanguinetti & Xu 1999; Vemana et al. 2004; Bruening-Wright & Larsson 2007). hERG D540K channels re-open to an open state at negative membrane voltage that is different from the depolarization-induced open state (Sanguinetti & Xu 1999). In V659P channels, the hyperpolarization-activated conductance and the voltage independent trapped-open channel conductance each accounted for approximately half of the total open probability (Fig. 3.4B). I interpreted this to indicate one of two possibilities: (1) that at any given potential there are two populations of channels, those in the trapped-open state that conducts at all voltages, and those in the hyperpolarization-activated state that has approximately twice the conductance of the trapped-open state; or (2) that the trapped-open state reflects a partial conductance (~50% of the maximal open probability), perhaps from an incompletely open channel gate, and that hyperpolarization fully activates channels into the maximal conductance state. The latter would suggest that the proline scan mutagenesis (Fig. 3.2 and 3.3) trapped the gate in a partially, rather than fully open state and may explain the subtle variability in the degree of closing observed among different mutations (e.g. F656P, I662P; Fig. 3.3).

It is interesting to note that either scenario would differ from the description of hyperpolarization-activation in hERG D540K channels, which activate into a distinct open state upon hyperpolarization (O_h) that is separated in a linear gating scheme from the depolarization-activated open state (O) by closed channel states (Sanguinetti & Xu 1999). In this scheme, hERG D540K O and O_h states have a similar single channel conductance (J S Mitcheson et al. 2000). The unique phenotype of V659P channels enabled us to infer that additional voltage sensor motion occurs upon repolarization. I propose that upon strong hyperpolarization, the voltage sensor relaxes to a further down state and this is coupled to the opening of the pore in V659P channels, as has been suggested to gate HCN channels (Bruening-Wright et al. 2007; Vemana et al. 2004). It is interesting to note the strong dependence upon the voltage of the hyperpolarization-activated open state. The Boltzmann fit in Fig. 3.4 B revealed a *k* value of 8.9 mV, which is similar to that of 8.7 mV for the activation of hERG WT channels upon depolarization. This suggests that significant charge movement is associated with hyperpolarization-activation of V659P channels. Further study would be required to record and characterize such inward charge movement.

Previous mutagenesis studies of hERG S6 proposed that hydrophobic interactions may be involved in coupling between the S4-S5 linker and S6 (Wynia-Smith et al. 2008). Based on homology modelling, V659 was found to lie within the hydrophobic pocket formed by S5, S6 and the S4-S5 linker in the closed state. Substitution of V659 with residues possessing different physicochemical properties dramatically slowed deactivation gating or exhibited constitutive conductance (Wynia-Smith et al. 2008). These data suggested that V659 may play a critical role in hERG deactivation gating. However, the mechanism by which V659 modulates deactivation gating is unclear. I hypothesize that V659 may modify gating by forming interactions with the S4-S5 linker. To confirm this interaction, I propose a series of cysteine cross-linking experiments. Introducing a cysteine at position V659 and a series of cysteines along the length of the S4-S5 linker to probe possible interactions by perfusing a membrane permeable oxidizing agent that induces chemical-cross linking in these sites. Furthermore, to determine specificity of the functional effects of cross-linking I would use dithiothreitol (DTT) to reverse the cross-linking effect.

6.2 hERG Deactivation

6.2.1 Time-dependent voltage sensor relaxation in hERG channels

hERG channels mediate cardiac repolarization due to their unusual gating kinetics. In particular, the mechanism of slow deactivation is not well understood. Recently, it was shown that deactivation in hERG channels is modulated by voltage sensor relaxation (Tan et al. 2012; Hull et al. 2014; Goodchild et al. 2015; Thouta et al. 2017). Prolonged depolarization reconfigures voltage sensors (S4) into a stable relaxed state that results in a hyperpolarizing shift of the voltage-dependence of S4 return and subsequent pore closure compared to that of S4 activation and pore opening. Interestingly, among the channels in which mode-shift has been described, mode-shift in hERG appears to occur on a physiological time-scale (Tan et al. 2012; Goodchild et al. 2015). The molecular mechanisms underlying hERG voltage sensor relaxation are unknown, but cytosolic regions of the channel are thought to be involved (e.g. N-terminus) (Tan et al. 2012; Goodchild et al. 2015). However, these two studies reported conflicting data. Hence, a fundamental biophysical understanding of hERG voltage sensor relaxation process is lacking. In Chapter 4, I characterized the time-dependence of voltage sensor relaxation

in hERG channels. In *Shaker* channels, the time-dependence of relaxation of the voltage sensor has been measured by applying depolarizing steps of increasing duration and observing the progressive slowing of charge return as the voltage sensor becomes more and more likely to enter the relaxed state (Lacroix et al. 2011; Labro et al. 2012). These studies showed that transition of the voltage sensor in *Shaker* and Kv1.2 channels to the relaxed state was slow, occurring over 2-4 s. Using a similar approach, I measured the time-dependence of voltage sensor relaxation in hERG channels. The data revealed that prolonged depolarization induces two components of slowing of deactivation kinetics (Fig. 4.1) and charge return (Fig. 4.2). The fast component was kinetically concomitant with the time course of activation and therefore I proposed that it is caused by a stabilization of the activated voltage sensor by the open pore. The second slower component occurred over durations that exceeded channel activation and was consistent with the reconfiguration of the voltage sensor into the relaxed state. To the best of my knowledge, this is the first quantification of the time course of the voltage sensor relaxation process in hERG channels. These data suggested that relaxation contributes significantly to the unusually slow deactivation in hERG channels. I further extended this analysis to describe the mode-shift behaviour in hERG channels. Several studies have demonstrated mode-shift behaviour in hERG channels (Piper et al. 2003; Tan et al. 2012; Hull et al. 2014; Goodchild et al. 2015), but reported differing results, leaving questions regarding the role of stabilization of the activated voltage sensor in mode-shift behaviour. My data showed that the apparent mode-shift depended greatly on recording conditions. To better understand mode-shift in hERG channels, I measured activation and deactivation at steady-state. To achieve this, I measured the voltage-dependence of activation and deactivation in response to voltage steps of increasing duration (Fig. 4.4). The relation between the $V_{1/2}$ of activation and deactivation with increasing duration show that the “true mode-shift” in hERG channels is ~15 mV (Fig. 4.4). Interestingly, the “true” mode-shift of gating currents is ~40 mV, much greater than that of the pore gate (Fig. 4.5). This observation suggests that, upon repolarization, pore closing is energetically more favourable than the return of the voltage sensor to its resting state. This suggested that the pore can close when the voltage sensor remains in its extruded position in hERG channels. Interestingly, the recent cryo-EM structural prediction of the related *eag* channel showed that the pore can be closed while the voltage sensor is in the upward position (Whicher & MacKinnon 2016), consistent with my functional observations. These data thus dissected events that occur during the

transition of channels from the activated to the deactivated state and showed that events associated with opening of the pore, as well as those intrinsic to the voltage sensor itself control return of the voltage sensor upon repolarization.

6.2.2 **Coupling of voltage sensor relaxation to the pore gate**

The N-terminus is well recognized as an integral component of deactivation gating in hERG channels that stabilizes the open state of the channel (Morais Cabral et al. 1998; Wang et al. 1998; Wang et al. 2000; F.W. Muskett et al. 2011; Gustina & Trudeau 2011; Ng et al. 2011). However, the mechanism by which this occurs is still unknown. Using VCF to track voltage sensor movement, Tan et al., 2012 showed that deletion of the N-terminus abolished the mode-shift in ionic currents without altering the mode-shift of the voltage sensor. These data suggested that the pore gate can close even though the voltage sensor is stabilized in the relaxed state (Tan et al. 2012). In contrast, another study examining hERG voltage sensor gating currents proposed instead that deletion of the N-terminus accelerates charge return and that closure of the pore is the limiting step for voltage sensor return. In this study, deletion of the N-terminus moderately reduced both ionic and voltage sensor mode-shift (Goodchild et al. 2015). I reasoned that such discrepancy derives from measurement of mode-shift at non-steady-state time points, and that faster deactivation in any construct would then appear to reduce mode-shift. Our data reconciled these reports by measuring mode-shift in ∆2-135 channels at steady-state. I demonstrated that mode-shift of ionic currents in ∆2-135 channels is similar to that in WT channels (Fig. 4.6 A-C). Moreover, coupling between the voltage sensor and pore gate appears intact, because the slowing of charge return and deactivation kinetics induced by opening of the pore gate and by relaxation are retained and exhibited a biphasic nature similar to that observed in WT channels (Fig. 4.6 D-G). This suggested that deletion of the N-terminus does not alter the stabilization of the activated voltage sensor imparted by the open pore gate or by the reconfiguration into the relaxed state. However, I observed that the kinetics of the fast phase of slowing of charge return and of deactivation kinetics in response to increasing depolarization duration was accelerated in ∆2-135 channels. This suggested that pore gate stabilization of the activated voltage sensor occurs more rapidly in the absence of the N-terminus.

Previous studies identified the S4-S5 linker of hERG as a critical factor regulating deactivation gating. A recent VCF study showed that mutations in the S4-S5 linker affect

mode-shift of ionic current without altering voltage sensor mode-shift (Hull et al. 2014). Furthermore, Lorinczi et al showed that alterations in the S4-S5 linker affected deactivation gating (Lörinczi et al. 2015). Based on these observations, in chapter 4, I used G546L mutation as a tool to study the role of the S4-S5 linker in the coupling between the pore gate and the voltage sensor during deactivation gating. Previously, this site has been shown to play an important role in regulating activation gating. G546L dramatically altered the stability of the open state as did any substitution of G546 with amino acids that reduce alpha-helical propensity (Van Slyke et al. 2010). Our data from the G546L mutant channel shown in Fig 4.3 is interesting in that it showed a single phase of slowing of charge return and deactivation kinetics with increasing depolarization duration. The G546L mutation impeded the faster component of voltage sensor stabilization that is associated with pore gate opening, without attenuating the slower component that is associated with relaxation. This suggested that the S4-S5 linker is important for communication between the pore gate and the voltage sensor during deactivation. These data also demonstrated that the mechanisms of pore gate-opening induced and relaxation-induced voltage sensor stabilization are separable. Such an influence of the S4-S5 linker on the coupling between the pore gate and the activated voltage sensor that I demonstrate in chapter 5 is consistent with the voltage sensing mechanism recently suggested in *eag* channels. The high resolution *eag* structure showed that in the activated state of the voltage sensor, the S4-S5 linker alters interaction between S4 and inner S6 directing S4 towards the C-linker that loosens the helical bundle and opens the pore (Whicher & MacKinnon 2016). Thus, my functional data is consistent with structural data in portraying a key role for the S4-S5 linker in communicating between the pore and the voltage sensor to control deactivation gating.

6.2.3 Stabilization of the activated voltage sensor represents a novel potential therapeutic target

The discovery that stabilization of the voltage sensor contributes to the unusual slow deactivation in hERG channels (chapter 4) presents a novel target to activate hERG channels. My data suggested that the relaxed state of the voltage sensor may be an attractive target for the action of hERG activator small molecules. As mentioned previously (see section 1.8), hERG activators are of significant therapeutic interest given their potential to increase repolarizing current and shorten the cardiac action potential. Several activator small molecules have been discovered (Perry et al. 2010; Zhou et al.

2011) and their mechanism of action appear to be different (Sanguinetti 2014). Interestingly, some activators such as RPR260243 and ginsenoside Rg3 alter hERG channel deactivation, slowing its kinetics resulting in increased hERG current during cardiac repolarization (Kang et al. 2005; Choi et al. 2011; Wu et al. 2016). The mechanism by which these activators alter deactivation kinetics in hERG channels is unknown. I propose that these activators slow hERG deactivation by stabilizing the relaxed state of the voltage sensor. I also suggest that novel small compounds that interact with the extracellular surface of the voltage sensor may stabilize the activated state of the voltage sensor and be used to activate hERG channels. To explore this further, I would want to examine the effects of existing activator compounds on ionic and voltage sensor mode-shift. Given the slowing of deactivation caused by these activators, I expect that both will enhance the mode-shift. I would then characterize the effect of each activator on the time-dependent voltage sensor relaxation by measuring the dependence of ionic current deactivation and voltage sensor return kinetics on the duration of preceding step depolarization. These studies aim to understand the mechanism underlying the targeted slowing of hERG activator compounds. I would follow this up by screening for novel compounds that activate hERG channels by interacting with and stabilizing the activated voltage sensor.

6.3 Using VCF to understand voltage sensor dynamics in hERG channels

VCF has proven a powerful technique in investigating the protein rearrangements associated with channel gating (Mannuzzu et al. 1996; Cha & Bezanilla 1997; Bezanilla et al. 1999; Claydon & Fedida 2007). Previous studies suggested that fluorescence emission reports from the extracellular end of the S4 voltage sensor and S3-S4 linker regions provides a reliable approach to measure the movement of S4 during channel activation. A number of studies investigated the conformational rearrangements of the voltage sensor associated with the unusual gating properties in hERG channels using VCF (Smith & Yellen 2002; Van Slyke et al. 2010; Es-Salah-Lamoureux et al. 2010; Tan et al. 2012; Hull et al. 2014; Thouta et al. 2014). However, during the completion of my thesis studies, VCF measurements in hERG channels reported conflicting data on the voltage-dependence of the report of S4 movement and kinetic separation between the report of S4 movement and pore opening. This raised questions as to whether

fluorescence measurements from hERG channels report on S4 movement or some other related or unrelated event. In chapter 5, I determined the ability of fluorescence to track voltage sensor movement associated with activation gating by performing a broad approach to labelling hERG channels with either TMRM or MTSR at five individual cysteine-substituted positions near the external end of S4 (G516 to L520). Fluorescence from both TMRM and MTSR at most of the sites yielded similar profiles exhibiting one component of fluorescence change during depolarization and repolarization, respectively. I characterized the voltage-dependence of the fluorescence change (FV) and compared this with voltage-dependence of ionic current activation (GV). In these experiments, I compared between equivalent GV and FV curves recorded from the same pulse duration, because in Chapter 4 I showed that the GV and QV relations vary greatly dependent on the duration of the depolarizing duration. This suggested that steady-state measurements require protocols with enough time for channels to fully stabilize into a new state. I also examined the effect of holding potential on the FV relation, working on the idea that the voltage sensor may not be fully at rest at -80 mV. My data showed that the FV relation of TMRM-L520C differed significantly when measured from a holding potential of -120 mV compared to FV relation measured from holding potential of -80 mV, with the FV relation by ~-30 mV (Fig. 5.5). This suggested that the FV relation is ~-30 mV hyperpolarized with respect to GV relation. Such a report is consistent with voltage sensor movement preceding pore opening. This finding needs to be confirmed by fluorescence reports from other sites, such as G516C, S517C and E518C. Although the position of the FV relation in TMRM-L520C channels is left-shifted from the GV, comparisons will also be required to be made between equivalent VCF signals and charge movement from gating current recordings. The faster fluorescence change we observed at TMRM-E519C closely correlated the voltage-dependence of the fast gating charge component (Q1) described in hERG WT gating currents recorded in mammalian cells. The Q1 component had a $V_{1/2}$ of -55 mV, and was hyperpolarized in compared to GV relationship, just like the FV1 relation described in chapter 5. However, the more positive component of the E519C fluorescence does not correlate well with known gating steps and its origin will require further evaluation.

In addition to these measurements of the voltage-dependence of fluorescence changes upon depolarization, I also compared the kinetics of fluorescence quenching upon depolarization with the time course of ionic activation and showed that the hERG voltage

sensor moves ahead of pore opening (Fig. 5.6). Interestingly, comparing the time course of fluorescence from hERG channels with that in *Shaker* channels, shows that voltage sensor movement is significantly slower in hERG channels. This is further evidence that slow voltage sensor movement underlies the slow activation of hERG channels (Fig. 5.7). In conclusion, these results showed that in hERG channels, just as in other Kv channels, the time course and voltage-dependence of voltage sensor movement precedes pore gate. The kinetics of movement of the voltage sensor in hERG channels is, however, considerably slower than in *Shaker*-like channels. Moreover, these data clear up uncertainty and controversy in the literature regarding the events reported upon by fluorophores at the top of S4 and suggest that fluorescence changes reported during VCF experiments in hERG channels report faithfully upon voltage sensor movement.

6.4 Insights into alternative voltage-dependent gating mechanism described in *KCNH* family of K^+ channels

Based on the available X-ray crystal structures of voltage-gated ion channels as well as extensive mutagenesis and functional experiments, transmission of voltage sensor movements to the pore gate (electromechanical coupling) is widely accepted to occur via the S4-S5 linker (Lu et al. 2002; Long et al. 2005b; Labro et al. 2008; Batulan et al. 2010). It is evident that the S4-S5 linker forms an α-helix that runs parallel to the membrane and acts as a mechanical lever on the C-terminal portion of S6 helix which it passes over (Long et al. 2005b). However, this does not appear to be the case with the *KCNH* family channels. In hERG channels the covalent link between the voltage sensing and pore domains is not completely required to confer voltage-dependent gating properties as shown by the co-expression of two independent modules, by creating a split at S4-S5 linker (Lörinczi et al. 2015). These data have challenged the role of the S4-S5 linker in transducing voltage sensor motions to the pore gate described in *Shaker* and other Kv channels (Blunck & Batulan 2012). This raises the question as to what molecular players could be involved in coupling the voltage sensor to the pore in the presence of an interrupted S4-S5 linker in *KCNH* channels. Moreover, the recent cryo-EM structure of r*Eag*1 and hERG channel revealed that the S4-S5 linker is a short loop that is not domain swapped and thus, not able to function as a mechanical lever, and this has resulted in an alternative model of voltage-dependent gating in *Eag* family members (Whicher & MacKinnon 2016; Wang & MacKinnon 2017). It is proposed that in

its hyperpolarized or resting state the voltage sensor would interact directly with the C-linker and induce a bend in S6 to close the pore gate. The up or depolarized conformation of S4 would enable rotation of the C-linker such that it loosens the S6 thereby relieving the high-energy bend to open the pore. This mechanism also consequently allows interaction of the cytoplasmic domains of *KCNH* family members with the pore and voltage sensing domains. Therefore, any changes to the transmembrane or cytoplasmic gating modules would perturb their movements, and affect the biophysical properties of *KCNH* channels. More recently, it has been shown that disruption of the covalent link within the S4 helix produced constitutively conducting channels whereas disrupting the S4-S5 linker did not (Tomczak et al. 2017). These data further supported the idea that the S4 helix rather than S4-S5 linker is important to close the pore in *Eag* channels. Surprisingly, mutation of D342 (homologous to D540 in hERG, which causes channels to re-open at hyperpolarized potentials) restored WT-like gating behaviour in split channels within the C-terminal of S4 that showed constitutive conductance. This is interesting because in hERG channels D540 mutants show a preference for the open state (Sanguinetti & Xu 1999). This observation suggests to me that the new alternative gating model proposed for *Eag* channels is not restricted to the interaction between the S4 and C-linker under the closed state of the channel. Of particular interest, VCF and accessibility experiments showed that the *Eag* split channels did not influence the voltage-dependence of voltage sensor movement, suggesting that the constitutive conductance in split channels is due to altered coupling between the voltage sensors and pore domain rather than changes in voltage sensor movements.

Based on these observations, I propose that split channels provide an excellent experimental model to assess the functional coupling between the voltage sensing and pore domains. In light of the new structural (Whicher & MacKinnon 2016) and functional evidence shown in *Eag* channels (Lörinczi et al. 2015; Tomczak et al. 2017), I propose to generate hERG split channels at different positions down the length of S4 and within the S4-S5 linker with the aim of investigating the interactions at the interface between the voltage sensor and pore domain in hERG channels. In addition, from a different perspective, I am also interested in understanding the functioning of the voltage sensor independently, in isolation from the pore domain. To do this, I propose to measure gating currents and fluorescence from truncated hERG channels, G546X, which comprise up to and including the voltage sensing domain, but lack pore domain. I speculate that

characterization of the hERG G546X could provide a greater understanding of the mechanism of voltage-dependency in hERG channels. For example, G546X channels could help to dissect the gating steps in the activation pathway of hERG channels. Previously an undergraduate in our lab has tested the functional expression of the G546X construct by injecting cRNA into oocytes and used an enzyme-linked immunosorbent assay (ELISA) to detect surface membrane expression of G546X in comparison with WT channels. The data demonstrated that the voltage sensor can express independently of the pore domain, thus creating the opportunity to study the function of the voltage sensor in isolation of pore domain.

It is important to note that although the above-mentioned studies suggest that the S4-S5 linker is not required to confer voltage-dependent gating in *KCNH* channels, previous reports from our lab, and others, have shown that mutations within the S4-S5 linker dramatically influence the open-closed equilibrium in hERG channels (Van Slyke et al. 2010; Ng et al. 2012; Hull et al. 2014). For example, substitution of G546 with various amino acids shifted the voltage-dependence of activation by ~-50 mV (Van Slyke et al. 2010). Furthermore, in chapter 5, I have shown that, mutation of the S4-S5 linker (G546L) affected the coupling of voltage sensor movement with the pore gate during deactivation gating in hERG channels (Thouta et al. 2017). These results also further support the findings from Lorinczi et al 2015, who showed that alterations in the S4-S5 linker (Y545 split hERG channel) affected deactivation gating (Lörinczi et al. 2015). These data suggest that the S4-S5 linker plays an important role for proper functioning of hERG channels. Previous studies in hERG channels have shown that specific interactions between the S4-S5 linker and S6 is required to mediate pore opening, suggesting a crucial role for the S4-S5 linker in coupling voltage sensing to channel gating. Both charge reversal and neutralization of D540 in the S4-S5 linker suggested that this residue interacts with R665 in S6 and it has been proposed that D540 and R665 act together to stabilize the closed state of the channel (Tristani-Firouzi et al. 2002). This idea was further supported by observation that cysteine residues at these sites can be chemically cross-linked (Ferrer et al. 2006). Similarly, recent work from Malak et al 2017, demonstrated that covalent binding of an S4-S5 linker peptide with the C-terminus of S6 could completely inhibit hERG gating, suggesting that the S4-S5 linker is sufficient to stabilise the pore gate in its closed state. Interestingly, covalently binding an S6 peptide with the S4-S5 linker prevented its inhibiting effect and rendered channels almost

voltage-independent (Malak et al. 2017). These results further reinforce the idea that voltage-dependent gating in hERG channels involves the S4-S5 linker that acts a ligand that binds to the pore gate (receptor) and traps the channel in the closed state. This model is actually consistent with the cryo-EM structure of the r*EAG1* channels, which show that the S4-S5 linker may be involved in directing the C-terminus of S4 towards to C-linker by interacting with the S6 pore gate in the open state. The proper distance and orientation between the C-terminus of S4 and C-linker are necessary for their interaction when the voltage sensor is in its resting state. Hence, I propose that mutations of the S4-S5 linker could affect its role in coordinating movement of S4 towards the C-linker, and in this way influence activation and deactivation gating of the channel.

6.5 **Final summary**

In this thesis, I have provided a novel mechanism to describe the unusually slow activation and deactivation gating process of hERG channels. In my first study (Chapter 3), using a proline scan approach I have shown that the position of the intracellular activation gate in hERG channels is formed at Q664, at least one helical turn below the location of gate in *Shaker* channels creating an enlarged pore cavity capable of accommodating a variety of large drug molecules. Furthermore, by characterizing the voltage sensor movement in trapped-open channel (I663P), I demonstrated that the slow activation kinetics observed in hERG channels is an intrinsic property of the voltage-sensing unit. In my second study (Chapter 4), I have defined the key steps in the deactivation pathway and showed that voltage sensor stabilization slows deactivation gating in hERG channels. My data suggested that voltage sensor stabilization occurs via two separable mechanisms, one that derives from pore gate opening and the other from the voltage-sensing unit itself. In addition, I have provided functional evidence supporting the structural observation that the pore gate in hERG channels can close with voltage sensors in the activated state, suggesting that voltage sensor return is what limits deactivation. Finally, in Chapter 5, I have characterized the use of VCF to track hERG sensor movements associated with gating. Consistent with the findings in Chapter 3, my data suggested that slow voltage sensor movement underlies the slow activation gating. Taken together, my findings in this thesis provide a greater understanding of the mechanistic and structural basis of the unusual gating processes in hERG channels,

which could improve prevention and treatment of hERG associated cardiac repolarization disorders.

References

Abbott, G.W. et al., 1999. MiRP1 forms IKr potassium channels with HERG and is associated with cardiac arrhythmia. *Cell*, 97(2), pp.175–87. Available at: http://www.ncbi.nlm.nih.gov/pubmed/10219239 [Accessed December 28, 2016].

Abbruzzese, J. et al., 2010. Modification of hERG1 channel gating by Cd $^{2+}$. *The Journal of General Physiology*, 136(2), pp.203–224. Available at: http://www.ncbi.nlm.nih.gov/pubmed/20660661 [Accessed January 15, 2017].

Adaixo, R. et al., 2013. Structural Properties of PAS Domains from the KCNH Potassium Channels Z. Zhang, ed. *PLoS ONE*, 8(3), p.e59265. Available at: http://dx.plos.org/10.1371/journal.pone.0059265 [Accessed January 10, 2017].

Aggarwal, S.K. & MacKinnon, R., 1996. Contribution of the S4 segment to gating charge in the Shaker K+ channel. *Neuron*, 16(6), pp.1169–77. Available at: http://www.ncbi.nlm.nih.gov/pubmed/8663993 [Accessed December 19, 2016].

Ahern, C.A. & Horn, R., 2004. Stirring up controversy with a voltage sensor paddle. *Trends in Neurosciences*, 27(6), pp.303–307.

Alabi, A.A. et al., 2007. Portability of paddle motif function and pharmacology in voltage sensors. *Nature*, 450(7168), pp.370–5. Available at: http://www.ncbi.nlm.nih.gov/pubmed/18004375 [Accessed December 27, 2016].

Alonso-Ron, C. et al., 2008. Thermodynamic and kinetic properties of amino-terminal and S4-S5 loop HERG channel mutants under steady-state conditions. *Biophysical journal*, 94(10), pp.3893–911. Available at: http://www.ncbi.nlm.nih.gov/pubmed/18222997 [Accessed January 8, 2017].

Armstrong, C.M., 1971. Interaction of tetraethylammonium ion derivatives with the potassium channels of giant axons. *The Journal of general physiology*, 58(4), pp.413–37. Available at: http://www.ncbi.nlm.nih.gov/pubmed/5112659 [Accessed December 19, 2016].

Armstrong, C.M., 1974. Ionic pores, gates, and gating currents. *Quarterly reviews of biophysics*, 7(2), pp.179–210. Available at: http://www.ncbi.nlm.nih.gov/pubmed/4449982 [Accessed December 19, 2016].

Armstrong, C.M., 1966. Time course of TEA(+)-induced anomalous rectification in squid giant axons. *The Journal of general physiology*, 50(2), pp.491–503. Available at: http://www.ncbi.nlm.nih.gov/pubmed/11526842 [Accessed December 19, 2016].

Armstrong, C.M. & Hille, B., 1972. The inner quaternary ammonium ion receptor in potassium channels of the node of Ranvier. *The Journal of general physiology*, 59(4), pp.388–400. Available at: http://www.ncbi.nlm.nih.gov/pubmed/4112955 [Accessed December 19, 2016].

Barlow, D.J. & Thornton, J.M., 1988. Helix geometry in proteins. *Journal of molecular biology*, 201(3), pp.601–19. Available at: http://www.ncbi.nlm.nih.gov/pubmed/3418712 [Accessed December 19, 2016].

Batulan, Z., Haddad, G.A. & Blunck, R., 2010. An Intersubunit Interaction between S4-S5 Linker and S6 Is Responsible for the Slow Off-gating Component in Shaker K^+ Channels. *Journal of Biological Chemistry*, 285(18), pp.14005–14019. Available at: http://www.ncbi.nlm.nih.gov/pubmed/20202932 [Accessed December 27, 2016].

Bezanilla, F. et al., 1999. Atomic scale movement of the voltage-sensing region in a potassium channel measured via spectroscopy. *Nature*, 402(6763), pp.809–813. Available at: http://www.ncbi.nlm.nih.gov/pubmed/10617201 [Accessed December 16, 2016].

Bezanilla, F., 1982. Gating charge movements and kinetics of excitable membrane proteins. *Progress in clinical and biological research*, 79, pp.3–16. Available at: http://www.ncbi.nlm.nih.gov/pubmed/6283564 [Accessed December 21, 2016].

Bezanilla, F. et al., 1991. Molecular basis of gating charge immobilization in Shaker potassium channels. *Science (New York, N.Y.)*, 254(5032), pp.679–83. Available at: http://www.ncbi.nlm.nih.gov/pubmed/1948047 [Accessed March 5, 2017].

Bezanilla, F., 2000. The Voltage Sensor in Voltage-Dependent Ion Channels. *Physiological Reviews*, 80(2).

Blunck, R. & Batulan, Z., 2012. Mechanism of Electromechanical Coupling in Voltage-Gated Potassium Channels. *Frontiers in Pharmacology*, 3, p.166. Available at: http://www.ncbi.nlm.nih.gov/pubmed/22988442 [Accessed April 12, 2017].

Bossi, E., Fabbrini, M.S. & Ceriotti, A., 2007. Exogenous Protein Expression in Xenopus Oocytes. In *In Vitro Transcription and Translation Protocols*. Totowa, NJ: Humana Press, pp. 107–131. Available at: http://link.springer.com/10.1007/978-1-59745-388-2_6 [Accessed December 16, 2016].

Brelidze, T.I. et al., 2013. Structure of the C-terminal region of an ERG channel and functional implications. *Proceedings of the National Academy of Sciences*, 110(28), pp.11648–11653. Available at: http://www.ncbi.nlm.nih.gov/pubmed/23801759 [Accessed January 10, 2017].

Brelidze, T.I. et al., 2012. Structure of the carboxy-terminal region of a KCNH channel. *Nature*, 481(7382), pp.530–533. Available at: http://www.ncbi.nlm.nih.gov/pubmed/22230959 [Accessed January 10, 2017].

Bruening-Wright, A., Elinder, F. & Larsson, H.P., 2007. Kinetic Relationship between the Voltage Sensor and the Activation Gate in spHCN Channels. *The Journal of General Physiology*, 130(1), pp.71–81. Available at: http://www.ncbi.nlm.nih.gov/pubmed/17591986 [Accessed March 8, 2017].

Bruening-Wright, A. & Larsson, H.P., 2007. Slow Conformational Changes of the

Voltage Sensor during the Mode Shift in Hyperpolarization-Activated Cyclic-Nucleotide-Gated Channels. *Journal of Neuroscience*, 27(2), pp.270–278. Available at: http://www.ncbi.nlm.nih.gov/pubmed/17215386 [Accessed January 10, 2017].

del Camino, D. et al., 2000. Blocker protection in the pore of a voltage-gated K+ channel and its structural implications. *Nature*, 403(6767), pp.321–325.

Del Camino, D. & Yellen, G., 2001. Tight steric closure at the intracellular activation gate of a voltage-gated K+ channel. *Neuron*, 32(4), pp.649–656.

Casis, O., Olesen, S.-P. & Sanguinetti, M.C., 2005. Mechanism of Action of a Novel Human ether-a-go-go-Related Gene Channel Activator. *Molecular Pharmacology*, 69(2), pp.658–665. Available at: http://www.ncbi.nlm.nih.gov/pubmed/16284303 [Accessed January 8, 2017].

Cha, A. et al., 1999. Voltage sensors in domains III and IV, but not I and II, are immobilized by Na+ channel fast inactivation. *Neuron*, 22(1), pp.73–87. Available at: http://www.ncbi.nlm.nih.gov/pubmed/10027291 [Accessed January 12, 2017].

Cha, A. & Bezanilla, F., 1997. Characterizing voltage-dependent conformational changes in the Shaker K+ channel with fluorescence. *Neuron*, 19(5), pp.1127–40. Available at: http://www.ncbi.nlm.nih.gov/pubmed/9390525 [Accessed December 16, 2016].

Chanda, B. et al., 2005. Gating charge displacement in voltage-gated ion channels involves limited transmembrane movement. *Nature*, 436(7052), pp.852–856. Available at: http://www.nature.com/doifinder/10.1038/nature03888 [Accessed January 12, 2017].

Chen, F.S., Steele, D. & Fedida, D., 1997. Allosteric effects of permeating cations on gating currents during K+ channel deactivation. *The Journal of general physiology*, 110(2), pp.87–100. Available at: http://www.ncbi.nlm.nih.gov/pubmed/9236203 [Accessed March 5, 2017].

Chen, J. et al., 1999. Long QT syndrome-associated mutations in the Per-Arnt-Sim (PAS) domain of HERG potassium channels accelerate channel deactivation. *The Journal of biological chemistry*, 274(15), pp.10113–8. Available at: http://www.ncbi.nlm.nih.gov/pubmed/10187793 [Accessed December 30, 2016].

Chen, J., Seebohm, G. & Sanguinetti, M.C., 2002. Position of aromatic residues in the S6 domain, not inactivation, dictates cisapride sensitivity of HERG and eag potassium channels. *Proceedings of the National Academy of Sciences*, 99(19), pp.12461–12466. Available at: http://www.ncbi.nlm.nih.gov/pubmed/12209010 [Accessed January 8, 2017].

Cheng, Y.M. et al., 2013. Functional interactions of voltage sensor charges with an S2 hydrophobic plug in hERG channels. *The Journal of general physiology*, 142(3), pp.289–303. Available at: http://www.ncbi.nlm.nih.gov/pubmed/23980197 [Accessed December 29, 2016].

Cheng, Y.M. & Claydon, T.W., 2012. Voltage-Dependent Gating of hERG Potassium Channels. *Frontiers in Pharmacology*, 3, p.83. Available at: http://www.ncbi.nlm.nih.gov/pubmed/22586397 [Accessed December 28, 2016].

Choe, S., 2002. ION CHANNEL STRUCTUREPOTASSIUM CHANNEL STRUCTURES. *Nature Reviews Neuroscience*, 3(2), pp.115–121. Available at: http://www.nature.com/doifinder/10.1038/nrn727 [Accessed December 14, 2016].

Choi, K.L. et al., 1993. The internal quaternary ammonium receptor site of Shaker potassium channels. *Neuron*, 10(3), pp.533–41. Available at: http://www.ncbi.nlm.nih.gov/pubmed/8461140 [Accessed March 5, 2017].

Choi, K.L., Aldrich, R.W. & Yellen, G., 1991. Tetraethylammonium blockade distinguishes two inactivation mechanisms in voltage-activated K+ channels. *Proceedings of the National Academy of Sciences of the United States of America*, 88(12), pp.5092–5. Available at: http://www.ncbi.nlm.nih.gov/pubmed/2052588 [Accessed January 7, 2017].

Choi, S.-H. et al., 2011. Ginsenoside Rg3 decelerates hERG K+ channel deactivation through Ser631 residue interaction. *European Journal of Pharmacology*, 663(1–3), pp.59–67. Available at: http://www.ncbi.nlm.nih.gov/pubmed/21586280 [Accessed January 8, 2017].

Clarke, C.E. et al., 2006. Effect of S5P α-helix charge mutants on inactivation of hERG K + channels The human ether a-go-go related gene (hERG) K. *J Physiol*, 5732, pp.291–304.

Claydon, T.W. et al., 2006. 4-Aminopyridine Prevents the Conformational Changes Associated with P/C-Type Inactivation in Shaker Channels. *Journal of Pharmacology and Experimental Therapeutics*, 320(1), pp.162–172. Available at: http://www.ncbi.nlm.nih.gov/pubmed/17015639 [Accessed December 16, 2016].

Claydon, T.W. et al., 2007. 4-Aminopyridine Prevents the Conformational Changes Associated with P / C-Type Inactivation in Shaker Channels. *Pharmacology*, 320(1), pp.162–172.

Claydon, T.W. & Fedida, D., 2007. Voltage clamp fluorimetry studies of mammalian voltage-gated K(+) channel gating. *Biochemical Society transactions*, 35(Pt 5), pp.1080–2. Available at: http://www.ncbi.nlm.nih.gov/pubmed/17956284.

Corbin-Leftwich, A. et al., 2016. Retigabine holds KV7 channels open and stabilizes the resting potential. *The Journal of general physiology*, 147(3), pp.229–41. Available at: http://www.ncbi.nlm.nih.gov/pubmed/26880756 [Accessed January 10, 2017].

Cordes, F.S., Bright, J.N. & Sansom, M.S.P., 2002. Proline-induced distortions of transmembrane helices. *Journal of Molecular Biology*, 323(5), pp.951–960.

Curran, M.E. et al., 1995. A molecular basis for cardiac arrhythmia: HERG mutations cause long QT syndrome. *Cell*, 80(5), pp.795–803. Available at:

http://www.ncbi.nlm.nih.gov/pubmed/7889573.

Doyle, D.A. et al., 1998. The Structure of the Potassium Channel: Molecular Basis of K sup + Conduction and Selectivity. *Science*, 280(April 3), pp.69–77.

Durdagi, S. et al., 2012. Structure-Guided Topographic Mapping and Mutagenesis to Elucidate Binding Sites for the Human Ether-a-Go-Go-Related Gene 1 Potassium Channel (KCNH2) Activator NS1643. *Journal of Pharmacology and Experimental Therapeutics*, 342(2), pp.441–452. Available at: http://www.ncbi.nlm.nih.gov/pubmed/22573844 [Accessed January 8, 2017].

Elliott, D.J.S. et al., 2009. Movement of the S4 segment in the hERG potassium channel during membrane depolarization. *Molecular Membrane Biology*, 26(8), pp.435–447. Available at: papers3://publication/doi/10.3109/09687680903321081.

Es-Salah-Lamoureux, Z. et al., 2010. Fluorescence-Tracking of Activation Gating in Human ERG Channels Reveals Rapid S4 Movement and Slow Pore Opening M. N. Nitabach, ed. *PLoS ONE*, 5(5), p.e10876. Available at: http://dx.plos.org/10.1371/journal.pone.0010876 [Accessed December 30, 2016].

Fedida, D., Bouchard, R. & Chen, F.S.P., 1996. Slow gating charge immobilization in the human potassium channel Kv1.5 and its prevention by 4-aminopyridine. *Journal of Physiology*, 494(2), pp.377–387. Available at: https://www.ncbi.nlm.nih.gov/pmc/articles/PMC1160641/pdf/jphysiol00397-0066.pdf [Accessed March 5, 2017].

Fernandez, D. et al., 2004. Physicochemical Features of the hERG Channel Drug Binding Site. *Journal of Biological Chemistry*, 279(11), pp.10120–10127. Available at: http://www.ncbi.nlm.nih.gov/pubmed/14699101 [Accessed December 29, 2016].

Ferrer, T. et al., 2006. The S4-S5 linker directly couples voltage sensor movement to the activation gate in the human ether-a'-go-go-related gene (hERG) K+ channel. *The Journal of biological chemistry*, 281(18), pp.12858–64. Available at: http://www.ncbi.nlm.nih.gov/pubmed/16524878 [Accessed December 30, 2016].

Ficker, E. et al., 1998. Molecular determinants of dofetilide block of HERG K+ channels. *Circulation research*, 82(3), pp.386–95. Available at: http://www.ncbi.nlm.nih.gov/pubmed/9486667 [Accessed January 7, 2017].

Ficker, E. et al., 1994. Spermine and spermidine as gating molecules for inward rectifier K+ channels. *Science*, 266(5187).

Ficker, E., Jarolimek, W. & Brown, A.M., 2001. Molecular determinants of inactivation and dofetilide block in ether a-go-go (EAG) channels and EAG-related K(+) channels. *Molecular pharmacology*, 60(6), pp.1343–8. Available at: http://www.ncbi.nlm.nih.gov/pubmed/11723241 [Accessed January 8, 2017].

Gagnon, D.G. & Bezanilla, F., 2009. A single charged voltage sensor is capable of gating the *Shaker* K^+ channel. *The Journal of General Physiology*, 133(5), pp.467–

483. Available at: http://www.ncbi.nlm.nih.gov/pubmed/19398775 [Accessed March 5, 2017].

Gandhi, C.S. & Isacoff, E.Y., 2002. Molecular models of voltage sensing. *The Journal of general physiology*, 120(4), pp.455–63. Available at: http://www.ncbi.nlm.nih.gov/pubmed/12356848 [Accessed January 12, 2017].

Gerlach, A.C., Stoehr, S.J. & Castle, N.A., 2010. Pharmacological Removal of Human Ether-a-go-go-Related Gene Potassium Channel Inactivation by 3-Nitro-N-(4-phenoxyphenyl) Benzamide (ICA-105574). *Molecular Pharmacology*, 77(1), pp.58–68. Available at: http://www.ncbi.nlm.nih.gov/pubmed/19805508 [Accessed January 8, 2017].

Gianulis, E.C., Liu, Q. & Trudeau, M.C., 2013. Direct interaction of eag domains and cyclic nucleotide-binding homology domains regulate deactivation gating in hERG channels. *The Journal of general physiology*, 142(4), pp.351–66. Available at: http://www.ncbi.nlm.nih.gov/pubmed/24043860 [Accessed December 30, 2016].

Goldin, A.L., 1991. Chapter 25 Expression of Ion Channels by Injection of mRNA into Xenopus Oocytes. *Methods in Cell Biology*, 36, pp.487–509.

Goodchild, S.J. & Fedida, D., 2014. Gating charge movement precedes ionic current activation in hERG channels. *Channels (Austin, Tex.)*, 8(1), pp.84–9. Available at: http://www.ncbi.nlm.nih.gov/pubmed/24126078 [Accessed December 29, 2016].

Goodchild, S.J., Macdonald, L.C. & Fedida, D., 2015. Sequence of gating charge movement and pore gating in HERG activation and deactivation pathways. *Biophysical journal*, 108(6), pp.1435–47. Available at: http://www.ncbi.nlm.nih.gov/pubmed/25809256 [Accessed December 29, 2016].

Guo, J. et al., 2015. NS1643 interacts around L529 of hERG to alter voltage sensor movement on the path to activation. *Biophysical journal*, 108(6), pp.1400–13. Available at: http://www.ncbi.nlm.nih.gov/pubmed/25809253 [Accessed January 8, 2017].

Guo, J., Gang, H. & Zhang, S., 2006. Molecular Determinants of Cocaine Block of Human Ether-a-go-go-Related Gene Potassium Channels. *Journal of Pharmacology and Experimental Therapeutics*, 317(2), pp.865–874. Available at: http://www.ncbi.nlm.nih.gov/pubmed/16397089 [Accessed January 8, 2017].

Gustina, A.S. & Trudeau, M.C., 2011. hERG potassium channel gating is mediated by N- and C-terminal region interactions. *The Journal of general physiology*, 137(3), pp.315–25. Available at: http://www.ncbi.nlm.nih.gov/pubmed/21357734 [Accessed December 30, 2016].

Gutman, G.A. et al., 2005. International Union of Pharmacology. LIII. Nomenclature and Molecular Relationships of Voltage-Gated Potassium Channels. *Pharmacological Reviews*, 57(4), pp.473–508. Available at: http://www.ncbi.nlm.nih.gov/pubmed/16382104 [Accessed December 14, 2016].

Hackos, D.H., Chang, T.-H. & Swartz, K.J., 2002. Scanning the intracellular S6 activation gate in the shaker K+ channel. *The Journal of general physiology*, 119(6), pp.521–32. Available at: http://www.ncbi.nlm.nih.gov/pubmed/12034760 [Accessed December 19, 2016].

Haddad, G.A. & Blunck, R., 2011. Mode shift of the voltage sensors in Shaker K+ channels is caused by energetic coupling to the pore domain. *The Journal of General Physiology*, 137(5).

Haitin, Y., Carlson, A.E. & Zagotta, W.N., 2013. The structural mechanism of KCNH-channel regulation by the eag domain. *Nature*, 501(7467), pp.444–448. Available at: http://www.nature.com/doifinder/10.1038/nature12487 [Accessed December 30, 2016].

Hardman, R.M. et al., 2007. Activation gating of hERG potassium channels: S6 glycines are not required as gating hinges. *Journal of Biological Chemistry*, 282(44), pp.31972–31981.

von Heijne, G., 1991. Proline kinks in transmembrane alpha-helices. *Journal of molecular biology*, 218(3), pp.499–503. Available at: http://www.ncbi.nlm.nih.gov/pubmed/2016741 [Accessed March 5, 2017].

Herzberg, I.M., Trudeau, M.C. & Robertson, G.A., 1998. Transfer of rapid inactivation and sensitivity to the class III antiarrhythmic drug E-4031 from HERG to M-eag channels. *The Journal of physiology*, (Pt 1), pp.3–14. Available at: http://www.ncbi.nlm.nih.gov/pubmed/9679158 [Accessed January 7, 2017].

Hille, B., 2001. Ion Channel Excitable Membranes. *Book*, pp.1–37.

Ho, S.N. et al., 1989. Site-directed mutagenesis by overlap extension using the polymerase chain reaction. *Gene*, 77(1), pp.51–9. Available at: http://www.ncbi.nlm.nih.gov/pubmed/2744487 [Accessed December 16, 2016].

Hodgkin, A.L. & Huxley, A.F., 1952. A quantitative description of membrane current and its application to conduction and excitation in nerve. *The Journal of Physiology*, 117(4), pp.500–544. Available at: http://doi.wiley.com/10.1113/jphysiol.1952.sp004764 [Accessed March 12, 2017].

Holmgren, M., Smith, P.L. & Yellen, G., 1997. Trapping of organic blockers by closing of voltage-dependent K+ channels: evidence for a trap door mechanism of activation gating. *The Journal of general physiology*, 109(5), pp.527–35. Available at: http://www.ncbi.nlm.nih.gov/pubmed/9154902 [Accessed January 14, 2017].

Horne, A.J. et al., 2010. Fast and slow voltage sensor rearrangements during activation gating in Kv1.2 channels detected using tetramethylrhodamine fluorescence. *The Journal of general physiology*, 136(1), pp.83–99. Available at: http://www.pubmedcentral.nih.gov/articlerender.fcgi?artid=2894543&tool=pmcentrez&rendertype=abstract.

Hoshi, T. & Armstrong, C.M., 2013. C-type inactivation of voltage-gated K+ channels: Pore constriction or dilation? *The Journal of General Physiology*, 141(2).

Hoshi, T. & Ta, W.N.Z.I., 1994. Shaker Potassium Channel Gating I : Transitions Near the Open State. , 103(February), pp.249–278.

Hoshi, T., Zagotta, W.N. & Aldrich, R.W., 1990. Biophysical and molecular mechanisms of Shaker potassium channel inactivation. *Science (New York, N.Y.)*, 250(4980), pp.533–8. Available at: http://www.ncbi.nlm.nih.gov/pubmed/2122519 [Accessed January 7, 2017].

Hoshi, T., Zagotta, W.N. & Aldrich, R.W., 1991. Two types of inactivation in Shaker K+ channels: Effects of alterations in the carboxy-terminal region. *Neuron*, 7(4), pp.547–556.

Hull, C.M. et al., 2014. Regional flexibility in the S4–S5 linker regulates hERG channel closed-state stabilization. *Pflügers Archiv - European Journal of Physiology*, 466(10), pp.1911–1919. Available at: http://www.ncbi.nlm.nih.gov/pubmed/24407947 [Accessed December 30, 2016].

Isacoff, E.Y. et al., 1999. Spectroscopic mapping of voltage sensor movement in the Shaker potassium channel. *Nature*, 402(6763), pp.813–817. Available at: http://www.nature.com/doifinder/10.1038/45561 [Accessed January 12, 2017].

Jan, L.Y. & Jan, Y.N., 1997. CLONED POTASSIUM CHANNELS FROM EUKARYOTES AND PROKARYOTES. *Annual Review of Neuroscience*, 20(1), pp.91–123. Available at: http://www.ncbi.nlm.nih.gov/pubmed/9056709 [Accessed December 14, 2016].

Jentsch, T.J. et al., 2000. A constitutively open potassium channel formed by KCNQ1 and KCNE3. *Nature*, 403(6766), pp.196–199. Available at: http://www.nature.com/doifinder/10.1038/35003200 [Accessed December 28, 2016].

Jiang, M., Dun, W. & Tseng, G.-N., 1999. Mechanism for the effects of extracellular acidification on HERG-channel function. *American Journal of Physiology - Heart and Circulatory Physiology*, 277(4).

Jiang, Y. et al., 2002a. Crystal structure and mechanism of a calcium-gated potassium channel. *Nature*, 417(6888), pp.515–522. Available at: http://www.nature.com/doifinder/10.1038/417515a%5Cnpapers3://publication/doi/10.1038/417515a.

Jiang, Y. et al., 2002b. The open pore conformation of potassium channels. *Nature*, 417(6888), pp.523–546. Available at: http://www.ncbi.nlm.nih.gov/pubmed/12037560%5Cnhttp://www.ncbi.nlm.nih.gov/entrez/query.fcgi?cmd=Retrieve&db=PubMed&dopt=Citation&list_uids=12037560.

Jiang, Y. et al., 2003. X-ray structure of a voltage-dependent K+ channel. *Nature*,

423(6935), pp.33–41. Available at: http://www.nature.com/nature/journal/v423/n6935/pdf/nature01580.pdf%5Cnhttp://www.ncbi.nlm.nih.gov/pubmed/12721618.

Jin, T. et al., 2002. The (beta)gamma subunits of G proteins gate a K(+) channel by pivoted bending of a transmembrane segment. *Molecular cell*, 10(3), pp.469–81. Available at: http://www.ncbi.nlm.nih.gov/pubmed/12408817 [Accessed January 14, 2017].

Jones, D.K. et al., 2014. hERG 1b is critical for human cardiac repolarization. *Proceedings of the National Academy of Sciences*, 111(50), pp.18073–18077. Available at: http://www.ncbi.nlm.nih.gov/pubmed/25453103 [Accessed December 28, 2016].

Jones, E.M.C. et al., 2004. Cardiac I_{Kr} Channels Minimally Comprise hERG 1a and 1b Subunits. *Journal of Biological Chemistry*, 279(43), pp.44690–44694. Available at: http://www.ncbi.nlm.nih.gov/pubmed/15304481 [Accessed December 28, 2016].

Kamiya, K. et al., 2006. Molecular Determinants of hERG Channel Block. *Molecular Pharmacology*, 69(5), pp.1709–1716. Available at: http://www.ncbi.nlm.nih.gov/pubmed/16474003 [Accessed January 8, 2017].

Kang, J. et al., 2005. Discovery of a Small Molecule Activator of the Human Ether-a-go-go-Related Gene (HERG) Cardiac K+ Channel. *Molecular Pharmacology*, 67(3).

Kaplan, W.D. & Trout, W.E., 1969. The behavior of four neurological mutants of Drosophila. *Genetics*, 61(2), pp.399–409. Available at: http://www.ncbi.nlm.nih.gov/pubmed/5807804 [Accessed December 28, 2016].

Keynes, R.D. & Elinder, F., 1999. The screw-helical voltage gating of ion channels. *Proceedings. Biological sciences*, 266(1421), pp.843–52. Available at: http://www.ncbi.nlm.nih.gov/pubmed/10343407 [Accessed January 12, 2017].

Kitaguchi, T., Sukhareva, M. & Swartz, K.J., 2004. Stabilizing the closed S6 gate in the Shaker Kv channel through modification of a hydrophobic seal. *The Journal of general physiology*, 124(4), pp.319–32. Available at: http://www.ncbi.nlm.nih.gov/pubmed/15365093 [Accessed January 14, 2017].

Korn, S.J. & Trapani, J.G., 2005. Potassium Channels. *IEEE Transactions on Nanobioscience*, 4(1), pp.21–33. Available at: http://ieeexplore.ieee.org/document/1402407/ [Accessed December 14, 2016].

Kuchel, P.W. et al., 2004. The HERG K + channel: progress in understanding the molecular basis of its unusual gating kinetics. *European Biophysics Journal*, 33(2), pp.89–97. Available at: http://www.ncbi.nlm.nih.gov/pubmed/13680209 [Accessed December 28, 2016].

Kurata, H.T. & Fedida, D., 2006. A structural interpretation of voltage-gated potassium channel inactivation. *Progress in Biophysics and Molecular Biology*, 92(2), pp.185–

208.

de la Pena, P. et al., 2011. Demonstration of Physical Proximity between the N Terminus and the S4-S5 Linker of the Human ether-a-go-go-related Gene (hERG) Potassium Channel. *Journal of Biological Chemistry*, 286(21), pp.19065–19075. Available at: http://www.ncbi.nlm.nih.gov/pubmed/21474444 [Accessed December 30, 2016].

Labro, A.J. et al., 2003. Gating of Shaker-type Channels Requires the Flexibility of S6 Caused by Prolines. *Journal of Biological Chemistry*, 278(50), pp.50724–50731.

Labro, A.J. et al., 2015. Kv3.1 uses a timely resurgent K+ current to secure action potential repolarization. *Nature Communications*, 6, p.10173. Available at: http://www.nature.com/doifinder/10.1038/ncomms10173 [Accessed January 10, 2017].

Labro, A.J. et al., 2008. Kv Channel Gating Requires a Compatible S4-S5 Linker and Bottom Part of S6, Constrained by Non-interacting Residues. *The Journal of General Physiology*, 132(6), pp.667–680. Available at: http://www.ncbi.nlm.nih.gov/pubmed/19029374 [Accessed December 27, 2016].

Labro, A.J. et al., 2012. Molecular mechanism for depolarization-induced modulation of Kv channel closure. *The Journal of general physiology*, 140(5), pp.481–93. Available at: http://www.ncbi.nlm.nih.gov/pubmed/23071266 [Accessed December 16, 2016].

Labro, A.J. & Snyders, D.J., 2012. Being Flexible: The Voltage-Controllable Activation Gate of Kv Channels. *Frontiers in Pharmacology*, 3, p.168. Available at: http://journal.frontiersin.org/article/10.3389/fphar.2012.00168/abstract [Accessed December 19, 2016].

Lacroix, J.J. et al., 2012. Intermediate state trapping of a voltage sensor. , 140(6).

Lacroix, J.J., Labro, A.J. & Bezanilla, F., 2011. Properties of deactivation gating currents in Shaker channels. *Biophysical journal*, 100(5), pp.L28-30. Available at: http://www.ncbi.nlm.nih.gov/pubmed/21354387 [Accessed December 21, 2016].

Larsson, H.P. et al., 1996. Transmembrane movement of the shaker K+ channel S4. *Neuron*, 16(2), pp.387–97. Available at: http://www.ncbi.nlm.nih.gov/pubmed/8789953 [Accessed January 12, 2017].

Ledwell, J.L. & Aldrich, R.W., 1999. Mutations in the S4 Region Isolate the Final Voltage-dependent Cooperative Step in Potassium Channel Activation. , 113(March).

Li, Q., Ng, H.Q., et al., 2014. Insight into the molecular interaction between the cyclic nucleotide-binding homology domain and the eag domain of the hERG channel. *FEBS Letters*, 588(17), pp.2782–2788. Available at: http://www.ncbi.nlm.nih.gov/pubmed/24931372 [Accessed January 10, 2017].

Li, Q. et al., 2010. *NMR solution structure of the N-terminal domain of hERG and its interaction with the S4–S5 linker*,

Li, Q., Wong, Y.L., et al., 2014. Structural insight into the transmembrane segments 3 and 4 of the hERG potassium channel. *Journal of Peptide Science*, 20(12), pp.935–944. Available at: http://doi.wiley.com/10.1002/psc.2704 [Accessed January 10, 2017].

Li, Y. et al., 2016. Structure of the Cyclic Nucleotide-Binding Homology Domain of the hERG Channel and Its Insight into Type 2 Long QT Syndrome. *Scientific Reports*, 6, p.23712. Available at: http://www.nature.com/articles/srep23712 [Accessed December 28, 2016].

Liman, E.R. & Hess, P., 1991. Voltage-sensing residues in the S4 region of a mammalian K+ channel. *Nature*, 353(6346), pp.752–756. Available at: http://www.nature.com/doifinder/10.1038/353752a0 [Accessed December 19, 2016].

Liu, J. et al., 2003. Negative charges in the transmembrane domains of the HERG K channel are involved in the activation- and deactivation-gating processes. *The Journal of general physiology*, 121(6), pp.599–614. Available at: http://www.pubmedcentral.nih.gov/articlerender.fcgi?artid=2217355&tool=pmcentrez&rendertype=abstract.

Liu, J. et al., 2002. Structural and functional role of the extracellular s5-p linker in the HERG potassium channel. *The Journal of general physiology*, 120(5), pp.723–37. Available at: http://www.ncbi.nlm.nih.gov/pubmed/12407082 [Accessed January 7, 2017].

Liu, Y. et al., 1997. Gated access to the pore of a voltage-dependent K+ channel. *Neuron*, 19(1), pp.175–84. Available at: http://www.ncbi.nlm.nih.gov/pubmed/9247273 [Accessed December 19, 2016].

Logothetis, D.E. et al., 1992. Incremental reductions of positive charge within the S4 region of a voltage-gated K+ channel result in corresponding decreases in gating charge. *Neuron*, 8(3), pp.531–40. Available at: http://www.ncbi.nlm.nih.gov/pubmed/1550676 [Accessed December 21, 2016].

Long, S.B. et al., 2007. Atomic structure of a voltage-dependent K+ channel in a lipid membrane-like environment. *Nature*, 450(7168), pp.376–382. Available at: http://www.nature.com/doifinder/10.1038/nature06265 [Accessed December 27, 2016].

Long, S.B., Campbell, E.B. & Mackinnon, R., 2005a. Crystal Structure of a Mammalinan Voltage-Dependent Shaker Family K+ Channel. *Science*, 897(August), pp.897–903.

Long, S.B., Campbell, E.B. & Mackinnon, R., 2005b. Voltage Sensor of Kv1 . 2 : Structural Basis of Electromechanical Coupling. *Science*, 32(July), pp.903–908.

López-Barneo, J. et al., 1993. Effects of external cations and mutations in the pore region on C-type inactivation of Shaker potassium channels. *Receptors & channels*, 1(1), pp.61–71. Available at: http://www.ncbi.nlm.nih.gov/pubmed/8081712 [Accessed January 7, 2017].

Lopez, G.A., Jan, Y.N. & Jan, L.Y., 1991. Hydrophobic substitution mutations in the S4 sequence alter voltage-dependent gating in Shaker K+ channels. *Neuron*, 7(2), pp.327–36. Available at: http://www.ncbi.nlm.nih.gov/pubmed/1873032 [Accessed December 21, 2016].

Lörinczi, É. et al., 2015. Voltage-dependent gating of KCNH potassium channels lacking a covalent link between voltage-sensing and pore domains. *Nature communications*, 6, p.6672. Available at: http://www.nature.com/ncomms/2015/150330/ncomms7672/full/ncomms7672.html?WT.ec_id=NCOMMS-20150401.

Lu, Z., Klem, A.M. & Ramu, Y., 2002. Coupling between voltage sensors and activation gate in voltage-gated K+ channels. *The Journal of general physiology*, 120(5), pp.663–76. Available at: http://www.ncbi.nlm.nih.gov/pubmed/12407078 [Accessed December 27, 2016].

MacArthur, M.W. & Thornton, J.M., 1991. Influence of proline residues on protein conformation. *Journal of Molecular Biology*, 218(2), pp.397–412.

MacKinnon, R. & Yellen, G., 1990. Mutations affecting TEA blockade and ion permeation in voltage-activated K+ channels. *Science (New York, N.Y.)*, 250(4978), pp.276–9. Available at: http://www.ncbi.nlm.nih.gov/pubmed/2218530 [Accessed January 7, 2017].

Malak, O.A., Es-Salah-Lamoureux, Z. & Loussouarn, G., 2017. hERG S4-S5 linker acts as a voltage-dependent ligand that binds to the activation gate and locks it in a closed state. *Scientific Reports*, 7(1), p.113. Available at: http://www.ncbi.nlm.nih.gov/pubmed/28273916 [Accessed April 12, 2017].

Mannuzzu, L.M., Moronne, M.M. & Isacoff, E.Y., 1996. Direct physical measure of conformational rearrangement underlying potassium channel gating. *Science (New York, N.Y.)*, 271(5246), pp.213–6. Available at: http://www.ncbi.nlm.nih.gov/pubmed/8539623 [Accessed December 16, 2016].

McDonald, T. V. et al., 1997. A minK|[ndash]|HERG complex regulates the cardiac potassium current IKr. *Nature*, 388(6639), pp.289–292. Available at: http://www.nature.com/doifinder/10.1038/40882 [Accessed December 28, 2016].

Miller, C. et al., 2000. An overview of the potassium channel family. *Genome Biology*, 1(4), p.reviews0004.1. Available at: http://genomebiology.biomedcentral.com/articles/10.1186/gb-2000-1-4-reviews0004 [Accessed December 14, 2016].

Mitcheson, J.S. et al., 2000. A structural basis for drug-induced long QT syndrome.

Proceedings of the National Academy of Sciences, 97(22), pp.12329–12333. Available at: http://www.ncbi.nlm.nih.gov/pubmed/11005845 [Accessed December 28, 2016].

Mitcheson, J.S., 2008. hERG Potassium Channels and the Structural Basis of Drug-Induced Arrhythmias. *Chemical Research in Toxicology*, 21(5), pp.1005–1010. Available at: http://www.ncbi.nlm.nih.gov/pubmed/18447395 [Accessed December 28, 2016].

Mitcheson, J.S., Chen, J. & Sanguinetti, M.C., 2000. Trapping of a methanesulfonanilide by closure of the HERG potassium channel activation gate. *The Journal of general physiology*, 115(3), pp.229–40. Available at: http://www.ncbi.nlm.nih.gov/pubmed/10694252 [Accessed December 29, 2016].

Mitcheson, J.S. & Perry, M.D., 2003. Molecular determinants of high-affinity drug binding to HERG channels. *Current opinion in drug discovery & development*, 6(5), pp.667–74. Available at: http://www.ncbi.nlm.nih.gov/pubmed/14579516 [Accessed January 8, 2017].

Morais-Cabral, J.H. & Robertson, G.A., 2015. The enigmatic cytoplasmic regions of KCNH channels. *Journal of molecular biology*, 427(1), pp.67–76. Available at: http://www.ncbi.nlm.nih.gov/pubmed/25158096 [Accessed January 10, 2017].

Morais Cabral, J.H. et al., 1998. Crystal structure and functional analysis of the HERG potassium channel N terminus: a eukaryotic PAS domain. *Cell*, 95(5), pp.649–55. Available at: http://www.ncbi.nlm.nih.gov/pubmed/9845367 [Accessed December 30, 2016].

Muskett, F.W. et al., 2011. Mechanistic Insight into Human ether-a-go-go-related Gene (hERG) K+ Channel Deactivation Gating from the Solution Structure of the EAG Domain. *Journal of Biological Chemistry*, 286(8), pp.6184–6191. Available at: http://www.ncbi.nlm.nih.gov/pubmed/21135103 [Accessed December 30, 2016].

Muskett, F.W. et al., 2011. Mechanistic insight into human ether-à-go-go-related gene (hERG) K + channel deactivation gating from the solution structure of the EAG domain. *Journal of Biological Chemistry*, 286(8).

Nakano, Y. & Shimizu, W., 2016. Genetics of long-QT syndrome. *Journal of Human Genetics*, 61(1), pp.51–55. Available at: http://www.nature.com/doifinder/10.1038/jhg.2015.74 [Accessed March 12, 2017].

Ng, C.A. et al., 2011. The N–Terminal Tail of hERG Contains an Amphipathic α–Helix That Regulates Channel Deactivation V. N. Uversky, ed. *PLoS ONE*, 6(1), p.e16191. Available at: http://dx.plos.org/10.1371/journal.pone.0016191 [Accessed December 30, 2016].

Ng, C.A. et al., 2012. The S4–S5 Linker Acts as a Signal Integrator for hERG K+ Channel Activation and Deactivation Gating B. Attali, ed. *PLoS ONE*, 7(2), p.e31640. Available at: http://www.ncbi.nlm.nih.gov/pubmed/22359612 [Accessed

January 10, 2017].

Noble, D. & Tsien, R.W., 1969. Outward membrane currents activated in the plateau range of potentials in cardiac Purkinje fibres. *The Journal of physiology*, 200(1), pp.205–31. Available at: http://www.ncbi.nlm.nih.gov/pubmed/5761944 [Accessed December 28, 2016].

Olcese, R. et al., 1997. Correlation between charge movement and ionic current during slow inactivation in Shaker K+ channels. *The Journal of general physiology*, 110(5), pp.579–89. Available at: http://www.ncbi.nlm.nih.gov/pubmed/9348329 [Accessed December 21, 2016].

Osteen, J.D. et al., 2010. KCNE1 alters the voltage sensor movements necessary to open the KCNQ1 channel gate. *Proceedings of the National Academy of Sciences of the United States of America*, 107(52), pp.22710–5. Available at: http://www.ncbi.nlm.nih.gov/pubmed/21149716 [Accessed March 11, 2017].

Pages, G. et al., 2009. Structure of the pore-helix of the hERG K+ channel. *European Biophysics Journal*, 39(1), pp.111–120. Available at: http://link.springer.com/10.1007/s00249-009-0433-1 [Accessed January 10, 2017].

Pantazis, A. et al., 2014. Functional heterogeneity of the four voltage sensors of a human L-type calcium channel. *Proceedings of the National Academy of Sciences of the United States of America*, 111(51), pp.18381–6. Available at: http://www.ncbi.nlm.nih.gov/pubmed/25489110 [Accessed March 12, 2017].

Papazian, D.M. et al., 1987. Cloning of genomic and complementary DNA from Shaker, a putative potassium channel gene from Drosophila. *Science (New York, N.Y.)*, 237(4816), pp.749–53. Available at: http://www.ncbi.nlm.nih.gov/pubmed/2441470 [Accessed December 14, 2016].

Papazian, D.M. et al., 1995. Electrostatic interactions of S4 voltage sensor in Shaker K+ channel. *Neuron*, 14(6), pp.1293–301. Available at: http://www.ncbi.nlm.nih.gov/pubmed/7605638 [Accessed January 12, 2017].

Papke, R.L. & Smith-Maxwell, C., 2009. High throughput electrophysiology with Xenopus oocytes. *Combinatorial chemistry & high throughput screening*, 12(1), pp.38–50. Available at: http://www.ncbi.nlm.nih.gov/pubmed/19149490 [Accessed December 16, 2016].

Pathak, M. et al., 2004. The Cooperative Voltage Sensor Motion that Gates a Potassium Channel. *The Journal of General Physiology*, 125(1).

Perozo, E. et al., 1994. S4 mutations alter gating currents of Shaker K channels. *Biophysical journal*, 66(2 Pt 1), pp.345–54. Available at: http://www.ncbi.nlm.nih.gov/pubmed/8161688 [Accessed December 21, 2016].

Perrin, M.J. et al., 2008a. Drug Binding to the Inactivated State Is Necessary but Not Sufficient for High-Affinity Binding to Human Ether-a-go-go-Related Gene

Channels. *Molecular Pharmacology*, 74(5), pp.1443–1452. Available at: http://molpharm.aspetjournals.org/cgi/doi/10.1124/mol.108.049056 [Accessed January 8, 2017].

Perrin, M.J. et al., 2008b. Drug Binding to the Inactivated State Is Necessary but Not Sufficient for High-Affinity Binding to Human Ether-a-go-go-Related Gene Channels. *Molecular Pharmacology*, 74(5), pp.1443–1452. Available at: http://www.ncbi.nlm.nih.gov/pubmed/18701618 [Accessed January 8, 2017].

Perry, M., Sachse, F.B. & Sanguinetti, M.C., 2007. Structural basis of action for a human ether-a-go-go-related gene 1 potassium channel activator. *Proceedings of the National Academy of Sciences of the United States of America*, 104(34), pp.13827–32. Available at: http://www.ncbi.nlm.nih.gov/pubmed/17693551 [Accessed January 8, 2017].

Perry, M., Sanguinetti, M. & Mitcheson, J., 2010. Revealing the structural basis of action of hERG potassium channel activators and blockers. *The Journal of physiology*, 588(Pt 17), pp.3157–3167.

Perry, M.D. et al., 2015. Getting to the heart of hERG K^+ channel gating. *The Journal of Physiology*, 593(12), pp.2575–2585. Available at: http://www.ncbi.nlm.nih.gov/pubmed/25820318 [Accessed January 7, 2017].

Perry, M.D. et al., 2013. Hydrophobic interactions between the voltage sensor and pore mediate inactivation in Kv11.1 channels. *The Journal of General Physiology*, 142(3), pp.275–288. Available at: http://www.ncbi.nlm.nih.gov/pubmed/23980196 [Accessed January 7, 2017].

Perry, M.D. et al., 2016. Rescue of protein expression defects may not be enough to abolish the pro-arrhythmic phenotype of long QT type 2 mutations. *The Journal of Physiology*, 594(14), pp.4031–4049. Available at: http://www.ncbi.nlm.nih.gov/pubmed/26958806 [Accessed April 1, 2017].

Perry, M.D., Ng, C.A. & Vandenberg, J.I., 2013. Pore Helices Play a Dynamic Role as Integrators of Domain Motion during Kv11.1 Channel Inactivation Gating. *Journal of Biological Chemistry*, 288(16), pp.11482–11491. Available at: http://www.ncbi.nlm.nih.gov/pubmed/23471968 [Accessed January 7, 2017].

Piper, D.R. et al., 2008. Cooperative Interactions Between R531 and Acidic Residues in the Voltage Sensing Module of hERG1 Channels. *Cellular Physiology and Biochemistry*, 21(1–3), pp.037–046. Available at: http://www.ncbi.nlm.nih.gov/pubmed/18209470 [Accessed December 29, 2016].

Piper, D.R. et al., 2003. Gating currents associated with intramembrane charge displacement in HERG potassium channels. *Proceedings of the National Academy of Sciences of the United States of America*, 100(18), pp.10534–9. Available at: http://www.ncbi.nlm.nih.gov/pubmed/12928493.

Piper, D.R. et al., 2005. Regional Specificity of Human ether-a'-go-go-related Gene

Channel Activation and Inactivation Gating. *Journal of Biological Chemistry*, 280(8), pp.7206–7217. Available at: http://www.ncbi.nlm.nih.gov/pubmed/15528201 [Accessed December 29, 2016].

Posson, D.J. & Selvin, P.R., 2008. Extent of voltage sensor movement during gating of shaker K+ channels. *Neuron*, 59(1), pp.98–109. Available at: http://www.ncbi.nlm.nih.gov/pubmed/18614032 [Accessed January 12, 2017].

Priest, M.F. et al., 2013. S3-S4 linker length modulates the relaxed state of a voltage-gated potassium channel. *Biophysical journal*, 105(10), pp.2312–22. Available at: http://www.ncbi.nlm.nih.gov/pubmed/24268143 [Accessed March 5, 2017].

Raschi, E. et al., 2008. The hERG K+ channel: target and antitarget strategies in drug development. *Pharmacological Research*, 57(3), pp.181–195. Available at: http://www.ncbi.nlm.nih.gov/pubmed/18329284 [Accessed January 8, 2017].

Rasmusson, R.L. et al., 1998. Inactivation of Voltage-Gated Cardiac K+ Channels. *Circulation Research*, 82(7).

Robertson, G.A., Jones, E.M.C. & Wang, J., 2005. Gating and assembly of heteromeric hERG1a/1b channels underlying I(Kr) in the heart. *Novartis Foundation symposium*, 266, pp.4-15–8, 44–5. Available at: http://www.ncbi.nlm.nih.gov/pubmed/16050259 [Accessed December 28, 2016].

Roden, D.M. et al., 2002. Cardiac Ion Channels. *Annual Review of Physiology*, 64(1), pp.431–475. Available at: http://www.ncbi.nlm.nih.gov/pubmed/11826275 [Accessed December 18, 2016].

Ruta, V., Chen, J. & MacKinnon, R., 2005. Calibrated Measurement of Gating-Charge Arginine Displacement in the KvAP Voltage-Dependent K+ Channel. *Cell*, 123(3), pp.463–475. Available at: http://www.ncbi.nlm.nih.gov/pubmed/16269337 [Accessed January 12, 2017].

Sanchez-Chapula, J.A. et al., 2002. Molecular Determinants of Voltage-dependent Human Ether-a-Go-Go Related Gene (HERG) K+ Channel Block. *Journal of Biological Chemistry*, 277(26), pp.23587–23595. Available at: http://www.ncbi.nlm.nih.gov/pubmed/11960982 [Accessed December 28, 2016].

Sanguinetti, M.C. et al., 1995. A mechanistic link between an inherited and an acquird cardiac arrthytmia: HERG encodes the IKr potassium channel. *Cell*, 81(2), pp.299–307.

Sanguinetti, M.C., 2014. HERG1 channel agonists and cardiac arrhythmia. *Current Opinion in Pharmacology*, 15, pp.22–27. Available at: http://www.ncbi.nlm.nih.gov/pubmed/24721650 [Accessed January 8, 2017].

Sanguinetti, M.C. et al., 1996. Spectrum of HERG K+-channel dysfunction in an inherited cardiac arrhythmia. *Proc.Natl.Acad.Sci.U.S.A*, 93(0027–8424 SB–IM), pp.2208–2212.

Sanguinetti, M.C. & Jurkiewicz, N.K., 1990. Two components of cardiac delayed rectifier K+ current. Differential sensitivity to block by class III antiarrhythmic agents. *J Gen Physiol*, 96(1), pp.195–215.

Sanguinetti, M.C. & Tristani-Firouzi, M., 2006. hERG potassium channels and cardiac arrhythmia. *Nature*, 440(7083), pp.463–469. Available at: http://www.nature.com/doifinder/10.1038/nature04710 [Accessed December 14, 2016].

Sanguinetti, M.C. & Xu, Q.P., 1999. Mutations of the S4-S5 linker alter activation properties of HERG potassium channels expressed in Xenopus oocytes. *The Journal of physiology*, pp.667–75. Available at: http://www.ncbi.nlm.nih.gov/pubmed/9882738 [Accessed December 30, 2016].

Savalli, N. et al., 2006. Voltage-dependent conformational changes in human Ca(2+)- and voltage-activated K(+) channel, revealed by voltage-clamp fluorometry. *Proceedings of the National Academy of Sciences of the United States of America*, 103(33), pp.12619–24. Available at: http://www.ncbi.nlm.nih.gov/pubmed/16895996 [Accessed January 12, 2017].

Schonherr, R. & Heinemann, S.H., 1996. Molecular determinants for activation and inactivation of HERG, a human inward rectifier potassium channel. *J Physiol (Lond)*, 493(Pt 3), pp.635–642.

Schönherr, R. & Heinemann, S.H., 1996. Molecular determinants for activation and inactivation of HERG, a human inward rectifier potassium channel. *The Journal of physiology*, pp.635–42. Available at: http://www.ncbi.nlm.nih.gov/pubmed/8799887 [Accessed December 30, 2016].

Schoppa, N.E. et al., 1992. The size of gating charge in wild-type and mutant Shaker potassium channels. *Science (New York, N.Y.)*, 255(5052), pp.1712–5. Available at: http://www.ncbi.nlm.nih.gov/pubmed/1553560 [Accessed December 21, 2016].

Seoh, S.A. et al., 1996. Voltage-sensing residues in the S2 and S4 segments of the Shaker K+ channel. *Neuron*, 16(6), pp.1159–67. Available at: http://www.ncbi.nlm.nih.gov/pubmed/8663992 [Accessed December 21, 2016].

Shi, W. et al., 1997. Identification of two nervous system-specific members of the erg potassium channel gene family. *The Journal of neuroscience : the official journal of the Society for Neuroscience*, 17(24), pp.9423–32. Available at: http://www.ncbi.nlm.nih.gov/pubmed/9390998 [Accessed December 28, 2016].

Shirokov, R. et al., 1992. Two classes of gating current from L-type Ca channels in guinea pig ventricular myocytes. *The Journal of general physiology*, 99(6), pp.863–95. Available at: http://www.ncbi.nlm.nih.gov/pubmed/1322450 [Accessed January 10, 2017].

Shirokov, R., 2011. What's in gating currents? Going beyond the voltage sensor movement. *Biophysical journal*, 101(2), pp.512-4-6. Available at:

http://www.ncbi.nlm.nih.gov/pubmed/21767505 [Accessed March 5, 2017].

Sigworth, F.J. et al., 1994. Voltage gating of ion channels. *Quarterly Reviews of Biophysics*, 27(1), p.1. Available at: http://www.journals.cambridge.org/abstract_S0033583500002894 [Accessed December 21, 2016].

Van Slyke, A.C. et al., 2010. Mutations within the S4-S5 linker alter voltage sensor constraints in hERG K+ channels. *Biophysical journal*, 99(9), pp.2841–52. Available at: http://www.ncbi.nlm.nih.gov/pubmed/21044581 [Accessed December 29, 2016].

Smith-maxwell, C.J., Ledwell, J.L. & Aldrich, R.W., 1998. Uncharged S4 Residues and Cooperativity in Voltage-dependent Potassium Channel Activation. , 111(March).

Smith-Maxwell, C.J., Ledwell, J.L. & Aldrich, R.W., 1998. Role of the S4 in cooperativity of voltage-dependent potassium channel activation. *The Journal of general physiology*, 111(3), pp.399–420. Available at: http://www.ncbi.nlm.nih.gov/pubmed/9482708 [Accessed December 21, 2016].

Smith, P.L., Baukrowitz, T. & Yellen, G., 1996. The inward rectification mechanism of the HERG cardiac potassium channel. *Nature*, 379(6568), pp.833–836. Available at: http://www.ncbi.nlm.nih.gov/pubmed/8587608 [Accessed December 29, 2016].

Smith, P.L. & Yellen, G., 2002. Fast and slow voltage sensor movements in HERG potassium channels. *The Journal of general physiology*, 119(3), pp.275–93. Available at: http://www.ncbi.nlm.nih.gov/pubmed/11865022 [Accessed December 29, 2016].

Spector, P.S. et al., 1996. Class III Antiarrhythmic Drugs Block HERG, a Human Cardiac Delayed Rectifier K+ Channel. *Circulation Research*, 78(3).

Spector, P.S. et al., 1996. Fast inactivation causes rectification of the IKr channel. *The Journal of general physiology*, 107(5), pp.611–9. Available at: http://www.ncbi.nlm.nih.gov/pubmed/8740374 [Accessed December 29, 2016].

Starace, D.M. & Bezanilla, F., 2004. A proton pore in a potassium channel voltage sensor reveals a focused electric field. *Nature*, 427(6974), pp.548–553. Available at: http://www.nature.com/doifinder/10.1038/nature02270 [Accessed January 12, 2017].

Starace, D.M., Stefani, E. & Bezanilla, F., 1997. Voltage-dependent proton transport by the voltage sensor of the Shaker K+ channel. *Neuron*, 19(6), pp.1319–27. Available at: http://www.ncbi.nlm.nih.gov/pubmed/9427254 [Accessed January 12, 2017].

Stefani, E. & Bezanilla, F., 1998. Cut-open oocyte voltage-clamp technique. *Methods in enzymology*, 293, pp.300–18. Available at: http://www.ncbi.nlm.nih.gov/pubmed/9711615 [Accessed January 15, 2017].

Su, Z. et al., 2009. Electrophysiologic characterization of a novel hERG channel activator. *Biochemical Pharmacology*, 77(8), pp.1383–1390. Available at: http://www.ncbi.nlm.nih.gov/pubmed/19426677 [Accessed January 8, 2017].

Subbiah, R.N. et al., 2004. Molecular basis of slow activation of the human ether-a-go-go related gene potassium channel. *The Journal of physiology*, 558(2004), pp.417–431.

Subbiah, R.N. et al., 2005. Tryptophan scanning mutagenesis of the HERG K^+ channel: the S4 domain is loosely packed and likely to be lipid exposed. *The Journal of Physiology*, 569(2), pp.367–379. Available at: http://www.ncbi.nlm.nih.gov/pubmed/16166152 [Accessed December 29, 2016].

Swartz, K.J., 2004. Towards a structural view of gating in potassium channels. *Nature reviews. Neuroscience*, 5(12), pp.905–916. Available at: http://www.ncbi.nlm.nih.gov/pubmed/15550946%5Cnhttp://www.nature.com/doifinder/10.1038/nrn1559.

Taglialatela, M., Toro, L. & Stefani, E., 1992. Novel voltage clamp to record small, fast currents from ion channels expressed in Xenopus oocytes. *Biophysical journal*, 61(1), pp.78–82. Available at: http://www.ncbi.nlm.nih.gov/pubmed/1311612%5Cnhttp://www.pubmedcentral.nih.gov/articlerender.fcgi?artid=PMC1260224.

Tan, P.S. et al., 2012. Voltage-sensing domain mode shift is coupled to the activation gate by the N-terminal tail of hERG channels. *The Journal of General Physiology*, 140(3), pp.293–306. Available at: http://www.ncbi.nlm.nih.gov/pubmed/22891279 [Accessed December 12, 2016].

Tao, X. et al., 2010. A Gating Charge Transfer Center in Voltage Sensors. *Science*, 328(5974), pp.67–73. Available at: http://www.ncbi.nlm.nih.gov/pubmed/20360102%5Cnhttp://www.pubmedcentral.nih.gov/articlerender.fcgi?artid=PMC2869078%5Cnhttp://www.sciencemag.org/cgi/doi/10.1126/science.1185954.

Tao, X., Hite, R.K. & MacKinnon, R., 2016. Cryo-EM structure of the open high-conductance Ca2+-activated K+ channel. *Nature*, 541(7635), pp.46–51. Available at: http://www.nature.com/doifinder/10.1038/nature20608 [Accessed February 18, 2017].

Thouta, S. et al., 2014. Proline scan of the hERG channel S6 helix reveals the location of the intracellular pore gate. *Biophysical Journal*, 106(5), pp.1057–1069.

Thouta, S. et al., 2017. Stabilization of the Activated hERG Channel Voltage Sensor by Depolarization Involves the S4-S5 Linker. *Biophysical Journal*, 112(2).

Tombola, F., Pathak, M.M. & Isacoff, E.Y., 2006. How Does Voltage Open an Ion Channel? *Annual Review of Cell and Developmental Biology*, 22(1), pp.23–52. Available at:

http://www.annualreviews.org/doi/10.1146/annurev.cellbio.21.020404.145837 [Accessed December 27, 2016].

Tombola, F., Pathak, M.M. & Isacoff, E.Y., 2005. Voltage-Sensing Arginines in a Potassium Channel Permeate and Occlude Cation-Selective Pores. *Neuron*, 45(3), pp.379–388. Available at: http://www.ncbi.nlm.nih.gov/pubmed/15694325 [Accessed January 12, 2017].

Tomczak, A.P. et al., 2017. A new mechanism of voltage-dependent gating exposed by K_V 10.1 channels interrupted between voltage sensor and pore. *The Journal of General Physiology*, p.jgp.201611742. Available at: http://www.ncbi.nlm.nih.gov/pubmed/28360219 [Accessed April 12, 2017].

Torres, A.M. et al., 2003. Structure of the HERG K+ channel S5P extracellular linker: role of an amphipathic alpha-helix in C-type inactivation. *The Journal of biological chemistry*, 278(43), pp.42136–48. Available at: http://www.ncbi.nlm.nih.gov/pubmed/12902341 [Accessed January 7, 2017].

Tristani-Firouzi, M. et al., 2001. Molecular biology of K(+) channels and their role in cardiac arrhythmias. *The American journal of medicine*, 110(1), pp.50–9. Available at: http://www.ncbi.nlm.nih.gov/pubmed/11152866 [Accessed December 28, 2016].

Tristani-Firouzi, M., Chen, J. & Sanguinetti, M.C., 2002. Interactions between S4-S5 linker and S6 transmembrane domain modulate gating of HERG K+ channels. *The Journal of biological chemistry*, 277(21), pp.18994–9000. Available at: http://www.ncbi.nlm.nih.gov/pubmed/11864984 [Accessed December 29, 2016].

Trudeau, M.C. et al., 1995. HERG, a human inward rectifier in the voltage-gated potassium channel family. *Science*, 269(5220), pp.92–95. Available at: http://www.ncbi.nlm.nih.gov/pubmed/7604285.

Vaid, M. et al., 2008. Voltage clamp fluorimetry reveals a novel outer pore instability in a mammalian voltage-gated potassium channel. *The Journal of general physiology*, 132(2), pp.209–22. Available at: http://www.ncbi.nlm.nih.gov/pubmed/18625849 [Accessed January 12, 2017].

Vandenberg, J.I. et al., 2012. hERG K+ Channels: Structure, Function, and Clinical Significance. *Physiological Reviews*, 92(3).

Vandenberg, J.I., Walker, B.D. & Campbell, T.J., 2001. HERG K+ channels: friend and foe. *Trends in pharmacological sciences*, 22(5), pp.240–6. Available at: http://www.ncbi.nlm.nih.gov/pubmed/11339975 [Accessed December 28, 2016].

Varga, Z. et al., 2015. Direct Measurement of Cardiac Na^+ Channel Conformations Reveals Molecular Pathologies of Inherited Mutations. *Circulation: Arrhythmia and Electrophysiology*, 8(5), pp.1228–1239. Available at: http://www.ncbi.nlm.nih.gov/pubmed/26283144 [Accessed February 18, 2017].

Vemana, S., Pandey, S. & Larsson, H.P., 2004. S4 movement in a mammalian HCN

channel. *The Journal of general physiology*, 123(1), pp.21–32. Available at: http://www.ncbi.nlm.nih.gov/pubmed/14676284 [Accessed March 8, 2017].

Villalba-Galea, C.A. et al., 2008. S4-based voltage sensors have three major conformations. *Proceedings of the National Academy of Sciences of the United States of America*, 105(46), pp.17600–7. Available at: http://www.ncbi.nlm.nih.gov/pubmed/18818307 [Accessed December 21, 2016].

Viloria, C.G. et al., 2000. Differential effects of amino-terminal distal and proximal domains in the regulation of human erg K(+) channel gating. *Biophysical journal*, 79(1), pp.231–46. Available at: http://www.ncbi.nlm.nih.gov/pubmed/10866950 [Accessed March 5, 2017].

Wang, D.T. et al., 2011. Mapping the sequence of conformational changes underlying selectivity filter gating in the Kv11.1 potassium channel. *Nature Structural & Molecular Biology*, 18(1), pp.35–41. Available at: http://www.ncbi.nlm.nih.gov/pubmed/21170050 [Accessed January 7, 2017].

Wang, J. et al., 1998. Regulation of deactivation by an amino terminal domain in human ether-à-go-go-related gene potassium channels. *The Journal of general physiology*, 112(5), pp.637–47. Available at: http://www.ncbi.nlm.nih.gov/pubmed/9806971 [Accessed December 30, 2016].

Wang, J., Myers, C.D. & Robertson, G.A., 2000. Dynamic control of deactivation gating by a soluble amino-terminal domain in HERG K(+) channels. *The Journal of general physiology*, 115(6), pp.749–58. Available at: http://www.ncbi.nlm.nih.gov/pubmed/10828248 [Accessed December 30, 2016].

Wang, S. et al., 1997. A quantitative analysis of the activation and inactivation kinetics of HERG expressed in Xenopus oocytes. *J Physiol (Lond)*, 502(Pt 1), pp.45–60.

Wang, W. & MacKinnon, R., 2017. Cryo-EM Structure of the Open Human Ether-à-go-go -Related K + Channel hERG. *Cell*, 169(3), p.422–430.e10. Available at: http://www.ncbi.nlm.nih.gov/pubmed/28431243 [Accessed June 21, 2017].

Wang, Z. et al., 2013. Components of gating charge movement and S4 voltage-sensor exposure during activation of hERG channels. *The Journal of general physiology*, 141(4), pp.431–43. Available at: http://jgp.rupress.org/content/141/4/431.long.

Warmke, J.W. & Ganetzky, B., 1994. A family of potassium channel genes related to eag in Drosophila and mammals. *Proceedings of the National Academy of Sciences of the United States of America*, 91(8), pp.3438–3442.

Weerapura, M., Nattel, S., et al., 2002. A comparison of currents carried by HERG, with and without coexpression of MiRP1, and the native rapid delayed rectifier current. Is MiRP1 the missing link? *The Journal of physiology*, 540(Pt 1), pp.15–27. Available at: http://www.ncbi.nlm.nih.gov/pubmed/11927665 [Accessed February 14, 2017].

Weerapura, M., Hébert, T.E. & Nattel, S., 2002. Dofetilide block involves interactions

with open and inactivated states of HERG channels. *Pflugers Archiv : European journal of physiology*, 443(4), pp.520–31. Available at: http://link.springer.com/10.1007/s004240100720 [Accessed January 8, 2017].

Whicher, J.R. & MacKinnon, R., 2016. Structure of the voltage-gated K^+ channel Eag1 reveals an alternative voltage sensing mechanism. *Science (New York, N.Y.)*, 353(6300), pp.664–9.

Wu, W. et al., 2016. Ginsenoside Rg3, a Gating Modifier of EAG Family K+ Channels. *Molecular Pharmacology*, 90(4), pp.469–482. Available at: http://www.ncbi.nlm.nih.gov/pubmed/27502018 [Accessed March 8, 2017].

Wu, W., Gardner, A. & Sanguinetti, M.C., 2015. The Link between Inactivation and High-Affinity Block of hERG1 Channels. *Molecular pharmacology*, 87(6), pp.1042–50. Available at: http://www.ncbi.nlm.nih.gov/pubmed/25855787 [Accessed March 8, 2017].

Wynia-Smith, S.L. et al., 2008. hERG gating microdomains defined by S6 mutagenesis and molecular modeling. *The Journal of general physiology*, 132(5), pp.507–520.

Yang, B. et al., 2004. Inactivation gating determines drug potency: a common mechanism for drug blockade of HERG channels. *Acta pharmacologica Sinica*, 25(5), pp.554–60. Available at: http://www.ncbi.nlm.nih.gov/pubmed/15132818 [Accessed January 7, 2017].

Yellen, G., 1998. The moving parts of voltage-gated ion channels. *Quarterly reviews of biophysics*, 31(3), pp.239–95. Available at: http://www.ncbi.nlm.nih.gov/pubmed/10384687 [Accessed December 19, 2016].

Yellen, G., 2002. The voltage-gated potassium channels and their relatives. *Nature*, 419(6902), pp.35–42. Available at: http://www.nature.com/doifinder/10.1038/nature00978 [Accessed December 14, 2016].

Zagotta, W.N., Hoshi, T., Dittman, J., et al., 1994. Shaker potassium channel gating. II: Transitions in the activation pathway. *The Journal of general physiology*, 103(2), pp.279–319. Available at: http://www.ncbi.nlm.nih.gov/pubmed/8189207 [Accessed December 21, 2016].

Zagotta, W.N., Hoshi, T. & Aldrich, R.W., 1990. Restoration of inactivation in mutants of Shaker potassium channels by a peptide derived from ShB. *Science (New York, N.Y.)*, 250(4980), pp.568–71. Available at: http://www.ncbi.nlm.nih.gov/pubmed/2122520 [Accessed January 7, 2017].

Zagotta, W.N., Hoshi, T. & Aldrich, R.W., 1994. Shaker potassium channel gating. III: Evaluation of kinetic models for activation. *The Journal of general physiology*, 103(2), pp.321–62. Available at: http://www.ncbi.nlm.nih.gov/pubmed/8189208 [Accessed December 21, 2016].

Zhang, M. et al., 2005. Interactions Between Charged Residues in the Transmembrane Segments of the Voltage-sensing Domain in the hERG Channel. *Journal of Membrane Biology*, 207(3), pp.169–181. Available at: http://www.ncbi.nlm.nih.gov/pubmed/16550488 [Accessed December 29, 2016].

Zhang, M., Liu, J. & Tseng, G.-N., 2004. Gating charges in the activation and inactivation processes of the HERG channel. *The Journal of general physiology*, 124(6), pp.703–18. Available at: http://www.ncbi.nlm.nih.gov/pubmed/15545400 [Accessed December 29, 2016].

Zhao, J. & Blunck, R., 2016. The isolated voltage sensing domain of the Shaker potassium channel forms a voltage-gated cation channel. *eLife*, 5. Available at: http://www.ncbi.nlm.nih.gov/pubmed/27710769 [Accessed January 10, 2017].

Zhao, Y., Yarov-Yarovoy, V., et al., 2004. A gating hinge in Na+ channels; a molecular switch for electrical signaling. *Neuron*, 41(6), pp.859–65. Available at: http://www.ncbi.nlm.nih.gov/pubmed/15046719 [Accessed December 19, 2016].

Zhao, Y. et al., 2017. The intrinsically liganded cyclic nucleotide–binding homology domain promotes KCNH channel activation. *The Journal of General Physiology*.

Zhao, Y., Scheuer, T. & Catterall, W.A., 2004. Reversed voltage-dependent gating of a bacterial sodium channel with proline substitutions in the S6 transmembrane segment. *Proceedings of the National Academy of Sciences of the United States of America*, 101(51), pp.17873–8. Available at: http://www.ncbi.nlm.nih.gov/pubmed/15583130 [Accessed January 15, 2017].

Zhou, P.Z. et al., 2011. Activation of human ether-a-go-go related gene (hERG) potassium channels by small molecules. *Acta Pharmacol Sin*, 32(6), pp.781–788. Available at: http://www.ncbi.nlm.nih.gov/pubmed/21623390.